Mathematical Modeling of the Tryptophan Metabolism During 1-Methyltryptophan Administration in Pigs in the Face of Infection

I n a u g u r a l d i s s e r t a t i o n

zur

Erlangung des akademischen Grades eines

Doktors der Naturwissenschaften
(Dr. rer. Nat.)

der

Mathematisch-Naturwissenschaftlichen Fakultät

der

Universität Greifswald

vorgelegt von

Dana Kleimeier

Greifswald, 24. Januar 2023

Dekan:	Prof. Dr. Gerald Kerth
1. Gutachter*in:	Prof. Dr. Barbara Bröker
2. Gutachter*in:	Prof. Dr. Lars Kaderali
3. Gutachter*in:	Prof. Dr. Marc Thilo Figge
Tag der Promotion:	31. Mai 2023

Contents

1. Introduction **1**

1.1. Tryptophan Metabolism 1
1.2. Tryptophan Metabolism in Inflammatory Diseases 5
1.3. Mathematical Modeling with Ordinary Differential Equations 7
1.3.1. The Law of Mass Action and Michaelis-Menten Kinetics 9
1.3.2. Parameter Fitting 14
1.3.3. Model Selection 15
1.3.4. Profile Likelihood 16
1.3.5. Sensitivity Analysis 17
1.4. Previous Mathematical Models of the TRP Metabolism 17
1.4.1. Effects of Vitamin B6 18
1.4.2. Parameter fitting Based on Tissue-Specific Gene Expression Data 20
1.4.3. Further Models 22
1.5. Aim of the Thesis 22

2. Materials and Methods **25**

2.1. Ordinary Differential Equation Models of Tryptophan Metabolism 25
2.1.1. Standard Model 26
2.1.2. Model Considering Infection 30
2.1.3. Model Considering 1-Methyltryptophan Administration 33
2.1.4. Hypotheses of 1-Methyltryptophan Degradation 36
2.1.5. Model of 1-Methyltryptophan Effects Facing Infection 51
2.2. Data used for validation of the mathematical models 56
2.2.1. A Pig Model of Indoleamine 2,3-Dioxygenase Activation by Lipopolysaccharides 56
2.2.2. A Pig Model of the Interactions of 1-Methyltryptophan and IDO . 57
2.3. Mathematical Methods used for Model Fitting and Analysis 61
2.3.1. Software 61
2.3.2. Approaches for Parameter Calculation 61
2.3.3. Conditions for Parameters and Literature Values 62
2.3.4. Identifiablity Analysis 66
2.3.5. Sensitivity Analysis 66
2.3.6. Modeling the Uptake of Tryptophan and 1-Methyltryptophan . . 66
2.3.7. Model Evaluation 67
2.3.8. Validation of Results of Simulation of 1-Methyltryptophan Hypotheses 67

3. Results **69**
3.1. 1-Methyltryptophan is Directly Degraded to Kynurenic Acid 69
3.1.1. Calculation of Parameters by Using the Data of Lipopolysaccharide-Treated Pigs 71
3.1.2. Calculations of Parameters by Using a Selection of Lipopolysaccharide-Treated Pigs 78
3.1.3. Estimation of Parameters fitted to Data of a Selection of Lipopolysaccharide-treated Pigs by a Parameter Scan 81
3.1.4. Sensitivity Analysis of Kynurenic Acid 83
3.1.5. Fitting Hypotheses to the Data of 1-Methyltryptophan/Lipopolysaccharide Experiment, Subset 1-Methyltryptophan-Treated Pigs 84
3.1.6. Results of the Validation Experiment 101
3.2. Modeling 1-Methyltryptophan's Ability to inhibit Indoleamine 2,3-Dioxygenase102
3.2.1. Parameters Fixed to the Parameter Values Fitted to the Data of Lipopolysaccharide-Treated Pigs (Approach 1) 102
3.2.2. Parameters Fixed to the Parameter Values Fitted to the Data of a Selection of Lipopolysaccharide-Treated Pigs (Approach 2) . . . 104
3.2.3. Parameters Fitted to the Data of a Selection of 1-Methyltryptophan-Treated Pigs by a Parameter Scan (Approach 3) 106

4. Discussion **109**
4.1. 1-Methyltryptophan is Directly Degraded to Kynurenic Acid 109
4.1.1. Classical Pathway 109
4.1.2. Hypothesis 1 110
4.1.3. Hypothesis 2 110
4.1.4. Hypothesis 3 110
4.1.5. Hypothesis 4 111
4.1.6. Hypothesis 5 111
4.1.7. Hypothesis 6 111
4.1.8. Hypothesis 7 111
4.2. Inhibition of Indoleamine 2,3-Dioxygenase by 1-Methyltryptophan 112
4.3. Potential Therapeutic Targets 112
4.4. Modeling Food Intake 113
4.5. Parameter Calculation based on Data Measured in Pigs 113
4.6. Comparison of the Fitted Parameters to Literature Values 114
4.7. Parameter Scan 115
4.8. Limitations 115
4.8.1. Using LL, AIC, and BIC for Model Selection 116
4.8.2. Different Approaches Reveal Different Results 116
4.8.3. Reduced Reproducibility of Parameters 116
4.8.4. Literature Values and Calculated Parameters 117
4.8.5. Mathematical Modeling of the Tryptophan Metabolism 118
4.9. Future Directions 118
4.10. Conclusion 119

5. Summary **121**

A. Data Description **147**
A.1. LPS - Treated Pigs 147
A.2. 1-MT and LPS-treated Pigs 151

B. Identifiability Analysis **161**

C. Comparison of literature and fitted parameters **163**

D. Parameters Fitted to the Data of 1-MT/LPS Experiment, Second Data Set with a Parameter Scan, AIC values **165**

List of Figures

1.1. TRP metabolism 3
1.2. Activation of IDO 6
1.3. Schematic of the TRP metabolism in different compartments published by Rios-Avila et al. 19
1.4. Schematic of the TRP metabolism in different compartments published by Stavrum et al. 21

2.1. Schematic of the standard model of the TRP metabolism 27
2.2. Schematic of the LPS model 30
2.3. Schematic of the 1-MT Model 33
2.4. Summary of hypotheses of 1-MT degradation processes 36
2.5. Schematic of hypothesis 1 of 1-MT degradation processes 37
2.6. Schematic of hypothesis 2 of 1-MT degradation processes 39
2.7. Schematic of hypothesis 3 of 1-MT degradation processes 41
2.8. Schematic of hypothesis 4 of 1-MT degradation processes 43
2.9. Schematic of hypothesis 5 of 1-MT degradation processes 45
2.10. Schematic of hypothesis 6 of 1-MT degradation processes 47
2.11. Schematic of hypothesis 7 of 1-MT degradation processes 49
2.12. Schematic of 1-MT/LPS model including 1-MT's inhibitory effects 52
2.13. Schematic of 1-MT/LPS model not including 1-MT's inhibitory effects . 54
2.14. Experimental Set-up of LPS Experiment I and II 57
2.15. Experimental Set-up of 1-MT/LPS Experiment 58
2.16. Experimental Set-up of 1-MT/LPS experiment, subset LPS-treated . . . 59
2.17. Experimental Set-up of 1-MT/LPS experiment, subset 1-MT-treated . . 60

3.1. Simulations with parameters fitted to data of LPS experiment I 72
3.2. Identifiability analysis of parameters of the LPS model fitted to data of LPS experiment I 73
3.3. Simulations with parameters fitted to data of LPS experiment I, applied to LPS experiment II for validation 75
3.4. Simulations with parameters fitted to data of LPS experiment I, applied to 1-MT/LPS experiment, subset LPS-treated 77
3.5. Simulations with parameters fitted to data of 1-MT/LPS experiment, LPS-treated pigs 79
3.6. Identifiability analysis of parameters of the LPS model fitted to data of 1-MT/LPS experiment, LPS-treated pigs 80

3.7. Simulations with parameters fitted to the data measured in 1-MT/LPS experiment, LPS-treated pigs, 100 times 82
3.8. Sensitivity Analysis of KYNA 83
3.9. Simulations of all hypotheses with parameters fitted to data of 1-MT/LPS experiment, subset 1-MT-treated pigs, first data set (approach 1) 87
3.10. Simulations of all hypotheses with parameters fitted to data of 1-MT/LPS experiment, subset 1-MT-treated pigs, second data set (approach 1) . . . 88
3.11. Simulations of all hypotheses with parameters fitted to data of 1-MT/LPS experiment, subset 1-MT-treated pigs, first data set (approach 2) 91
3.12. Simulations of all hypotheses with parameters fitted to data of 1-MT/LPS experiment, subset 1-MT-treated pigs, second data set (approach 2) . . . 92
3.13. Box plot of AIC values of all hypotheses fitted 100 times to the data of 1-MT/LPS experiment, subset 1-MT-treated pigs, first data set (approach 3) 93
3.14. Simulations of all hypotheses fitted 100 times to the data of 1-MT/LPS experiment, subset 1-MT-treated pigs, first data set (approach 3) 96
3.15. Box plot of AIC values of all hypotheses fitted 100 times to the data of 1-MT/LPS experiment, subset 1-MT-treated pigs, second data set (approach 3) 98
3.16. Simulations of all hypotheses fitted 100 times to the data of 1-MT/LPS experiment, subset 1-MT-treated pigs, second data set (approach 3) . . . 100
3.17. Results of the experiment to validate the results of the hypotheses 101
3.18. Simulations of the models with inhibition and without inhibition (approach 1) 103
3.19. Simulations of the models with inhibition and without inhibition (approach 2) 105
3.20. Simulations of the models with inhibition and without inhibition (approach 3) 108

A.1. LPS Experiment I and II 148
A.2. Data measured in LPS experiment I 149
A.3. Data measured in LPS experiment II 150
A.4. 1-MT/LPS experiment 151
A.5. Data measured in 1-MT/LPS experiment 153
A.6. 1-MT/LPS experiment, subset LPS-treated 154
A.7. Data measured in 1-MT/LPS experiment, subset LPS-treated 155
A.8. 1-MT/LPS experiment, subset 1-MT-treated 156
A.9. Data measured in 1-MT/LPS experiment, subset 1-MT-treated pigs (first data set) 157
A.10. Data measured in 1-MT/LPS experiment, subset 1-MT-treated pigs (second data set) 158
A.11. Data measured in 1-MT/LPS experiment (second data set) 160

D.1. Boxplot of AIC values of hypotheses based on the data of 1-MT/LPS experiment (second data set) 165

List of Tables

2.1. **Chemical reactions and signaling pathways of the TRP metabolism** . . . 28
2.2. **Chemical reactions and signaling pathways of the TRP metabolism including the IDO activation by LPS administration** . . . 31
2.3. **Chemical reactions and signaling pathways of the TRP metabolism, including the administration of 1-MT** . . . 34
2.4. **Chemical reactions and signaling pathways of the TRP metabolism, including the IDO activation by LPS administration and 1-MT's inhibitory effects on IDO** . . . 51
2.5. **Literature values for simulations with Michaelis-Menten Kinetics:** 64

3.1. **Results of all three *in silico* experiments to find the most likely degradation process of 1-MT** . . . 70
3.2. **LL, AIC, BIC values of different hypotheses fitted to data of LPS experiment I (approach 1)** . . . 85
3.3. **LL, AIC, BIC values of different hypotheses fitted to data of 1-MT/LPS experiment, subset 1-MT-treated pigs (approach 2)** 89
3.4. **LL, AIC, BIC values of the classical pathway and all hypotheses fitted to the data of 1-MT/LPS experiment, first data set (approach 3)** . . . 94
3.5. **p-values of pairwise comparison of AIC values for each hypothesis fitted to the data of 1-MT/LPS experiment, subset 1-MT-treated pigs, first data set, 100 times (approach 3)** . . . 95
3.6. **LL, AIC, BIC values of the classical pathway and all hypotheses fitted to data of 1-MT/LPS experiment, Second Data Set (approach 3)** . . . 97
3.7. **p-values of pairwise comparison of AIC values for each hypotheses fitted to the data of 1-MT/LPS experiment, subset 1-MT-treated pigs, second data set, 100 times (approach 3)** . . . 99
3.8. **LL, AIC, BIC values of simulations with and without inhibition fitted to data of LPS experiment I** . . . 102
3.9. **LL, AIC, BIC values of simulations with and without inhibition fitted to data of 1-MT/LPS experiment** . . . 104
3.10. **LL, AIC, BIC, values of the LPS model extended by hypothesis 2 and with and without inhibition were fitted to data of the 1-MT/LPS experiment, second data set** . . . 106

B.1. **Upper and lower boundary of Identifiability analysis for the LPS model** 161

C.1. **Overview of fitted parameters of the LPS model on different data sets and literature values** 164

Abbreviations

1-MT	1-methyltryptophan
AA	anthranilic acid
AAD	aromatic L-amino acid decarboxylase
AANAT	N-acetyltransferase
ACD	2-amino-3-carboxymuconate semialdehyde-decarboxylase
ACMS	2-amino-3-monooxygenase
AFD	arylformamidase
AhR	aryl hydrocarbon receptor
AMSA	2-aminoconate semialdehyde
CD	cluster of differentiation
eq.	equation
EU	endotoxin units
HAA	3-hydroxy-anthranilic acid
HAO	3-hydroxyanthranilic acid oxidase
HIOMT	hydroxy-O-methyltransferase
HK	3-hydroxykynurenine
hyp	hypothesis
IDO	indoleamine 2,3-dioxygenase
IFN-γ	Interferon gamma - γ
IL	Interleukin
KAT	kynurenine aminotransferase
KMO	kynurenine 3-monooxygenase
KP	kynurenine pathway
KAT	kynurenine amino transferase
KQE	kynurenine to quinolinic acid degrading enzyme
KYN	kynurenine
KYNA	kynurenic acid
KYNU	kynureninase
LAT	L-amino acid transporter
LBP	lipopolysaccharide binding protein
LHS	latin hypercube symapling
LPS	lipopolysaccharides
MM	Michaelis-Menten
NF-κB	nuclear factor kappa-light-chain-enhancer of activated B cells
NFK	N-formyl-kynurenine
NMDA	N-methyl-d-aspartate

ODE	ordinary differential equations
PICO	picolinic acid
PLP	pyridoxal 5'-phosphate
QUIN	quinolinic acid
T_{reg} cells	regulatory T cells
SER	serotonin
STAT1	signal transducer and activator of transcription 1
TDO	tryptophan 2,3-dioxygenase
TPH	tryptophan hydroxylase
TLR-4	toll-like receptor 4
TNF-α	tumor necrosis factor α
TNFR	tumor necrosis factor α receptor
TRP	tryptophan
XA	xanthurenic acid

1. Introduction

In this study, the tryptophan (TRP) metabolism and its dynamics, without interference, in the face of infection and drug intervention are in focus. To decipher the mechanisms of the altered dynamics of TRP metabolites, mathematical modeling with systems of ordinary differential equations (ODE) was applied. To emphasize the relevance of TRP metabolism, a detailed explanation of its reactions and its relation to disease, is given in the following introductory part. The reactions were translated into mathematical models. To understand the simulations based on these models, mathematical modeling with ODEs is introduced. Both sections are connected by the aim of the thesis, which completes this chapter.

1.1. Tryptophan Metabolism

Biological processes are the basis of mathematical modeling. In this study, the dynamics of the TRP metabolism are in focus. Its detailed explanation helps to understand the composition of a model, which represents the dynamics of the TRP metabolism with the help of data measured in pig's blood. Since the blood vessels are the railway of the body, connecting the organs, the turnover rates of enzymes are mixed. Thus, it is crucial look closely at different enzyme variants in different organs. Alterations of the TRP metabolism due to infection, drug application, and food intake must be considered for model extension. These topics are introduced in more detail in this section, beginning with the TRP metabolism in general and alterations of the metabolism during infection. Moreover, the effects of drug application on TRP metabolites and associated enzymes with different variants are explained in more detail. Lastly, the impact of TRP increase after food intake and the properties of drug administration are presented.
The TRP metabolism can be divided into two branches: the serotonin (SER) pathway and the kynurenine pathway (KP). Via the SER pathway, TRP is degraded to 5-hydroxytryptophan (HT) by tryptophan hydroxylase (TPH, see Figure 1.1) [1]. HT is further degraded to SER by aromatic L-amino acid decarboxylase (AAD) [2, 3]. SER acts as a hormone and neurotransmitter in the central nervous system and the periphery [4]. The modulation of SER levels can lead e.g., to mood disorders, pulmonary and system hypertension [4]. SER is also further degraded to melatonin by N-acetyltransferase (AANAT) and hydroxy-O-methyltransferase (HIOMT) [1]. Melatonin regulates the sleep/wake cycle, and other circadian and seasonal rhythms and acts as an immunostimulator [5]. The enzyme indoleamine 2,3-dioxygenase (IDO) degrades melatonin further to N-acetyl-5-methoxy-kynuramine, which affects the cardiovascular system [6]. A dis-regulation of the SER pathway due to infection [7] is one reason for

sickness behavior [8, 9, 10]. Sickness behavior is characterized by general malaise, decreased activity, loss of energy or fatigue, decreased social investigation, loss of interest in usual activities and reduced appetite [11].

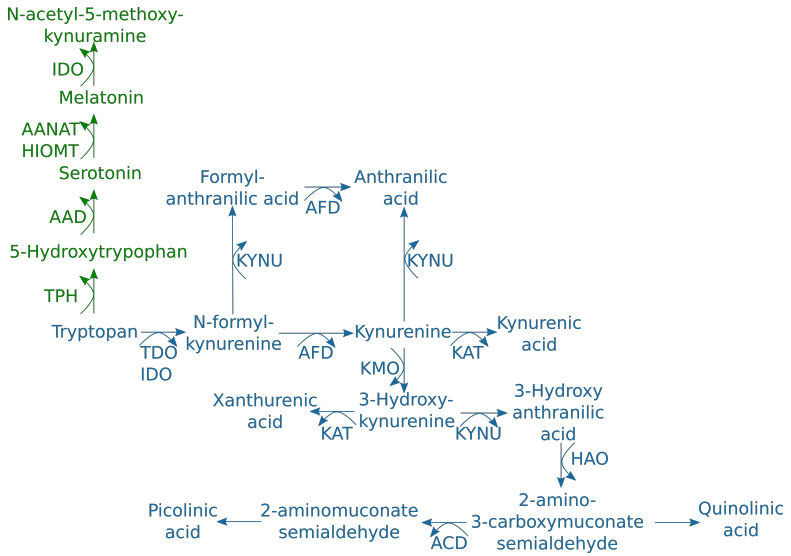

Figure 1.1.: **TRP metabolism:** The TRP pathway is divided into two branches: the serotonin pathway (in green font), including 5-hydroxytryptophan, serotonin, melatonin, N-acetyl-5-methoxy-kynuramine and the kynurenine pathway (in blue font) including tryptophan, N-formyl-kynurenine, formyl anthranilic acid, anthranilic acid, kynurenine, kynurenic acid, 3-hydroxykynurenine, 3-hydroxy-anthranilic acid, 2-amino-3-carboxymuconate semialdehyde, 2-aminomuconate-semialdehyde, picolinic acid and quinolinic acid. Bent arrows show enzymatic reactions with the enzyme names next to the arrow. AAD - aromatic L-amino acid decarboxylase, AANAT - N-acetyltransferase, ACD - 2-amino-3-carboxymuconate semialdehyde-decarboxylase, AFD - Arylformamidase, HAO - 3-hydroxynalic acid oxygenase, HIOMT - hydroxy-O-methyltransferase, IDO - indoleamine 2,3-dioxygenase, KAT - kynurenine aminotransferase, KMO - kynurenine 3-monooxygenase, KYNU - kynureninase, TDO - tryptophan 2,3- dioxygenase, TPH - Tryptophan hydroxylase

Along the KP, TRP is degraded via two different enzymes. The first one is IDO, which is activated during infection. The activation of IDO is presented in more detail in section 1.2. The second degradation process is mediated via the hepatic enzyme tryptophan 2,3-dioxygenase (TDO) [12, 13]. It is responsible for the homeostasis of TRP and catalyzes the degradation of TRP to N-formyl-kynurenine [14]. N-formyl-kynurenine can be degraded to formyl-anthranilic acid by the enzyme kynureninase (KYNU), which is further degraded to anthranilic acid by aryl formamidase (AFD) [15]. AFD also catalyzes N-formyl-kynurenine degradation to KYN (see Figure 1.1) [14]. KYN has immunomodulatory properties affecting T-cells, which mediate the adaptive immune response [16]. KYN can also be degraded to anthranilic acid by KYNU [17]. KYN is further degraded to quinolinic acid (QUIN) via three different enzymes (see Figure 1.1): Kynurenine 3-monooxygenase (KMO) degrades KYN to 3-hydroxykynurenine, which KYNU further degrades to 3-hydroxyanthranilic acid [14]. 3-Hydroxyanthranilic acid is degraded to QUIN via 2-amino-3-carboxymuconate semialdehyde by 3-hydroxyanthranilic acid oxidase (HAO) [18, 19] and spontaneously to QUIN [15, 20]. QUIN and 3-hydroxykynurenine lead to excessive glutamatergic activity, leading, together with a decreased SER production, to cytokine-induced depression [8]. QUIN is an N-methyl-d-aspartate (NMDA) receptor agonist [21]. The NMDA receptor belongs to glutamate receptors [22]. In the brain, the NMDA receptor affects synaptic plasticity and synapse formation [22]. It is also a neurotoxin, gliotoxin, proinflammatory mediator and pro-oxidant molecule and can alter the integrity and cohesion of the blood–brain barrier [21]. 3-Hydroxykynurenine can also be degraded to xanthurenic acid by kynurenine aminotransferases (KAT). Xanthurenic acid activates NMDA receptors [23]. Lowered levels of xanthurenic acid are associated with schizophrenia [23]. 2-amino-3-carboxymuconate semialdehyde is degraded via 2-amino-3-carboxymuconate semialdehyde decarboxylase (ACD) to 2-aminomuconate semialdehyde, which is further degraded non-enzymeatical to picolinic acid (PICO). PICO has neuroprotective, immunological, and antiproliferative effects [24]. Besides QUIN, KYNA is also a product of KYN, which is degraded by a group of enzymes called kynurenine aminotransferases (KAT, see Figure 1.1) [1]. This group consists of four different variants. All differ in the locations where they are expressed. KATI and KATIII are expressed in kidney, liver, heart, lung, and neuroendocrine organs [25]. In mitochondria, KATII, III and IV are located [26]. KATII is also located in the brain [27, 28, 29]. The production of KYNA in the brain is necessary since KYNA only poorly crosses the blood-brain barrier [30]. In contrast, KYN can pass the blood-brain barrier [31]. Thus, KAT catalyzes the degradation of KYN to KYNA in the brain. All in all, 60% to 80% of brain KYN originate from non-brain compartments of the body [30, 31]. The presence of some KATs in the brain leads to mental disorders like psychosis and schizophrenia [28, 32, 33] because KYNA is an NMDA receptor antagonist. An inhibition of KAT is discussed as a potential therapeutic application to treat mental disorders [34] and influence hypermotility and inflammatory processes in the intestine [35].

1.2. Tryptophan Metabolism in Inflammatory Diseases

In the face of infection, e.g., by gram-negative bacteria, which secrete lipopolysaccharides (LPS), IDO transcription is initiated (see Figure 1.2, arrow 1) [2]. The detection of LPS is one of the most sensitive processes of animals during infection of those bacteria [36, 37, 38, 39, 40] and leads to the activation of the innate immune system [41]. After secretion, LPS binds to the lipopolysaccharide binding protein (LBP) (see Figure 1.2, arrow 2). Afterward, the LPS/LBP complex binds to toll-like receptor 4 (TLR-4, see Figure 1.2, 3)[42, 43, 44]. The activation of TLR-4 via the aryl hydrocarbon receptor (AhR) pathway leads to IDO-transcription of either the IDO variant IDO1 or the variant IDO2 [45, 46, 47]. Depending on the activated cells. Many different cells produce IDO. For example, it can be translated into immune cells like macrophages [48] or monocytes [1], dendritic cells [49, 50], but also in tissue like intestinal epithelial [51] or brain tissue [52]. Independent of the activation via LPS/LBP complexes, IDO transcription is also activated by TNF-α and IFN-γ secretion [53, 54] (see Figure 1.2, 4). While the IFN-γ receptor activates STAT1 [55], the TNF-α receptor and TLR-4 activate NF-κB (see Figure 1.2, 5) [43, 56]. This activation also leads to IDO transcription (see Figure 1.2, arrow 6), which occurs in the lung, small and large intestine, colon, spleen, kidney, stomach and brain [57]. Afterward, IDO mRNA is translated to the IDO protein (see Figure 1.2, arrow 7), which catalyzes the degradation of TRP to KYN in the cell (see Figure 1.2, arrow 8) [1, 2]. To enter the cell, TRP uses the L-amino acid transporter (LAT), while KYN exits the cell through LAT [58]. KYN is further degraded to QUIN via several other metabolites (see Figure 1.2, arrow 12) or to KYNA (see Figure 1.2, arrow 13). But TRP is not only degraded to KYN, it is also degraded to SER. Whereat, the proportion of TRP degraded to SER is reduced during infection [7].

IDO production is increased during severe sepsis and septic shock. High IDO levels are also associated with increased mortality [59]. In the early phase of sepsis, patients with enhanced IDO levels have poor outcome [60]. The increased IDO levels accompanied by increased levels of KYN and KYNA and cytokine production [61, 62]. This increase, in turn, leads to an increased generation of regulatory T cells (T_{reg}) ending up in immunoparalysis [1]. Immunoparalysis is the persistence of a marked compensatory anti-inflammatory innate immune response after an insult such as sepsis. Anti-inflammatory cytokines are TGF-β and interleukin (IL)-10 [60], whereas TNF-α and IFN-γ are proinflammatory cytokines. TNF-α is involved in pathological processes such as chronic inflammation [63], like inflammatory bowel diseases. Patients with inflammatory bowel diseases like ulcerative colitis and Crohn's disease have increased KYN and KYNA levels [64] due to increased production of TNF-α, which activates IDO. However, KYNA has neuroprotective properties that counter QUIN's effects [65]. On the one hand, KYNA attenuates inflammation by activating G protein-coupled receptor 35 (GPR35) in the intestinal wall [66, 67, 68, 69]. On the other hand, KYNA reduces the production of inflammatory factors [70, 71], such as TNF-α [68], and activates T_{reg} cells [72].

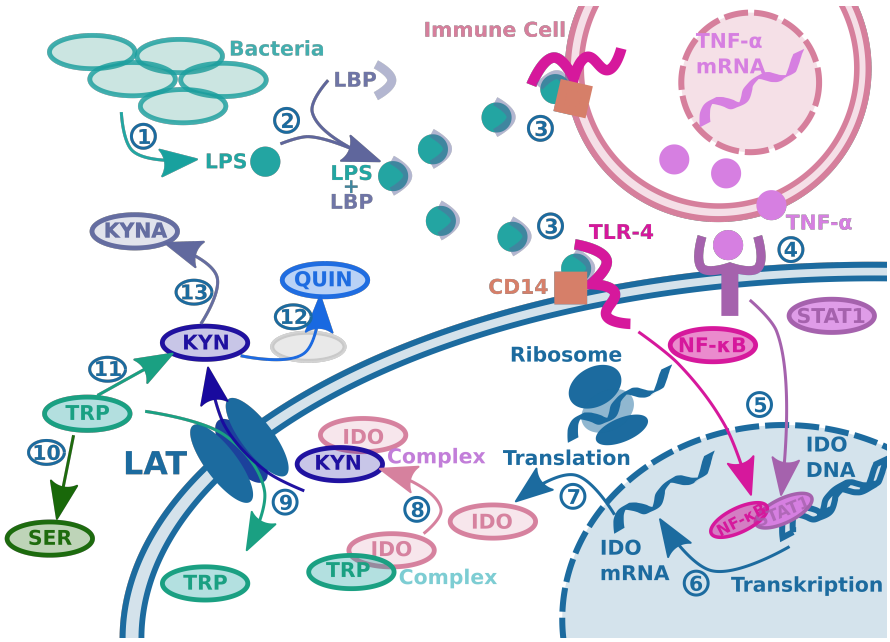

Figure 1.2.: **Activation of IDO:** gram-negative bacteria secrete lipopolysaccharides (LPS, 1). LPS is bound to lipopolysaccharide-binding protein (LBP, 2). The complex binds to toll-like receptor-4 (TLR-4, 3) and cluster of differentiation (CD) 40. This induces interferon-γ (IFN-γ) and tumor necrosis factor α (TNF-α, 4) production in immune cells. TNF-α binds to its receptor (TNFR, 4) and induces signal transducer and activator of transcription 1 (STAT1, 5), leading to transcription of indoleamine 2,3-dioxygenase (IDO) mRNA (6). The binding of LPS/LBP complexes to TLR4/CD14 to its receptors leads to the activation of nuclear factor (NF)-κB (5) and also to IDO mRNA transcription in the nucleus (6). Further, IDO mRNA is translated to the active enzyme leading to the degradation of tryptophan (TRP) to kynurenine (KYN, 8). TRP gets into and KYN out of the cell by crossing the amino acid transporter (LAT, 9). Afterward KYN can be degraded by kynurenine aminotransferases (KATs) to kynurenic acid (KYNA, 13) or by kynurenine 3-monooxygenase (KMO), kynureninase (KYNU) and 3-hydroxyanthranilic acid oxidase (HAO) via 3-hydroxyanthranilic acid to quinolinic acid (QUIN, 12). In addition, TRP can be degraded by tryptophan-2,3-dioxygenase to KYN in the liver and by tryptophan hydroxylase to serotonin (SER, 10). CD - cluster of differentiation, IDO - indoleamine 2,3-dioxygenase, KYN - kynurenine, KYNA - kynurenic acid, LAT - L-amino acid transporter, LBP - lipopolysaccharide-binding protein, LPS - lipopolysaccharide, NF-κB - nuclear factor kappa-light-chain-enhancer of activated B cells, QUIN - quinolinic acid, SER - serotonin, STAT1 - signal transducer and activator of transcription 1, TLR-4 - toll-like receptor 4, TNF-α - tumor necrosis factor α, TRP - tryptophan

T_{reg} cells secrete TGF-β [73], which is an immunoinhibitory cytokine [73] preventing organ damage by the immune system during infection [74]. Thus, KYNA acts as a counter-regulator to prevent overshooting inflammation leading to tissue damage [75]. It also mediates immune tolerance by activating the aryl hydrocarbon receptor (AhR). In breast cancer cells, activation of the AhR by KYNA leads to IL-6 secretion. IL-6 initiates processes allowing cancer cells to bypass crucial checkpoints in cell cycle progression and evade apoptotic signals [76]. Thus, an increased IL-6 secretion is associated with poor prognosis in cancer patients [77, 78].
In sepsis, inflammatory bowel disease, and cancer, the TRP metabolism is associated with disease outcomes. Thus, the TRP metabolism could be a target of therapeutic intervention, especially manipulation of KYNA levels [62]. This regulation can be disturbed via 1-methyltryptophan (1-MT). It was discovered to inhibit IDO since it is structurally very similar to TRP. The only difference is a methyl group (CH_3) [79], which does not prohibit the ability of 1-MT to bind IDO. However, with its binding, 1-MT inhibits the degradation of TRP to KYN by IDO1 and IDO2 [80], leading to a competitive inhibition [81]. By administering 1-MT, lowered levels of downstream metabolites such as KYN and KYNA are expected. It was reported that the survival of 1-MT-treated mice suffering from sepsis increased compared to mice, not treated with 1-MT [82, 83, 84]. Surprisingly, in healthy mice and in pigs, an increase in KYNA after 1-MT administration was reported [85, 86]. Nevertheless only weak inhibition of 1-MT was recognizable concerning the proportion of TRP to KYN [86, 87, 88]. This lack of IDO inhibition may be due to the low affinity of 1-MT to IDO *in vivo* or due to the limited accumulation of 1-MT to serum levels compared to those of TRP [89]. Those unexpected metabolite alterations after 1-MT administration and the mode of action, were not the focus of recent research.

1.3. Mathematical Modeling with Ordinary Differential Equations

This work focuses on the dynamics of the TRP metabolism and its interference by LPS and 1-MT. Mathematical modeling helps to understand processes' internal nature and dynamics [90, 91]. Different ODE models have already been invented to answer particular questions about metabolisms [92] or drug treatment [93, 94].
This thesis used mathematical models based on ODEs, because many biological laws and reactions appear mathematically in the form of differential equations [95]. A short introduction to several mathematical modeling methods using ODEs is given below. Firstly, the development of systems of ODEs according to chemical respective biological processes is described since it is the fundamental method used in this study. In the following this method is called modeling, ODE modeling, or mathematical modeling. The law of mass action is the basis of modeling biochemical kinetics by ODEs [96, 97]. In this study, Michaelis-Menten (MM) kinetics extended equations of biochemical kinetics [98] because enzymes catalyze reactions of the TRP metabolism. The resulting ODE models

were adjusted to data (for example, on data shown in Figure A.5), especially the parameters were chosen so that the data and the trajectories of the models agree with each other. A visualization of such an adjustment of parameters is called simulation. This adjustment is performed by fitting them to the data by approximation of the underlying solution of the ODEs. lsqnonlin [99] and CVODES [100, 101] are used for parameter fitting in this study. To solve a system of ODEs, an initial value has to be determined. But only for some mathematical models initial values are available. Therefore, suitable initial values have to be chosen, e.g. with LHS fit [102]. The certainty of the fitted parameters is determined by a profile likelihood estimation [98]. In addition, the evaluation of different ODE models determined a degradation process of 1-MT explaining the increased levels of TRP and KYNA. Those models were compared by methods based on the maximum likelihood approach [103, 104, 105]. This approach calculates a value describing how likely the parameters describe experimental data. Finally, a sensitivity analysis [106] was performed to determine further drug targets.
Predictions about future development and the effects of interactions with the environment can be made by mathematical modeling [90]. Only certain aspects of a system are included. Some are neglected or simplified [90] because biological processes, e.g. of metabolism [92], infection [107, 108, 109], immune response [110, 111, 112, 113], or drug treatment [93, 94] can be very extensive and complex. Thus, models are only approximations to full reality [114]. During model development, it is essential to remember what a specific model's goal is. In general, the goals of modeling can be

1. explaining the phenomenon, they are modeling [99]
2. answer particular questions [90]
3. making predictions from the model [99]

In this study, the first goal corresponds to the ODE model of IDO activation due to LPS administration and its effects on TRP metabolism. The second goal corresponds to answering the questions of section 1.5, where the aim of the thesis is stated.
Mathematical models in the form of ODEs describe alterations of a concentration x (here called species) depending on the time t, with $x(t), x, t \in \mathbb{R}$ as derivative of x to t

$$\frac{dx}{dt} = F(x(t, \theta), \theta)$$

Thus, the only independent variable is the time t, while the dependent variable is the rate of change of the function [99]. The dynamical behavior also depends on the model parameters $\theta = (\theta_1, \ldots, \theta_n)$, such as rate constants and initial concentrations [115]. In biology, species are often dependent on the presence of other species, e.g., KYN can only be produced if there is enough TRP. Thereby, a system of ODEs is necessary, whose species interact with each other. Those models are kept as simple as possible [90]. Therefore, degradation steps of the TRP metabolism have to be aggregated. The time-dependent variables x are mapped to m model outputs y. These are the quantities measured in experiments at time points t [115].

1.3.1. The Law of Mass Action and Michaelis-Menten Kinetics

Biochemical kinetics, as they are translated in this study, are based on the *law of mass action* [96, 97]. This law assumes that the reaction rate is proportional to the probability of a collision of species (in this case, reactants) [90]. The probability is, in turn, proportional to the concentration of a species. With this, a prediction can be made for a quantity C by measuring quantities A and B. This prediction is in the form of a formula [116]. For example, the chemical reaction

$$A + B \underset{k_2}{\overset{k_1}{\Leftrightarrow}} C \tag{1.1}$$

yields the system of ODEs:

$$\begin{aligned} \frac{dA(t)}{dt} = \frac{dB(t)}{dt} &= -k_1 \cdot A(t) \cdot B(t) + k_2 \cdot C(t) \\ \frac{dC(t)}{dt} &= +k_1 \cdot A(t) \cdot B(t) - k_2 \cdot C(t) \end{aligned}$$

with A, B, and C as reactants, and k as reaction rate. The reaction rate can also be written as $v = 2 \cdot (k_1 \cdot A(t) \cdot B(t) - k_2 \cdot C(t)^2)$. The units of the reactants depend on their measurements (concentration, amount) and on time (seconds, minutes, hours, days).
Ten years after the fundamental equation regarding enzyme kinetics was set up by Victor Henri in 1903, Leonor Michaelis and Maud Leonora Menten invented the well-known MM kinetics. They postulated that enzymatic reactions are initiated by binding enzyme and substrate [117].
Michaelis and Menten investigated the sucrase's kinetics, also called invertase. It accelerates the hydrolysis of sucrose into glucose and fructose [117].

$$Saccharose + H_2O \xrightarrow{\text{enzyme}} glucose + fructose$$

They confirmed the findings of Henri and developed a mathematical description of this reaction. With this, enzymatic reactions became quantifiable. The chemical reaction is modeled as follows:

$$E + S \underset{k_2}{\overset{k_1}{\Leftrightarrow}} ES \xrightarrow{k_3} E + P$$

with E as the enzyme, S as substrate, P as product, ES as enzyme-substrate-complex [117] and k_1 as the formation of enzyme-substrate-complex formation, k_2 as the decay of ES, and k_3 as dissociation of enzyme and product. The interconnected system of ordinary differential equations (ODE) can be used to calculate concentrations of the different components or masses. It is given as follows:

$$\frac{dS(t)}{dt} = -k_1 \cdot E(t) \cdot S(t) + k_2 \cdot ES(t) \tag{1.2}$$

$$\frac{dE(t)}{dt} = -k_1 \cdot E(t) \cdot S(t) + k_2 \cdot ES(t) + k_3 \cdot ES(t)$$

$$\frac{dE(t)}{dt} = -k_1 \cdot E(t) \cdot S(t) + (k_2 + k_3) \cdot ES(t) \tag{1.3}$$

$$\frac{dES(t)}{dt} = k_1 \cdot E(t) \cdot S(t) - (k_2 + k_3) \cdot ES(t) \tag{1.4}$$

$$\frac{dP(t)}{dt} = +k_3 \cdot ES(t) \tag{1.5}$$

Since the reactions start at time point $t = 0$, no enzyme-substrate complex or product is present. The initial concentration of the substrate and enzyme are named S_0 and E_0 ($S(0) = S_0$, $E(0) = E_0$) [117]. To solve this system of ODEs, two different approaches can be used, which differ in their assumptions:

- **Michaelis/Menten (1913) [117]:** k_3 is very small compared to k_2. K_S was introduced as a constant for complex formation or substrate constant with

$$K_m = K_S = \frac{k_2}{k_1}$$

- **Briggs/Haldane (1925) [118]:** k_3 is manageable for some enzymes, leading to the following substrate constant,

$$K_m = \frac{k_2 + k_3}{k_1} = \frac{k_2}{k_1} + \frac{k_3}{k_1}$$

with $\frac{k_2}{k_1}$ as equilibrium constants and $\frac{k_3}{k_1}$. The last kinetic constant describes a subsequent reaction of the form

$$A \rightarrow B \rightarrow C$$

According to the different assumptions of Michaelis, Menten and, Briggs, Haldane, the system of ODEs can be solved as follows:

- **Michaelis/Menten [117]:** If equation 1.2 and equation 1.4 are summed up,

$$\frac{dS(t)}{dt} + \frac{dES(t)}{dt} = 0$$

results. Thus

$$\begin{aligned} S(t) + ES(t) =& constant = E_0 \\ E(t) =& E_0 - ES(t) \end{aligned} \tag{1.6}$$

It is assumed that the first reaction enters equilibrium, this means that

$$\begin{aligned} \frac{dS(t)}{dt} =& 0 \\ \frac{dES(t)}{dt} =& 0. \end{aligned}$$

In equilibrium, it is also valid for equation 1.2

$$0 = \frac{dS(t)}{dt} = -k_1 \cdot E(t) \cdot S(t) + k_2 \cdot ES(t)$$

with equation 1.6

$$\begin{aligned} 0 =& - k_1(E_0 - ES(t)) \cdot S(t) + k_2 \cdot ES(t) \\ \Rightarrow ES(t) =& \frac{k_1 \cdot E_0 \cdot S(t)}{k_1 \cdot S(t) + k_2} = \frac{E_0 \cdot S(t)}{S(t) + \frac{k_2}{k_1}} \end{aligned} \tag{1.7}$$

$ES(t)$ is not measurable and has to be replaced. The velocity of the reactions depends on the overall reaction of the decomposition of ES to P.

$$\begin{aligned} \frac{dP(t)}{dt} =& k_3 \cdot ES(t) = \frac{k_3 \cdot S(t)}{S(t) + \frac{k_2}{k_1}} \\ \frac{dP(t)}{dt} \cdot \frac{1}{k_3 \cdot E_0} =& \frac{S(t)}{S(t) + K_m} \leq 1 \end{aligned}$$

For

$$\begin{aligned} \frac{dP(t)}{dt} \leq& k_3 \cdot E_0 := V_{max} \\ \Rightarrow \frac{dP(t)}{dt} =& \frac{V_{max} \cdot S(t)}{S(t) + K_m} \end{aligned}$$

Set

$$\begin{aligned}\frac{dP(t)}{dt} &= \frac{1}{2} \cdot V_{max} \\ \frac{1}{2} \cdot V_{max} &= \frac{V_{max} \cdot S(t)}{S(t) + K_m} \iff K_m = S(t)\end{aligned}$$

Thus, K_m is the substrate concentration $S = S(t_x)$ at a certain time point t_x, so that the velocity of the generation of P is half of V_{max}. For the substrate concentration, we know that

$$\frac{dS(t)}{dt} + \frac{dS(t)}{dt} = -k_3 \cdot ES(t)$$

An equilibrium is assumed, thus

$$\begin{aligned}\frac{dES(t)}{dt} &= 0 \\ \Rightarrow \frac{dES(t)}{dt} &= -k3 \cdot ES(t)\end{aligned} \tag{1.8}$$

with equation 1.7 it is valid that

$$\begin{aligned}\frac{dS(t)}{dt} &= -\frac{k_3 \cdot E_0 \cdot S(t)}{S(t) + K_m} \\ \frac{dS(t)}{dt} &= -\frac{dP(t)}{dt}\end{aligned}$$

For $S(t) \gg K_m$ leading to

$$\frac{dS(t)}{dt} = -k_3 \cdot E_0 = V_{max}$$

and for $K_m \gg S(t)$ leading to

$$\frac{dS(t)}{dt} = -\frac{k_3 \cdot E_0}{K_m} \cdot S(t)$$

leading to a steep decrease in S in the early phase and a moderate decrease in the later phase. For P, it is yielded that

$$\frac{dP(t)}{dt} = \frac{k_3 \cdot E_0}{K_m} \cdot P(t).$$

in the early phase. In the later phase

$$\frac{dP(t)}{dt} = k_3 \cdot E_0$$

is valid.

- **Briggs/Haldane [118]:** The generation of ES is a reaction of the second order, and it is valid that

$$\frac{dES(t)}{dt} = k_1 \cdot ES(t).$$

The degradation of ES is a reaction of first order and

$$-\frac{dES(t)}{dt} = k_2 \cdot + k_3 \cdot ES(t) = (k_2 + k_3) \cdot ES(t)$$

is yielded. In the steady state, both reaction velocities are equal. Thus

$$\begin{aligned} k_1 \cdot E(t) \cdot S(t) =& (k_2 + k_3) \cdot ES(t) \\ E(t) \cdot S(t) =& \frac{k_2 + k_3}{k_1} \cdot ES(t) = K_m \cdot ES(t) \end{aligned}$$

This leads to the k_m value in terms of Briggs and Haldane:

$$\begin{aligned} K_m =& \frac{k_2 + k_3}{k_1} \\ =& \frac{k_2}{k_1} + \frac{k_3}{k_1} \end{aligned}$$

k_2/k_3 is the equilibrium constant, according to Michaelis and Menten, and is called the „substrate constant“ (K_s). k_2/k_3 is the kinetic constant of product formation. For $k_2 \ll k_1$,

$$K_s = K_m$$

With equation 1.6 and 1.3.1

$$(E_0 - ES(t)) \cdot S(t) = K_m \cdot ES(t)$$

leads to

$$ES(t) = \frac{E_0 \cdot S(t)}{K_m + S(t)}.$$

This is the exact solution of the system of ODEs with the approach of Michaelis and Menten.

In conclusion, for MM, it is valid that

$$\begin{aligned} \frac{dES(t)}{dt} &= 0 \\ K_m &= \frac{k_2}{k_1} \end{aligned}$$

For Briggs and Haldane, the generation velocity of ES is the same as the degradation velocity of ES with

$$K_m = \frac{k_2 + k_3}{k_1} \tag{1.3}$$

1.3.2. Parameter Fitting

A mathematical model consists of equations which correspond to the concentration or amount of different compounds in the model. Those compounds are also called species. The equations consist of parameters and species. For the species, often measurements from different time points are available. On the theoretical face of parameter fitting, the parameter has to be determined in a way that the predicted model output agrees with the underlying experimental data for parameters θ [115]. To check whether a system of ODEs represents the dynamics of a process, parameters are fitted to the corresponding data. Therefore, initial values problems (IVP) have to be solved. They have the form:

$$\begin{aligned} \frac{dx(t)}{dt} &= F(x(t)) \\ x(t_0) &= x_0 \end{aligned}$$

To measure the agreement between data points $y(t_i)$ (with $i = 1, \ldots, d_k$ and d_k the amount of data points) and the model output an objective function provides such a measure. Commonly the weighted sum of squared residuals

$$\chi^2(\theta) = \sum_{k=1}^{m} \sum_{i=1}^{d_k} \frac{1}{\sigma_{ki}^2} (y(t_i) - F(x(t_i, \theta), \theta)) \tag{1.4}$$

where d_k denotes the number of data points for each observable $k = 1, \ldots, m$, measured at time points t_i with $i = 1, \ldots, dk$ is used. The variances σ_{ki}^2 of the measurement noise are assumed to be known. The parameters can be estimated by finding the parameter values $\hat{\theta}$ that minimize $\chi^2(\theta)$, for normally distributed measurement noise $\chi^2(\theta)$ is proportional to the log-likelihood (LL) and minimizing equation 1.4 corresponds to the maximum likelihood estimation (MLE) [98, 115].

Calculating an ODE model's parameters with respect to data is problematic, because most models include stiff differential equations. With this, the solution depends on the selection of the initial values. Moreover, when an optimal parameter set is found, the uniqueness of the solution is uncertain [119].
On the practical face of parameter fitting, the process, which is executed to fit the parameters to the data, consists of four steps. The first step is to make a first guess about the parameters. Secondly, the model equations have to be solved. Afterward, it has to be checked whether optimal conditions are achieved. If this is the case, the algorithm can stop. If not, another value for the parameters has to be chosen, and the process has to restart. The starting point x_0 of an optimization method [120] can be chosen so that the algorithm is stuck in a local optimum. Therefore, latin hypercube sampling (LHS) was invented. This algorithm prohibits randomly selected starting points lying too close to each other [102]. It ensures that the entire parameter space is covered optimally. Therefore, the parameter space is divided in regions in a way, that a single sample represents each region. This procedure generates a fixed number of starting points [120, 121]. Now initial guesses for parameters are chosen. The next step is to solve the system of ODEs, e.g., by CVODES [100]. This algorithm solves the system of ODEs numerically with multi-step methods. A detailed explanation of the algorithm can be found in [101].
This thesis performs a simulation by fixing calculated parameters in a model with corresponding parameters. The values (e.g., concentration) for each species are calculated for a specific time interval and visualized by plotting data points and trajectories of the different species in the selected time interval.

1.3.3. Model Selection

To answer a particular question, often several answers are possible. These answers are translated into different mathematical models. A model is good as long it explains the corresponding data [98]. However, it is often difficult to decide whether a model fits the data. Therefore, models are compared. Model selection is a broad field [122, 123], but not much work was done in the context of ODEs [99]. A criterion must be consulted, which is estimable from the data for each fitted model [114]. This implies that one of the models is the actual model [114]. Primarily, model selection has been performed

by using the Akaike information criterion (AIC) [103, 104], which is the most popular selection criterion [124] and is based on the likelihood (L). The AIC is calculated by $2 \cdot k - 2 \cdot ln(L)$, with k as the number of parameters. To compare models fitted to data sets with different amounts of data, the Bayesian information criterion (BIC) is used. The BIC is calculated by $k \cdot ln(n) - 2 \cdot ln(L)$, with n as the amount of the measurements, which are used to calculate the parameters [105].

1.3.4. Profile Likelihood

The profile likelihood enables to calculation of likelihood-based confidence intervals. This approach detects the flatness of the likelihood and a high dimensional space by exploring each parameter in the direction of the least increase in $\chi^2(\theta)$ with

$$\chi^2_{PL}(\theta) = \min_{\theta_j \neq i}(\chi^2(\theta))$$

For each parameter θ_i, a section is computed along the minimum of the objective function concerning all the other parameters $\theta_{j \neq i}$. A certain threshold Δ_α defines a confidence region given the following equation 1.5

$$\{\theta | \chi^2(\theta) - \chi^2(\hat{\theta}) < \Delta_\alpha)\} \tag{1.5}$$

Its borders represent confidence intervals. the threshold Δ_α is the α quantile of the χ^2 distribution [115].
For the calculation of the confidence intervals, an optimization method is used, which calculates the minimum of constrained nonlinear multi-variable functions (fmincon) of the form:

$$\min_x f(x) \text{ such that } \begin{cases} c(x) \leq 0 \\ seq(x) = 0 \\ A\dot{x} = 0 \\ Aeq\dot{x} = beq \\ lb \leq x \leq ub \end{cases}$$

e.g. with b, beq are vectors, A and Aeq are matrices, $c(x)$ and $ceq(x)$ are functions that return vectors. $f(x)$ is a function that returns a scalar. $f(x)$, $c(x)$ and $ceq(x)$ can be nonlinear functions, and x, lb, and ub can be passed as vectors or matrices [125]. This approach is also used for the profile likelihood estimation. It determines whether parameters are definitely calculated based on derived measurements [98]. A model is called structurally identifiable, whose solution $x(t)$, $t \in [0, T]$ of an initial value problem determines the initial values ψ and the parameter vector θ [125].
A perfectly flat profile characterizes a structural non-identifiability. indicating that the parameter cannot be determined. A practical non-identifiability is characterized by a profile that flattens out and stays below the threshold Δ_α for confidences intervals [115, 126].

1.3.5. Sensitivity Analysis

If the actual ODE model is detected, it is also of interest which inputs substantially influence different species. The influence can be determined by sensitivity analysis (SA) [106]. It identifies relations between the inputs and outputs of a system of ODEs [127]. Different approaches were developed to perform a SA [128]: derivative-based sensitivity measure [129, 130, 131, 132], regression-based sensitivity measure [133, 134], variance-based sensitivity measure [135, 136], moment-independent sensitivity measures [137, 138] and qualitative (or screening) sensitivity measure [106, 139, 140, 141, 142].
This study used the morris elementary effects screening method (morris screening), which belongs to the last group. The morris screening identifies important factors and is a reliable and efficient SA technique [135]. f is denoted as a model with k independent inputs $X(X_1, \cdots, X_k)$, Y is denoted as the model output $Y = f(X)$. $x = x_1, \ldots, x_k$ are values, which were assigned to X. Only x_i is varied by a given Δ. All other input values remain unchanged. The corresponding model output is $f(x_1, \ldots, x_{i-1}, x_{i+\Delta}, x_{i+1}, \ldots, x_k)$. Elementary effects (EE) for x_i are given by

$$EE_i = \frac{f(x_1, \ldots, x_{i-1}, x_{i+\Delta}, x_{i+1}, \ldots, x_k) - f(x)}{\Delta}$$

This corresponds to the one-at-a-time (OAT) design, repeated N times. Thus, N EEs are obtained for X_i. Measures for the influence of a species are given with

$$\begin{aligned} \mu_i &= \frac{1}{N} \sum_{r=1}^{N} EE_{i,r} \\ \sigma_i &= \sqrt{\frac{1}{N-1} \sum_{r=1}^{N} (EE_{i,r} - \mu_1)^2} \end{aligned} \tag{1.6}$$

The EE_{i_r} corresponds to the r-th EE of X_i.

1.4. Previous Mathematical Models of the TRP Metabolism

To develop a model based on ODEs, already published models of the TRP metabolism were reviewed to configure them according to the natural setting, which is relevant to this work. Four different ODE models with relation to the TRP metabolism or the effects of 1-MT were found and are presented in the following. None of the models explains the effects of LPS or 1-MT. They describe alterations of the TRP metabolism due to digestion [14] or pathological changes like cancer [15, 143, 144]. Two of the four models are presented in more detail. Both consider almost all of the degradation pathways of the TRP metabolism. Therefore, the models developed in this thesis are simplifications of both models.

1.4.1. Effects of Vitamin B6

The mathematical model of Rios-Avila published in 2013 [14] was developed to investigate the dynamics of the TRP metabolism influenced by the amount of pyridoxal 5'-phosphate (PLP) in the liver. PLP is the active form of vitamin B6 [14]. However, TRP transport from the gut, brain and muscle was also involved. PLP serves as a coenzyme for KYNU and KAT [14].
The ODE model presented in the paper of Rios-Avila et al. is presented as a schematic in Figure 1.3. It is based on the following biological degradation processes: In the liver, TRP is oxidized to NFK by TDO. AFD further degraded NFK to KYN. KYNU catalyzes the hydrolysis of KYN to AA. Moreover, KYN is converted by KAT to KYNA. KMO degrades KYN to HK, which is further converted by KAT to XA and by KYNU to HAA. HAA is further degraded to QUIN by HAO. The activity of KYNU and KAT depend on PLP, to which KYNU is more susceptible than KAT to the effects of PLP.
The ODE model includes TRP input in the intestinal lumen, transport of tryptophan from the intestinal lumen to circulation by the L-transporter, delivery of TRP to the liver, and exchange of circulating tryptophan with muscle and brain [14]. The effects of IDO were omitted since IDO is not synthesized by liver cells [57]. SER was omitted too, but it occurs in the liver [145]. Probably, it was omitted since it is not related to vitamin B6 and the focus of the paper was on the KP and not on the whole TRP metabolism. The schematic of the model given in Figure 1.3 was transferred into a system of ODEs consisting of 15 equations. The system includes the TRP metabolites TRP, KYN, QUIN, KYNA and the intermediate metabolites. The degradation of one species to the other was modeled as an enzymatic reaction by using MM kinetics. K_m values were fixed to literature values. For the K_m and V_{max} values of KYNU I and II and KATI and II, different enzyme activities were assumed. Both enzymes were included with two different variants, catalyzing the degradation of two different substrates. This model was applied to data found in the literature [14].
With this whole-body model, the TRP metabolism via the KP in the liver is simulated to gain insight into the effects of vitamin B6 deficiency, TRP loading and induction of TDO on TRP metabolites. The results of those validation studies showed good agreement between the model with published data [14]. Rios-Avila et al. report the results of in silico experiments with the model to investigate the effects of various levels of vitamin B6 deficiency, the effects of TDO induction, and the interaction of vitamin B6 deficiency [14]. Moderate deficiency yielded increased HK levels and decreased KYNA and AA levels. More severe deficiency also increased KYN and XA levels and had more pronounced effects on the other metabolites[14]. TRP load simulations with and without vitamin B6 deficiency showed altered metabolite concentrations consistent with published data. Induction of TDO caused an increase in all metabolites, and TDO induction, together with a simulated vitamin B6 deficiency, yielded increases in KYN, HK, and XA and decreases in KYNA and AA levels [14].
Rios-Avila et al. give a detailed model of the KP and also provide an overview of literature values, which are used to create simulations of human B6 deficiency based on data. Therefore, detailed descriptions of the calculations of the volumes of the different

compartments are given. Unfortunately, the references to the data should be mentioned and also figures showing data and simulations in comparison should be included. The model only includes the TRP levels of different compartments, but it does not account for other compartments' metabolite levels. The reproducibility is lowered by missing information about the used software. It should be noted that assumptions on the volumes of the different compartments (liver, gut, brain, and muscle) were made for conditions valid for humans, but the fixed parameter values were determined in rodents. [14]

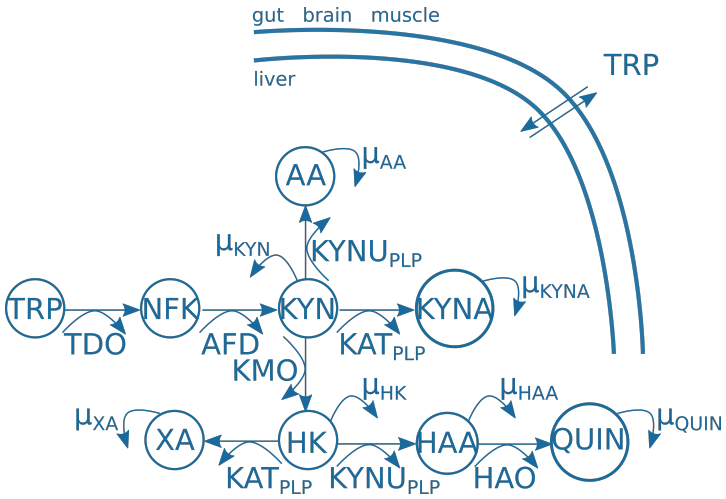

Figure 1.3.: **Schematic of the TRP metabolism in different compartments published by Rios-Avila et al.:** The interaction network of the TRP metabolism published by Rios-Avlia et al. in 2013 [14] includes the degradation of TRP to NFK by TDO. NFK is degraded to KYN by AFD, and KYN is degraded to the downstream metabolites KYNA (by KAT depending on PLP), AA (by KYNU dependent on PLP) and HK (by KMO). HK is further degraded to XA by KAT (dependent on PLP) and to HAA by KYNU (dependent on PLP). HAO further degrades HAA to QUIN. Metabolites are shown in circles, arrows show reactions with the enzyme names next to an additional bent arrow. Bent arrows with $\mu_{metabolite}$ specify degradation pathways of the corresponding metabolite. The bi-directional arrow crossing the plasma membrane shows the transport of TRP from the different compartments gut, brain and muscle to the liver. AA - anthranilic acid, AFD - aryl formamidase, HAA - 3-hydroxyanthranilic acid, HAO - 3-hydroxynalic acid oxygenase, HK - 3-hydroxykynurenine, KAT - kynurenine aminotransferase, KMO - kynurenine 3-monooxygenase, KYN - kynurenine, KYNA - kynurenic acid, KYNU - kynureninase, NFK - N-formyl-kynurenine, QUIN - quinolinic acid, PLP - pyridoxal 5'-phosphate, TDO - tryptophan 2,3- dioxygenase, TRP - tryptophan, XA - xanthurenic acid, μ degradation parameter

1.4.2. Parameter fitting Based on Tissue-Specific Gene Expression Data

Stavrum et al. developed an ODE model of the TRP metabolism [15] intending to the aim to estimate enzyme concentrations of neuroactive TRP metabolites like KYNA and QUIN [146] which are based on gene expression data in the brain and liver. A considerable impact of the KP in the liver on the concentrations of neuroactive derivatives in the brain were made. A simplified schematic of the model is shown in Figure 1.4. The model was adapted to cancer and *tuberculosis meningitis*. A multiplicity of metabolites are included in the model developed by Stavrum et al. [15]. They included the branch of the SER pathway consisting of HT and SER as well as downstream metabolites like melatonin. Also, the KP with TRP, KYN, KYNA, and QUIN is included as well as intermediate metabolites like NFK or downstream metabolites like cinnabarinic acid. More precisely, TRP is degraded to SER via HT by TPH and DDC. TRP is also degraded to tryptamine by DDC and further downstream metabolites. Along the KP, TRP is degraded to NFK by IDO or TDO. NFK is further degraded to FAA by KYNU and by AFD to KYN. Both FAA and AA are degraded to AA by KYNU or AFD. The model includes an exchange of TRP and KYN with other compartments, like brain and blood via the blood stream. KYN is further degraded to KYNA by KAT or to HK by KMO. HK can be degraded to XA by KAT or to HAA by KYNU. HAA is further degraded to cinnabarinic acid and ACMS by HAO, which is further degraded to QUIN by KYNU and to AMSA by ACD. AMSA is further degraded to PICO [15].
The schematic presented in Figure 1.4 of the TRP metabolism was transferred into a system of ODEs. Mass action kinetics were used to model non enzymatic reactions, whereas enzymatic reactions were modeled as MM kinetics. The turnover number k_{cat} and the enzyme concentration calculate K_m and V_{max}. K_m and k_{cat} were fixed to literature values, while the enzyme concentration had to be measured. If there was more than one literature value, minimal and maximal values were set as the lower and upper boundaries of the parameter search space [15]. Each optimization was repeated 20 times to get an estimate of the variability of optimized expression values [15] because the parameter search space for expression values was huge, there could be several optimal parameter combinations that would result in similar results [15]. This approach is also called a „parameter scan“.
Simulations based on gene expression data were performed, and prediction of metabolic changes in cancer and *tuberculosis meningitis* were made. Those predictions were in line with data measured in patients. The model developed by Stavrum et al. provides a diagnostic tool to predict pathological changes in TRP metabolism based on a limited number of clinical measurements [15].

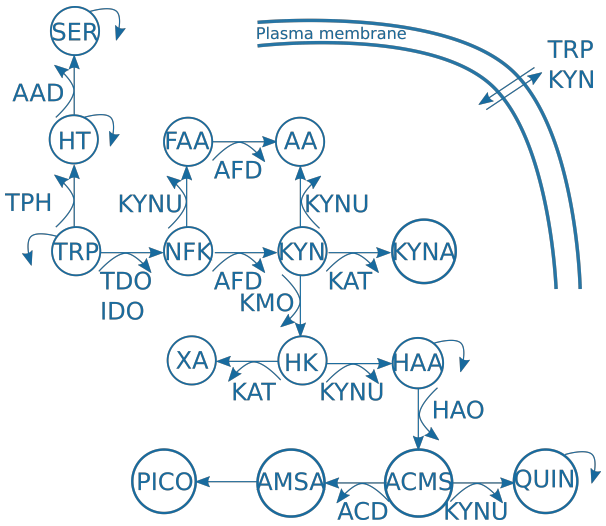

Figure 1.4.: **Schematic of the TRP metabolism in different compartments published by Stavrum et al.:** The interaction network of the TRP metabolism published by Stavrum et al. in 2013 [15] includes the SER and KP as well as other degradation pathways and their metabolites. TRP is degraded via HT to SER by TPH and AAD along the SER pathway. TRP is degraded via the KYN-pathway to NFK by TDO or IDO. NFK is further degraded to FAA and then to AA by KYNU and AFD. NFK is degraded to KYN by AFD. KYN is also degraded to AA by KYNU or by KAT to KYNA. Moreover, it is degraded to HK by KMO. KAT degrades HK to XA and KYNU degrades HK to HAA. HAO degrades HAA to ACMS. KYNU degrades ACMS to QUIN. ACMS is also degraded to AMSA by ACD, which is further degraded to PICO. Metabolites are shown in circles, arrows show reactions with the enzyme names next to an additional bent arrow. Arrows without enzyme names sum up several enzymatic reactions. Bent arrows with μ replace reactions not included in the SER and KP. The bi-directional arrow crossing the plasma membrane shows the transport of TRP and KYN. AA - anthranilic acid, ACD - 2-amino-3-carboxymuconate semialdehyde-decarboxylase, ACMS - 2-amino-3-carboxymuconate semialdehyde, AFD - aryl formamidase, AMSA - 2-aminomuconate semialdehyde, DDC - aromatic L-amino acid decarboxylase, FAA - formyl-AA, HAA - 3-hydroxyanthranilic acid, HAO - 3-hydroxynalic acid oxygenase, HK - 3-hydroxykynurenine, HT - 5-hydroxy-tryptophan, IDO - indoleamine 2,3-dioxygenase, KAT - kynurenine aminotransferase, KMO - kynurenine 3-monooxygenase, KYN - kynurenine, KYNA - kynurenic acid, KYNU - kynureninase, NFK - N-formyl-kynurenine, PICO - picolinic acid, QUIN - quinolinic acid, PLP - pyridoxal 5'-phosphate, SER - serotonin, TDO - tryptophan 2,3- dioxygenase, TRP - tryptophan, XA - xanthurenic acid, μ degradation parameter

An overview of all literature values is given in the supplementary tables. They only used data on mammals, but they did not specify the species in which the values were measured. But there were simulations made for human liver and brain and rat liver and its cortex. To improve the clarity, the schematic of reduced models is shown. Unfortunately, no explicit written system of ODEs is given. Thus, the developed models are not reproducible. Moreover, no figure was included displaying the changes in metabolite levels over the time.
Although IDO was considered in the model, the calculations revealed that no reaction was catalyzed based on the used data [15]. The lack of infection can explain this. Unfortunately, the results of predicting TRP metabolites during *tuberculosis meningitis* infection are not shown.

1.4.3. Further Models

The following ODE models are mentioned for the sake of completeness. For the model development in this study, the models were not used. One model concerns the TRP metabolism in patients with pancreatic adenocarcinoma. It was developed to find treatment targets [143]. Therefore, the expression of mRNA of TRP, KYN and IDO and of several markers of the immune system were measured. Remaining TRP metabolites were omitted. 12 equations with 35 parameters built the ODE system. All parameters were estimated and MM kinetics were not used [143]. The second model includes immunotherapy with 1-MT concerning cancer therapy of glioblastoma [144]. This model focuses on tumor cells, radiotherapy, and immune cells and immunotherapy with 1-MT. The model aimed to predict the survival time of cancer patients. 1-MT, IDO, radiotherapy, and tumor-associated antigens were included. Inhibition of the effects of IDO by 1-MT was included in the model. All other TRP metabolites were not included in the model [144].

1.5. Aim of the Thesis

As mentioned in section 1.2 there is no explanation for the 1-MT induced increase of TRP and KYNA, while the intermediate metabolite KYN does not change. In this study, mathematical modeling with systems of ordinary differential equations (ODEs) was applied to clarify two questions using data measured in pigs [147, 148]:

1. How do TRP and KYNA increase while the intermediate metabolite KYN does not change?

2. In the face of infection, does TRP only degrade to KYN via TDO or IDO during 1-MT administration?

Therefore, the thesis aims to:

1. develop a mathematical model of the TRP metabolism (standard model)

2. extend this model by an LPS administration and the effects of LPS (LPS model)
3. extend the standard model by an 1-MT administration (1-MT model)
4. develop different possible degradation processes of 1-MT along the TRP metabolism
5. extend the 1-MT model by different pathways explaining the increase of TRP and KYNA (hypotheses)
6. combine the LPS model with the most likely hypothesis of TRP and KYNA increase (1-MT/LPS model)
7. compare a 1-MT/LPS model including inhibitory effects of 1-MT with one 1-MT/LPS model excluding those effects
8. fit the parameters of all models and hypotheses to appropriate data and test their reliability

To process the different aims, this thesis will proceed as follows. After the introduction, the thesis is further divided into the commonly used structure with a „Materials and Methods“, „Results“as well as „Discussion“section. The models, data and methods are introduced in sections 2.1, 2.2 and 2.3 of the „Materials and Methods“ part. The presented models are a result of this work. They are not presented in the „Results“, because, in most publications of mathematical modeling with ODEs, the models are introduced in the „Materials and Methods“part. It was decided to hold this convention. The „Results“section is divided into two parts: In section 3.1, the results of ODE modeling different degradation processes of 1-MT along the TRP pathway are presented. In the second section 3.2 two ODE models are compared. One model includes the inhibitory effects of 1-MT, and one does not. In the section 4, the results of this work are compared to results from the literature. Moreover, limitations of the work are discussed in section 4.8, as well as future research directions 4.9. The thesis closes with a conclusion in section 4.10. In the appendix a detailed description of the experimental design (see appendix section A) and additional information on literature, fitted parameters (see appendix section C) as well as more detailed information of the results of the identifiability analysis (see appendix section B) are shown.

2. Materials and Methods

Data were gained from experiments conducted in pigs to investigate the degradation processes of 1-MT and reproduce its inhibitory effects on IDO. Those pigs received LPS to activate IDO [149]. This study was performed to establish a pig model of IDO activation by LPS for further research [149]. LPS and 1-MT were administered in another study to investigate the protective and immunomodulatory effects of 1-MT against endotoxin-induced shock in a porcine *in vivo* model [86]. The purpose of both studies was not to conduct analysis using systems of ODEs. Nevertheless, data can be used to test different degradation processes of 1-MT and reproduce 1-MT's inhibitory effects in a mathematical model using ODEs. The different degradation processes of 1-MT were tested in three ways:

- parameters were fixed to parameter values, which were fitted to data measured in LPS-treated pigs (approach 1)
- parameters were fixed to parameter values, which were fitted to a subset of the data measured in 1-MT and LPS-treated pigs (approach 2)
- parameters were fitted to the data measured in 1-MT and LPS-treated pigs (approach 3)

The developed models are introduced in section 2.1. The parameters of those models are adapted to data, which are described in section 2.2 and in more detail in the appendix A. The methods used for the adaptation of parameters to the data and consequent analysis are described in section 2.3.

2.1. Ordinary Differential Equation Models of Tryptophan Metabolism

Three different models were developed to investigate the alterations on the dynamics of TRP metabolites during infection (LPS administration), during 1-MT administration and during a combination of 1-MT and LPS administration. The models are based on a standard model of the TRP metabolism (including TRP, KYN, KYNA, QUIN, and SER), which is based on the existing models presented in section 1.4 [14, 15]. The standard model is extended by LPS, 1-MT, or 1-MT and LPS administration. The first ODE model includes the activation of IDO by LPS administration (LPS model). The administration of 1-MT extends the second ODE model to decipher degradation mechanisms of 1-MT belonging to the TRP metabolism (1-MT model). Therefore, this model was

extended by possible degradation pathways, which were subsequently compared by LL, AIC, and BIC values (see section 1.3.3). The ODE model of the degradation pathway describing the data the best was extended by the LPS administration. Thus, a model combining the LPS and 1-MT model resulted (1-MT/LPS model). To decipher the inhibitory effects of 1-MT on LPS induced IDO in pigs, models were developed. The first ODE model considers the inhibitory effects of 1-MT on IDO, the second does not. Both models were compared by LL, AIC, and BIC values. In the following, all models are introduced.

2.1.1. Standard Model

The model presented in this section is called the „standard model“. It is developed based on the models of the TRP metabolism published by Rios-Avila et al. [14] and Stavrum et al. [15] in section 1.4. Based on both models, the standard model was simplified. Several reactions were summarized, resulting in an ODE model only containing species for which measurements are available to increase the identifiability of the model parameters.
According to Rios-Avila et al., degradation parameters of both models were maintained in the standard model [14]. Several reactions of the model of Stavrum et al. [15] were summed up as degradation reactions μ. MM-kinetics were applied, and K_m values were set to literature values, while V_{max}-values were calculated [14, 15]. As opposed to Stavrum et al., parameters of k_{cat}-values and enzyme concentrations were calculated using V_{max} [15].
The levels of all metabolites were calculated for the whole body, as it was performed by Rios-Avila et al. disregarding TRP. Although it is a disadvantage fixing parameters to literature values from different species, it proceeded similarly due to the lag of pig-specific literature values.
The standard model was used to simulate the dynamics of the TRP metabolism without any interference. Its parameters were fitted to the data of control pigs, which were not treated with LPS or 1-MT (see section 2.2). This model was extended for further investigations concerning LPS and 1-MT administration. A schematic of the reactions of the standard model is shown in Figure 2.1.

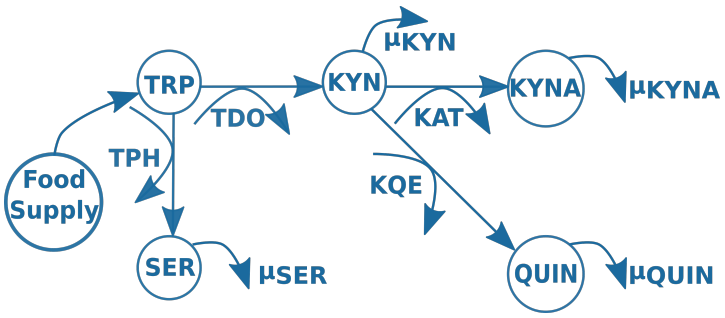

Figure 2.1.: **Schematic of the standard model of the TRP metabolism:** The schematic of the TRP metabolism includes the degradation of TRP to SER by TPH. TRP is degraded to KYN by TDO, and KYN is degraded to the downstream metabolites KYNA (by KAT) and QUIN (by KQE). Bent arrows show enzymatic reactions bent arrows next to a straight arrow. KAT - kynurenine aminotransferase, KQE - kynurenine to quinolinic acid degrading enzyme, KYN - kynurenine, KYNA - kynurenic acid, QUIN - quinolinic acid, SER - serotonin, TDO - tryptophan-2,3-dioxygenase, TPH - tryptophan hydroxylase, TRP - tryptophan, μ - degradation parameter

The schematic of the reactions of the standard model is based on biological processes, which are described in more detail in the following: TRP is degraded to KYN by hepatic TDO (V_{max}^{TDO}, K_{TDO}, 2.2) [150] (see Table 2.1 reaction 1). This degradation of TRP is an enzymatic reaction, and therefore, the MM equation was used. Since TRP is degraded via TDO, it is modeled as a decrease in eq. 2.2 and as an increase in eq. 2.3 The product of the TRP degradation via TDO is KYN, which is degraded to KYNA by kynurenine aminotransferase (KAT, see Table 2.1 reaction 3). KAT leads to an increase in eq. 2.4 and a decrease in eq. 2.3. KYN is also degraded to QUIN by several consecutive reactions (kynurenine 3-monooxygenase, kynureninase, 3-hydroxyanthranilic acid oxidase). These reactions were summed up in one enzymatic reaction by a fictitious enzyme named KQE (KYN to QUIN degrading enzyme, see Table 2.1 reaction 4). The increase of QUIN was accounted in eq. 2.5, and the decrease of KYN was modeled in eq. 2.3. Moreover, KYN is degraded to anthranilic acid [15], leading to a degradation term of KYN (μ_{KYN} in eq. 2.3, see Table 2.1 reaction 7). KYNA (in eq. 2.4) and QUIN (in eq.(2.5)) are further degraded (see Table 2.1 reaction 6 and 8), resulting in loss terms [147]. TRP is not only degraded by TDO. The enzyme tryptophan hydroxylase (TPH) and aromatic L-amino acid decarboxylase degrade TRP via 5 Hydroxytryptophan to SER [151]. These degradation steps were summed up to one reaction by TPH (see Table 2.1 reaction 2), resulting in a gaining term in eq. 2.6 and a loss term in eq. 2.2. Also, SER is degraded (see Table 2.1 reaction 5), like QUIN and KYNA, leading to a decrease in eq. 2.6. Those reactions are summed up in Figure 2.1. The reactions are concordant with the chemical reactions of the TRP metabolism shown in Table 2.1. The following reactions are included in the standard model: TRP is degraded via TPH to SER (see Table 2.1,

Table 2.1.: **Chemical reactions and signaling pathways of the TRP metabolism**

reaction	source		product	reaction type
1	TRP	$\xrightarrow{\text{TDO}}$	KYN	enzymatic
2	TRP	$\xrightarrow{\text{TPH}}$	SER	enzymatic
3	KYN	$\xrightarrow{\text{KAT}}$	KYNA	enzymatic
4	KYN	$\xrightarrow{\text{KQE}}$	QUIN	enzymatic
5	SER	$\xrightarrow{\mu}$		degradative
6	KYNA	$\xrightarrow{\mu}$		degradative
7	KYN	$\xrightarrow{\mu}$		degradative
8	QUIN	$\xrightarrow{\mu}$		degradative
9		$\xrightarrow{\text{FoodSupply}}$	TRP	receiving

Concordant with the interaction network in Figure 2.1, TRP is degraded to SER by TPH (reaction 2). TRP is degraded to KYN by TDO (reaction 1), and KYN is degraded to the downstream metabolites KYNA (by KAT, reaction 3) and QUIN (by KQE, reaction 4), SER, KYN, KYNA and QUIN are further degraded with degradation rates μ (reactions 5, 6, 7, 8). The TRP levels increase after food intake (reaction 9, *FoodSupply*). KAT - kynurenine aminotransferase, KQE - kynurenine to quinolinic acid degrading enzyme, KYN - kynurenine, KYNA - kynurenic acid, QUIN - quinolinic acid, SER - serotonin, TDO - tryptophan-2,3-dioxygenase, TPH - tryptophan hydroxylase, TRP - tryptophan, μ - degradation parameter

reaction 2) and to KYN via TDO (see Table 2.1, reaction 1). KYN is degraded by KAT to KYNA and KQE to QUIN (see Table 2.1, reaction 3 and 4). Each species is degraded separately with degradation parameter μ (see Table 2.1, reactions 5 to 8). Since the pigs had access to food and TRP is a ubiquitous amino acid, contained in food (see section 2.2), an increase of TRP was modeled by *FoodSupply* (see Table 2.1 reaction 9).

The system of ODEs corresponds to the standard model of Table 2.1 and Figure 2.1. Since several degradation steps of the TRP metabolism are catalyzed by enzymes, Michaelis-Menten(MM) kinetics were used [152] corresponding to eq. 2.1.

$$\frac{dS(t)}{dt} = \frac{V_{max}^{enzyme} \cdot S(t)}{S(t) + K_{enzyme}}, \tag{2.1}$$

with V_{max}^{enzyme} as the maximal turnover rate, and $K_{enzyme} = K_m$ as the MM-constant of the corresponding enzyme. This constant represents the substrate concentration, at which the velocity of the enzymatic reaction is half of the maximal turnover rate V_{max}^{enzyme}. All enzymatic reactions were assumed to be irreversible for two reasons:

1. Reactions involving oxygenation, acetylation, ring forming, and ring breaking are unlikely to be reversed [15]

2. Potentially reversible reactions in the network follow fast non-enzymatic reactions, which drive preceding enzymatic reactions in a forward direction [15]

The system of ODEs corresponding to the standard model is given as follows:

$$\frac{dTRP(t)}{dt} = + FoodSupply - \frac{TRP(t) \cdot V_{max}^{TPH}}{K_{TPH} + TRP(t)} - \frac{TRP(t) \cdot V_{max}^{TDO}}{K_{TDO} + TRP(t)} \tag{2.2}$$

$$\frac{dKYN(t)}{dt} = + \frac{TRP(t) \cdot V_{max}^{TDO}}{K_{TDO} + TRP(t)} - \frac{KYN(t) \cdot V_{max}^{KQE}}{K_{KQE} + KYN(t)} - \frac{KYN(t) \cdot V_{max}^{KAT}}{K_{KAT} + KYN(t)} - \mu_{KYN} \cdot KYN(t) \tag{2.3}$$

$$\frac{dKYNA(t)}{dt} = + \frac{KYN(t) \cdot V_{max}^{KAT}}{K_{KAT} + KYN(t)} - \mu_{KYNA} \cdot KYNA(t) \tag{2.4}$$

$$\frac{dQUIN(t)}{dt} = + \frac{KYN(t) \cdot V_{max}^{KQE}}{K_{KQE} + KYN(t)} - \mu_{QUIN} \cdot QUIN(t) \tag{2.5}$$

$$\frac{dSER(t)}{dt} = + \frac{TRP(t) \cdot V_{max}^{TPH}}{K_{TPH} + TRP(t)} - \mu_{SER} \cdot SER(t) \tag{2.6}$$

2.1.2. Model Considering Infection

The ODE model described in this section includes the activation of IDO by LPS. It was invented to describe the altered dynamics of the TRP metabolism during infection. The model is based on the standard model (see Figure 2.2, blue) and extended by an LPS administration with consequent TNF-*alpha* production induced IDO activation (see Figure 2.2, pink).

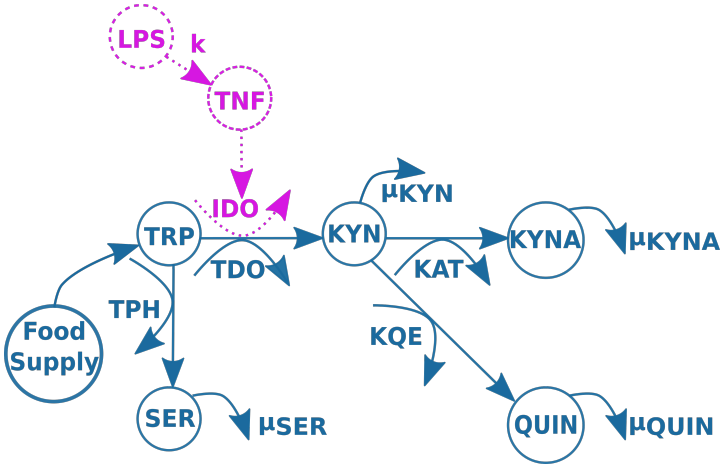

Figure 2.2.: **Schematic of the LPS model:** The standard model is extended (dotted lines) by an application of LPS, which leads to an increase in TNF (TNF-α) concentration, TNF leads to the activation of IDO, which increases the degradation rate of TRP to KYN. Bent arrows show enzymatic reactions next to a straight arrow. k - activating reaction, KAT - kynurenine aminotransferase, KQE - kynurenine to quinolinic acid degrading enzyme, KYN - kynurenine, KYNA - kynurenic acid, LPS - lipopolysaccharide, QUIN - quinolinic acid, SER - serotonin, IDO - indolamin-2,3-dioxygenase, TDO - tryptophan-2,3-dioxygenase, TNF - tumor necrosis factor -α, TPH - tryptophan hydroxylase, TRP - tryptophan, μ - degradation parameter

This ODE model is called the „LPS model“ and is based on the chemical reactions and signaling pathways shown in Table 2.2, which reactions 1 to 9 equal the reactions of the standard model shown in Table 2.1.

Table 2.2.: **Chemical reactions and signaling pathways of the TRP metabolism including the IDO activation by LPS administration**

reaction	source		product	reaction type
1	TRP	$\xrightarrow{\text{TDO}}$	KYN	enzymatic
2	TRP	$\xrightarrow{\text{TPH}}$	SER	enzymatic
3	KYN	$\xrightarrow{\text{KAT}}$	KYNA	enzymatic
4	KYN	$\xrightarrow{\text{KQE}}$	QUIN	enzymatic
5	SER	$\xrightarrow{\mu}$		degradative
6	KYNA	$\xrightarrow{\mu}$		degradative
7	KYN	$\xrightarrow{\mu}$		degradative
8	QUIN	$\xrightarrow{\mu}$		degradative
9		$\xrightarrow{\text{FoodSupply}}$	TRP	receiving
10	LPS	$\xrightarrow{\text{k}}$	TNF-α	activating
11	TNF-α + TRP	$\xrightarrow{\text{IDO}}$	TNF-α + KYN	producing
12	LPS	$\xrightarrow{\mu}$		degradative
13	TNF-α	$\xrightarrow{\mu}$		degradative

The standard model, which is represented in Table 2.1, is extended by the following reactions: LPS is degraded (12), TNF$-\alpha$ is produced by LPS (10), TNF$-\alpha$ is degraded (13), TNF-α is associated with IDO levels. Thus the degradation of TRP to KYN (11) depends on TNF-α and on IDO-parameters. KAT - kynurenine aminotransferase, KQE - kynurenine to quinolinic acid degrading enzyme, KYN - kynurenine, KYNA - kynurenic acid, LPS - lipopolysaccharide, QUIN - quinolinic acid, SER - serotonin, IDO - indolamin-2,3-dioxygenase, TDO - tryptophan-2,3-dioxygenase, TNF - tumor necrosis factor -α, TPH - tryptophan hydroxylase, TRP - tryptophan, μ - degradation parameter

The model is based on the following assumptions: LPS is administered, and this activates TNF-α with rate k. TNF-α leads to IDO production, which catalyzes the degradation of TRP to KYN. Those reactions were added to the system of ODEs corresponding to the standard model (eq. 2.2 to eq. 2.6). The added terms are shown in pink in the associated system of ODEs, which is given by the following equations (eq. 2.7 to 2.14):

$$\frac{dLPS(t)}{dt} = +Application - \mu_{LPS} \cdot LPS(t) \tag{2.7}$$

$$\frac{dTRP(t)}{dt} = + FoodSupply - \frac{TRP(t) \cdot V_{max}^{TPH}}{K_{TPH} + TRP(t)} - \frac{TNF(t) \cdot TRP(t) \cdot V_{max}^{IDO}}{K_{IDO} + TRP(t)} \tag{2.8}$$

$$- \frac{TRP(t) \cdot V_{max}^{TDO}}{K_{TDO} + TRP(t)}$$

$$\frac{dKYN(t)}{dt} = + \frac{TRP(t) \cdot V_{max}^{TDO}}{K_{TDO} + TRP(t)} + \frac{TNF(t) \cdot TRP(t) \cdot V_{max}^{IDO}}{K_{IDO} + TRP(t)} \tag{2.9}$$

$$- \frac{KYN(t) \cdot V_{max}^{KQE}}{K_{KQE} + KYN(t)} - \frac{KYN(t) \cdot V_{max}^{KAT}}{K_{KAT} + KYN(t)} - \mu_{KYN} \cdot KYN(t) \tag{2.10}$$

$$\frac{dKYNA(t)}{dt} = + \frac{KYN(t) \cdot V_{max}^{KAT}}{K_{KAT} + KYN(t)} - \mu_{KYNA} \cdot KYNA(t) \tag{2.11}$$

$$\frac{dQUIN(t)}{dt} = + \frac{KYN(t) \cdot V_{max}^{KQE}}{K_{KQE} + KYN(t)} - \mu_{QUIN} \cdot QUIN(t) \tag{2.12}$$

$$\frac{dSER(t)}{dt} = + \frac{TRP(t) \cdot V_{max}^{TPH}}{K_{TPH} + TRP(t)} - \mu_{SER} \cdot SER(t) \tag{2.13}$$

$$\frac{dTNF(t)}{dt} = +k \cdot LPS(t) - \mu_{TNF} \cdot TNF(t) \tag{2.14}$$

This system of ODEs is based on the following biological processes: With the LPS administration, IDO transcription is activated in two ways:

1. IDO production is initiated by LPS administration in a direct way [153] by binding LPS to TLR4 of IDO-expressing cells. This binding activates $NF - \kappa B$ and leads to the transcription of IDO mRNA and, subsequently to the translation of its mRNA [147].

2. TNF-α production is initiated by LPS, which binds to TLR4 of immune cells and thus activates IDO production via STAT1 [154, 155]. TNF-α binds to TLR4 and leads to the production of IDO.

Only the IDO activation by TNF-α was included since IFN-γ levels were not measured (see section 2.2.1). TNF-α increases due to LPS (see Table 2.2, reaction 10, see eq. 2.14, k). Also, IDO levels were not measured. Hence the degradation of TRP to KYN by IDO was simplified. IDO levels depend on TNF-α levels. Therefore, the degradation of TRP to KYN is mediated by TNF-α (see Table 2.2, reaction 11) [156]. By binding to TLR-4, TNF-α is degraded with rate $\mu_{TNF-\alpha}$ (see Table 2.2 reaction 13, eq. 2.14). The IDO activation leads to an increase in eq. 2.10 and to a decrease in eq. 2.9. The degradation of TLR-4 is not responsible for LPS internalization [157], and the uptake of LPS is probably mediated by scavenger receptor-dependent pathways [158]. Thus LPS

is not reduced by IDO activation. It was shown, that hepatocytes degrade LPS. This degradation leads to a decrease of LPS with a rate of μ_{LPS} in eq. 2.7 [159] (see Table 2.2, reaction 12).

2.1.3. Model Considering 1-Methyltryptophan Administration

To investigate the 1-MT induced increase of TRP and KYNA, while the intermediate metabolite KYN stays unchanged, the standard model was extended by a 1-MT administration. The resulting ODE model is called the „1-MT model“ and is shown in Figure 2.1. The extension of the standard model is indicated in orange.

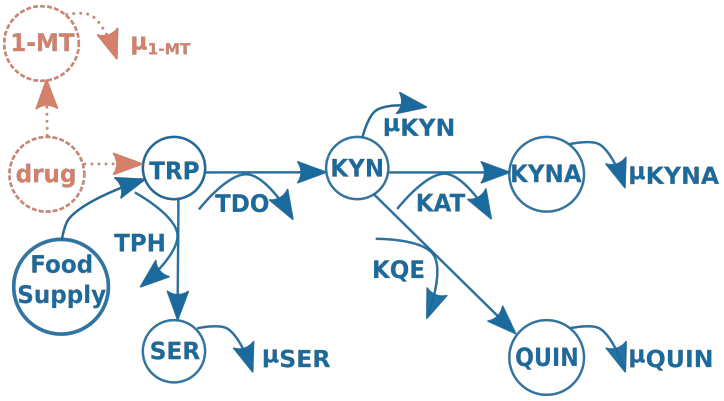

Figure 2.3.: **Schematic of the 1-MT Model:** standard model is extended (dotted lines) by a drug application, which leads to an increase in 1-MT (1-MT) and TRP due to contamination of the drug 1-MT with TRP, 1-MT is further degraded with a rate of μ_{OMT}. Bent arrows show enzymatic reactions next to a straight arrow. 1-MT - 1-methyltryptophan, IDO - indolamin-2,3-dioxygenase, KQE - kynurenine to quinolinic acid degrading enzyme, KAT - kynurenine aminotransferase, KYN - kynurenine, KYNA - kynurenic acid, QUIN - quinolinic acid, SER - serotonin, TDO - tryptophan-2,3-dioxygenase, TPH - tryptophan hydroxylase, TRP - tryptophan, μ - degradation parameter

This model corresponds to the state of the art concerning the knowledge of the administration of 1-MT. Therefore, this model is called the „classical pathway “ or just „classic“. All chemical reactions and signaling pathways included in the 1-MT model are shown in Table 2.3, at which reactions 1 to 9 are equal to the reactions of the standard model shown in table 2.1.

Table 2.3.: **Chemical reactions and signaling pathways of the TRP metabolism, including the administration of 1-MT**

reaction	source		product	reaction type
1	TRP	$\xrightarrow{\text{TDO}}$	KYN	enzymatic
2	TRP	$\xrightarrow{\text{TPH}}$	SER	enzymatic
3	KYN	$\xrightarrow{\text{KAT}}$	KYNA	enzymatic
4	KYN	$\xrightarrow{\text{KQE}}$	QUIN	enzymatic
5	SER	$\xrightarrow{\mu}$		degradative
6	KYNA	$\xrightarrow{\mu}$		degradative
7	KYN	$\xrightarrow{\mu}$		degradative
8	QUIN	$\xrightarrow{\mu}$		degradative
9		$\xrightarrow{\text{FoodSupply}}$	TRP	receiving
10		$\xrightarrow{\text{ApplicationMT}}$	1-MT	receiving
11		$\xrightarrow{\text{ApplicationMT}}$	TRP	receiving
12	1MT	$\xrightarrow{\mu}$		degradative

1-MT increases during its application (reaction 10). It is also degraded (ApplicationMT, reaction 12). The drug 1-MT is contaminated with TRP according to manufacturer information. Thus TRP increases during 1-MT application (ApplicationMT, reaction 11). 1-MT - 1-methyltryptophan, IDO - indolamin-2,3-dioxygenase, KQE - kynurenine to quinolinic acid degrading enzyme, KAT - kynurenine aminotransferase, KYN - kynurenine, KYNA - kynurenic acid, QUIN - quinolinic acid, SER - serotonin, TDO - tryptophan-2,3-dioxygenase, TPH - tryptophan hydroxylase, TRP - tryptophan,

Reactions 10 and 11 of Table 2.3 increase 1-MT respective TRP by 1-MT administration (see Table 2.3, reaction 12, *ApplicationMT*). 1-MT is degraded (see Table 2.3, reaction 12, μ). The reaction of *FoodSupply* is only included when food is supplied. Those reactions were added to the system of ODEs corresponding to the standard model (see eq. 2.2 to eq. 2.6). The reactions are shown in orange in the system of ODEs, which is given by the following equations (eq. 2.15 to 2.20):

$$\frac{d1MT(t)}{dt} = +ApplicationMT - \mu_{1MT} \cdot 1MT(t) \tag{2.15}$$

$$\begin{aligned}\frac{dTRP(t)}{dt} =& + FoodSupply + ApplicationMT - \frac{TRP(t) \cdot V_{max}^{TPH}}{K_{TPH} + TRP(t)} \\ & - \frac{TRP(t) \cdot V_{max}^{TDO}}{K_{TDO} + TRP(t)}\end{aligned} \tag{2.16}$$

$$\begin{aligned}\frac{dKYN(t)}{dt} =& + \frac{TRP(t) \cdot V_{max}^{TDO}}{K_{TDO} + TRP(t)} - \frac{KYN(t) \cdot V_{max}^{KQE}}{K_{KQE} + KYN(t)} - \frac{KYN(t) \cdot V_{max}^{KAT}}{K_{KAT} + KYN(t)} \\ & - \mu_{KYN} \cdot KYN(t)\end{aligned} \tag{2.17}$$

$$\frac{dKYNA(t)}{dt} = + \frac{KYN(t) \cdot V_{max}^{KAT}}{K_{KAT} + KYN(t)} - \mu_{KYNA} \cdot KYNA(t) \tag{2.18}$$

$$\frac{dQUIN(t)}{dt} = + \frac{KYN(t) \cdot V_{max}^{KQE}}{K_{KQE} + KYN(t)} - \mu_{QUIN} \cdot QUIN(t) \tag{2.19}$$

$$\frac{dSER(t)}{dt} = + \frac{TRP(t) \cdot V_{max}^{TPH}}{K_{TPH} + TRP(t)} - \mu_{SER} \cdot SER(t) \tag{2.20}$$

The producer claimed a purity of 95%, while the remaining 5% consisted of TRP ($ApplicationMT$, see Table 2.3, reaction 10, eq. 2.16) [86]. 1-MT is degraded (see Table 2.3, reaction 12) with a loss term μ_{1MT}.

2.1.4. Hypotheses of 1-Methyltryptophan Degradation

1-MT leads to increased TRP and KYNA concentrations, while the levels of the intermediate metabolite KYN does not change [86]. To determine the degradation process of 1-MT, the 1-MT model (see section 2.1.3 and eq. 2.15 to eq. 2.20) was extended. Seven different degradation processes were included in the 1-MT model. Their corresponding ODE models were enumerated and are below called „hypothesis“. A summary of all hypotheses is shown in Figure 2.4.

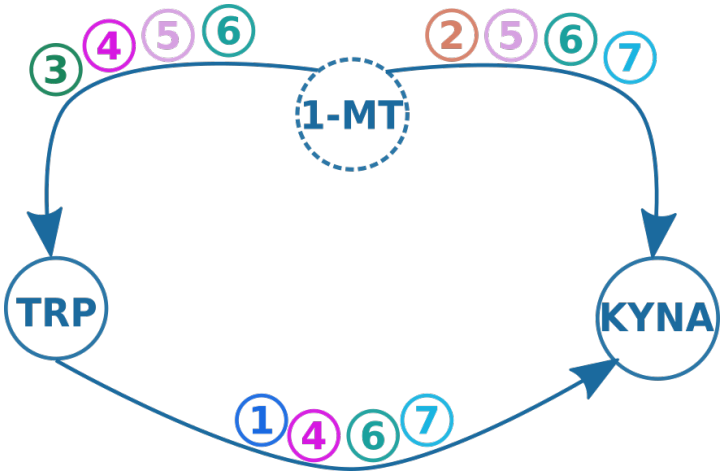

Figure 2.4.: **Summary of hypotheses of 1-MT degradation processes:** Direct degradation of TRP to KYNA (*1*), direct degradation of 1-MT to KYNA (*2*), direct degradation of 1-MT to TRP to KYN, and KYNA (*3*), direct degradation of 1-MT to TRP and directly to KYNA (*4*), direct degradation of 1-MT to TRP and of 1-MT to KYNA (*5*), direct degradation of 1-MT to KYNA and of 1-MT to TRP and further to KYNA (*6*), direct degradation of 1-MT to KYNA and of TRP to KYNA (*7*), 1-MT - 1-methyltryptophan, KYNA - kynurenic acid, TRP - tryptophan

The first hypothesis is developed by adding a direct degradation of TRP to KYNA to the 1-MT model. This degradation was already reported by Han et al. in 2008 ([201]). The second hypothesis adds a direct degradation of 1-MT to KYNA. The third hypothesis is also based on the 1-MT model, including a direct degradation of 1-MT to TRP. The four remaining hypotheses are combinations of hypotheses 1 to 3. Hypothesis 4 combines hypothesis 1 and 3, hypothesis 5 combines hypotheses 2 and 3. Hypothesis 6 combines hypotheses 1, 2 and 3 and hypothesis 7 combines hypotheses 1 and 2. In the following, the hypotheses are explained separately.

Hypothesis 1 The first hypothesis („Hyp 1“) is based on the findings of Han et al. [160]. The enzyme KAT catalyzes the degradation of KYN to KYNA and exists in four variants (KATI -IV). The variant KATII was shown to degrade TRP to KYNA. This reaction was included in the 1-MT model. The degradation of this hypothesis is assumed to be enzymatic. Because it is not known, which enzyme catalyzes this reaction, a fictitious enzyme here named „tryptophan to kynurenic acid degrading enzyme“(TKE) is introduced (see Figure 2.5).

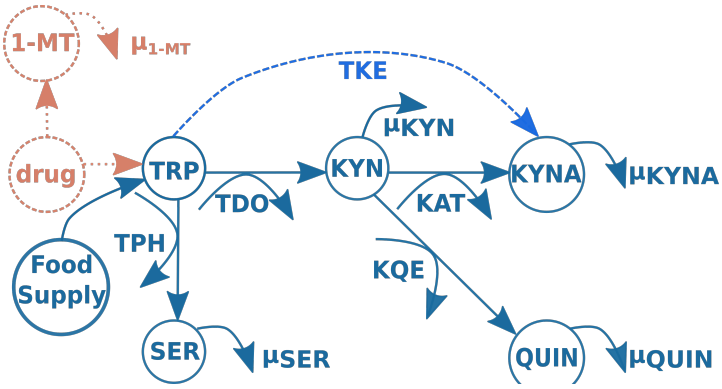

Figure 2.5.: **Schematic of hypothesis 1 of 1-MT degradation processes:** The interaction network of the TRP metabolism includes the degradation of TRP to SER by TPH. TRP is degraded to KYN by TDO, and KYN is degraded to the downstream metabolites KYNA (by KAT) and QUIN (by KQE). The direct degradation of TRP to KYNA by TKE is included due to 1-MT administration. Bent arrows show enzymatic reactions next to a straight arrow. 1-MT - 1-methyltryptophan, KAT - kynurenine aminotransferase, KQE - kynurenine to quinolinic acid degrading enzyme, KYN - kynurenine, KYNA - kynurenic acid, QUIN - quinolinic acid, SER - serotonin, TDO - tryptophan-2,3-dioxygenase, TKE - tryptophan to kynurenic acid degrading enzyme, TPH - tryptophan hydroxylase, TRP - tryptophan, μ - degradation parameter

The chemical reaction added to the Table 2.3 is as follows:

$$TRP \xrightarrow{\text{TKE}} KYNA$$

This reaction leads to the system of ordinary differential equations given in eq. 2.21 to 2.26. It is based on the ODE system of the standard model (eq.2.2 to 2.6). Its extension by 1-MT administration (eq. 2.15 to 2.20) is marked in orange. The added degradation of TRP to KYNA is marked in blue:

$$\frac{d1MT(t)}{dt} = +ApplicationMT - \mu_{1MT} \cdot 1MT(t) \tag{2.21}$$

$$\begin{aligned}\frac{dTRP(t)}{dt} = &+ FoodSupply + ApplicationMT - \frac{TRP(t) \cdot V_{max}^{TPH}}{K_{TPH} + TRP(t)} \\ &- \frac{TRP(t) \cdot V_{max}^{TDO}}{K_{TDO} + TRP(t)} - \frac{TRP(t) \cdot V_{max}^{TKE}}{K_{TKE} + TRP(t)}\end{aligned} \tag{2.22}$$

$$\begin{aligned}\frac{dKYN(t)}{dt} = &+ \frac{TRP(t) \cdot V_{max}^{TDO}}{K_{TDO} + TRP(t)} - \frac{KYN(t) \cdot V_{max}^{KQE}}{K_{KQE} + KYN(t)} - \frac{KYN(t) \cdot V_{max}^{KAT}}{K_{KAT} + KYN(t)} \\ &- \mu_{KYN} \cdot KYN(t)\end{aligned} \tag{2.23}$$

$$\frac{dKYNA(t)}{dt} = + \frac{KYN(t) \cdot V_{max}^{KAT}}{K_{KAT} + KYN(t)} + \frac{TRP(t) \cdot V_{max}^{TKE}}{K_{TKE} + TRP(t)} - \mu_{KYNA} \cdot KYNA(t) \tag{2.24}$$

$$\frac{dQUIN(t)}{dt} = + \frac{KYN(t) \cdot V_{max}^{KQE}}{K_{KQE} + KYN(t)} - \mu_{QUIN} \cdot QUIN(t) \tag{2.25}$$

$$\frac{dSER(t)}{dt} = + \frac{TRP(t) \cdot V_{max}^{TPH}}{K_{TPH} + TRP(t)} - \mu_{SER} \cdot SER(t) \tag{2.26}$$

Hypothesis 2 KATII degrades TRP to KYNA [160]. 1-MT and TRP are structurally similar, disregarding the methylation group. Therefore, it was assumed that an enzyme exists that degrades 1-MT to KYNA. Hence, hypothesis 2 („Hyp 2“), includes the enzymatic degradation of 1-MT to KYNA by a fictitious enzyme called „1-methyltryptophan to kynurenic acid degrading enzyme“(MTKE). This reaction was included in the 1-MT model and is shown in Figure 2.6 as the blue dashed line.

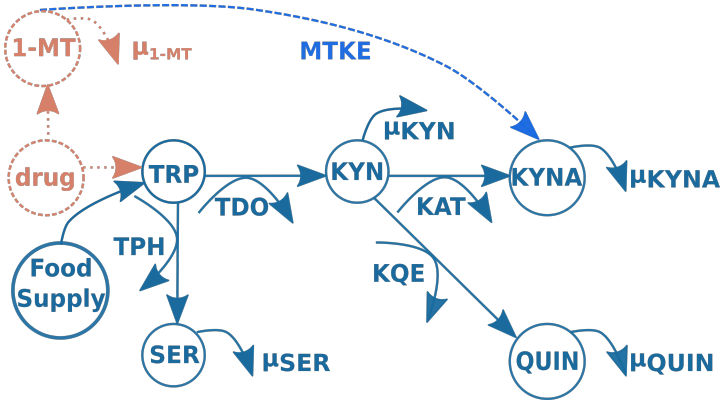

Figure 2.6.: **Schematic of hypothesis 2 of 1-MT degradation processes:** The interaction network of the TRP metabolism includes the degradation of TRP to SER by TPH. TRP is degraded to KYN by TDO, and KYN is degraded to the downstream metabolites KYNA (by KAT) and QUIN (by KQE). The direct degradation of 1-MT to KYNA by MTKE is included due to 1-MT administration. Bent arrows show enzymatic reactions next to a straight arrow. 1-MT - 1-methyltryptophan, KAT - kynurenine aminotransferase, KQE - kynurenine to quinolinic acid degrading enzyme, KYN - kynurenine, KYNA - kynurenic acid, MTKE - 1-methyltryptophan to kynurenic acid degrading enzyme, QUIN - quinolinic acid, SER - serotonin, TDO - tryptophan-2,3-dioxygenase, TPH - tryptophan hydroxylase, TRP - tryptophan, μ - degradation parameter

The chemical reaction added to the Table 2.3 is as follows:

$$1MT \xrightarrow{\text{MTKE}} KYNA$$

This leads to the following system of differential equations given in equations 2.27 to 2.32, where the added degradation of 1-MT to KYNA by MTKE is marked in blue:

$$\frac{d1MT(t)}{dt} = +ApplicationMT - \frac{1MT(t) \cdot V_{max}^{MTKE}}{K_{MTKE} + 1MT(t)} - \mu_{1MT} \cdot 1MT(t) \tag{2.27}$$

$$\begin{aligned}\frac{dTRP(t)}{dt} &= +FoodSupply + ApplicationMT - \frac{TRP(t) \cdot V_{max}^{TPH}}{K_{TPH} + TRP(t)} \\ &\quad - \frac{TRP(t) \cdot V_{max}^{TDO}}{K_{TDO} + TRP(t)}\end{aligned} \tag{2.28}$$

$$\begin{aligned}\frac{dKYN(t)}{dt} &= + \frac{TRP(t) \cdot V_{max}^{TDO}}{K_{TDO} + TRP(t)} - \frac{KYN(t) \cdot V_{max}^{KQE}}{K_{KQE} + KYN(t)} - \frac{KYN(t) \cdot V_{max}^{KAT}}{K_{KAT} + KYN(t)} \\ &\quad - \mu_{KYN} \cdot KYN(t)\end{aligned} \tag{2.29}$$

$$\frac{dKYNA(t)}{dt} = + \frac{KYN(t) \cdot V_{max}^{KAT}}{K_{KAT} + KYN(t)} + \frac{1MT(t) \cdot V_{max}^{MTKE}}{K_{MTKE} + 1MT(t)} - \mu_{KYNA} \cdot KYNA(t) \tag{2.30}$$

$$\frac{dQUIN(t)}{dt} = + \frac{KYN(t) \cdot V_{max}^{KQE}}{K_{KQE} + KYN(t)} - \mu_{QUIN} \cdot QUIN(t) \tag{2.31}$$

$$\frac{dSER(t)}{dt} = + \frac{TRP(t) \cdot V_{max}^{TPH}}{K_{TPH} + TRP(t)} - \mu_{SER} \cdot SER(t) \tag{2.32}$$

Hypothesis 3 As already mentioned, 1-MT and TRP are structurally similar except for the methylation group. Demethylases can remove the methyl group from proteins [161]. Thus, in hypothesis 3 („Hyp 3“) it is assumed demethylation degrades 1-MT by the fictitious enzyme called „1-methyltryptophan to tryptophan degrading enzyme“ MTTE. The reactions are shown in Figure 2.7.

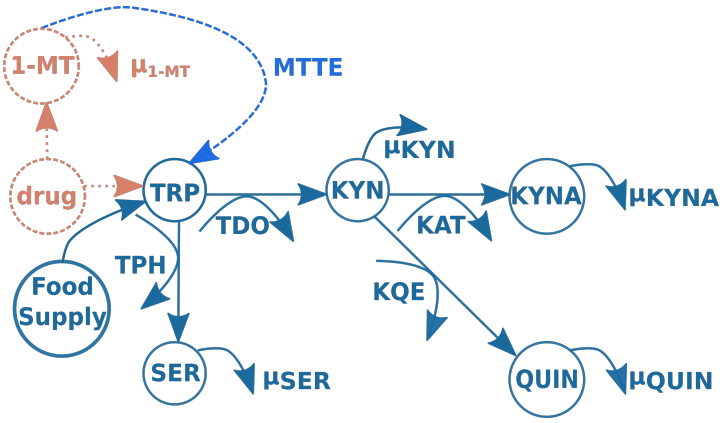

Figure 2.7.: **Schematic of hypothesis 3 of 1-MT degradation processes:** The interaction network of the TRP metabolism includes the degradation of TRP to SER by TPH. TRP is degraded to KYN by TDO, and KYN is degraded to the downstream metabolites KYNA (by KAT) and QUIN (by KQE). The direct degradation of 1-MT to TRP by MTTKE is included due to 1-MT administration. Bent arrows show enzymatic reactions next to a straight arrow. 1-MT - 1-methyltryptophan, KAT - kynurenine aminotransferase, KQE - kynurenine to quinolinic acid degrading enzyme, KYN - kynurenine, KYNA - kynurenic acid, MTTE - 1-methyltryptophan to tryptophan degrading enzyme, QUIN - quinolinic acid, SER - serotonin, TDO - tryptophan-2,3-dioxygenase, TPH - tryptophan hydroxylase, TRP - tryptophan, μ - degradation parameter

The chemical reaction added to the Table 2.3 is as follows:

$$1MT \xrightarrow{\text{MTTE}} TRP$$

This leads to the following system of differential equations given in equation 2.33 to 2.38. The degradation of 1-MT to TRP by MTTE is added to the standard model (eq.2.2 to 2.6). Its extension by 1-MT administration (eq. 2.15 to 2.20) is marked in orange. The added degradation of TRP to KYNA is marked in blue:

$$\frac{d1MT(t)}{dt} = +ApplicationMT - \frac{1MT(t) \cdot V_{max}^{MTTE}}{K_{MTTE} + 1MT(t)} - \mu_{1MT} \cdot 1MT(t) \tag{2.33}$$

$$\begin{aligned}\frac{dTRP(t)}{dt} = &+ FoodSupply + ApplicationMT - \frac{TRP(t) \cdot V_{max}^{TPH}}{K_{TPH} + TRP(t)} \\ &- \frac{TRP(t) \cdot V_{max}^{TDO}}{K_{TDO} + TRP(t)} + \frac{1MT(t) \cdot V_{max}^{MTTE}}{K_{MTTE} + 1MT(t)}\end{aligned} \tag{2.34}$$

$$\begin{aligned}\frac{dKYN(t)}{dt} = &+ \frac{TRP(t) \cdot V_{max}^{TDO}}{K_{TDO} + TRP(t)} - \frac{KYN(t) \cdot V_{max}^{KQE}}{K_{KQE} + KYN(t)} - \frac{dKYN(t) \cdot V_{max}^{KAT}}{K_{KAT} + KYN(t)} \\ &- \mu_{KYN} \cdot KYN(t)\end{aligned} \tag{2.35}$$

$$\frac{dKYNA(t)}{dt} = + \frac{KYN(t) \cdot V_{max}^{KAT}}{K_{KAT} + KYN(t)} - \mu_{KYNA} \cdot KYNA(t) \tag{2.36}$$

$$\frac{dQUIN(t)}{dt} = + \frac{KYN(t) \cdot V_{max}^{KQE}}{K_{KQE} + KYN(t)} - \mu_{QUIN} \cdot QUIN(t) \tag{2.37}$$

$$\frac{dSER(t)}{dt} = + \frac{TRP(t) \cdot V_{max}^{TPH}}{K_{TPH} + TRP(t)} - \mu_{SER} \cdot SER(t) \tag{2.38}$$

Hypothesis 4 Hypothesis 4 („Hyp 4“) combines Hyp 1 and Hyp 3, including a direct degradation of TRP to KYNA via the fictitious enzyme TKE and the demethylation of 1-MT to TRP by MTTE are included. In Figure 2.8, both reactions are shown as blue dashed lines.

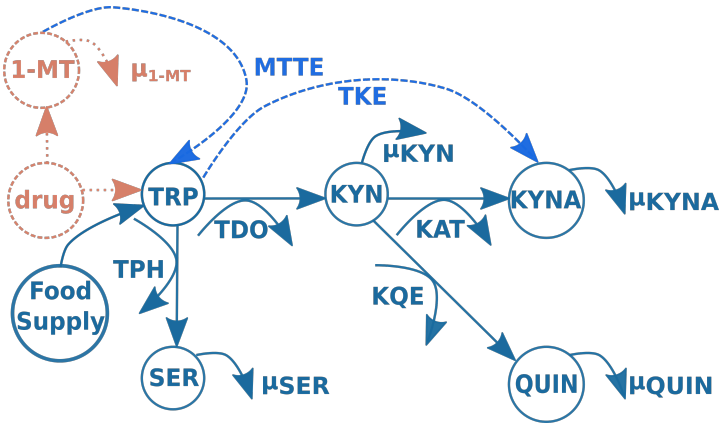

Figure 2.8.: **Schematic of hypothesis 4 of 1-MT degradation processes:** The interaction network of the TRP metabolism includes the degradation of TRP to SER by TPH. TRP is degraded to KYN by TDO, and KYN is degraded to the downstream metabolites KYNA (by KAT) and QUIN (by KQE). The direct degradation of TRP to KYNA by TKE and of 1-MT to TRP by MTTE are included due to 1-MT administration. Bent arrows show enzymatic reactions next to a straight arrow. 1-MT - 1-methyltryptophan, KAT - kynurenine aminotransferase, KQE - kynurenine to quinolinic acid degrading enzyme, KYN - kynurenine, KYNA - kynurenic acid, MTTE - 1-methyltryptophan to tryptophan degrading enzyme, fictional enzyme, QUIN - quinolinic acid, SER - serotonin, TDO - tryptophan-2,3-dioxygenase, TKE - tryptophan to kynurenic acid degrading enzyme, TRP - tryptophan, TPH - tryptophan hydroxylase, μ - degradation parameter

The chemical reactions added to the Table 2.3 are as follows:

$$1MT \xrightarrow{\text{MTTE}} TRP$$
$$TRP \xrightarrow{\text{TKE}} KYNA$$

These reactions lead to the following system of differential equations given in eq. 2.39 to 2.44, where the added degradation of 1-MT to TRP by MTTE and of TRP to KYNA by TKE are marked in blue:

$$\frac{d1MT(t)}{dt} = +ApplicationMT - \frac{1MT(t) \cdot V_{max}^{MTTE}}{K_{MTTE} + 1MT(t)} - \mu_{1MT} \cdot 1MT(t) \tag{2.39}$$

$$\begin{aligned}\frac{dTRP(t)}{dt} = &+ FoodSupply + ApplicationMT - \frac{TRP(t) \cdot V_{max}^{TPH}}{K_{TPH} + TRP(t)} \\ &- \frac{TRP(t) \cdot V_{max}^{TDO}}{K_{TDO} + TRP(t)} + \frac{1MT(t) \cdot V_{max}^{MTTE}}{K_{MTTE} + 1MT(t)} - \frac{TRP(t) \cdot V_{max}^{TKE}}{K_{TKE} + TRP(t)}\end{aligned} \tag{2.40}$$

$$\begin{aligned}\frac{dKYN(t)}{dt} = &+ \frac{TRP(t) \cdot V_{max}^{TDO}}{K_{TDO} + TRP(t)} - \frac{KYN(t) \cdot V_{max}^{KQE}}{K_{KQE} + KYN(t)} - \frac{KYN(t) \cdot V_{max}^{KAT}}{K_{KAT} + KYN(t)} \\ &- \mu_{KYN} \cdot KYN(t)\end{aligned} \tag{2.41}$$

$$\begin{aligned}\frac{dKYNA(t)}{dt} = &+ \frac{KYN(t) \cdot V_{max}^{KAT}}{K_{KAT} + KYN(t)} + \frac{TRP(t) \cdot V_{max}^{TKE}}{K_{TKE} + TRP(t)} \\ &- \mu_{KYNA} \cdot KYNA(t)\end{aligned} \tag{2.42}$$

$$\frac{dQUIN(t)}{dt} = + \frac{KYN(t) \cdot V_{max}^{KQE}}{K_{KQE} + KYN(t)} - \mu_{QUIN} \cdot QUIN(t) \tag{2.43}$$

$$\frac{dSER(t)}{dt} = + \frac{TRP(t) \cdot V_{max}^{TPH}}{K_{TPH} + TRP(t)} - \mu_{SER} \cdot SER(t) \tag{2.44}$$

Hypothesis 5 Hypothesis 5 („Hyp 5“) combines the degradation processes of Hyp 1 to Hyp 3. This hypothesis combines the degradation of 1-MT to KYNA by MTKE (Hyp 2), and the demethylation of 1-MT to TRP by MTTE (Hyp 3). In Figure 2.9, both reactions are shown as blue dashed lines.

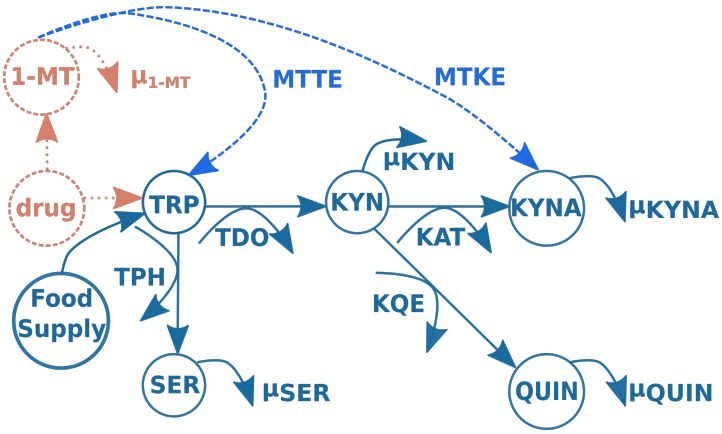

Figure 2.9.: **Schematic of hypothesis 5 of 1-MT degradation processes:** The interaction network of the TRP metabolism includes the degradation of TRP to SER by TPH. TRP is degraded to KYN by TDO, and KYN is degraded to the downstream metabolites KYNA (by KAT) and QUIN (by KQE). The direct degradation of 1-MT to TRP by MTTE and 1-MT to KYNA by MTKE are included due to 1-MT administration. Bent arrows show enzymatic reactions next to a straight arrow. 1-MT - 1-methyltryptophan, KYN - kynurenine, KQE - kynurenine to quinolinic acid degrading enzyme, KYNA - kynurenic acid, QUIN - quinolinic acid, MTKE- 1-methyltryptophan to kynurenic acid degrading enzyme, MTTE - methyltryptophan to tryptophan degrading enzyme, SER - serotonin, TDO - tryptophan-2,3-dioxygenase, KAT - kynurenine aminotransferase, TPH - tryptophan hydroxylase, TRP - tryptophan, μ - degradation parameter

The chemical reactions added to Table 2.3 are as follows:

$$1MT \xrightarrow{\text{MTTE}} TRP$$
$$1MT \xrightarrow{\text{MTKE}} KYNA$$

These reactions lead to the system of differential equations given in equations 2.45 to 2.50. The added degradation of 1-MT to TRP by MTTE and 1-MT to KYNA by MTKE are marked in blue:

$$\frac{d1MT(t)}{dt} = +ApplicationMT - \frac{1MT(t) \cdot V_{max}^{MTKE}}{K_{MTKE} + 1MT(t)} - \frac{1MT(t) \cdot V_{max}^{MTTE}}{K_{MTTE} + 1MT(t)} - \mu_{1MT} \cdot 1MT(t) \tag{2.45}$$

$$\frac{dTRP(t)}{dt} = + FoodSupply + ApplicationMT - \frac{TRP(t) \cdot V_{max}^{TPH}}{K_{TPH} + TRP(t)} - \frac{TRP(t) \cdot V_{max}^{TDO}}{K_{TDO} + TRP(t)} + \frac{1MT(t) \cdot V_{max}^{MTTE}}{K_{MTTE} + 1MT(t)} \tag{2.46}$$

$$\frac{dKYN(t)}{dt} = + \frac{TRP(t) \cdot V_{max}^{TDO}}{K_{TDO} + TRP(t)} - \frac{KYN(t) \cdot V_{max}^{KQE}}{K_{KQE} + KYN(t)} - \frac{KYN(t) \cdot V_{max}^{KAT}}{K_{KAT} + KYN(t)} - \mu_{KYN} \cdot KYN(t) \tag{2.47}$$

$$\frac{dKYNA(t)}{dt} = + \frac{KYN(t) \cdot V_{max}^{KAT}}{K_{KAT} + KYN(t)} + \frac{1MT(t) \cdot V_{max}^{MTKE}}{K_{MTKE} + 1MT(t)} - \mu_{KYNA} \cdot KYNA(t) \tag{2.48}$$

$$\frac{dQUIN(t)}{dt} = + \frac{KYN(t) \cdot V_{max}^{KQE}}{K_{KQE} + KYN(t)} - \mu_{QUIN} \cdot QUIN(t) \tag{2.49}$$

$$\frac{dSER(t)}{dt} = + \frac{TRP(t) \cdot V_{max}^{TPH}}{K_{TPH} + TRP(t)} - \mu_{SER} \cdot SER(t) \tag{2.50}$$

Hypothesis 6 Hypothesis 6 („Hyp 6“) combines the degradation of 1-MT to KYNA by MTKE (Hyp 2), the degradation of TRP to KYNA by TKE (Hyp 1), and the degradation of 1-MT to TRP by MTTE (Hyp 3). In Figure 2.10, all reactions are shown as blue dashed lines.

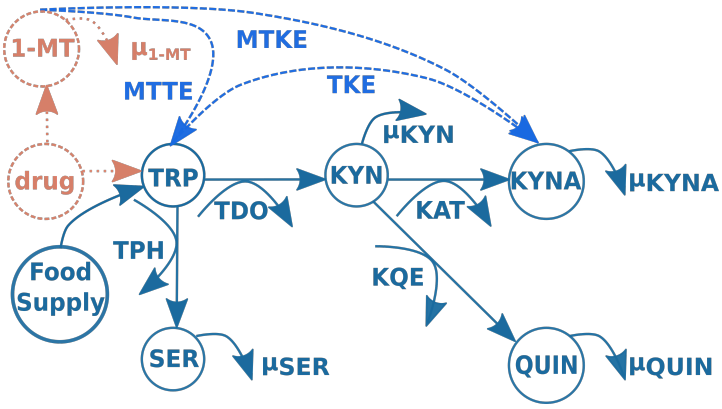

Figure 2.10.: **Schematic of hypothesis 6 of 1-MT degradation processes:** The interaction network of the TRP metabolism includes the degradation of TRP to SER by TPH. TRP is degraded to KYN by TDO, and KYN is degraded to the downstream metabolites KYNA (by KAT) and QUIN (by KQE). The direct degradation of TRP to KYNA by TKE, of 1-MT to TRP by MTTE and 1-MT to KYNA by MTKE are included due to 1-MT administration. Bent arrows show enzymatic reactions next to a straight arrow. 1-MT - 1-methyltryptophan, KAT - kynurenine aminotransferase, KQE - kynurenine to quinolinic acid degrading enzyme, KYN - kynurenine, KYNA - kynurenic acid, QUIN - quinolinic acid, MTTE- 1-methyltryptophan to tryptophan degrading enzyme, MTKE - 1-methyltryptophan to kynurenic acid degrading enzyme, SER - serotonin, TDO - tryptophan-2,3-dioxygenase, TKE - tryptophan to kynurenic acid degrading enzyme, TPH - tryptophan hydroxylase, TRP - tryptophan, μ - degradation parameter

The chemical reactions added to the Table 2.3 are as follows:

$$TRP \xrightarrow{\text{TKE}} KYNA$$
$$1MT \xrightarrow{\text{MTTE}} TRP$$
$$1MT \xrightarrow{\text{MTKE}} KYNA$$

These reactions lead to the following system of differential equations given in eq. 2.51 to 2.56. This system of ODEs is based on the standard model (eq.2.2 to 2.6). Its extension by the 1-MT administration (eq. 2.15 to 2.20), is marked in orange. The

added degradation of 1-MT to KYNA by TKE and 1-MT to KYNA by MTKE are marked in blue:

$$\frac{d1MT(t)}{dt} = +ApplicationMT - \frac{1MT(t) \cdot V_{max}^{MTKE}}{K_{MTKE} + 1MT(t)} - \frac{1MT(t) \cdot V_{max}^{MTTE}}{K_{MTTE} + 1MT(t)} - \mu_{1MT} \cdot 1MT(t) \tag{2.51}$$

$$\frac{dTRP(t)}{dt} = + FoodSupply + ApplicationMT - \frac{TRP(t) \cdot V_{max}^{TPH}}{K_{TPH} + TRP(t)} - \frac{TRP(t) \cdot V_{max}^{TDO}}{K_{TDO} + TRP(t)} + \frac{1MT(t) \cdot V_{max}^{MTTE}}{K_{MTTE} + 1MT(t)} - \frac{TRP(t) \cdot V_{max}^{TKE}}{K_{TKE} + TRP(t)} \tag{2.52}$$

$$\frac{dKYN(t)}{dt} = + \frac{TRP(t) \cdot V_{max}^{TDO}}{K_{TDO} + TRP(t)} - \frac{KYN(t) \cdot V_{max}^{KQE}}{K_{KQE} + KYN(t)} - \frac{KYN(t) \cdot V_{max}^{KAT}}{K_{KAT} + KYN(t)} - \mu_{KYN} \cdot KYN(t) \tag{2.53}$$

$$\frac{dKYNA(t)}{dt} = + \frac{KYN(t) \cdot V_{max}^{KAT}}{K_{KAT} + KYN(t)} + \frac{1MT(t) \cdot V_{max}^{MTKE}}{K_{MTKE} + 1MT(t)} + \frac{TRP(t) \cdot V_{max}^{TKE}}{K_{TKE} + TRP(t)} - \mu_{KYNA} \cdot KYNA(t) \tag{2.54}$$

$$\frac{dQUIN(t)}{dt} = + \frac{KYN(t) \cdot V_{max}^{KQE}}{K_{KQE} + KYN(t)} - \mu_{QUIN} \cdot QUIN(t) \tag{2.55}$$

$$\frac{dSER(t)}{dt} = + \frac{TRP(t) \cdot V_{max}^{TPH}}{K_{TPH} + TRP(t)} - \mu_{SER} \cdot SER(t) \tag{2.56}$$

Hypothesis 7 Hypothesis 7 („Hyp 7“) is a combination of Hyp 2 (degradation of 1-MT to KYNA by MTKE) and Hyp 1 (degradation of TRP to KYNA by TKE). Both reactions are shown as blue dashed lines in Figure 2.11.

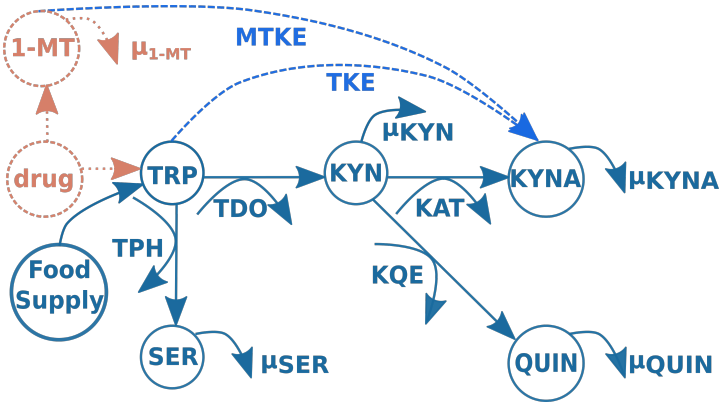

Figure 2.11.: **Schematic of hypothesis 7 of 1-MT degradation processes:** The interaction network of the TRP metabolism includes the degradation of TRP to SER by TPH. TRP is degraded to KYN by TDO, and KYN is degraded to the downstream metabolites KYNA (by KAT) and QUIN (by KQE). The direct degradation of TRP to KYNA by TKE and of 1-MT to KYNA by MTKE are included due to 1-MT administration. Bent arrows show enzymatic reactions next to a straight arrow. 1-MT - 1-methyltryptophan, KAT - kynurenine aminotransferase, KQE - kynurenine to quinolinic acid degrading enzyme, KYN - kynurenine, KYNA - kynurenic acid, MTKE - 1-methyltryptophan to kynurenic acid degrading enzyme, QUIN - quinolinic acid, SER - serotonin, TKE - tryptophan to kynurenic acid degrading enzyme, TDO - tryptophan-2,3-dioxygenase, TPH - tryptophan hydroxylase, TRP - tryptophan, μ - degradation parameter,

The chemical reactions added to the Table 2.3 are as follows:

$$TRP \xrightarrow{\text{TKE}} KYNA$$
$$1MT \xrightarrow{\text{MTKE}} KYNA$$

These reactions lead to the system of ODEs given in equations 2.57 to 2.62. The added degradation of 1-MT to KYNA by TKE and 1-MT to KYNA by MTKE are marked in blue:

$$\frac{d1MT(t)}{dt} = +ApplicationMT - \frac{1MT(t) \cdot V_{max}^{MTKE}}{K_{MTKE} + 1MT(t)} - \mu_{1MT} \cdot 1MT(t) \tag{2.57}$$

$$\frac{dTRP(t)}{dt} = +FoodSupply + ApplicationMT - \frac{TRP(t) \cdot V_{max}^{TPH}}{K_{TPH} + TRP(t)} - \frac{TRP(t) \cdot V_{max}^{TDO}}{K_{TDO} + TRP(t)} - \frac{TRP(t) \cdot V_{max}^{TKE}}{K_{TKE} + TRP(t)} \tag{2.58}$$

$$\frac{dKYN(t)}{dt} = +\frac{TRP(t) \cdot V_{max}^{TDO}}{K_{TDO} + TRP(t)} - \frac{KYN(t) \cdot V_{max}^{KQE}}{K_{KQE} + KYN(t)} - \frac{KYN(t) \cdot V_{max}^{KAT}}{K_{KAT} + KYN(t)} - \mu_{KYN} \cdot KYN(t) \tag{2.59}$$

$$\frac{dKYNA(t)}{dt} = +\frac{KYN(t) \cdot V_{max}^{KAT}}{K_{KAT} + KYN(t)} + \frac{1MT(t) \cdot V_{max}^{MTKE}}{K_{MTKE} + 1MT(t)} + \frac{TRP(t) \cdot V_{max}^{TKE}}{K_{TKE} + TRP(t)} - \mu_{KYNA} \cdot KYNA(t) \tag{2.60}$$

$$\frac{dQUIN(t)}{dt} = +\frac{KYN(t) \cdot V_{max}^{KQE}}{K_{KQE} + KYN(t)} - \mu_{QUIN} \cdot QUIN(t) \tag{2.61}$$

$$\frac{dSER(t)}{dt} = +\frac{TRP(t) \cdot V_{max}^{TPH}}{K_{TPH} + TRP(t)} - \mu_{SER} \cdot SER(t) \tag{2.62}$$

2.1.5. Model of 1-Methyltryptophan Effects Facing Infection

It was already shown that 1-MT inhibits IDO [86], but a sufficient 1-MT level for an entire IDO inhibition was not achieved *in vivo*. To investigate the ability of the 1-MT model to represent the inhibitory effects of 1-MT on IDO *in vivo*, the model of the most likely hypothesis of section 2.1.4 has to be anticipated. The most likely degradation pathway of 1-MT is hypothesis 2. The ODE model of hypothesis 2 is merged with the LPS model.

Table 2.4.: **Chemical reactions and signaling pathways of the TRP metabolism, including the IDO activation by LPS administration and 1-MT's inhibitory effects on IDO**

reaction	source		product	reaction type
1	TRP	$\xrightarrow{\text{TDO}}$	KYN	enzymatic
2	TRP	$\xrightarrow{\text{TPH}}$	SER	enzymatic
3	KYN	$\xrightarrow{\text{KAT}}$	KYNA	enzymatic
4	KYN	$\xrightarrow{\text{KQE}}$	QUIN	enzymatic
5	SER	$\xrightarrow{\mu}$		degradative
6	KYNA	$\xrightarrow{\mu}$		degradative
7	KYN	$\xrightarrow{\mu}$		degradative
8	QUIN	$\xrightarrow{\mu}$		degradative
9		$\xrightarrow{\text{ApplicationMT}}$	TRP	receiving
10		$\xrightarrow{\text{ApplicationMT}}$	1MT	receiving
11	LPS	$\xrightarrow{\text{k}}$	TNF-α	activating
12	TNF-α + TRP	$\xrightarrow{\text{IDO}}$	KYN	enzymatic
13	LPS	$\xrightarrow{\mu}$		degradative
14	TNF-α	$\xrightarrow{\mu}$		degradative
15	1MT	$\xrightarrow{\mu}$		degradative
16	1MT	$\xrightarrow{\text{MTKE}}$	KYNA	producing

The 1-MT model, which is represented in Table 2.3, is merged with the LPS model (see Table-2.2) extended by the degradation process of 1-MT to KYNA, which is catalyzed by the fictitious enzyme MTKE (16), 1-MT - 1-methyltryptophan, KAT - kynurenine aminotransferase, KYN - kynurenine, KYNA - kynurenic acid, LPS - lipopolysaccharide, QUIN - quinolinic acid, SER - serotonin, IDO - indolamin-2,3-dioxygenase, TDO - tryptophan-2,3-dioxygenase, TNF - tumor necrosis factor -α, TPH - tryptophan hydroxylase, TRP - tryptophan

The model's chemical reactions and signaling pathways are shown in Table 2.4. The merged model was duplicated so two models result. One model was extended by the inhibitory effects of 1-MT on IDO, and the other model does not include the inhibitory effects of 1-MT on IDO. Both models are presented in more detail in the following.

Model of 1-Methyltryptophan Induced Indoleamine 2,3-Dioxygenase Inhibition The inhibitory properties of 1-MT are represented in the system of ODEs corresponding to the model of 1-MT induced IDO inhibition by a term deduced from the following equation:

$$K_i = \frac{IC_{50}^{1MT}}{1 + \frac{TNF \cdot TRP}{K_{IDO}}}, \tag{2.63}$$

with IC_{50}^{1MT} as half maximal inhibitory concentration and K_{IDO} as MM constant. K_i is the binding affinity of the inhibitor. In Figure 2.12, the composition of the ODE model of 1-MT inhibition facing infection is shown.

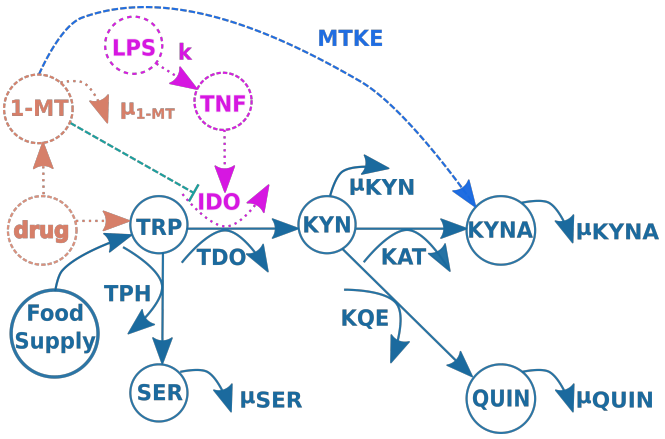

Figure 2.12.: **Schematic of 1-MT/LPS model including 1-MT's inhibitory effects:** The standard model is extended (dotted lines) by an application of LPS, which increases TNF-α concentration. TNF-α leads to the activation of IDO, which increases the degradation rate of TRP to KYN. The standard model is further extended (dotted lines) by the drug application of 1-MT (MT), increases 1-MT and TRP. Due to the contamination of the drug 1-MT with TRP, 1-MT is degraded with a rate of μ_{OMT}. A direct degradation of 1-MT to KYNA is assumed based on the results of the simulations of the different hypotheses of 1-MT degradation (dashed line), 1-MT's ability of IDO inhibition is here included and presented as dashed line. Bent arrows show enzymatic reactions next to a straight arrow. 1-MT - 1-methyltryptophan, IDO - indolamin-2,3-dioxygenase, KAT - kynurenine aminotransferase, KYN - kynurenine, KYNA - kynurenic acid, MTKE - 1-methyltryptophan to kynurenic acid degrading enzyme, QUIN - quinolinic acid, SER - serotonin, TDO - tryptophan-2,3-dioxygenase, TPH - tryptophan hydroxylase, TRP - tryptophan, μ - degradation parameter

The interconnected system of ODEs is also colored according to its composition as it is given in Figure 2.12. The system of ordinary differential equations dedicated to Table 2.4 and Figure 2.12 is given by the equation 2.64 to 2.71 of the following system of ODEs:

$$\frac{d1MT(t)}{dt} = +ApplicationMT - \frac{1MT(t) \cdot V_{max}^{MTKE}}{K_{MTKE} + 1MT(t)} - \mu_{1MT} \cdot 1MT(t) \tag{2.64}$$

$$\frac{dLPS(t)}{dt} = +Application - \mu_{LPS} \cdot LPS(t) \tag{2.65}$$

$$\begin{aligned}\frac{dTRP(t)}{dt} = &+ FoodSupply + ApplicationMT - \frac{TRP(t) \cdot V_{max}^{TPH}}{K_{TPH} + TRP(t)} \\ &- \frac{IC_{50}^{1MT}}{1 + \frac{TNF(t) \cdot TRP(t)}{K_{IDO}}} \cdot \frac{TNF(t) \cdot TRP(t) \cdot V_{max}^{IDO}}{K_{IDO} + TRP(t)} - \frac{TRP(t) \cdot V_{max}^{TDO}}{K_{TDO} + TRP(t)}\end{aligned} \tag{2.66}$$

$$\begin{aligned}\frac{dKYN(t)}{dt} = &+ \frac{TRP(t) \cdot V_{max}^{TDO}}{K_{TDO} + TRP(t)} + \frac{IC_{50}^{1MT}}{1 + \frac{TNF(t) \cdot TRP(t)}{K_{IDO}}} \cdot \frac{TNF(t) \cdot TRP(t) \cdot V_{max}^{IDO}}{K_{IDO} + TRP(t)} \\ &- \frac{KYN(t) \cdot V_{max}^{KQE}}{K_{KQE} + KYN(t)} - \frac{KYN(t) \cdot V_{max}^{KAT}}{K_{KAT} + KYN(t)} - \mu_{KYN} \cdot KYN(t)\end{aligned} \tag{2.67}$$

$$\frac{dKYNA(t)}{dt} = + \frac{KYN(t) \cdot V_{max}^{KAT}}{K_{KAT} + KYN(t)} + \frac{1MT(t) \cdot V_{max}^{MTKE}}{K_{MTKE} + 1MT(t)} - \mu_{KYNA} \cdot KYNA(t) \tag{2.68}$$

$$\frac{dQUIN(t)}{dt} = + \frac{KYN(t) \cdot V_{max}^{KQE}}{K_{KQE} + KYN(t)} - \mu_{QUIN} \cdot QUIN(t) \tag{2.69}$$

$$\frac{dSER(t)}{dt} = + \frac{TRP(t) \cdot V_{max}^{TPH}}{K_{TPH} + TRP(t)} - \mu_{SER} \cdot SER(t) \tag{2.70}$$

$$\frac{dTNF(t)}{dt} = +k \cdot LPS(t) - \mu_{TNF} \cdot TNF(t) \tag{2.71}$$

Model of 1-Methyltryptophan Without Indoleamine 2,3-Dioxygenase Inhibition
The second model does not include the inhibitory properties of 1-MT on IDO, as it is shown in Figure 2.13.

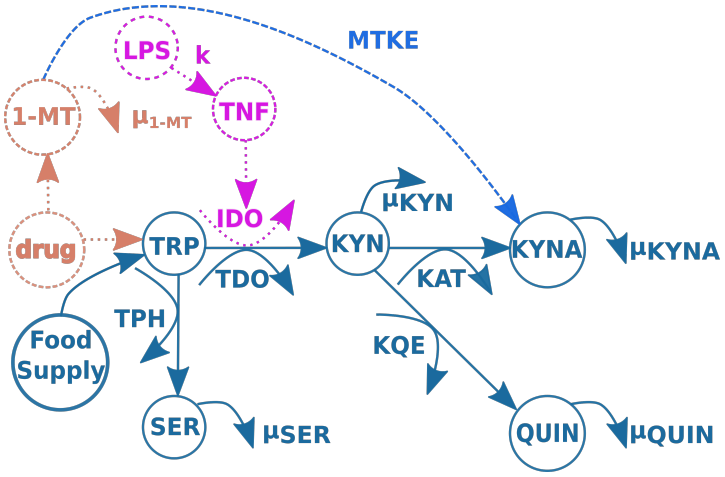

Figure 2.13.: **Schematic of 1-MT/LPS model not including 1-MT's inhibitory effects:** The standard model is extended (dotted lines) by an application of LPS, which leads to an increase in TNF-α concentration, TNF-α leads to the activation of IDO, which increases the degradation rate of TRP to KYN. The standard model is further extended (dotted lines) by the drug application of 1-MT (MT), which leads to an increase in 1-MT and TRP. Due to the contamination of the drug 1-MT with TRP, 1-MT is degraded with a rate of μ_{OMT}. A direct degradation of 1-MT to KYNA is assumed based on the results of the simulations of the different hypotheses of 1-MT degradation (dashed line), 1-MT's ability of IDO inhibition is here excluded. Enzymatic reactions are shown by bent arrows next to a straight arrow. 1-MT - 1-methyltryptophan, IDO - indolamin-2,3-dioxygenase, KAT - kynurenine aminotransferase, KYN - kynurenine, KYNA - kynurenic acid, MTKE - 1-methyltryptophan to kynurenic acid degrading enzyme, QUIN - quinolinic acid, SER - serotonin, TDO - tryptophan-2,3-dioxygenase, TPH - tryptophan hydroxylase, TRP - tryptophan, μ - degradation parameter

The interconnected system of ODEs is also colored according to its composition, as in Figure 2.13. The parts of the standard model are shown in black. The parts of the LPS model are shown in pink and the parts of the 1-MT model are presented in orange. The degradation of 1-MT to KYNA according to hypothesis 2 is depicted as a dashed line. The system of ODEs is given in equations 2.72 to 2.79:

$$\frac{d1MT(t)}{dt} = +ApplicationMT - \frac{1MT(t) \cdot V_{max}^{MTKE}}{K_{MTKE} + 1MT(t)} - \mu_{1MT} \cdot 1MT(t) \tag{2.72}$$

$$\frac{dLPS(t)}{dt} = +Application - \mu_{LPS} \cdot LPS(t) \tag{2.73}$$

$$\begin{aligned}\frac{dTRP(t)}{dt} = &+ FoodSupply + ApplicationMT - \frac{TRP(t) \cdot V_{max}^{TPH}}{K_{TPH} + TRP(t)} \\ &- \frac{TNF(t) \cdot TRP(t) \cdot V_{max}^{IDO}}{K_{IDO} + TRP(t)} - \frac{TRP(t) \cdot V_{max}^{TDO}}{K_{TDO} + TRP(t)}\end{aligned} \tag{2.74}$$

$$\begin{aligned}\frac{dKYN(t)}{dt} = &+ \frac{TRP(t) \cdot V_{max}^{TDO}}{K_{TDO} + TRP(t)} + \frac{TNF(t) \cdot TRP(t) \cdot V_{max}^{IDO}}{K_{IDO} + TRP(t)} \\ &- \frac{KYN(t) \cdot V_{max}^{KQE}}{K_{KQE} + KYN(t)} - \frac{KYN(t) \cdot V_{max}^{KAT}}{K_{KAT} + KYN(t)} - \mu_{KYN} \cdot KYN(t)\end{aligned} \tag{2.75}$$

$$\frac{dKYNA(t)}{dt} = + \frac{KYN(t) \cdot V_{max}^{KAT}}{K_{KAT} + KYN(t)} + \frac{1MT(t) \cdot V_{max}^{MTKE}}{K_{MTKE} + 1MT(t)} - \mu_{KYNA} \cdot KYNA(t) \tag{2.76}$$

$$\frac{dQUIN(t)}{dt} = + \frac{KYN(t) \cdot V_{max}^{KQE}}{K_{KQE} + KYN(t)} - \mu_{QUIN} \cdot QUIN(t) \tag{2.77}$$

$$\frac{dSER(t)}{dt} = + \frac{TRP(t) \cdot V_{max}^{TPH}}{K_{TPH} + TRP(t)} - \mu_{SER} \cdot SER(t) \tag{2.78}$$

$$\frac{dTNF(t)}{dt} = +k \cdot LPS(t) - \mu_{TNF} \cdot TNF(t) \tag{2.79}$$

2.2. Data used for validation of the mathematical models

Already published data and also unpublished data were used with the permission of the author's respective experimentalists to calculate the parameters of the mathematical models describing the TRP metabolism under different conditions (see section 2.1). In the following, a short explanation of the experimental models, and their connection to the ODE models of the TRP metabolism, is given. Detailed explanations and figures of the data are given in the appendix A or can be found in the publications [86, 149, **?**]. Those experiments were conducted to establish a pig model of IDO activation by LPS and to investigate the effects of 1-MT and 1-MT on IDO activation. The TRP metabolites TRP, SER, KYN, KYNA, and QUIN, as well as 1-MT and TNF-α, were measured. All blood samples were taken from the anterior vena cava of male pigs.

2.2.1. A Pig Model of Indoleamine 2,3-Dioxygenase Activation by Lipopolysaccharides

A reliable model of the TRP metabolism is necessary to investigate the effects of 1-MT administration on the TRP metabolites. Therefore, the parameters of the standard model and the LPS model were fitted to data representing the dynamics of the TRP metabolism in LPS-treated pigs. The calculated parameters were fixed in the models of the different hypotheses according to approach 1. The data were published by Wirthgen et al. [147]. In the following, the here presented experiment is called the „LPS experiment I“. The yielded parameters were verified on the measurements of an identical experiment („LPS experiment II“), which were not published. Both experiments were conducted during the summer season (August and September). In Figure 2.14, a schematic presentation of the experimental set-up is shown.

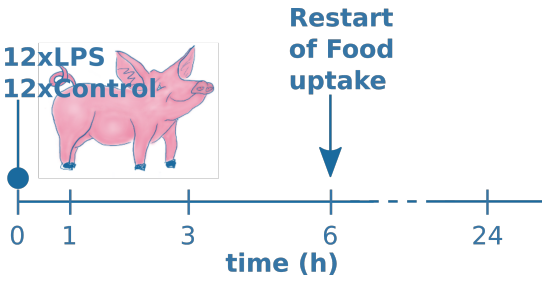

Figure 2.14.: **Experimental Setup of LPS Experiment I and II:** In LPS experiment I, 24 pigs, and in LPS experiment II 16 pigs were treated at 0 h with either LPS or NaCl as control (Control). At the indicated time points, blood samples were taken, and metabolites of the TRP metabolism (TRP, SER, KYN, KYNA, QUIN), as well as TNF-α were measured (see Figure A.2 and Figure A.3 in the appendix A). Before time point 0 h, food was subducted, 6 h later, food was supplied. At time point 6 h, twelve pigs of LPS experiment I and eight pigs of LPS experiment II were sacrificed. LPS - lipopolysaccharides

In LPS experiment I, 12 pigs received LPS and 12 NaCl and therefore served as the control group. In LPS experiment II, eight pigs received LPS and eight NaCl. 1 h before LPS or NaCl administration, food was removed in both experiments and restarted 6 h after LPS/NaCl administration. After 6 h, twelve respective eight pigs were slaughtered. Hence, the group size of twelve pigs was reduced to six pigs (respective four pigs) for LPS and six pigs for NaCl-treated pigs. Blood samples were taken shortly before LPS administration (0 h), 1 h, 3 h, 6 h, and 24 h after LPS/NaCl administration [149].

2.2.2. A Pig Model of the Interactions of 1-Methyltryptophan and IDO

Data from samples of 1-MT-treated pigs were needed to test the different hypotheses. Those data were published by Wirthgen et al. [86, 162]. In the following, this experiment is called the „1-MT/LPS experiment“. 16 pigs were included in the experiment, which was conducted in the winter season (January). Eight pigs received five times every 24 h 1 g 1-MT, as it is shown in Figure 2.15.

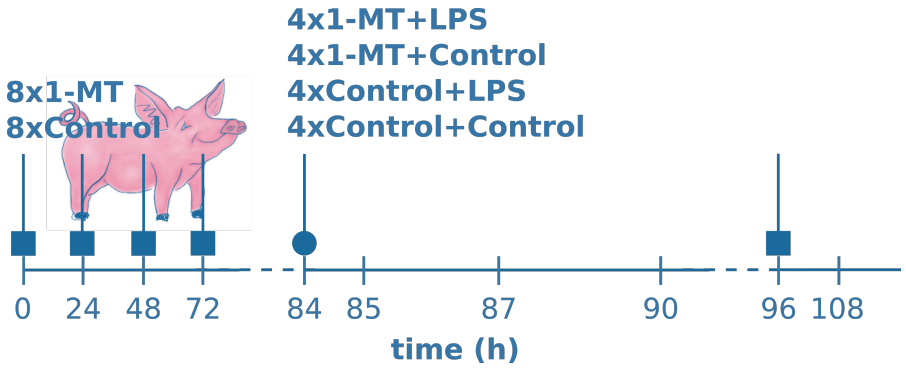

Figure 2.15.: **Experimental Set-up of 1-MT/LPS Experiment:** At time points indicated with arrows with a rectangualar head, 16 pigs were treated with 1-MT or Myritol as control (Control). At the time point indicated with an arrow with a circular arrowhead, pigs received either LPS or NaCl as control. At 90 h half of the pigs were sacrificed (eight of 16 remained, each treatment group was of equal group size). Pigs were starved from time point 72 h on till the end of the experiment. At each indicated time point samples from blood were taken. Measurements of TRP metabolites and 1-MT are shown in Figure A.5 in the appendix A, LPS - lipopolysaccharides, 1-MT - 1-methyltryptophan

The control group consisted of eight pigs and received Myritol (carrier solution for 1-MT). Blood samples were taken at 0 h, 24 h, 48 h, 72 h, and 96 h after each 1-MT/Myritol administration. 12 h after the fourth application (at 84 h) of 1-MT, eight pigs received LPS. Four of them were treated with 1-MT, and four pigs were treated with Myritol. The control group received NaCl consisting of four 1-MT-treated pigs and four Myritol-treated pigs. Thus, this leads to four treatment groups (each with four pigs):

- 1-MT & LPS - pigs that were treated with 1-MT and LPS
- 1-MT, Control - pigs that were treated with 1-MT and NaCl
- Control, LPS - pigs that were treated with NaCl and LPS
- Control & Control- pigs that were treated with 1-MT and NaCl

At time point 85 h, 87 h, 90 h, 96 h (before fifth 1-MT application), and 108 h after LPS/NaCl administration, blood samples were taken, too. Half of the treated animals were sacrificed equally distributed in the four treatment groups after 90 h (see Figure 2.14). Thus in each group, two pigs remain. The pigs were starved after the 1-MT administration at 72 h. Feeding did not restart. For parameter fitting, the data set was split up into different subsets according to their purposes, which are explained below.

Selection of Lipopolysaccharide-Treated Pigs Data of control animals of the 1-MT/LPS experiment (Myritol-treated) were used to model the dynamics of the LPS induced enzyme IDO with regard to the TRP metabolism. A summary of the experiment with a subset of the pigs is shown in Figure 2.16.

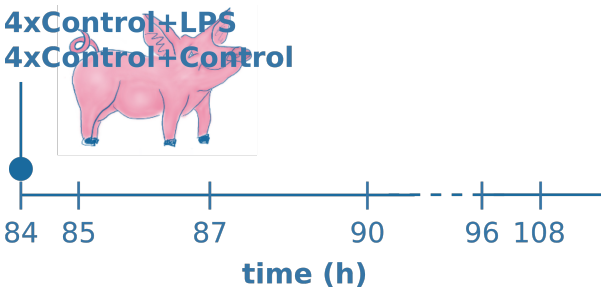

Figure 2.16.: **Experimental Setup of 1-MT/LPS experiment, subset LPS-treated:** Only a subset of pigs of 1-MT/LPS experiment (see Figure 2.15) is considered, Myritol-treated pigs received LPS or NaCl (Control) at the time point indicated with a circular arrowhead. At time point 90 h, half of the pigs were sacrificed (four of eight pigs remained). At each indicated time point, samples from blood were taken. The pigs had no access to food during the whole experiment. The measurements of TRP metabolites and 1-MT are shown in Figure A.7 in the appendix A, LPS - lipopolysaccharides

Measurements, including time point 84 h and later, were used for parameter fitting (see Figure A.7 in the appendix A). This subset is named „1-MT/LPS experiment, subset LPS-treated pigs“. Pigs were starved for the whole period and only eight pigs were included. For taking tissue samples, four pigs were slaughtered, two in each treatment group, at time point 90 h. With this subset, results based on the data measured in LPS experiments I and II were validated and parameters only based on 1-MT/LPS experiment, subset LPS-treated pigs, were estimated. Those parameters were also applied to data to explain the degradation process of 1-MT and its inhibitory effects on IDO (approach 2).

Selection of 1-Methyltryptophan-Treated Pigs To estimate parameters of the models including 1-MT degradation pathways leading to an increase of TRP and KYNA increase, only the subset of 1-MT-treated pigs is needed. This subset consists of eight pigs treated with 1-MT and Myritol, but not with LPS (see Figure 2.17).

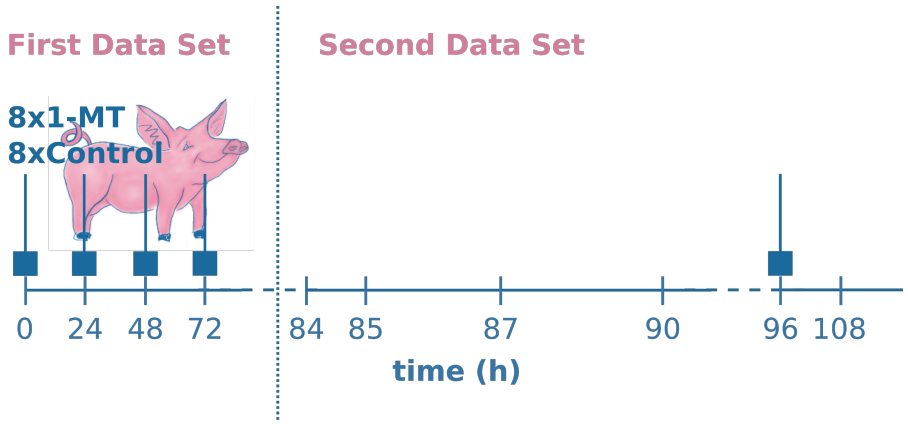

Figure 2.17.: **Experimental Setup of 1-MT/LPS experiment, subset 1-MT-treated:** At time points with arrows with rectangular arrowheads pigs were treated with 1-MT or Myritol as control (Control). At time point 90 h, half of the pigs were sacrificed (four of eight pigs remained, equally distributed in the treatment groups), pigs had access to food during time points 0 h and 72 h, from time point 72 h till the end of the experiment pigs were starved, at each indicated time point samples from blood were taken. The data set was divided into pigs, that received food (first data set), and pigs that did not receive food (second data set). Measurements of the TRP metabolites and 1-MT with *FoodSupply* (first data set) are shown in Figure A.9 and without *FoodSupply* (second data set) are shown in Figure A.10 in the appendix A, 1-MT - 1-methyltryptophan

This subset is named „1-MT/LPS experiment, subset 1-MT-treated pigs“. This experiment was further split up into two periods depending on the food supply. Since food contains TRP, the increase of TRP due to food intake has to be considered in the models. To investigate the impact of additional TRP increase, one data set includes food uptake, the other does not. In the first period, pigs were fed (see Figure 2.17, first data set). In the second period (including time point 84 h and later), pigs were starved. For further studies, pigs were slaughtered at time point 90 h so 2 pigs in every treatment group remained (see Figure 2.17, second data set). With this subset, parameters estimated on data measured in LPS experiment I and II, and 1-MT/LPS experiment, subset LPS-treated pigs, were applied on different models, which describe possible degradation processes of 1-MT.

Selection of Lipopolysaccharide and 1-Methyltryptophan-Treated Pigs To investigate 1-MT's inhibitory effects on IDO, two models of 1-MT effects facing infection were developed. One 1-MT/LPS model includes the inhibitory effects of 1-MT. The other does not. The Parameters of both models were fitted on a subset of measurements of the 1-MT/LPS experiment. Data of pigs treated with 1-MT or Myritol and LPS or

NaCl, including time point 84 h, and later were used. This subset is called „1-MT/LPS experiment, second data set “.

2.3. Mathematical Methods used for Model Fitting and Analysis

The parameters of the models presented in section 2.1 were fitted to the data presented in section 2.2. The combination of the model and corresponding data set is presented below. Moreover, several assumptions to initial values, boundaries of fitted parameters, and fixed parameters were made before simulations started. Those frame conditions, the methods used for parameter fitting, the three different approaches for choosing parameters, and methods for model analysis are explained in this section.

2.3.1. Software

To implement the models, the software Matlab [125] was used. An additional toolbox, called „Data 2 Dynamics“ [163], was used to define the equations of the models, import the data files and assign the data to the corresponding models. The used data CSV files, model and data-definition files, and the setup files are available via the CD, which is located at the back inner cover, or via the Institut of Bioinformatics of the University Medicine Greifswald.All plots including simulations, data presenteation, sensitivity and identifiability analysis were created with R statistics in R studio [164] with the package ggplot2 [165]. The sensitivity analysis was performed in R [164], with the package „ODESensitivity“ and the function „ODEmorris“ [166].

2.3.2. Approaches for Parameter Calculation

Data (see section 2.2) were used to fit the parameters of the models, which were introduced in section 2.1. Data from control pigs of the LPS model, the 1-MT model, the different hypotheses models of 1-MT degradation, and the 1-MT/LPS model (pigs treated with Myritol and NaCl), were used to calculate parameters of the standard model (see Figure 2.1 and eq. 2.2 to eq. 2.6). This is necessary due to two reasons:

1. TRP is degraded to KYN by TDO and by IDO. TDO is active in every pig. At which IDO is only active in LPS treated pigs because LPS leads to IDO production. By fitting NaCl-treated and LPS-treated pigs together, the degradation of TRP by TDO and by IDO can be discriminated.

2. TRP is degraded to KYNA via KYN. Thus, an increase in KYNA depends on the activity of TDO and KAT in Myritol-treated pigs. For pigs treated with 1-MT, a substantial increase in KYNA was shown. Thus, it is possible that 1-MT is degraded to TRP and then to KYN and KYNA, leading to a strong increase. Another possibility is the degradation of 1-MT via an unknown pathway to KYNA.

By fitting the parameters of both treatment groups at once, a differentiation between the degradation of TRP to KYNA via KYN or an independent pathway is possible.

For parameter fitting, the LPS model (see Figure 2.2) was fitted to data of LPS experiment I (see Figure A.2 in the appendix A). The resulting parameter set was verified on data of LPS experiment II (see Figure A.3 in the appendix A) and 1-MT/LPS experiment, subset LPS-treated pigs. Moreover, the LPS model was fitted to data of 1-MT/LPS experiment, subset LPS treated pigs (see Figure A.7 in the appendix A). Since LPS experiment I/II differ from 1-MT/LPS experiment in the number of pigs, in the metabolite levels of some species (e.g. TRP) and in the season in which the experiments were conducted (LPS experiment I/II in summer, 1-MT/LPS experiment in winter), parameters were fitted to both (LPS experiment I and 1-MT/LPS experiment, subset LPS-treated pigs). The models of the seven hypotheses of 1-MT degradation (see Figure 2.3 and Figure 2.4) were fitted to data of 1-MT/LPS experiment, subset 1-MT-treated pigs, first data set, and second data set. Therefore, three different approaches were used:

1. parameters were fixed to the parameters fitted to LPS experiment I (approach 1)
2. parameters were fixed to the parameters fitted to 1-MT/LPS experiment, LPS-treated pigs (approach 2)
3. parameters of each hypothesis were fitted separately multiple times to find an optimal parameter combination [15]. The parameters were fitted 100 times according to the approach of Stavrum et al. and Cornforth et al. [15, 167]. The parameters of all models of the different hypotheses were fitted at once. (approach 3)

The 1-MT/LPS model including inhibitory effects (see Figure 2.12 and eq. 2.64 to eq. 2.71) and the one omitting inhibitory effects (see Figure 2.13 and eq. 2.72 to eq. 2.79) of 1-MT were fitted to data of 1-MT/LPS experiment, second data set. The three approaches described for testing the hypotheses were also used for fitting the parameters to the 1-MT/LPS experiment, second data set.
Matlab [125] and the Data 2 Dynamics toolbox [163] were used to calculate parameters of the different models. Parameter fitting was initialized from random parameter sets generated by latin hypercube sampling [163] to find a global optimum. Those initial values were then used to initialize the CVODES algorithm, which solves IVPs. Here the numerical method lsqnonlin was used. The parameters were estimated on a log scale, as recommended [168]. For parameter fitting, the data of each pig were imported separately. Subsequently, the LL was calculated for each pig.

2.3.3. Conditions for Parameters and Literature Values

To obtain parameters, which are in a physiological range of pigs, some assumptions were made. Boundaries for initial parameters TRP_0, SER_0, KYN_0, $KYNA_0$, $QUIN_0$, and

$1MT_0$ were estimated in a range of $mean \pm 2 \cdot standard\ deviations$ of the measured data of all pigs at time point 0. This assumption was made because 95% of the data are in this range for normal distribution [169]. The initial values were calculated for each data set and subset for the measurements at time point 0 h respective 84 h for the parameters of the models, which were estimated on the data of the 1-MT/LPS experiment, second data set. As already mentioned, the data are not normally distributed, and a skewed distribution is present. Thus $mean - 2 \cdot standard\ deviations < 0$ is possible. In these cases, the initial value was set to 0.00001. Boundaries for V_{max}^{enzyme} and k were set broadly. In other studies, the boundaries were set to the maximal and minimal values found in the literature [15]. Those studies were performed for organisms like a human. However, in this study, samples were taken from the blood of pigs, but no K_m, V_{max}^{enzyme} or degradation parameters μ were established for pigs. LPS_0 was set to 100 000 (EU) for models applied on LPS experiment I and II data, since pigs got administered this amount of LPS in the beginning of the experiment (see section 2.2). For data from 1-MT/LPS experiment, subset LPS-treated pigs, and 1-MT/LPS experiment, second data set LPS_0 was set to 150 000 (EU), since the pigs got administered this amount of LPS (see section 2.2). Initial values of LPS (LPS_0) for control animals and for TNF-α ($TNF - \alpha_0$) for treatment groups of LPS experiment I, II, and 1-MT/LPS experiment, subset LPS-treated pigs, first data set and second data set were set to zero (see Figure A.9 in the appendix A). The initial value of 1-MT ($1MT_0$) was set to zero for all pigs of the 1-MT/LPS experiment, first data set. In the second data set, $1MT_0$ was set to zero for Myritol-treated pigs (Myritol and NaCl-treated). For 1-MT-treated pigs, $1MT_0$ was set to $mean \pm 2 \cdot standard\ deviations$.
To reduce the parameter erstimation complexity and maintain the model's identifiability, K_m-values and degradation parameters μ were fixed to values found in literature (see Table 2.5).

Table 2.5.: **Literature values for simulations with Michaelis-Menten Kinetics:**

Parameter	Value	Reference organism	Reference
K_{IDO}	$4\ \mu M$	human T24 cells	[170]
K_{IDO}	$10^{-5}\mu M$	epididymis of mice	[171]
K_{IDO}	$7\ \mu M$	human	[172]
K_{IDO}	$3\ \mu M$	human fibroblasts	[173]
V_{max}^{IDO}	$14.851 \cdot 10^3 \mu M/h$	epididymis of mice	[171]
V_{max}^{IDO}	$50 \mu M/h$	human T24 cells	[170]
K_{TDO}	$222\ \mu M$	human	[172]
K_{TDO}	$82.5 \mu M$	human	[174]
K_{TDO}	$20 \mu M$	rabbit intestine	[175]
V_{max}^{TDO}	$11.424 \cdot 10^3 \mu M/h$	rabbit intestine	[175]
V_{max}^{TDO}	$3934.072 \mu M/h$	mice liver	[153]
V_{max}^{TDO}	$94.112 \cdot 10^6 \mu M/h$	rat lung	[176]
K_{TPH}	$90 \mu M$	rats	[177]
K_{TPH}	$108 \mu M$	male albino rat	[178]
V_{max}^{TPH}	$81,6 \cdot 10^{12} \mu M/h$	rats	[177]
V_{max}^{TPH}	$5.168 \cdot 10^6 \mu M/h$	male albino rat	[178]
V_{max}^{TPH}	$195.84 \mu M/h$	human brain	[179]
V_{max}^{TPH}	$78.88 \mu M/h$	rat brain	[180]
V_{max}^{TPH}	$2.6928 \cdot 10^3 \mu M/h$	murine mast cells	[181]
K_{KYNU}	$240 \mu M$	rat liver	[182]
K_{KYNU}	$28.5 \mu M$	human	[183]
K_{KYNU}	$3 \mu M/h$	Human	[184]
V_{max}^{KYNU}	$1.69218 \cdot 10^3 \mu M/h$	rat liver	[182]

Continued on next page

Table 5 - continued from previous page

Parameter	Value	Reference organism	Reference
K_{KAT}	$4.7 \cdot 10^3 \mu M$	human liver cDNA	[185]
K_{KAT}	$53 \mu M$	KATI, rat brain	[186]
K_{KAT}	$2000 \mu M$	KATI, human brain	[187]
V_{max}^{KAT}	$271.286 \cdot 10^{-3} \mu M/h$	rat brain	[186]
V_{max}^{KAT}	$2820.3 \mu M/h$	human brain	[187]
μ_{SER}	$0.01444057 \mu M/h$	rabbit	[188]
μ_{QUIN}	$0.4892802 \mu M/h$	Male Sprague-Dawley rats	[189]
μ_{QUIN}	$1.039731 \mu M/h$	gerbil	[190]
μ_{QUIN}	$1.890401 \mu M/h$	Adult male C57BL/6 mice	[191]
μ_{QUIN}	$0.165035 \mu M/h$	rabbit	[192]
μ_{KYN}	$0.2\ \mu M$	human	[14]
μ_{KYNA}	$0.6931472 \mu M/h$	Non Human Primates	[193]
$\mu_{TNF-\alpha}$	$1.386294 \mu M/h$	human Monocytes	[194, 195]
$\mu_{TNF-\alpha}$	$0.6931472 \mu M/h$	not specified	[196]
Application1MT	137.129	pig	[162]

Values for K_m, V_{max}, and the degradation parameters μ were gathered from literature. Only degradation parameters μ and K_m values were fixed and V_{max} values were fitted to the data. This approach is according to Rios-Avila et al. [14]. Values for K_m and degradation rates μ, which were fixed in the LPS model, are colored in pink. The parameters specific to the 1-MT model are colored in orange. The parameters fixed in the standard model are colored in blue. The parameter Application1MT is the amount of 1-MT, which was measured in blood after one 1-MT administration in [162], K_{KYNU} equals K_{KQE}. TNF-α - tumor necrosis factor α, TRP - tryptophan, KYN - kynurenine, KYNA - kynurenic acid, QUIN - quinolinic acid, SER - serotonin, IDO - indoleamine 2,3-dioxygenase, , KAT - kynurenine aminotransferase, KYNU - kynureninase, TDO - tryptophan-2,3-dioxygenase, TPH - tryptophanhydroxylase

In the literature, no pig specific measurements were found. Moreover, parameters obtained from different experiments on different experimental models were used to measure degradation rates of KYN, KYNA, QUIN, and SER or enzyme activities of IDO, TDO, TPH, KQE (=KYNU), or KAT. The organisms used for the experiments range from human and rodents to primates, from cells of the brain to cells of the liver. Nevertheless, no experiment was conducted in the cells of pigs. The degradation parameters μ and K_m of the LPS model were fixed. The initial parameter values and V_{max} values were fitted to the data of LPS experiment I. This approach was adapted from Rios-Avila et al. [14]. Since more than one literature value for the K_m values and degradation parameters μ were found, different combinations of literature values were fixed. The principle of trial and error created the combinations of parameters. The combination leading to the best approximation given by the LPS model to the data of LPS experiment I was chosen. The parameters, which were fixed in the LPS model, were also used in the models of 1-MT degradation as well as IDO inhibition by 1-MT.

2.3.4. Identifiablity Analysis

Parameter identifiability and confidence bounds were determined by profile likelihood estimation at a confidence level of 95% using functions of D2D (arPLEInit and ple(), [126]).

2.3.5. Sensitivity Analysis

The purpose of this thesis is to investigate the 1-MT induced increase of KYNA. Therefore it is necessary to determine the parameters with the most significant impact on KYNA levels. A sensitivity analysis is the appropriate tool to determine those parameters and was performed in R [164]. The method of „Morris Screening“ of the package „ODESensitivity“ and function „ODEmorris“ [166] was applied to the LPS model with parameters fitted to data of LPS experiment I. The sensitivity of initial values, V_{max} values, K_m values, and the degradation values μ, were determined. The sensitivity analysis was performed for all species, but only the results for KYNA were evaluated. The corresponding plot was created with R statistics in R studio [164] with the package ggplot2 [165].

2.3.6. Modeling the Uptake of Tryptophan and 1-Methyltryptophan

Three different processes can be regarded as drug applications. The first one is the administration of 1-MT ($Application1MT$), administered multiple times during the 1-MT/LPS experiment. The drug 1-MT was contaminated with TRP, leading to a TRP increase. Thus, during 1-MT administration, also TRP is administered, which represents the second process. The third process is initiated by food intake because food was supplied ($FoodSupply$) and removed. This food supply led to two phases of TRP increase. D2D's function called „Bolus Injection“ implemented these processes regarded as drug application. In general, a bolus injection is a single dose of a drug D. For the Bolus injection implemented in this study, it was assumed that the dynamics of D increase according to the trajectory of the normal distribution, which is in line with the findings of Wirthgen et al. [162]. Therefore the density function of the normal distribution

$$F(x) = \frac{1}{\sqrt{2 \cdot \pi \cdot \sigma^2}} \cdot exp(-\frac{(t-\mu)^2}{2 \cdot \sigma^2}) \tag{2.80}$$

was adapted with w_t as the injection time point, which equals the mean of the normal distribution. $w_d = injection\_duration$ equals the standard deviation. To account for the drug increase, the bolus amount w_a is multiplied by the eq. 2.80, because the area under the curve of a probability density is always 1, but the increase of the drug differs from 1. These assumptions lead to the following equation:

$$\frac{D(t)}{dt} = \frac{w_a}{\sqrt{2 \cdot \pi \cdot w_d^2}} \cdot exp(-\frac{(t-w_t)^2}{2 \cdot w_d^2}) \tag{2.81}$$

This equation depends on t with w_t as time point when the peak of the drug concentration occurs. If w_t is chosen as the actual injection time point, the increase of D, would start before the drug was administered. Thus, w_t has to be delayed. For models whose parameters were fitted to data from LPS experiment I and II, the injection time point was shifted from 6 h (start of food intake) to 20 h with an injection duration w_d of 7 h. Several parameter fittings obtained those values with altering values for w_d and w_t. The results of a study of 1-MT's pharmacokinetics [162] were used. The calculation of 1-MT's dosage is simplified. The area under the concentration curve was reported to be $959.9\mu M$ [162]. This concentration was divided by five since 1-MT was injected five times (at time points 0 h, 24 h, 48 h, 72 h, and 96 h). The purity of the drug 1-MT was reported with 95% [162], leading to a TRP increase of 9.599 μM. The peak of 1-MT in blood was observed after 12 h [162], leading to a later injection time point (w_t = 12 h). TRP ($FoodSupply$), 1-MT (drug application) and TRP (drug contamination) administration were assigned four times between 0 h and 84 h (12 h, 36 h, 60 h, 84 h, 1-MT/LPS experiment, subset 1-MT-treated pigs, first data set). For models whose parameters were fitted to data of 1-MT/LPS experiment, subset 1-MT-treated pigs, second data set, 1-MT (drug application), and TRP (drug contamination) administration were assigned to two time points. The first time point corresponds to the 1-MT administration at time point 72 h, which was chosen with 84 h. The second time point (108 h) corresponds to the 1-MT administration at time point 96 h. Thus, again a shift of 12 h was assumed.

2.3.7. Model Evaluation

The Log-Likelihood, AIC and BIC were calculated to compare simulations TRP metabolism's dynamics. $-2ln(L)$ values for each pig were summed up to get an overall LL value. To compare simulations with different amounts of parameters, the Akaike information criterion (AIC) was used. It is calculated by $2 \cdot k - 2 \cdot ln(L)$, with k as the number of parameters and the likelihood L [197]. To compare simulations with different amounts of parameters and data, the Bayesian information criterion (BIC) is used. The BIC is calculated by $k \cdot ln(n) - 2 \cdot ln(L)$, with k as the number of parameters and n as the amount of data. For parameter validation, it was necessary to use the BIC since data sets differ in the number of measurements. Generally, the model with the lowest AIC value can be selected for inference [198]. In this study, all three chraracteristic numbers (LL, AIC, and BIC) were calculated in R statistics [164], by using the equations introduced in section 1.3.3 and compared.

2.3.8. Validation of Results of Simulation of 1-Methyltryptophan Hypotheses

To validate the results of the different hypotheses of 1-MT degradation, an experiment was developed and performed (by Elisa Wirthgen). This experiment was based on calculations performed on data of 1-MT/LPS experiment, subset 1-MT-treated pigs. 1-MT or TRP was added to cell-free assays to investigate the ability of KAT to catalyze the

degradation of 1-MT or TRP. On the one hand, 1-MT was added with and without KAT. On the other hand, TRP was added with and without KAT. Measurements of TRP, KYN, and KYNA were made in medium and PBS. As control, measurements of TRP, KYN, and KYNA in the medium and PBS were made.
In more detail, the experiments were performed in cell-free assays. The assays were performed to investigate the potential spontaneous and enzymatic degradation of 1-MT to KYNA. Therefore, 1-MT (L-isomer, purity 95%; Sigma-Aldrich, Deisenhofen, Germany) was dissolved in 1 N NaOH to a stock concentration of 1M, and further dilutions were made in either PBS or RPMI 1640 medium (both PAN-Biotech, Aidenbach, Germany) to a final concentration of 700 μM. In contrast to RPMI 1640, PBS contains no supplemented TRP or TRP metabolites. A NaOH solvent control was prepared by adding 1 N NaOH to PBS or cell culture medium to the same volume as used for L-1-MT. 1-MT contains between 2 and 5% L-TRP [199, 200]. Therefore, the effect of 35 μM L-TRP (Sigma-Aldrich, Deisenhofen, Germany) on KYNA production was investigated, corresponding to 5% of the applied 1-MT concentration. *In vivo*, the enzymatical production of KYNA is generated by kynurenine aminotransferases (KATs), which catalyze KYN to KYNA. However, also TRP was described to be a potential substrate for KATs. 1-MT and TRP were incubated for 60 min at 37°C and 5% CO_2 in the presence or absence of Glutamic-Oxaloacetic Transaminase 1 in triplicates (GOT1 = KATIV, antibodies-online GmbH, Aachen, Germany) at a final concentration of 1.25 μg/ml as recommended by the manufacturer. After incubation, the assay supernatants were harvested and stored at $-80°C$. Triplicates of each group were pooled to analyze TRP and its metabolites KYN and KYNA by mass spectrometry.

3. Results

This study aims to propose a degradation process of 1-MT leading to increased levels of TRP and KYNA while the intermediate metabolite KYN does not change. Therefore, different degradation processes were developed and translated to systems of ODEs (see section 2.1.4). Moreover, it was investigated whether those systems of ODEs can reproduce the inhibitory effects of 1-MT on IDO (see section 2.1.5). The parameters of the different models were fitted to the data of experiments conducted in pigs (see section 2.2). At first, general findings are presented. Afterward, the exact results of the parameter fittings and the comparison of the different models are presented. More precisely, the results of 1-MT's degradation are shown, including the different approaches and the validation experiment. The results of the models concerning 1-MT's inhibitory effects on IDO's activity are shown to be separated by the three different approaches.

3.1. 1-Methyltryptophan is Directly Degraded to Kynurenic Acid

Models of seven different degradation processes were developed to investigate the degradation of 1-MT leading to increases of TRP and KYNA levels (see section 2.1.4). Those models were applied in different settings to the data of 1-MT/LPS experiment, subset 1-MT-treated pigs on the first and the second data set. The LL, AIC, and BIC values were compared. The parameters fitted to the data of LPS experiment I (approach 1) and 1-MT/LPS experiment, subset LPS-treated pigs (approach 2), were fixed. The models of the different hypotheses with fixed parameters were used to investigate their ability to reflect the dynamics of the TRP metabolism. Moreover, the parameters of the hypotheses were fitted 100 times (approach 3). Here, LL, AIC, and BIC values were determined for all 100 iterations, and mean and minimal values were calculated and compared. By computing LL, AIC, and BIC values of models, which used different approaches for parameter fitting on two data sets (1-MT/LPS experiment, subset 1-MT-treated pigs, first and second data set), 18 times, the most likely hypothesis was determined. The results are shown in Table 3.1.

Table 3.1.: **Results of all three *in silico* experiments to find the most likely degradation process of 1-MT**

approach	simulation	LL	AIC	BIC
1	first data set	Hyp 7	Hyp7	Hyp 7
	second data set	Hyp 2	Hyp 2	Hyp 2
2	first data set	Hyp 6	Hyp 6	Hyp 2
	second data set	Hyp 4	Hyp 4	Hyp 2
3	first data set	Hyp 7	Hyp 2	Hyp 2
	second data set	Hyp 2	Hyp 2	classic

To determine the most likely degradation process of 1-MT presented as models in section 2.1.4, different parameter set-ups were used to fit parameters to the data of 1-MT/LPS experiment, subset 1-MT-treated pigs, first data set, and second data set. For the first setting, parameters were fixed to values, which were fitted to the data of LPS experiment I. In the second setting, parameters were fixed to values, which were fitted to the data of 1-M/LPS experiment, subset LPS-treated pigs. In the third setting, parameters were fitted to the data of the 1-MT/LPS experiment, subset 1-MT-treated pigs, first data set and second data set 100 times, and the mean LL, AIC, and BIC values were calculated. The classical pathway includes no further degradation of one metabolite or 1-MT to another. Hypothesis 2 includes the direct degradation of 1-MT of KYNA. Hypothesis 4 includes the degradation of 1-MT to TRP, and TRP to KYNA. Hypothesis 6 includes the degradation of 1-MT to KYNA, of 1-MT to TRP, and TRP to KYNA. Hypothesis 7 includes the degradation of 1-MT to KYNA and of TRP to KYNA. AIC - Akaike Information Criterion, BIC - Bayesian information Criterion, Hyp - hypothesis, LL - Log-Likelihood

Hyp 2 was nine times the most likely one. Hyp 7 was four times the most likely one. Hyp 4 and 6 were only two times the most likely, and the classical pathway was once the most likely model. Concluding, the most likely degradation process is given by Hyp 2, assuming a direct degradation of 1-MT to KYNA. The increase in TRP degradation is explainable by contamination of the drug 1-MT.
The following results of these parameter fits include LL, AIC, and BIC values, results of indentifiability analysis and a comparison of all fitted parameters to their literature values. The results of the sensitivity analysis for KYNA and the results of the experiment validating the direct degradation of 1-MT to KYNA.

3.1.1. Calculation of Parameters by Using the Data of Lipopolysaccharide-Treated Pigs

To determine parameters, which were fixed in the models of the different hypotheses, parameters of the LPS model were fitted to the data of LPS experiment I. Those parameters were validated on LPS experiment II and 1-MT/LPS experiment, subset LPS-treated pigs.

Parameter Fitting The parameters fitted to the LPS experiment I consisting of 756 data points, yielded a LL value of -2140.261, an AIC value of -2100.261, and a BIC value of -2007.7. The simulations with those fitted parameters are shown in Figure 3.1. The calculated parameters are presented in the appendix C in column I. All are identifiable except V_{max}^{TPH}, which is not identifiable for low parameter values (see Figure 3.2). Since the degradation of TRP to SER is not in focus, the non-identifiability of this parameter can be neglected. The lower and upper bound of parameters and parameter values are represented in log_{10}-scale and are shown in the appendix B in Table B.1.

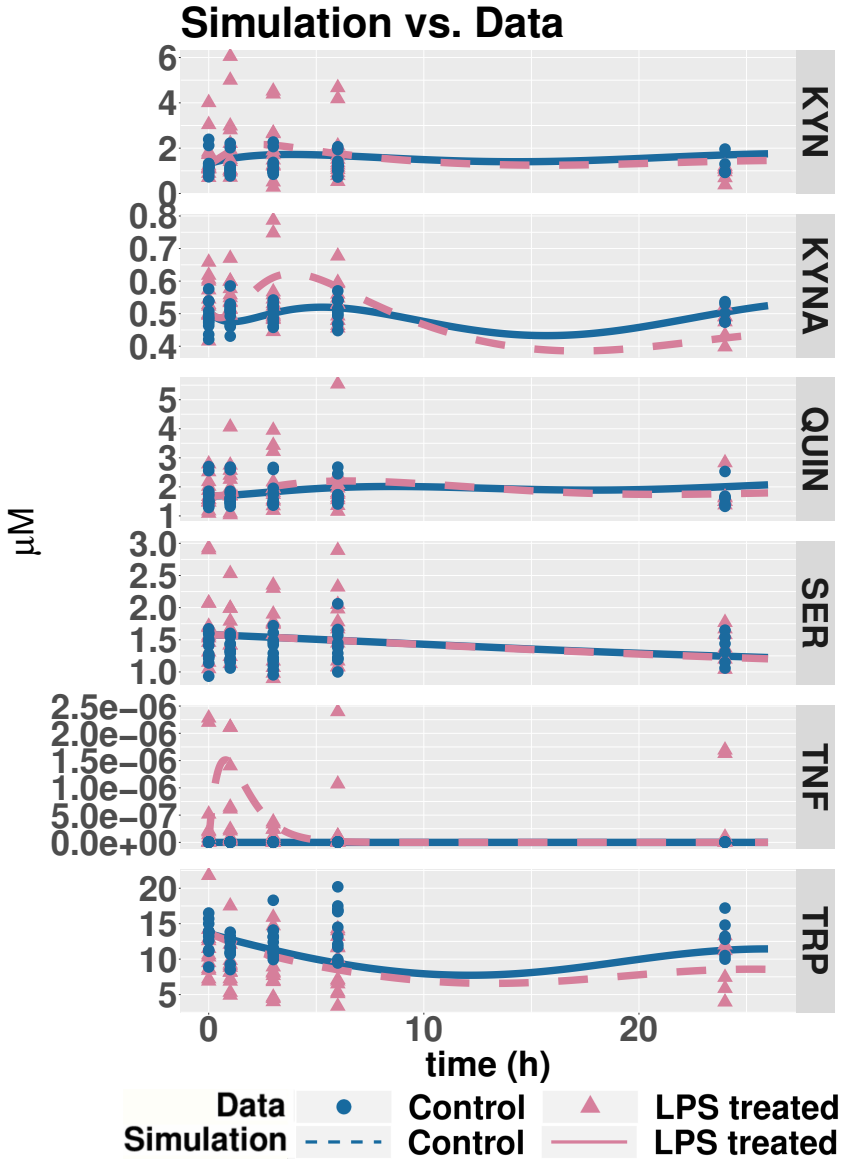

Figure 3.1.: **Simulations with parameters fitted to data of LPS experiment I:** Parameters are based on the LPS model and on data of LPS experiment I (see Figure A.2 in the appendix A). Simulations are shown in solid and dashed lines. The data are shown in triangles and dots. Pigs were treated at 0 h with LPS and starved in the time slot between 0 h and 6 h. Half of the pigs were sacrificed at time point 6 h. The immolation of pigs decreased the group size from twelve pigs to six pigs for LPS-treated pigs, and NaCl-treated pigs. KYN - kynurenine, KYNA - kynurenic acid, QUIN - quinolinic acid, SER - serotonin, TNF - tumor necrosis factor α, TRP - tryptophan

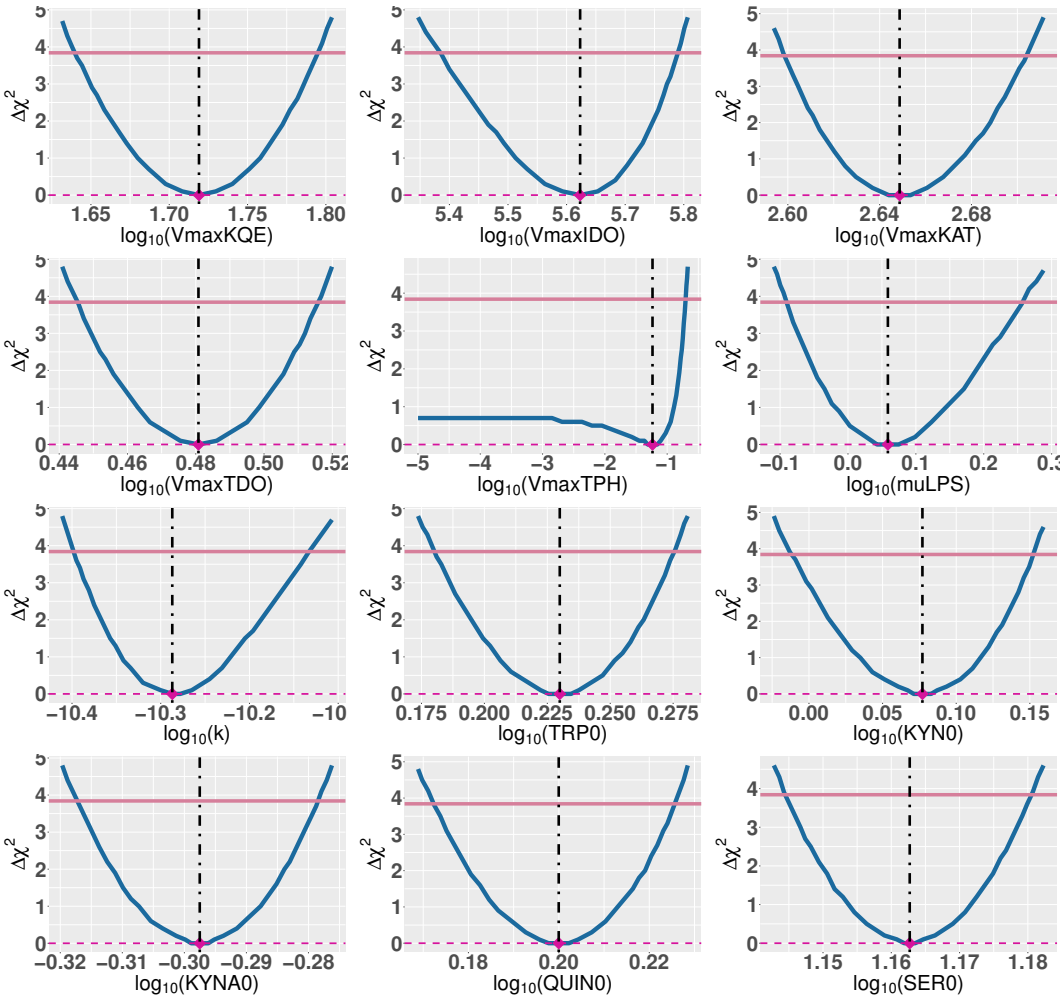

Figure 3.2.: **Identifiability analysis of parameters of the LPS model fitted to data of LPS experiment I:** An identifiability analysis was performed for the parameters fitted to data of LPS experiment I presented in Table C.1. The x-axis is depicted in log_{10} scale and *species*0 are the fitted initial values of the corresponding species. IDO - indoleamine 2,3-dioxygenase, k - parameter of tumor necrosis factor α activation, KAT- kynurenine aminotransferase, KQE- kynurenine to quinolinic acid degrading enzyme, KYN- kynurenine, KYNA - kynurenic acid, LPS - lipopolysaccharides, QUIN - quinolinic acid, SER - serotonin, TDO - tryptophan 2,3-dioxygenase, TPH - tryptophan hydroxylase, TRP - tryptophan

Parameter Validation on an Independent Data Set of Lipopolysaccharide-Treated Pigs The fitted parameters were validated by fixing those parameters in the LPS model. Initial values were excluded from fixing and were fitted to the data of LPS experiment II because differences in the initial levels of the different species show a considerable variability. The simulation of the LPS model with parameters fitted to the data of LPS experiment II, including 648 data points, yielded a LL value of -1191.488, an AIC value of -1169.488 and a BIC value of -1120.275 for parameter validation. The simulations with the validated parameters are presented in Figure 3.3. Parameters fitted to the data of LPS experiment I can represent the dynamics of data measured in LPS experiment II. The simulations correspond to the data. Both simulations yielded LL, AIC, and BIC values in the dimension of -10^3, which is comparable to the results of the simulations on data of LPS experiment I.

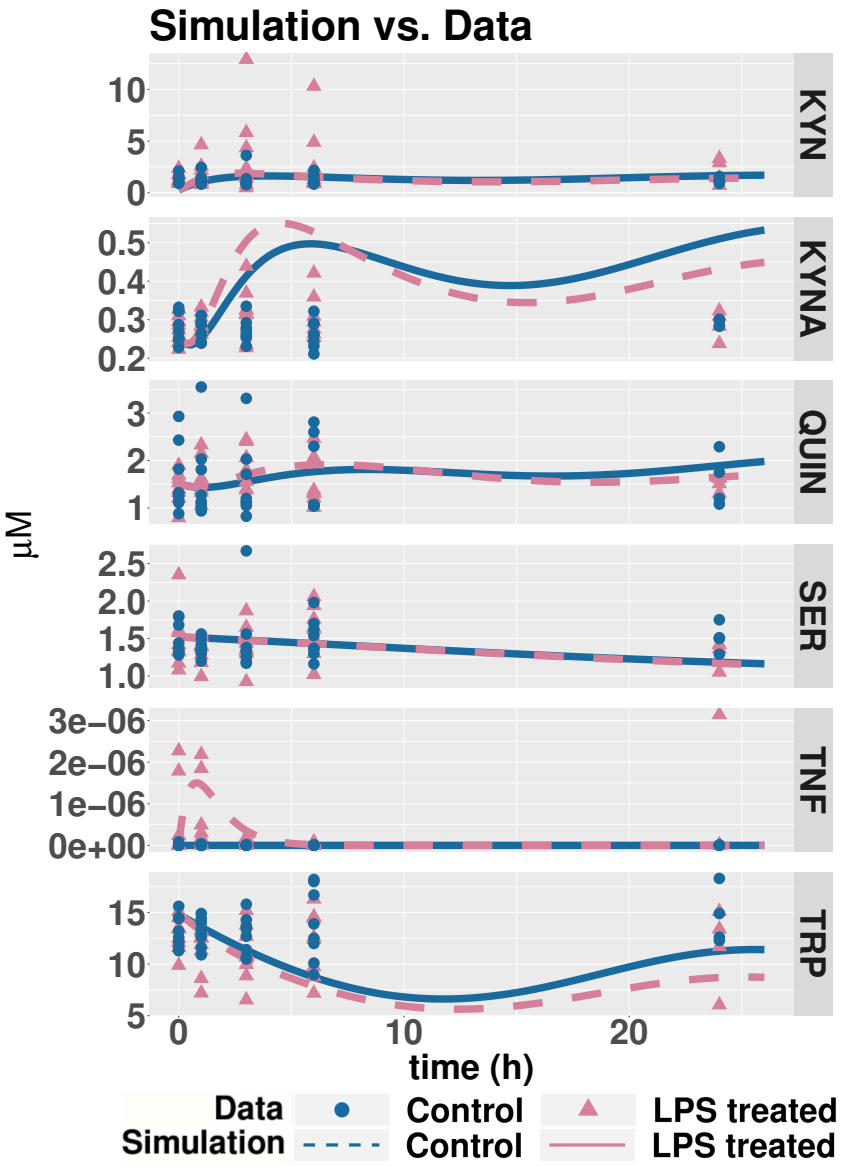

Figure 3.3.: **Simulations with parameters fitted to data of LPS experiment I, applied to LPS experiment II for validation:** Based on the LPS model and data of LPS experiment I(see Figure A.2 in the appendix A), parameters were fitted. Those parameters were then fixed in the LPS model, which was applied to the data measured in LPS experiment II (presented in Figure A.3 in the the appendix A) for parameter validation. Pigs were treated at 0 h with LPS and were starved between 0 h and 6 h. Half of the pigs were sacrificed at 6 h. The immolation of pigs decreased the group size from twelve to six pigs for LPS-treated pigs, and NaCl-treated pigs. KYN - kynurenine, KYNA - kynurenic acid, QUIN - quinolinic acid, SER - serotonin, TNF - tumor necrosis factor α, TRP - tryptophan

Parameter Validation on Data of a Selection of Lipopolysaccharide-Treated Pigs
Validation of parameters of Table C.1 was also performed on data of 1-MT/LPS experiment, subset LPS-treated pigs consisting of 236 data points, to check their applicability on those data. Therefore, the fitted parameters were fixed in the LPS model, except the initial values, because differences in the value levels of the different species show a considerable variability. The parameter fitting yielded a LL value of 4704448893, an AIC value of 4704448915, and a BIC value of 4704448953. These values are in the dimension of 10^9. Since comparing these results to the simulations based on data from LPS experiment I and II, which are in a dimension of -10^3, a huge difference is given. This difference shows, that the parameters fitted to the data of LPS experiment I cannot be validated on the data of 1-MT/LPS experiment, subset LPS-treated pigs. This fact can also be retraced by the simulations shown in Figure 3.4.

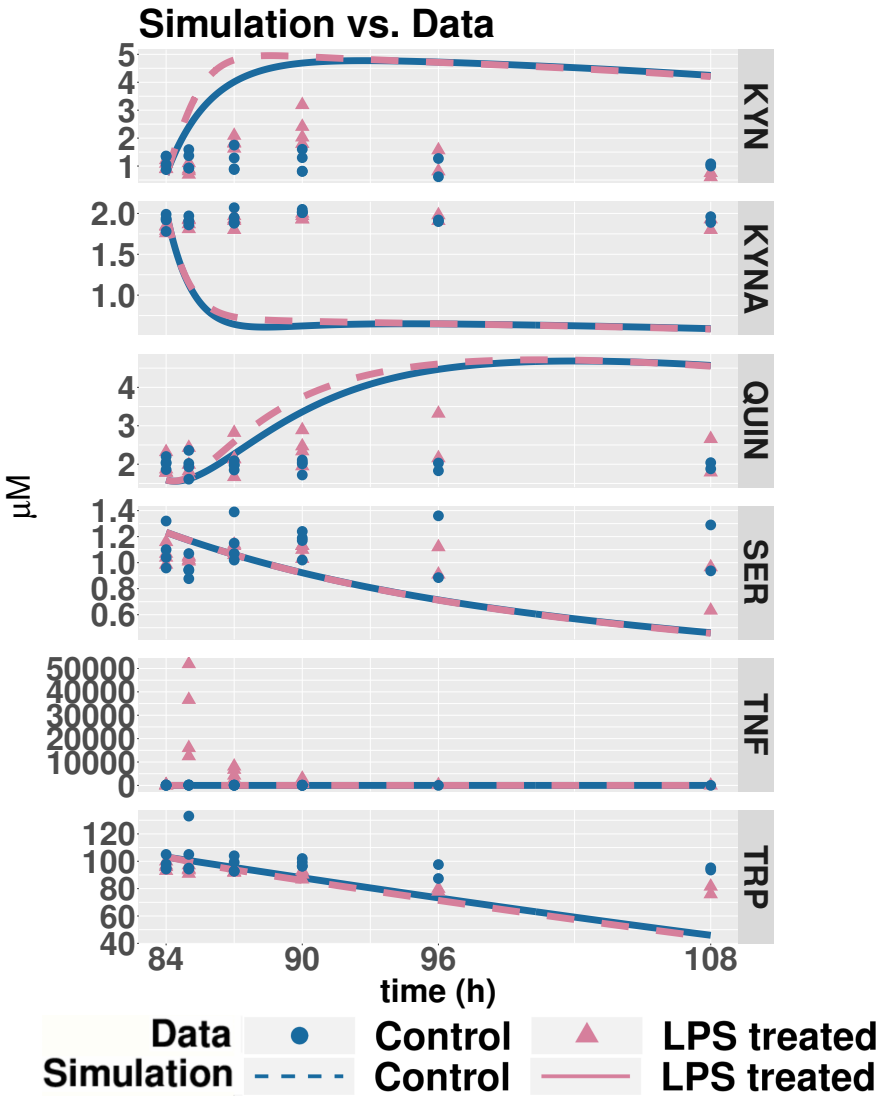

Figure 3.4.: **Simulations with parameters fitted to data of LPS experiment I, applied to 1-MT/LPS experiment, subset LPS-treated:** The parameters of the LPS model (see Figure 2.2) were fitted to the data of LPS experiment I (see Figure A.2 in the appendix A). These parameters were fixed in the LPS model and applied to the data measured in 1-MT/LPS experiment, subset LPS-treated pigs (presented in Figure A.7 in the appendix A) for parameter validation. Pigs were treated at 84 h with LPS and were starved the whole time. Half of the pigs were sacrificed at 90 h. The immolation of pigs decreased group size from four pigs to two pigs for LPS-treated pigs and NaCl-treated pigs. KYN - kynurenine, KYNA - kynurenic acid, QUIN - quinolinic acid, SER - serotonin, TNF - tumor necrosis factor α, TRP - tryptophan

3.1.2. Calculations of Parameters by Using a Selection of Lipopolysaccharide-Treated Pigs

Additionally, parameters of the LPS model were fitted to the data of 1-MT/LPS experiment, subset LPS-treated pigs, because a validation of parameters fitted to the data of LPS experiment I failed. To determine parameters, which were fixed in the models of the different hypotheses, parameters of the LPS model were fitted to the data of 1-MT/LPS experiment, subset LPS-treated pigs. Those pigs were starved the whole time. Thus a TRP increase due to $FoodSupply$ was not included. The K_m values presented in Table 2.6 and $\mu_{LPS} = 1.145 \mu M/h$, estimated based on LPS experiment I data, were fixed in the LPS model. The simulations yielded a LL value of 3167997327, an AIC value of 3167997365, and a BIC value of 3167997431. These values are in the dimension of 10^9. This numbers are comparable to the parameter validation in section 3.1.1. The simulations with the fitted parameters are shown in Figure 3.5.
The calculated parameters are presented in the appendix C in column II. However, those parameters do not fit the data, except the simulations of NaCl-treated pigs are comparable for TRP, QUIN and TNF-α to the data.
This discrepancy is explainable by the results of the identifiability analysis of the parameters. The calculated parameters are not identifiable as shown in Figure 3.6.

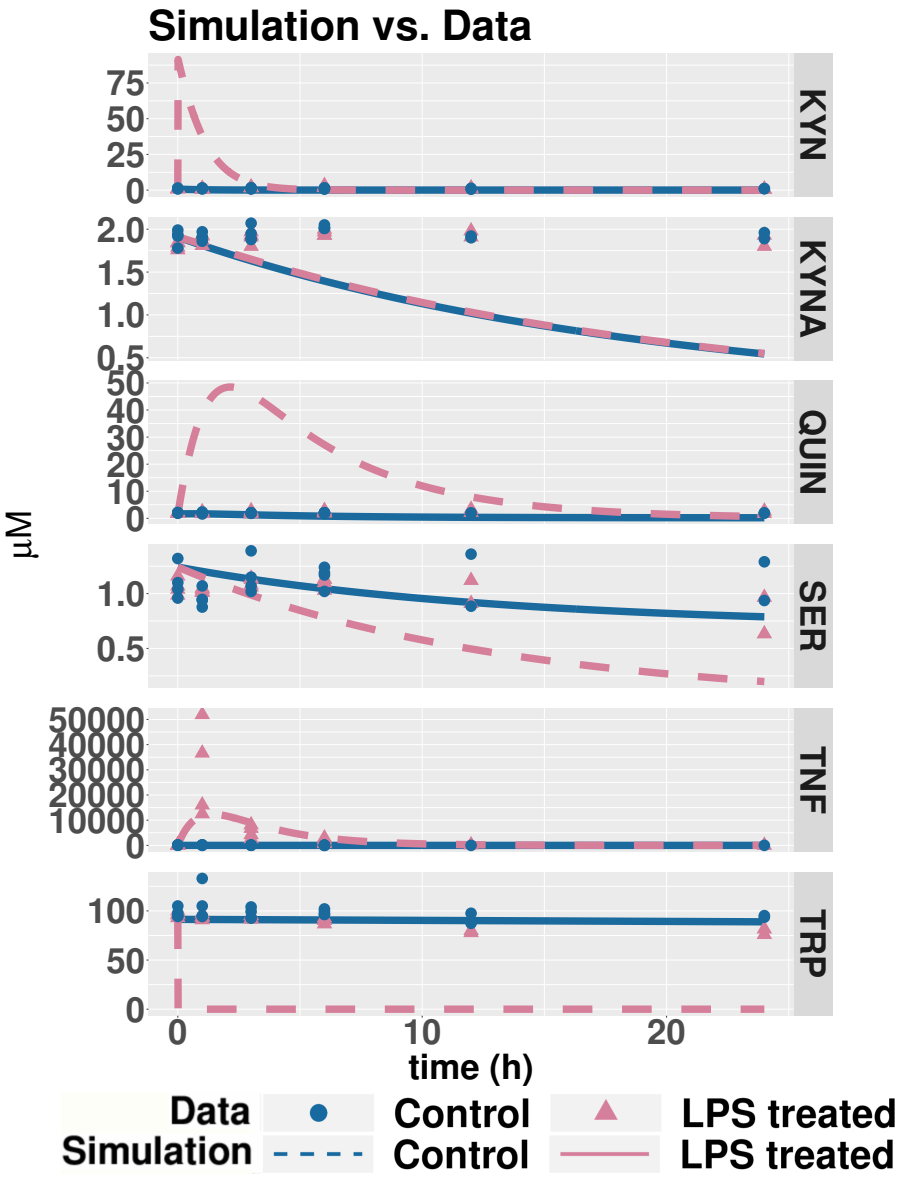

Figure 3.5.: **Simulations with parameters fitted to data of 1-MT/LPS experiment, LPS-treated pigs:** The parameters of the LPS model were fitted to the data of 1-MT/LPS experiment, LPS-treated pigs (see Figure A.7 in the appendix A). The simulations are shown in solid and dashed lines. The data are shown as triangles and dots. Pigs were treated at 84 h with LPS and were starved the whole time. Half of the pigs were sacrificed at 90 h. The immolation of pigs decreased the group size from four pigs to two pigs for LPS-treated pigs, and NaCl-treated pigs. KYN - kynurenine, KYNA - kynurenic acid, QUIN - quinolinic acid, SER - serotonin, TNF - tumor necrosis factor α, TRP - tryptophan

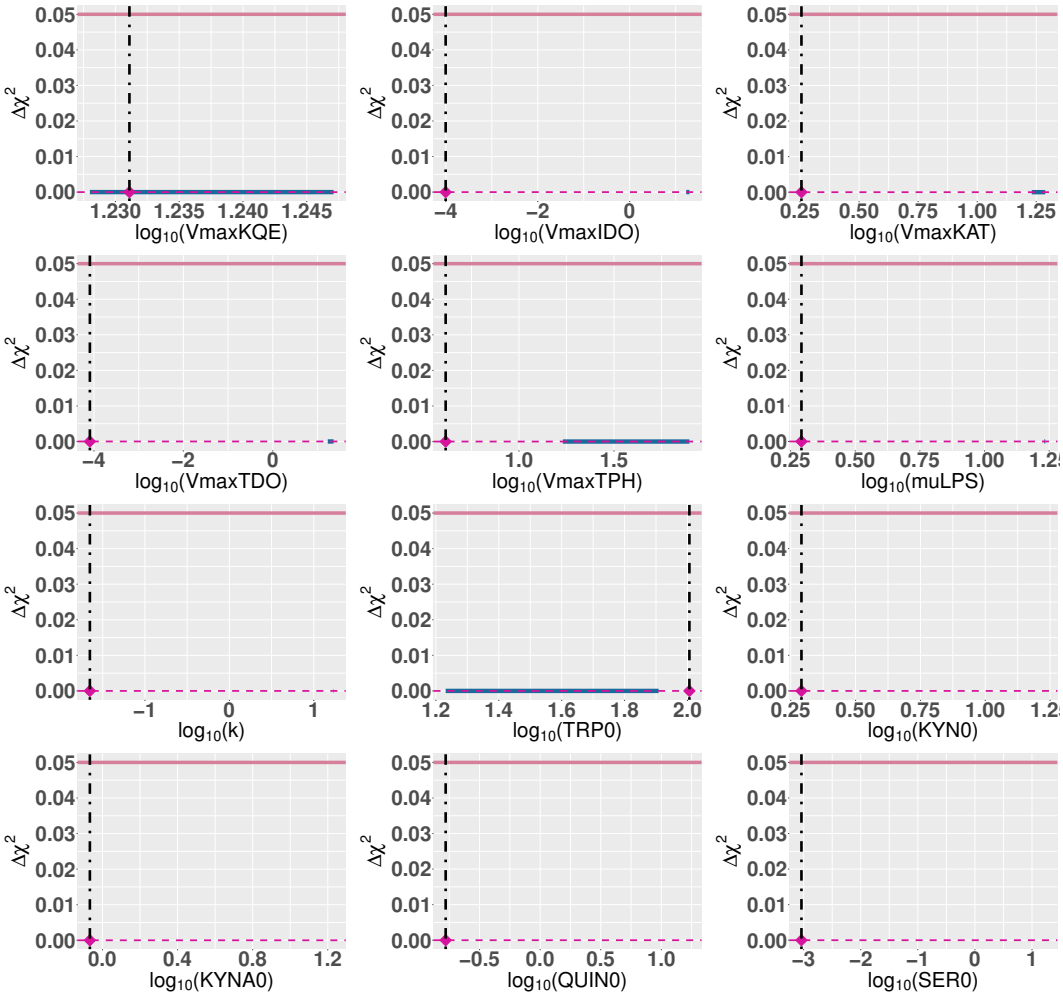

Figure 3.6.: **Identifiability analysis of parameters of the LPS model fitted to data of 1-MT/LPS experiment, LPS-treated pigs:** An identifiability analysis was performed for the parameters fitted to data of LPS experiment I presented in Table C.1. The x-axis is depicted in log_{10} scale, *species*0 are the fitted initial values of the corresponding species. IDO - indoleamine 2,3-dioxygenase, k - parameter of tumor necrosis factor α activation, KAT- kynurenine aminotransferase, KQE- kynurenine to quinolinic acid degrading enzyme, KYN- kynurenine, KYNA - kynurenic acid, LPS - lipopolysaccharides, QUIN - quinolinic acid, SER - serotonin, TDO - tryptophan 2,3-dioxygenase, TPH - tryptophan hydroxylase, TRP - tryptophan

3.1.3. Estimation of Parameters fitted to Data of a Selection of Lipopolysaccharide-treated Pigs by a Parameter Scan

Parameters of the LPS model were fitted 100 times to the data of 1-MT/LPS experiment, subset LPS-treated pigs according to approach 3. 100 fits were performed because the parameter fitting to data of 1-MT/LPS experiment, subset LPS-treated pigs failed (see section 3.1.2). Pigs of the 1-MT/LPS experiment, subset LPS-treated pigs, were starved the whole time. Thus a TRP increase due to $FoodSupply$ was not included. The K_m values presented in Table 2.6 and $\mu_{LPS} = 1.145 \mu M/h$, estimated based on data from LPS experiment I, were fixed in the LPS model. The simulations yielded LL values with a mean of 3115415212, a mean AIC value of 3115415252, and a mean BIC value of 3115415322, and all have the same standard deviation of 22893.09. These values are in the dimension of 10^9. The simulations with the lowest LL value is presented in Figure 3.7. Moreover, the mean values and standard deviation of the 100 calculated parameters are shown in the appendix C. The mean values are shown in column IV, and the standard deviation in column VI.

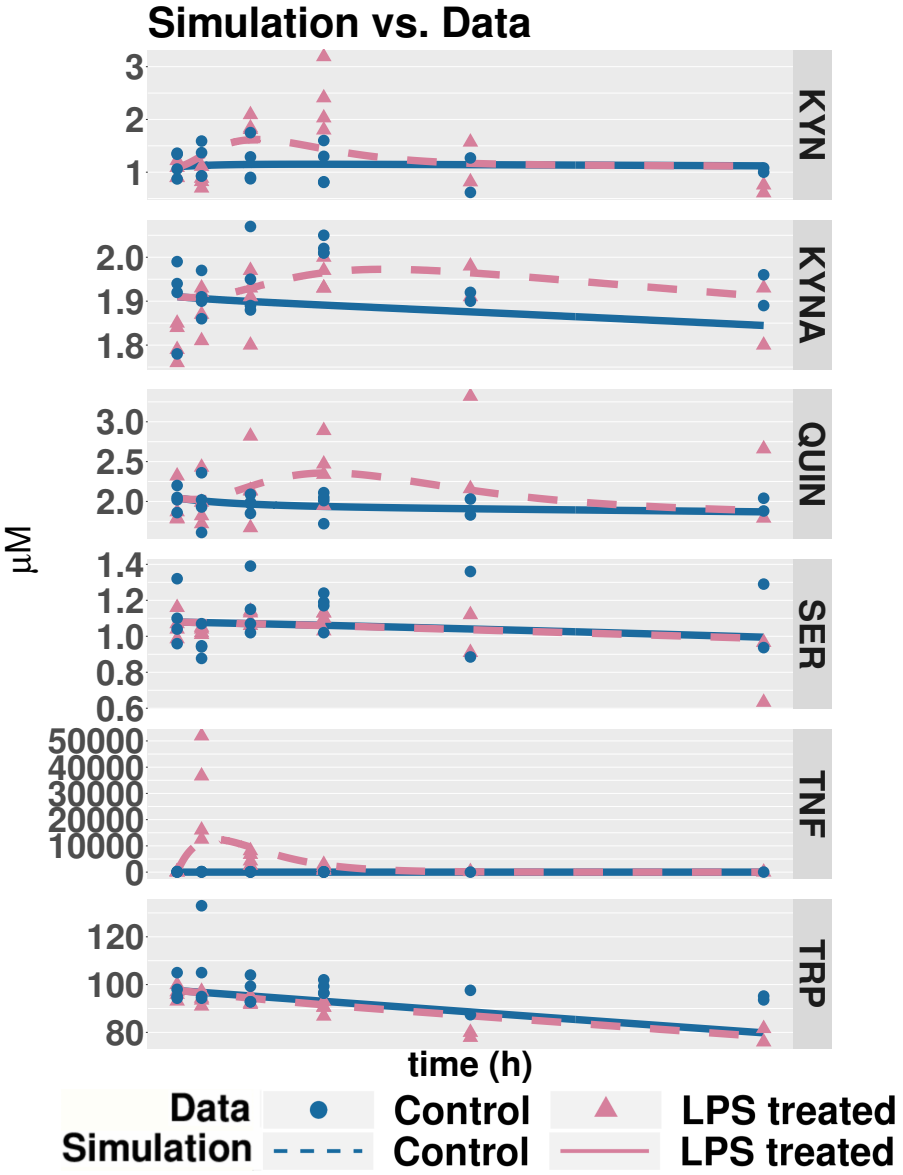

Figure 3.7.: **Simulations with parameters fitted to the data measured in 1-MT/LPS experiment, LPS-treated pigs, 100 times:** The parameters of the LPS model were fitted to the data of 1-MT/LPS experiment, LPS-treated pigs (see Figure A.7 in the appendix A). The simulations are shown in blue and purple lines. The data are shown in blue and in purple triangles and dots. Pigs were treated at 84 h with LPS and were starved the whole time. Half of the pigs were sacrificed at 90 h. The immolation of pigs decreased the group size from four pigs to two pigs for LPS-treated pigs, and NaCl-treated pigs. KYN - kynurenine, KYNA - kynurenic acid, QUIN - quinolinic acid, SER - serotonin, TRP - tryptophan

3.1.4. Sensitivity Analysis of Kynurenic Acid

Because of KYNA's importance in immunity and the effects of 1-MT on KYNA, a sensitivity analysis of the LPS model was performed, and parameters with the most significant impact on KYNA levels were determined. Here, the method „Morris Screening" was used to calculate the impact of the degradation parameters and V_{max}^{enzyme} parameters. The LPS model and parameters fitted to the data of LPS experiment I was used to perform the sensitivity analysis. μ was calculated for 24 h (0 h to 24 h). Those values can also become negative if they have a negative impact on the KYNA level. A plot of μ for KYNA is presented in Figure 3.8.

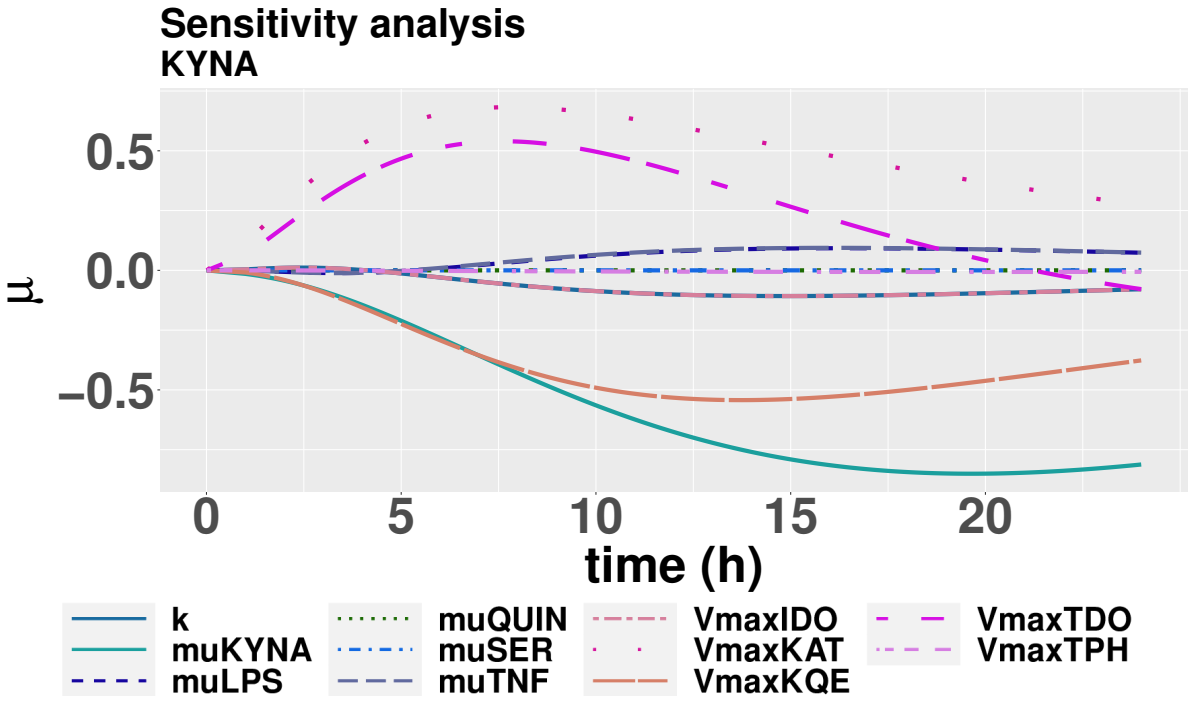

Figure 3.8.: **Sensitivity Analysis of KYNA:** Morris Screening was applied to the LPS model and parameters fitted to data of LPS experiment I. Only V_{max}^{enzyme}, degradation parameters μ, and k were investigated concerning their sensitivity. The impact on the KYNA level is shown as μ for a period of 24 h. IDO - indoleamine 2,3-dioxygenase, k - parameter of tumor necrosis factor α activation, KAT- kynurenine aminotransferase, KQE- kynurenine to quinolinic acid degrading enzyme, KYN- kynurenine, KYNA - kynurenic acid, LPS - lipopolysaccharides, QUIN - quinolinic acid, SER - serotonin, TDO - tryptophan 2,3-dioxygenase, TNF - tumor necrosis factor α, TPH - tryptophan hydroxylase, TRP - tryptophan

With decreasing maximal, absolute μ values, the following order of the impact of the parameters on KYNA's cencentration was determined:

1. $\mu_{KYNA} = 0.850572$
2. $V_{max}^{KAT} = 0.6826279$
3. $V_{max}^{KQE} = 0.5427479$
4. $V_{max}^{TDO} = 0.5398745$
5. $V_{max}^{IDO} = 0.1075437$
6. $k = 0.1074836$
7. $\mu_{TNF} = 0.09409497$
8. $\mu_{LPS} = 0.09247089$
9. $V_{max}^{TPH} = 0.006611762$
10. $\mu_{QUIN} = 1.366777 \cdot 10^{-7}$
11. $\mu_{SER} = 0$

The degradation rate of KYNA and the maximal velocity of KAT have the biggest impact on KYNA levels followed by the maximal velocity of KQE. Whereas, the lowest impact on KYNA levels was reported by the degradation of SER and QUIN and the maximal velocity of TPH.

3.1.5. Fitting Hypotheses to the Data of 1-Methyltryptophan/Lipopolysaccharide Experiment, Subset 1-Methyltryptophan-Treated Pigs

1-MT leads to increased TRP and KYNA cocentrations, while the intermediate metabolite KYN does not change [86]. There is no study explaining the degradation process of this phenomenon. Here, ODEs are applied to describe the 1-MT induced dynamics of TRP metabolites. Parameters calculated based on the data of LPS experiment I (approach 1) and the 1-MT/LPS experiment, LPS-treated pigs (approach 2), were fixed in the models of the different hypotheses (degradation parameters μ and V_{max} parameters). Afterward, the parameters of the models of the different hypotheses were fitted to the data of 1-MT/LPS experiment, subset 1-MT-treated pigs, first and second data set. Moreover, no parameters were fixed while the models of the hypotheses were fitted to the data of 1-MT/LPS experiment, subset 1-MT-treated pigs, first and second data set 100 times (approach 3). The mean value for LL, AIC, and BIC for each hypothesis was calculated and compared. The results of these three approaches are shown below.

Parameters Fixed to the Parameter Values Fitted to the Data of Lipopolysaccharide-Treated Pigs (Approach 1) Parameters were fixed to the parameter values fitted to the data of LPS experiment I (see Table C.1, approach 1). The models of the different hypotheses were fitted to the data of 1-MT/LPS experiment, subset 1-MT-treated pigs, to investigate their ability to reflect the dynamics of the TRP metabolism after 1-MT administration in pigs.
Data of 1-MT/LPS experiment, subset 1-MT-treated pigs, first data set include measurements for every 24 h. During this time, the pigs were fed, and $FoodSupply$ was included in the ODEs. By fitting the parameters of the LPS model to the data of LPS experiment I, a value of $26.6\mu M$ for NaCl-treated pigs was determined. Since pigs were fed in LPS experiment I only for 18 h, the TRP increase induced by $FoodSupply$ was adapted to 24 h. Thus, $FoodSupply$ was set to a value of $35.467\mu M$. Data of 1-MT/LPS experiment, subset 1-MT-treated pigs, second data set includes measurements in irregular, but more dense time intervals. During this time, the pigs were not fed and $FoodSupply$ was excluded from the ODEs. LL, AIC, and BIC values for simulations based on the first and the second data set are given in Table 3.2.

Table 3.2.: **LL, AIC, BIC values of different hypotheses fitted to data of LPS experiment I (approach 1)**

hypotheses	**LL**	**AIC**	**BIC**	**LL**	**AIC**	**BIC**
	First Data Set			Second Data Set		
classic	1627.47	1653.47	1704.83	364.67	392.67	452.22
Hyp 1	1583.12	1613.12	1672.38	366.08	398.08	466.14
Hyp 2	1527.15	1557.15	1616.41	**164.86**	**196.86**	**264.92**
Hyp 3	1577.91	1611.91	1679.07	165.64	201.64	278.21
Hyp 4	1528.89	1562.89	1630.05	165.64	201.64	278.21
Hyp 5	1580.50	1614.50	1681.66	165.64	201.64	278.21
Hyp 6	1496.26	1534.26	1609.32	167.46	207.46	292.53
Hyp 7	**1494.55**	**1528.55**	**1595.71**	166.67	202.67	279.23

The parameters of the models of the hypotheses were fixed to the parameter values, which were determined by fitting the LPS model to the data of LPS experiment I. The parameters of the models of the hypotheses with the fixed parameters were then fitted to the data of 1-MT/LPS experiment, subset 1-MT-treated pigs, on the first and the second data set. The lowest values are shown in bold numbers. AIC - Akaike Information Criterion, BIC - Bayesian information Criterion, Hyp - hypothesis, LL - Log-Likelihood.

For the first data set, the lowest LL, AIC, and BIC were calculated for Hyp 7. For the second data set, the lowest LL, AIC and BIC values were calculated for Hyp 2. In conclusion, Hyp 2 and 7 were three times the model, sufficiently representing the data. Simulations of all hypotheses for the first data set are presented in Figure 3.9 and for

the second data set in Figure 3.9.
LL, AIC, and BIC values are in the dimension of 10^3 for the first data set. For the second data set, the values are in the range of 10^2. For both data sets these values are much higher than the ones calculated for the parameters of the LPS model, which was fitted to LPS experiment I. Based on this and the simulations in Figure 3.11 and 3.12, one can conclude that the parameters fitted to the data of 1-MT/LPS experiment, subset LPS-treated pigs are not able to represent the dynamics of the TRP metabolism after 1-MT administration.

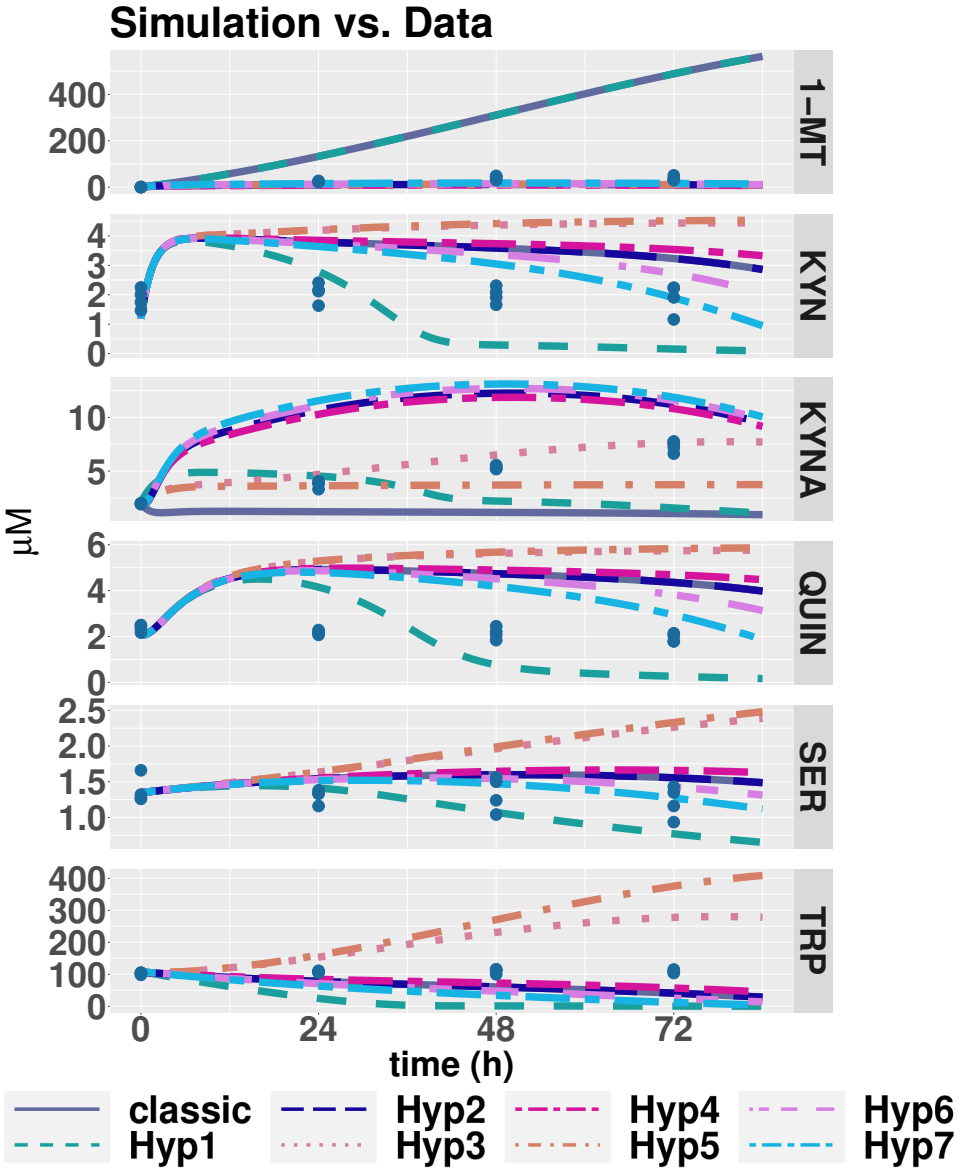

Figure 3.9.: **Simulations of all hypotheses with parameters fitted to data of 1-MT/LPS experiment, subset 1-MT-treated pigs, first data set (approach 1)** Parameters are fitted to the data of LPS experiment I in the models of the different hypotheses with fixed parameter values fitted to data of LPS experiment I. The models were then fitted to the data of 1-MT/LPS experiment, subset 1-MT-treated pigs, first data set (see Figure A.9). Pigs were treated at time points 0 h, 24 h, 48 h and 72 h with 1-MT and were starved between 72 h and 84 h. The data are shown in blue dots. The simulations are shown in lines. 1-methyltryptophan, KYN - kynurenine, KYNA - kynurenic acid, QUIN - quinolinic acid, SER - serotonin, TRP - tryptophan

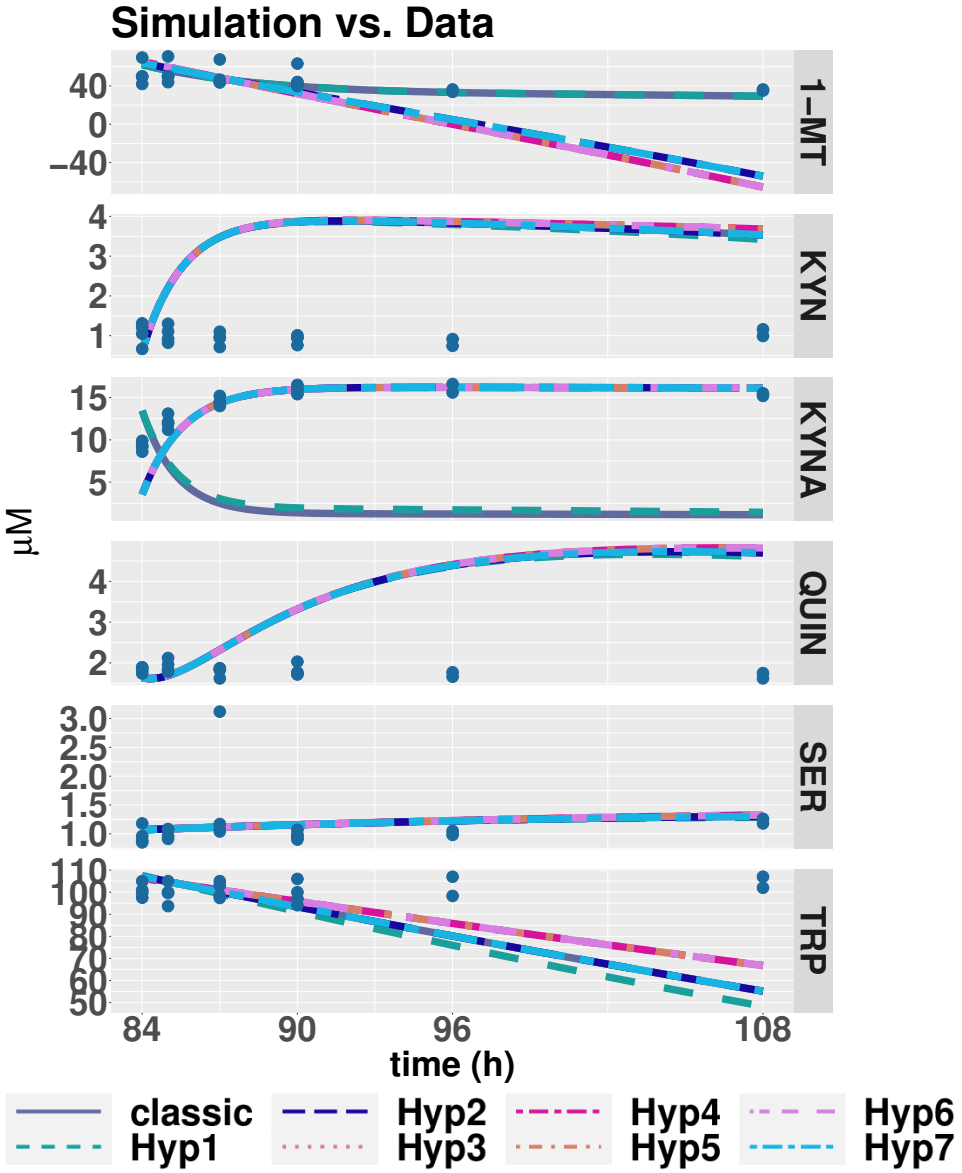

Figure 3.10.: **Simulations of all hypotheses with parameters fitted to data of 1-MT/LPS experiment, subset 1-MT-treated pigs, second data set (approach 1):** Parameters fitted to the data of LPS experiment I were fixed in the models of the hypotheses. Those were fitted to the data of 1-MT/LPS experiment, subset 1-MT-treated pigs, second data set (see Figure A.10 in the appendix A). Pigs were treated at 96 h with 1-MT and were starved the whole time. The data are shown in blue dots. The simulations are shown in lines. 1-methyltryptophan, KYN - kynurenine, KYNA - kynurenic acid, QUIN - quinolinic acid, SER - serotonin, TRP - tryptophan

Parameters Fixed to the Parameter Values Fitted to the Data of a Selection of Lipopolysaccharide-Treated Pigs (Approach 2) Parameters were fitted to the data of 1-MT/LPS experiment, subset LPS-treated pigs. Those parameters were fixed in the models of the different hypotheses (approach 2). Then the models were fitted to the data of 1-MT/LPS experiment, subset 1-MT-treated pigs, first and second data sets to investigate their ability to reflect the dynamics of the TRP metabolism after 1-MT administration in pigs.
The procedure of this *in silico* experiment differs from the one described in section 3.1.5 only in the parameter values used to fix model parameters. V_{max} and degradation parameters μ were fixed. The remaining parameters were fitted to the data of the 1-MT/LPS experiment, subset 1-MT-treated pigs, first and second data set. LL, AIC, and BIC values were determined and are shown in Table 3.3, including all hypotheses and the classical pathway.

Table 3.3.: **LL, AIC, BIC values of different hypotheses fitted to data of 1-MT/LPS experiment, subset 1-MT-treated pigs (approach 2)**

hypotheses	**LL**	**AIC**	**BIC**	**LL**	**AIC**	**BIC**
	First Data Set			Second Data Set		
classic	1397.71	1425.71	1481.02	67.39	97.39	161.20
Hyp 1	1298.57	1330.57	1393.78	10.40	44.40	116.71
Hyp 2	1264.31	1296.31	**1359.52**	-13.91	20.09	**92.41**
Hyp 3	1356.08	1392.08	1463.19	-9.00	29.00	109.82
Hyp 4	1266.15	1302.15	1373.27	**-24.59**	**13.41**	94.23
Hyp 5	1358.07	1394.07	1465.18	-9.00	29.00	109.82
Hyp 6	**1254.28**	**1294.28**	1373.29	-22.77	19.23	108.56
Hyp 7	1265.13	1301.13	1372.25	-23.77	14.23	95.06

The parameters of the models of the hypotheses were fixed to the parameter values, which were determined by fitting the LPS model to the data of 1-MT/LPS experiment, subset LPS-treated pigs. The parameters of the models of the hypotheses with the fixed parameters were then fitted to the data of 1-MT/LPS experiment, subset 1-MT-treated pigs, on the first and the second data set. The lowest values are shown in bold numbers. AIC - Akaike Information Criterion, BIC - Bayesian information Criterion, Hyp - hypothesis, LL - Log-Likelihood

For the first data set, the lowest LL and AIC were calculated for Hyp 6. The lowest BIC value was calculated for Hyp 2. For the second data set, the lowest LL and AIC values were calculated for Hyp 4. The lowest BIC values were calculated for Hyp 2. In conclusion, Hyps 2, 4 and 7 were the most likely ODE model twice each. Simulations of all hypotheses for the first data set are presented in Figure 3.11, and for the second data set in Figure 3.12. LL, AIC, and BIC values are in the dimension of 10^3 for the first data set. For the second data set, the values are in the range of 10^1. For both data

sets, these values are much higher than the ones calculated for the parameters of the LPS model, which was fitted to LPS experiment I. Based on this and the simulations in Figure 3.11, and 3.12, one can conclude that the parameters fitted to the data of 1-MT/LPS experiment, subset LPS-treated pigs cannot represent the dynamics of the TRP metabolism after 1-MT administration.

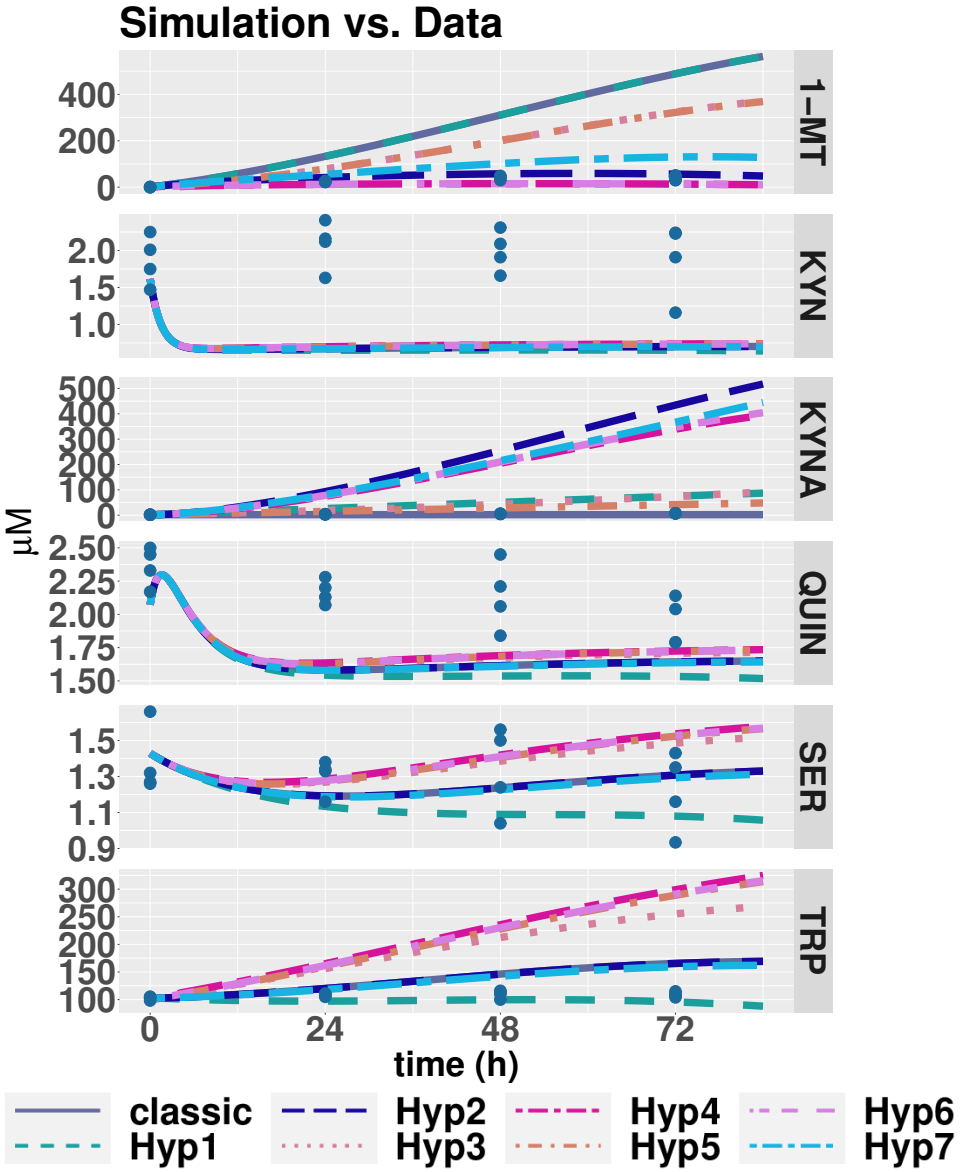

Figure 3.11.: **Simulations of all hypotheses with parameters fitted to data of 1-MT/LPS experiment, subset 1-MT-treated pigs, second data set (approach 2):** Parameters were fitted to the data of 1-MT/LPS experiment, subset LPS-treated pigs. The resulting parameters were fixed in the hypotheses' models and were fitted to the data of 1-MT/LPS experiment, subset 1-MT-treated pigs, first data set. Pigs were treated at 0 h, 24 h, 48 h, and 72 h with 1-MT and were starved in the time frame between 72 h and 84 h. The data are depicted in blue dots. The simulations are in lines. 1-methyltryptophan, KYN - kynurenine, KYNA - kynurenic acid, QUIN - quinolinic acid, SER - serotonin, TRP - tryptophan

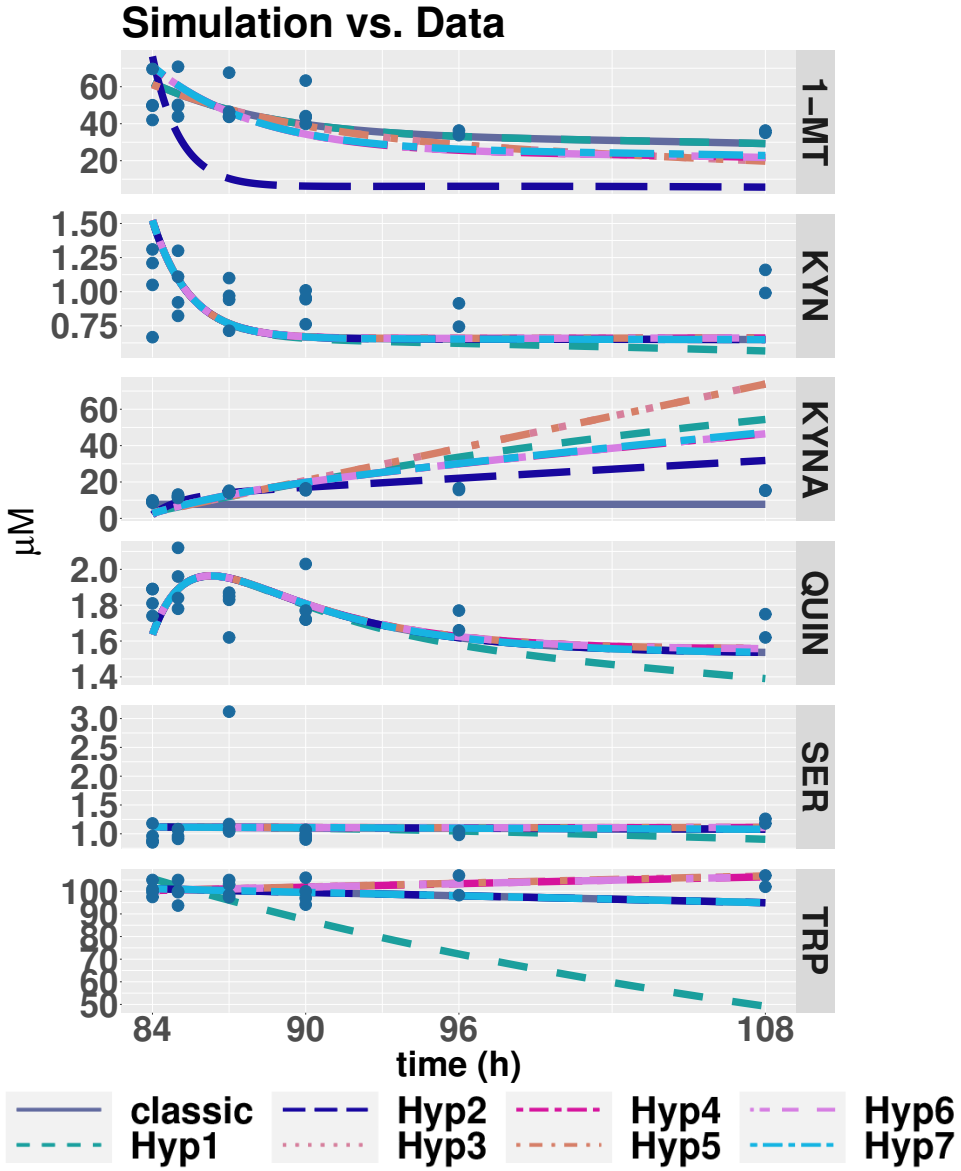

Figure 3.12.: **Simulations of all hypotheses with parameters fitted to data of 1-MT/LPS experiment, subset 1-MT-treated pigs, second data set (approach 2):** Parameters fitted to 1-MT/LPS experiment, subset 1-MT-treated pigs were fixed in the models of the hypotheses. The remaining parameters were fitted to the data of 1-MT/LPS experiment, subset 1-MT-treated pigs, second data set (see Figure A.10). Pigs were treated at 96 h with 1-MT and were starved the whole time. The data are depicted in blue dots. The simulations are in lines. 1-methyltryptophan, KYN - kynurenine, KYNA - kynurenic acid, QUIN - quinolinic acid, SER - serotonin, TRP - tryptophan

Parameters Fitted to the Data of a Selection of 1-Methyltryptophan-Treated Pigs Using a Parameter Scan (Approach 3) If parameters were fixed to parameter values obtained from parameter fits of the LPS model to the data of LPS experiment I or 1-MT/LPS experiment, subset LPS-treated pigs, the data of 1-MT/LPS experiment, subset 1-MT-treated pigs, first and second data set did not fit the data. Thus, parameters of the models of the different hypotheses have to be fitted to the data of 1-MT/LPS experiment, subset 1-MT-treated pigs, first and second data set. It was already shown that several parameters of the LPS model were not identifiable. Therefore, parameters of the models of the different hypotheses were fitted 100 times.
Again, this procedure is very similar to the one presented in section 3.1.5, except the parameter values of V_{max}^{enzyme} and degradation parameters μ were not fixed. The parameter fitting led to 100 parameter sets, and 100 LL, AIC, and BIC values. To determine which hypotheses is the most likely one, the AIC values of the 100 parameter fits were compared. In the following, the results of this comparison are shown.

First Data Set: The 100 AIC values are summarized in a box plot in Figure 3.13. The lowest values were calculated for Hyp 1, 2, and 3, at which the median AIC values were calculated for Hyp 7.

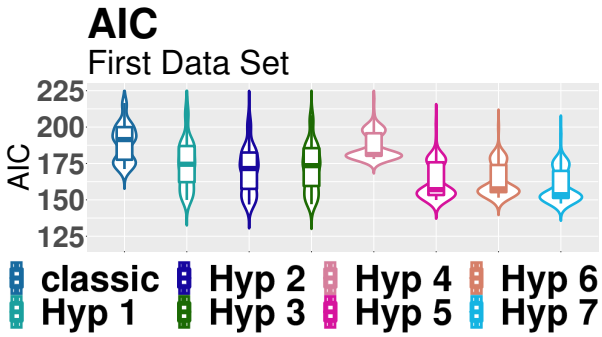

Figure 3.13.: **Boxplot of AIC values of all hypotheses fitted 100 times to the data of 1-MT/LPS experiment, subset 1-MT-treated pigs, first data set (approach 3):** The box plot depicts the results of the AIC values. Those values were obtained by 100 parameter fits to models of the hypothesis. The curve around the box plot shows the distribution of the data and is mirrored at the whiskers. AIC - Akaike Information Criterion, Hyp - hypothesis

A Kruskal-Wallis test was performed for AIC values for results based on data of 1-MT/LPS experiment, subset 1-MT-treated pigs, first data set, to determine whether there are significant differences between the AIC values of the seven hypotheses. A significant difference was detected ($p < 2.210^{-16}$). Subsequently, a pairwise comparison

with the Mann-Whitney-Wilcoxon test was conducted to find the hypotheses which differ from each other in their AIC value. P-values were corrected with Benjamini-Hochberg and are presented in Table 3.5.
Significant differences of the AIC values were found for every pair of hypotheses, except for the pairs of Hyp 3 with Hyp 1, Hyp 3 with Hyp 2, and Hyp 4 with the classical pathway (classic). The test with Hyp 6 and Hyp 4 also reveals a non significant p-value. The mean LL, AIC, and BIC values are shown in Table 3.4.

Table 3.4.: **LL, AIC, BIC values of the classical pathway and all hypotheses fitted to the data of 1-MT/LPS experiment, first data set (approach 3)**

hypothesis	**mean**			**min**		
	LL	**AIC**	**BIC**	**LL**	**AIC**	**BIC**
classic	189.45	189.45	189.45	171.18	171.18	171.18
1	170.31	174.31	182.21	145.95	149.95	157.85
2	165.81	169.81	177.71	142.83	**146.83**	**154.74**
3	167.70	171.70	179.60	143.03	147.03	154.93
4	178.77	186.77	202.58	170.10	178.10	193.91
5	154.51	162.51	178.32	141.89	149.89	165.69
6	151.32	163.32	187.02	**139.48**	151.48	175.19
7	**151.26**	**159.26**	**175.07**	**139.48**	147.48	163.29

Parameters of the models of the hypotheses were fitted to the data of 1-MT/LPS experiment, subset 1-MT-treated pigs, first data set, with 100 iterations. The mean and the minimum values were calculated. The lowest values are shown in bold numbers. AIC - Akaike Information Criterion, BIC - Bayesian information Criterion, Hyp - hypothesis, LL - Log-Likelihood

The mean and minimal LL, AIC, and BIC values of the models, whose parameters were fitted to the data of 1-MT/LPS experiment, subset 1-MT-treated pigs, first data set are in a range of 10^2. These values are ten times lower than those obtained from the models fitted with fixed parameter values. Thus the parameter scan approach reveals better results for the parameter fit.
Hyp 7 is the most likely one because mean LL, AIC, BIC, and minimum LL values revealed the lowest values. Hyp 6, has the same value for the minimum LL value. Minimum AIC and BIC values revealed the lowest value for Hyp 2. Simulations of all hypotheses of the model with the lowest LL value are shown in Figure 3.14.

Table 3.5.: **p-values of pairwise comparison of AIC values for each hypothesis fitted to the data of 1-MT/LPS experiment, subset 1-MT-treated pigs, first data set, 100 times (approach 3)**

	classic	Hyp 1	Hyp 2	Hyp 3	Hyp 4	Hyp 5	Hyp 6	Hyp7
classic	-	$8.93 \cdot 10^{-11}$	$5.14 \cdot 10^{-15}$	$3.02 \cdot 10^{-12}$	$9.41 \cdot 10^{-01}$	$3.42 \cdot 10^{-22}$	$3.42 \cdot 10^{-22}$	$1.35 \cdot 10^{-27}$
Hyp 1	-	-	$1.1 \cdot 10^{-02}$	$1.04 \cdot 10^{-01}$	$7.4 \cdot 10^{-09}$	$2.46 \cdot 10^{-06}$	$1.26 \cdot 10^{-06}$	$3.62 \cdot 10^{-11}$
Hyp 2	-	-	-	$9.25 \cdot 10^{-02}$	$4.04 \cdot 10^{-12}$	$2.72 \cdot 10^{-03}$	$4.4 \cdot 10^{-03}$	$1.64 \cdot 10^{-06}$
Hyp 3	-	-	-	-	$3.08 \cdot 10^{-11}$	$2.15 \cdot 10^{-04}$	$4.84 \cdot 10^{-04}$	$4.46 \cdot 10^{-07}$
Hyp 4	-	-	-	-	-	$4.83 \cdot 10^{-29}$	$1.16 \cdot 10^{-25}$	$5.95 \cdot 10^{-32}$
Hyp 5	-	-	-	-	-	-	$1.04 \cdot 10^{-01}$	$1.03 \cdot 10^{-03}$
Hyp 6	-	-	-	-	-	-	-	$4.73 \cdot 10^{-05}$
Hyp 7	-	-	-	-	-	-	-	-

The parameters of the hypotheses were fitted 100 times to the data of 1-MT/LPS experiment, subset 1-MT-treated pigs, first data set (see Figure A.9). AIC values for each hypotheses were pairwise compared by the Mann-Whitnex-Wilcoxon test. The results for the reversed test (e.g. Hyp 1 - Hyp 2, the reversed test is than Hyp 2 - Hyp 1) are equal and are omitted here. Hyp - hypothesis

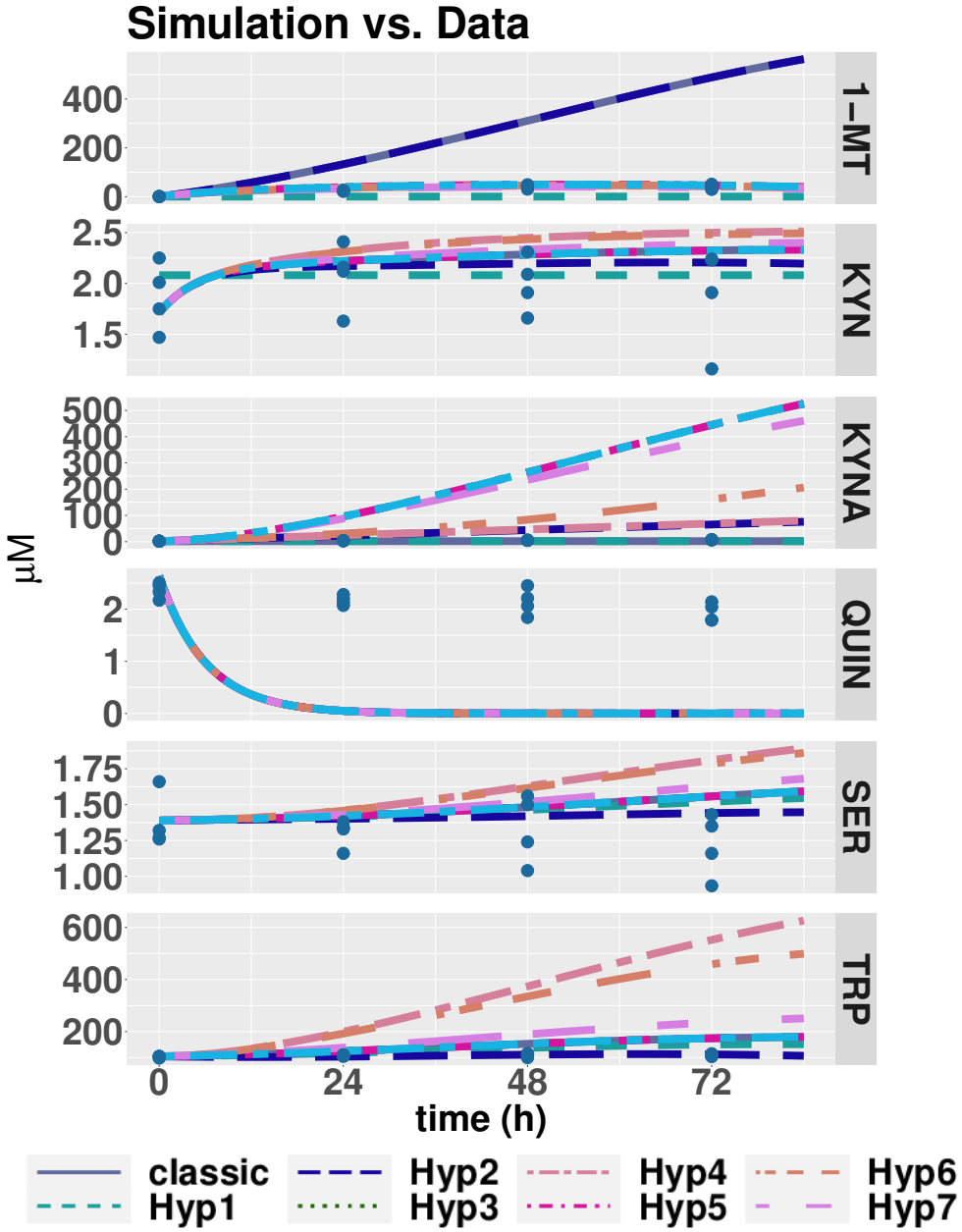

Figure 3.14.: **Simulations of all hypotheses fitted 100 times to the data of 1-MT/LPS experiment, subset 1-MT-treated pigs, first data set (approach 3):** Based on the 1-MT model, parameters were fitted 100 times to the data of 1-MT/LPs experiment, first data set. The model with the lowest AIC is shown. Pigs were treated at time points 0 h, 24 h, 48 h, 72 h with 1-MT and were starved in the time slot between 72 h and 84 h. The data are depicted in blue. 1-methyltryptophan, KYN - kynurenine, KYNA - kynurenic acid, QUIN - quinolinic acid, SER - serotonin, TRP - tryptophan

Second Data Set: The calculated characteristic numbers (mean and minimum LL, AIC, and BIC) are shown in Table 3.6 for comparison. By comparing mean and minimum LL and AIC values, Hyp 2 is the most probable. By comparing the minimum BIC value, the classical pathway (classic) is the most probable. The values range from -10^0 to 10^1. Compared to the results yielded by parameter fitting on 1-MT/LPS experiment, subset 1-MT-treated pigs, first data set, the characteristic numbers based on calculations on data without a TRP increase due to *FoodSupply* are lower.

Table 3.6.: **LL, AIC, BIC values of the classical pathway and all hypotheses fitted to data of 1-MT/LPS experiment, Second Data Set (approach 3)**

hypothesis	**mean**			**min**		
	LL	**AIC**	**BIC**	**LL**	**AIC**	**BIC**
classic	-4.71	-4.71	**-4.71**	-13.29	-13.29	**-13.29**
1	-12.12	-8.12	0.39	-19.32	-15.32	-6.81
2	**-16.31**	**-12.31**	-3.80	**-20.36**	**-16.36**	-7.85
3	-15.94	-11.94	-3.44	-20.13	-16.13	-7.63
4	-15.76	-7.76	9.25	-20.04	-12.04	4.98
5	-15.94	-7.94	9.08	-20.15	-12.15	4.87
6	-15.89	-3.89	21.63	-20.12	-8.12	17.41
7	-15.89	-8.30	8.71	-20.25	-12.25	4.77

Parameters of the models of the hypotheses were fitted to the data of 1-MT/LPS experiment, subset 1-MT-treated pigs, second data set, with 100 iterations. The mean and the minimum values were calculated. The lowest values are shown in bold numbers. AIC - Akaike Information Criterion, BIC - Bayesian information Criterion, LL - Log-Likelihood

A boxplot was created to determine whether there are significant differences between the AIC values of the hypotheses (see Figure 3.15). By comparing the AIC values shown in Figure 3.15, the most likely hypothesis is Hyp 2.

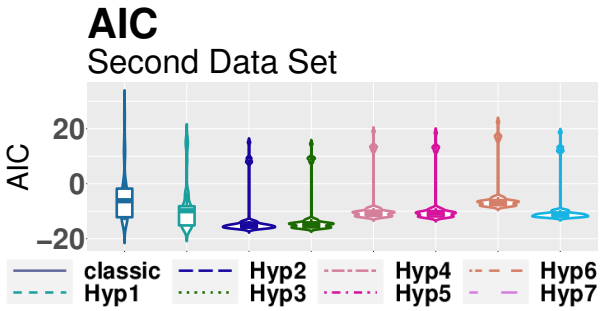

Figure 3.15.: **Boxplot of AIC values of all hypotheses fitted 100 times to the data of 1-MT/LPS experiment, subset 1-MT-treated pigs, second data set (approach 3):** The box plot shows the results of 100 iterations of the different hypotheses. The curve around the box plot shows the distribution of the data and is mirrored at the whiskers.

Moreover, a Kruskal-Wallis test was performed as it was done for the first data set. Again a significant difference was detected with a p-value smaller than 2.210^{-16}. To check for significant differences between the hypotheses, a pairwise comparison with the Mann-Whitney-Wilcoxon test was performed. The p-values, corrected with Benjamini-Hochberg, are presented in Table 3.7. All p-values are significant except the comparison of Hyp 4 with Hyp 1, Hyp 5 with Hyp 1, Hyp 6 with the classical pathway (classic), and Hyp 7 with Hyp 1. Simulations of all hypotheses are shown in Figure 3.16.

Table 3.7.: **p-values of pairwise comparison of AIC values for each hypotheses fitted to the data of 1-MT/LPS experiment, subset 1-MT-treated pigs, second data set, 100 times (approach 3)**

	classic	Hyp 1	Hyp 2	Hyp 3	Hyp 4	Hyp 5	Hyp 6	Hyp7
classic	-	$3.02 \cdot 10^{-06}$	$2.12 \cdot 10^{-21}$	$1.19 \cdot 10^{-20}$	$1.58 \cdot 10^{-04}$	$1.53 \cdot 10^{-04}$	$5.96 \cdot 10^{-01}$	$1.38 \cdot 10^{-04}$
Hyp 1	-	-	$5.04 \cdot 10^{-10}$	$1.41 \cdot 10^{-06}$	$7.91 \cdot 10^{-01}$	$5.79 \cdot 10^{-01}$	$3.83 \cdot 10^{-12}$	$2.12 \cdot 10^{-01}$
Hyp 2	-	-	-	$9.26 \cdot 10^{-03}$	$2.12 \cdot 10^{-21}$	$2.12 \cdot 10^{-21}$	$2.12 \cdot 10^{-21}$	$2.12 \cdot 10^{-21}$
Hyp 3	-	-	-	-	$2.12 \cdot 10^{-21}$	$2.12 \cdot 10^{-21}$	$2.12 \cdot 10^{-21}$	$2.12 \cdot 10^{-21}$
Hyp 4	-	-	-	-	-	$2.8 \cdot 10^{-02}$	$2.12 \cdot 10^{-21}$	$1.18 \cdot 10^{-03}$
Hyp 5	-	-	-	-	-	-	$2.12 \cdot 10^{-21}$	$1.41 \cdot 10^{-02}$
Hyp 6	-	-	-	-	-	-	-	$2.12 \cdot 10^{-21}$
Hyp 7	-	-	-	-	-	-	-	-

The parameters of the hypotheses were fitted 100 times to the data of 1-MT/LPS experiment, subset 1-MT-treated pigs, first data set (see Figure A.9). AIC values for each hypothesis were pairwise compared by the Mann-Whitnex-Wilcoxon test. The results for the reversed test (e.g. Hyp 1 - Hyp 2, the reversed test is than Hyp 2 - Hyp 1) are equal and are omitted here. Hyp - hypothesis

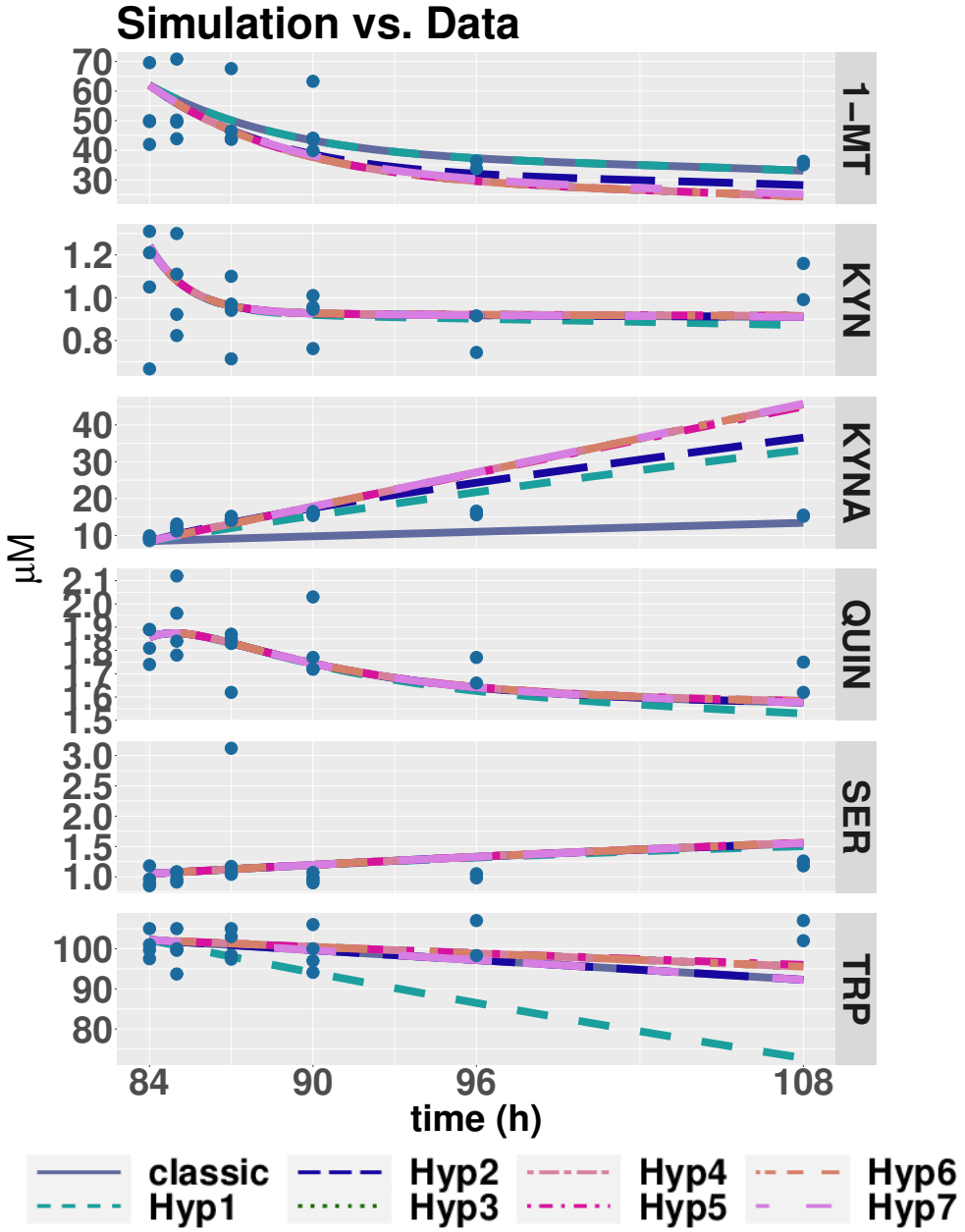

Figure 3.16.: **Simulations of all hypotheses fitted 100 times to the data of 1-MT/LPS experiment, subset 1-MT-treated pigs, second data set (approach 3):** Based on the 1-MT model, parameters were fitted 100 times to the data of 1-MT/LPS experiment, second data set. The model with the lowest AIC is shown. Pigs were treated at 96 h with 1-MT and were starved the whole time. The data are depicted in blue. 1-methyltryptophan, KYN - kynurenine, KYNA - kynurenic acid, QUIN - quinolinic acid, SER - serotonin, TRP - tryptophan

3.1.6. Results of the Validation Experiment

To validate Hyp 2, a biological experiment was developed and conducted by Elisa Wirthgen. Here, the experimental set-up is described, which is solely the work of Elisa Wirthgen.
1-MT, TRP, and KATIV were added in different combinations (1-MT and KAT, 1-MT, TRP and KAT, TRP, nothing) to PBS and medium. Medium contains TRP metabolites in addition to the given reactants 1-MT and TRP. In simulations, the enzyme KATIV is named KAT. TRP, KYN and KYNA were measured. The results are shown in Figure 3.17. Adding 1-MT and KATIV (KAT4) increased KYNA in the medium and PBS compared to the experiment without KATIV, indicating that 1-MT is degraded to KYNA. Since KYN did not change by adding KATIV, a direct degradation of 1-MT to KYNA can be assumed. Adding TRP, and KATIV increased KYN, while KYNA changed only slightly, compared to the experiment without KATIV. Thus, KATIV can catalyze the degradation of TRP to KYN. This degradation process was already reported by Han et al. [201], who used the KAT variant KATII. With these results, a direct degradation, as it is modeled in Hyp 2, is validated. TRP and KYN were measured in medium, without adding anything. Thus, both are included in the medium, but KYNA was not detected.

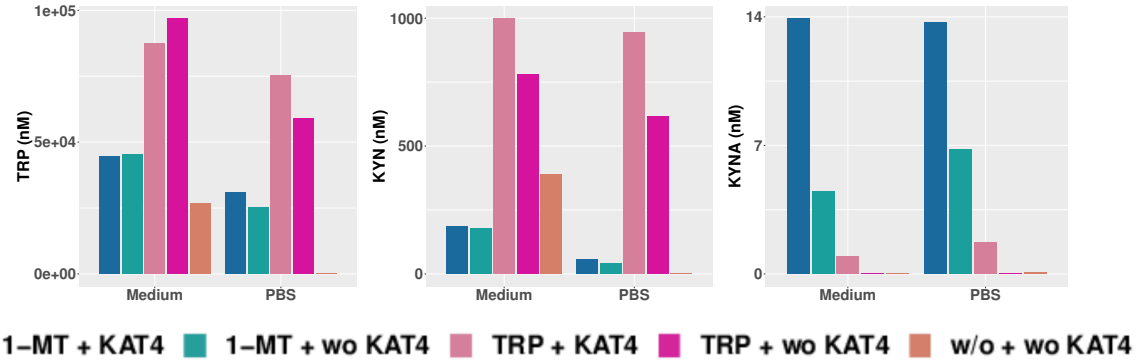

Figure 3.17.: **Results of the experimental to validate the results of the hypotheses:** Cell-free assays were performed in medium or PBS under different conditions. The results of the experiments with 1-MT are depicted in blue colored bars, with TRP in red colored bars, without adding anything in orange. The impact of KATIV (KAT4) was under investigation. Therefore experiments were conducted by adding KATIV. As a control, the same experiments were conducted without adding KATIV. The metabolites of the TRP metabolism TRP, KYN, and KYNA were measured, n=1. 1-methyltryptophan, KAT - kynurenine aminotransferase, KYN - kynurenine, KYNA - kynurenic acid, TRP - tryptophan

3.2. Modeling 1-Methyltryptophan's Ability to inhibit Indoleamine 2,3-Dioxygenase

To investigate the inhibitory effects of 1-MT on IDO, two models were applied to data of the 1-MT/LPS experiment, second data set. One model included a term of 1-MT induced IDO inhibition, and the other does not include a term for inhibitory effects in the system of ODEs. Parameter values fitted to the data of LPS experiment I (approach 1) and 1-MT/LPS experiment, subset LPS-treated pigs (approach 2), were fixed in both models. The most likely model was determined by comparing LL, AIC, and BIC values pointing to the model without inhibition for both parameter sets.
Moreover, degradation parameters and V_{max}^{enzyme} parameters were fitted to the data 100 times (approach 3). Also, mean and minimal LL, AIC, and BIC values were determined for all 100 fits and were compared. Results between mean and minimal values did not differ statistically. The comparison of mean LL, AIC, and BIC values revealed no inhibition. However, the model, including no inhibitory effects of 1-MT on IDO, does not represent the dynamics due to the high characteristic numbers.

3.2.1. Parameters Fixed to the Parameter Values Fitted to the Data of Lipopolysaccharide-Treated Pigs (Approach 1)

Parameters fitted to the data of LPS experiment I, were fixed in the model including inhibitory effects of 1-MT on IDO's activity, and in the model, without including inhibitory effects of 1-MT (approach 1). Then the parameters of the models were fitted to the data of the 1-MT/LPS experiment, second data set (without $FoodSupply$). LL, AIC, and BIC values were calculated, which are shown in Table 3.8.

Table 3.8.: **LL, AIC, BIC values of simulations with and without inhibition fitted to data of LPS experiment I**

	LL	AIC	BIC
with inhibition	9341367698	9341367742	9341367851
without inhibition	**9323927462**	**9341367740**	**9341367844**

The fitted parameters of the LPS model and the data of the LPS experiment were fixed in the model of hypothesis 2. Two models were compared. One model includes the inhibitory effects of 1-MT on IDO, the other does not. The lowest values are shown in bold numbers. AIC - Akaike Information Criterion, BIC - Bayesian information Criterion, LL - Log-Likelihood

Comparing the two model reveals the lowest values without inhibition. The values are in a range of 10^9 with and without inhibition. The corresponding simulations are presented in Figure 3.18.

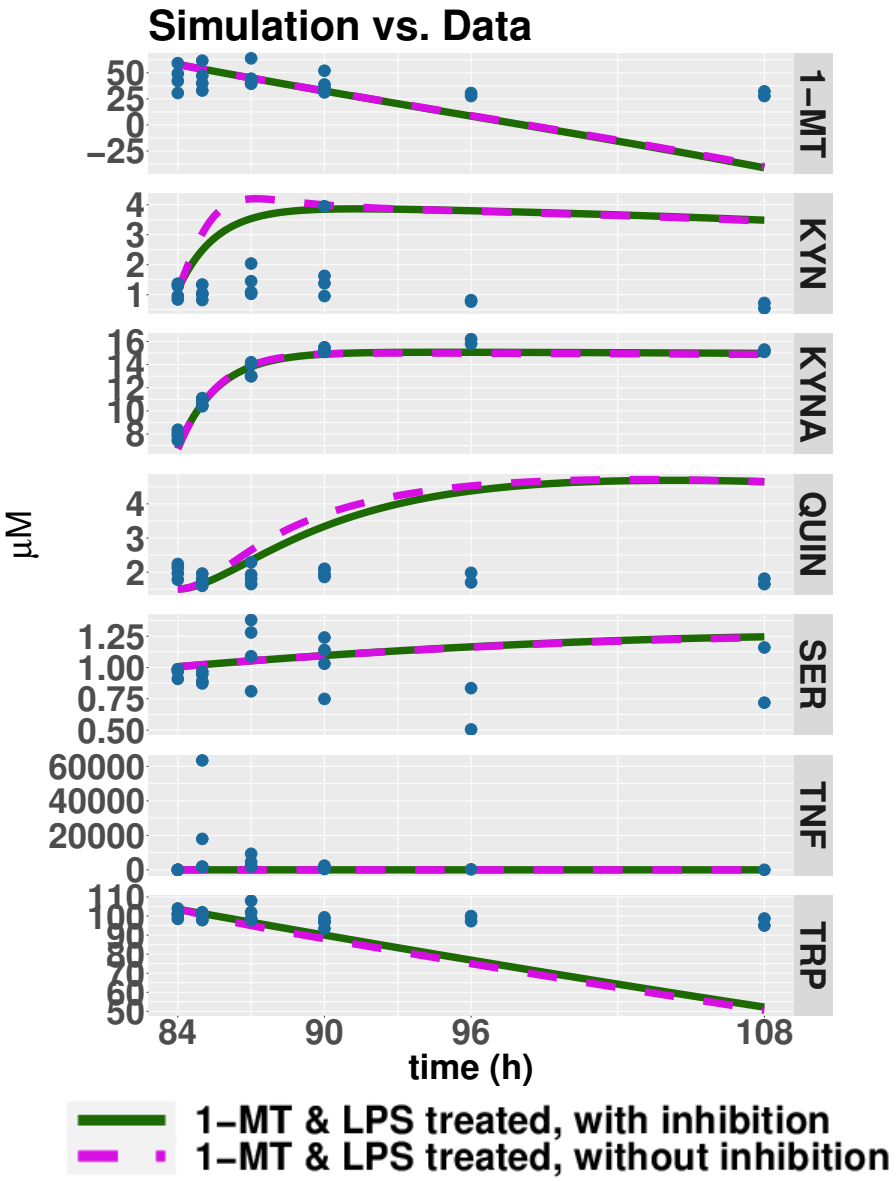

Figure 3.18.: **Simulations of the models with inhibition and without inhibition (approach 1):** Parameters fitted to data of LPS experiment I were fixed. The remaining parameters of the models, including and not including inhibitory effects of 1-MT on IDO, were fitted to the data of the 1-MT/LPS experiment, second data set. Pigs were treated at 96 h with 1-MT and were starved during the whole experiment. Simulations are shown in lines. Data are shown in blue dots. 1-methyltryptophan, KYN - kynurenine, KYNA - kynurenic acid, QUIN - quinolinic acid, SER - serotonin, TNF - tumor necrosis factor α, TRP - tryptophan

3.2.2. Parameters Fixed to the Parameter Values Fitted to the Data of a Selection of Lipopolysaccharide-Treated Pigs (Approach 2)

V_{max}^{enzyme} and degradation parameters, which were fitted to the data of 1-MT/LPS experiment, subset LPS treated pigs (approach 2), were fixed in two different models of 1-MT administration during infection. The first model includes 1-MT's inhibitory effects and the second omits those effects. The remaining parameters of the models were fitted to the data of the 1-MT/LPS experiment, second data set. The resulting LL, AIC, and BIC values are shown in Table 3.8.

Table 3.9.: **LL, AIC, BIC values of simulations with and without inhibition fitted to data of 1-MT/LPS experiment**

	LL	**AIC**	**BIC**
with inhibition	6906367180	6906367224	6906367333
without inhibition	**6893446416**	**6906367222**	**6906367326**

Fitted parameters of the LPS model and the data of 1-MT/LPS experiment, subset LPS-treated pigs were fixed in the model of hypothesis 2. Two models were compared. One model includes the inhibitory effects of 1-MT on IDO and the other does not. The lowest values are shown in bold numbers. AIC - Akaike Information Criterion, BIC - Bayesian information Criterion, LL - Log-Likelihood

The model without concerning inhibition reveals the lowest values. The values are in a range of 10^9 with and without inhibition. Compared with the models of 1-MT inhibition, whose parameters were fixed to parameter values fitted to the data of LPS experiment I, the LL, AIC, and BIC values, are higher. Simulations are presented in Figure 3.19.

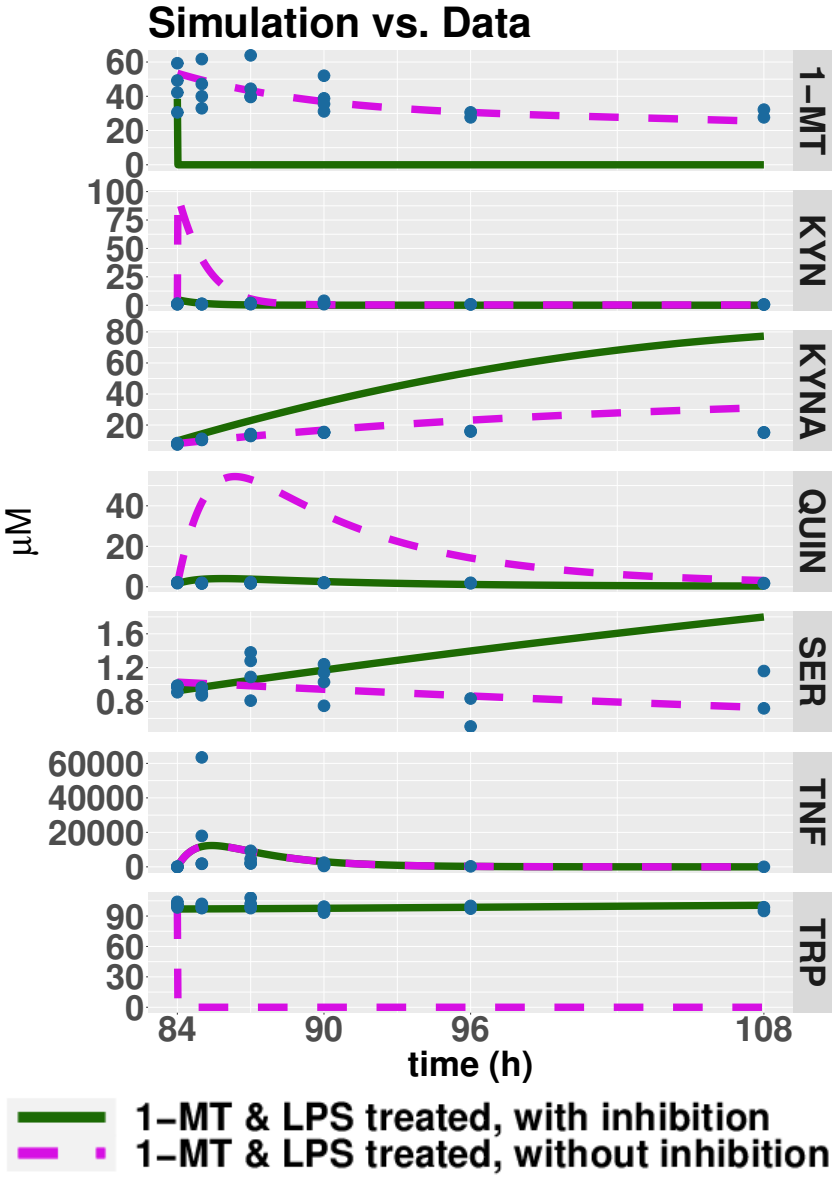

Figure 3.19.: **Simulations of the models with inhibition and without inhibition (approach 2):** Based on parameters fitted to data of 1-MT/LPS experiment, subset LPS-treated pigs, the parameters of the models with and without including inhibitory effects of 1-MT on IDO were fitted to the data of 1-MT/LPS experiment, second data set. Pigs were treated at 96 h with 1-MT and were starved during the whole experiment. Simulations are shown in lines. Data are shown in blue dots. 1-methyltryptophan, KYN - kynurenine, KYNA - kynurenic acid, QUIN - quinolinic acid, SER - serotonin, TNF - tumor necrosis factor α, TRP - tryptophan

3.2.3. Parameters Fitted to the Data of a Selection of 1-Methyltryptophan-Treated Pigs by a Parameter Scan (Approach 3)

In section 3.2.1 and section 3.2.2, parameters were fixed to parameter values obtained from parameter fits of the LPS model to the data of LPS experiment I (approach 1) or 1-MT/LPS experiment, subset LPS-treated pigs (approach 2). These set-ups led to fits with high LL, AIC, and BIC values when the parameters of the models with and without inhibitory effects were fitted to the data of 1-MT/LPS experiment, second data set. Thus, parameters of the model, including 1-MT's inhibitory effects and the parameters of the model without these effects, have to be fitted to the data of the 1-MT/LPS experiment, second data set. It was already shown that several parameters of the LPS model were not identifiable. In the models of IDO inhibition, the amount of parameters that were not fixed is higher compared to the models of the different hypotheses. Concluding, the parameters for these models are also not identifiable. The implementation of the identifiability analysis was abandoned. Consequently, a parameter scan was made. Thus, the models with and without including inhibitory effects of 1-MT were fitted 100 times to the data of the 1-MT/LPS experiment, second data set.
Parameter fitting led to 100 LL, AIC, and BIC values. Mean, median and minimal values were calculated. All values are shown in Table 3.10.

Table 3.10.: **LL, AIC, BIC, values of the LPS model extended by hypothesis 2 and with and without inhibition were fitted to data of the 1-MT/LPS experiment, second data set**

		LL	AIC	BIC
with inhibition	mean	$3.780471 \cdot 10^{17}$	$3.780471 \cdot 10^{17}$	$3.780471 \cdot 10^{17}$
	median	3719450000	3719450006	37194500214
	min	3719140000	3719140006	3719140021
without inhibition	mean	$3.723710 \cdot 10^{9}$	$3.723710 \cdot 10^{9}$	$3.723710 \cdot 10^{9}$
	median	3719455000	3719455002	3719455007
	min	3719140000	**3719140002**	**3719140007**

The parameters of the models with and without inhibitory effects of 1-MT were fitted 100 times to the data of the 1-MT/LPS experiment, second data set. The mean, median and minimum values were calculated. The lowest minimal values are shown in bold numbers. AIC - Akaike Information Criterion, BIC - Bayesian information Criterion, LL - Log-Likelihood

The lowest values were obtained for median LL values with inhibition. Mean, and minimum values do not differ. The lowest mean and minimum AIC and BIC values were obtained by modeling the IDO activation during 1-MT administration without an inhibition of IDO by 1-MT, at which the median AIC and BIC values are lower for the model including an inhibition.

To determine which model is the more likely one, the AIC values of the 100 parameter fits were compared. This comparison was done by a Kruskal-Wallis test. The p-values showed no significant difference between the two models (inhibition and no inhibition, $p = 0.2675$, the Figure D.1 of a box plot of the AIC values is shown in the appendix D). Median, and minimal LL, AIC, and BIC values are three times lower than the values calculated in section 3.2.1 and two times lower than those calculated in section 3.2.1. Simulations of the model with the lowest AIC are presented in Figure 3.20.

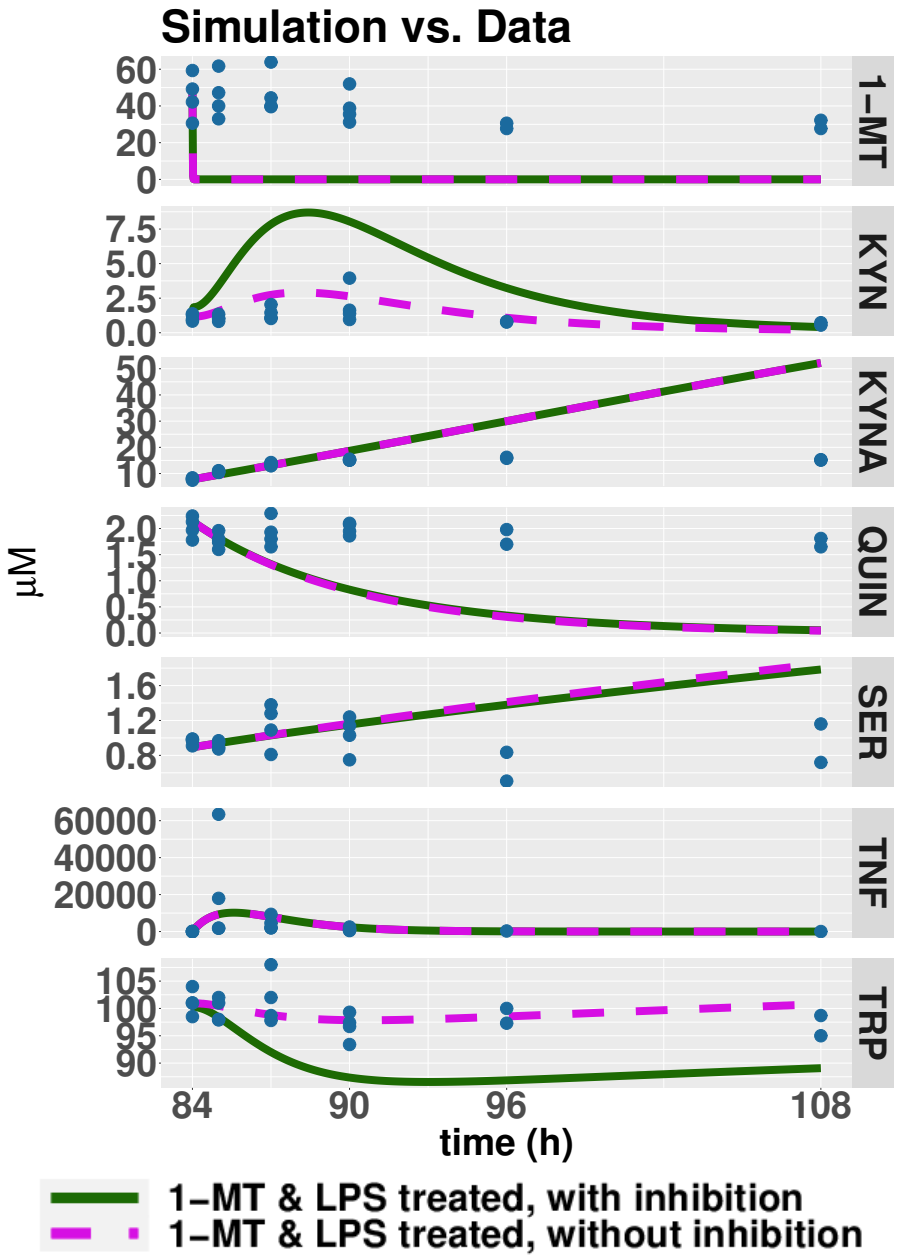

Figure 3.20.: **Simulations of the models with inhibition and without inhibition (approach 3):** The parameters of the models with and without inhibitory effects were fitted 100 times to the data of the 1-MT/LPS experiment. The model with the lowest AIC is shown. Pigs were treated at 84 h with LPS, and at 96 h with 1-MT. Pigs were starved during the whole time. Simulations are shown in lines. The data are shown in blue dots. 1-methyltryptophan, KYN - kynurenine, KYNA - kynurenic acid, QUIN - quinolinic acid, SER - serotonin, TNF-α - tumor necrosis factor α, TRP - tryptophan

4. Discussion

During 1-MT administration TRP and KYNA levels increase while the intermediate metabolite KYN does not change [85]. The administration of 1-MT led to increased survival of mice suffering from sepsis, compared to mice that were not treated with 1-MT [202]. Deciphering the mechanisms leading to those unexpected dynamics of the TRP metabolism will help to understand 1-MT's mode of action in the face of infection and will provide new drug targets. The 1-MT dependent increase of KYNA levels affect the parts of the immune system. KYNA's mode of action depends on whether inflammatory or homeostatic conditions prevail. In the face of infection, a dis-regulation of KYNA levels can lead to immunoparalysis, which is correlated with a poor prognosis [1].
In most studies of the TRP metabolism, only the KYN/TRP ratio or IDO mRNA is used to measure the IDO activity after 1-MT administration [203, 204]. Thus, measurements of KYNA levels still need to be included. In a couple of experiments, the KYNA increase after 1-MT administration was recognized [67, 86]. The processes mediating the altered TRP metabolite levels during 1-MT administration gained no attention. Thus, the aim of the thesis was to investigate possible degradation pathways of 1-MT as well as its ability to inhibit IDO to improve the understanding of 1-MT's mode of action.

4.1. 1-Methyltryptophan is Directly Degraded to Kynurenic Acid

To investigate the degradation processes of 1-MT, an ODE model of the TRP metabolism was developed and extended by an 1-MT administration. This ODE model was further extended by seven different hypothetical degradation processes based on the fact that KATII degrades KYN not only to KYNA [1], but also TRP to KYNA [201]. The results of this study revealed that 1-MT is directly degraded to KYNA (hyp 2). An *in vitro* cell-free assay experiment supported these findings. In this experiment, 1-MT or TRP with or without KATIV was added. TRP, KYN, and KYNA levels were measured. The experiment was only performed once; thus the results are only of low significance. In the following, all hypotheses are discussed in detail regarding their *in silico* and experimental results, and previous findings in the literature.

4.1.1. Classical Pathway

Hypotheses 1 to 7 are based on the ODE model of the classical pathway. These pathways assume that the TRP contamination of the drug 1-MT provokes the TRP increase. The

producer reported that the drug is contaminated with 5 % TRP [86]. Therefore, no additional degradation process was included in the system of ODEs. For this assumption, the degradation rates from TRP to KYN and from KYN to KYNA have to be equal. When parameters were fitted 100 times to the data of the 1-MT experiment (approach 3), 1-MT-treated pigs, second data set, the BIC of the classical pathway was the lowest one. The results of the cell-free essay experiment contradict these assumptions. By adding just TRP, TRP and KYN levels increased, but KYNA stayed at low levels. Therefore, the solely degradation of TRP via KYN to KYNA is unlikely.

4.1.2. Hypothesis 1

The finding of Han et al. [201] that TRP can be degraded to KYNA by KATII, was included in Hyp 1. This ODE model was never (LL, AIC, and BIC) the most likely one. Also, in the experiment where the enzyme KATIV instead of KATII was used, the findings of Han et al. [201] were not reproduced because adding TRP with and without KATIV leads to increases in TRP and KYN but not in KYNA levels.

4.1.3. Hypothesis 2

A direct degradation of 1-MT to KYNA (Hyp 2) was the most likely hypothesis in 50 % of the calculated LL, AIC, and BIC values. The validation experiment revealed that Hyp 2 is the most likely one since KYNA increase after 1-MT administration was high. After adding TRP, only low levels of KYNA were measured compared to the addition of 1-MT. There is no proof that 1-MT can be degraded to KYNA, and only assumptions can be made, about how KAT degrades 1-MT to KYNA. KAT is a transaminase [1], meaning that the α-amino nitrogen of an amino acid (here TRP respective 1-MT) is transferred to an α-keto acid with the synthesis of a second amino acid and a second α-keto acid [205]. An α amino nitrogen is a functional group of nitrogen (N) and hydrogen (H) [206]. 1-MT has two α-amino nitrogen groups, and KYNA has just one. A transfer of one α-amino nitrogen group seems plausible. A detailed description of this transamination is beyond the scope of this thesis.

4.1.4. Hypothesis 3

The assumption for Hyp 3 is that 1-MT is demethylated and TRP is generated. For this reaction, a demethylase is needed. To my knowledge, there are no reports of enzymes demethylating 1-MT. Hyp 3 did not reveal the lowest LL, AIC or BIC in any *in silico* experiment. In the validation experiment, TRP increased after 1-MT administration, and KYN and KYNA increased without adding the enzyme KATIV. Wirthgen et al. also proposed this[148]. The N-methyltryptophan ($N \in \mathbb{N}$) oxidase is able to demethylate its substrate, to which N-methyltryptophan is the best-known [207]. Thus, it is not distinguishable *in vivo* whether 1-MT is contaminated or demethylated. In cell-free experiments, it has to be clarified whether 1-MT can dissociate to TRP.

4.1.5. Hypothesis 4

Hyp 4 includes the degradation of TRP to KYNA (Hyp 1) and 1-MT to TRP (Hyp 3). It was the most likely hypothesis for LL and AIC values for approach 2. The validation experiment showed increases in TRP and KYNA concentrations after 1-MT administration with and without the addition of KATIV. It is a combination of hypotheses 1 and 3. The first hypothesis is possible since the degradation of TRP to KYNA was already reported [201]. Also, the demethylation of 1-MT to TRP is possible [207]. To prove this hypothesis, it has to be proven whether 1-MT can be demethylated to TRP.

4.1.6. Hypothesis 5

The combination of demethylation of 1-MT to TRP (Hyp 3) and a degradation of 1-MT to KYNA (Hyp 2) kept the lowest LL, AIC, and BIC value. The second part of the hypothesis is the one which was the most likely one. A combination of both is not reported in the literature. This result excludes the possibility of demethylation of 1-MT to TRP, since Hyp 5 was in no case the most likely one in the conducted *in silico* experiments.

4.1.7. Hypothesis 6

Hyp 6 is based on Hyp 2. It is further extended by a direct degradation of TRP to KYNA (Hyp 1) and 1-MT to TRP (Hyp 3). Hyp 6 revealed the lowest LL and AIC values by fixing parameters to values fitted to the data of 1-MT/LPS experiment, LPS-treated pigs while fitting the remaining values to data of 1-MT/LPS experiment first data set (approach 2). The part of Hyp 6, including Hyp 1, was not reproduced by the validation experiment. The remaining degradation processes, Hyp 2 and Hyp 3, are equal to Hyp 5, which never was the most likely one. Thus, Hyp 6 can be excluded as a possible degradation pathway of 1-MT.

4.1.8. Hypothesis 7

TRP and 1-MT are directly degraded to KYNA (Hyp 7). This degradation was the most likely hypothesis for approach 1 for LL, AIC, and BIC values. The remaining parameters were fitted to the data of the 1-MT/LPS experiment of 1-MT-treated pigs, first data set. These degradation processes are a combination of Hyp 1 and 2. A degradation of TRP to KYNA in Hyp 1 was reported by Han et al. [201]. Hyp 2 was the most likely one, and is also explainable by the validation experiment, but further chemical analysis for this degradation process still needs to be included.

4.2. Inhibition of Indoleamine 2,3-Dioxygenase by 1-Methyltryptophan

The second aim of this study was to investigate the model's ability to represent 1-MT's inhibitory effects on IDO. Three different approaches investigated this. LL, AIC, and BIC values of all approaches point to no inhibitory effects of 1-MT on IDO. For approach 3, where parameters were fitted 100 times, these findings remain true for mean and minimal values but not for median values. These findings align with previous research, where reduced inhibitory effects of 1-MT on IDO were determined *in vivo*. The authors concluded that the saturation of 1-MT was too low in pigs [162]. These low saturation levels were also reported in a phase I trial of tumor patients using 1-MT (D-isomer) as an IDO1 inhibitor. It was shown that doses higher than 1200 mg 1-MT/patient do not increase peak serum levels [82]. Thus IDO inhibition was not fully reached. In addition, this was also shown for the steady-state 1-MT concentration reached after the second 1-MT injection of 1000 $mg/animal/day$ [208].

4.3. Potential Therapeutic Targets

1-MT, and KYNA, activate the AhR [148, 209], which is known as a toxin clearance mediator [85]. Nevertheless, also in inflammation TRP metabolites, AhR contributed to immune homeostasis during e.g., repeated LPS administration by activating immunomodulatory signaling pathways [210]. The most potent activator of the AhR is KYNA. Thus it is a promising therapeutic intervention in inflammatory disorders [62]. In the first phase of sepsis, an overshooting immune response is prevented by appropriate KYNA production [147] by activating T_{reg} cells [211]. But, in the later phase of sepsis, this can lead to immunoparalysis correlated with a poor outcome [147]. To counteract this, inhibition of the AhR receptor by e.g., the antibiotic drug clofazimine [212] could be an appropriate way. It was already successfully tested in immunocompromised patients infected by parasites [213] or drug-resistant *Mycobacterium tuberculosis* [214].
Since the sensitivity analysis revealed V_{max}^{KAT} as a parameter with one of the highest impacts on the KYNA amount, manipulation of the enzyme KAT could also be a potent drug target. Especially for KATII, inhibitors were invented. By sufficient inhibition, significant effects can be expected since KATII catalyzes 70% of the KYNA amount in the brain [215]. Nematollahi et al. presented several KAT inhibitors, but there are few *in vivo* studies, even though there are serious claims of significant potency for them. They claim that systematic *in vivo* examinations of these and related compounds are desirable [215]. Most of them were invented to treat psychiatric disorders caused by the NMDA agonistic properties of KYNA [216, 217]. However, research on the administration of KAT inhibitors during infection is outside the middle of current research.
Since one option is to decrease the production of KYNA by inhibition of KATs, another option could be to increase the degradation of KYNA. KYNA is absorbed from the digestive tract after its oral ingestion. Further, it is mainly excreted via urine [218]. Elevated blood levels of KYNA have normalized already after two hours [219]. Thus,

the degradation of KYNA is already speedy.
The parameter V_{max}^{KQE} has the biggest influence on KYNA levels after μ_{KYNA} and V_{max}^{KAT}. An increase in the enzyme activity of KQE would lead to increased QUIN levels and a decrease on KYNA levels. An intervention of QUIN levels can have dramatic results since QUIN is an NMDA-receptor agonist [21]. It is an endogenous excitotoxin and can lead to acutely or chronic neuronal dysfunction or death by several mechanisms [21].

4.4. Modeling Food Intake

A TRP increase upon food intake was included to adjust the model to the experimental set up. It was reported that treated rats ate less than non-treated rats [220]. This was also reported for LPS-treated pigs [221]. Unfortunately, amount of food intake was not noted during the experiments. Besides, comparing the amount of TRP increase would not be possible because the increase of amino acids in the blood varies between experiments due to different model organisms or altered food composition [222]. To investigate a possible degradation of 1-MT to TRP in *in vivo* experiments, other sources of TRP, like food intake, should be avoided. However, food deprivation is regulated, accounting for animal welfare. For example, guidelines on animal fasting in Norway state that food deprivation for more than 24 h should be avoided in small mammals like rabbits or rats. In guinea pigs, ferrets, and shrews, fasting should be avoided at all [223].
Omitting the split up of data of the 1-MT/LPS experiment, 1-MT-treated pigs in the first and second data set would enable detection of the differences between 1-MT administration with and without food intake.

4.5. Parameter Calculation based on Data Measured in Pigs

Mostly, the boundaries for parameter fitting are set to the lowest and highest values reported in literature [14, 15]. Unfortunately, in literature, no values are reported for pigs. These missing values occur because protein-based techniques in farm animals are often limited compared to their use in humans and rodents due to the poor peptide mass database [224]. Of course, there are many similarities between pigs and humans [224], but also differences. Especially in the immune response [225] and metabolism [226], pigs show a large heterogeneity. Moreover, there needs to be more detailed information on similarities and differences between human and pig at the molecular level [227]. Thus, no a priori knowledge can be used, and values of other species cannot be converted.
The boundaries for initial values were set tightly by $mean - 2 \cdot standard\ deviation$. With this, a normal distribution of the measured data was presumed but not tested. Identifying the actual distribution was not possible for all treatment groups because some groups only consisted of four pigs. Evidence for a different distribution is given due to a non-symmetric distribution determined by negative values of $mean - 2 \cdot standard\ deviation$. Thus, estimating a mean and a standard deviation is not an appropriate tool. Another

approach for determining the initial values of all species is to fix the values to the measured data for time point 0 h for each pig individually [228].
This individualisation leads to individual-based models, which describe the temporal evolution of individual actions and events [229]. They introduce individual traits to build the rules that determine the behavior of a general system [230]. In this thesis, individual-based dynamics were not considered because this would result in a variation of parameter values fitted to different data sets and reduced comparability of data and simulations for all three approaches. The complexity of individual-based models might make the models and validation procedures, and parameterization difficult to implement or computationally prohibitive. Therefore, detailed and reliable observational data are required for comparison [229].

4.6. Comparison of the Fitted Parameters to Literature Values

Parameters were fitted to independent data sets, which differ in the levels of some species. These differences can be justified by altered dynamics caused by a seasonal factor [231] or by human error [232] conducting the measurements by a mass spectrometer [86, 149, 162], which will be discussed later in section 4.8.3. Consequential, fitted parameter values differ. For V_{max}^{KAT} the fitted parameter values are in the range of literature values. In most cases, the fitted value is in the dimension of 10^2. Only when the LPS model was fitted to the data of 1-MT/LPS experiment, subset LPS-treated pigs, the parameter is decreased (10^{-1}). For the parameter V_{max}^{TPH} all fitted parameter values are in the dimension of 10^{-2} to 10^{-1}, at which literature values are much higher. The fitted values of parameter V_{max}^{TDO} range between values of the dimension 10^{-1} to 10^2, at which literature values are again much higher. For the parameter V_{max}^{KQE} the fitted parameter values are between 10^1 and 10^2, this can only be compared to the literature value of the enzyme KYNU. KYNU is an enzyme catalyzing one of the three reactions degrading KYN to QUIN. This parameter is 10 times higher compared to the highest fitted parameter. For V_{max}^{IDO} the fitted parameters range from 10^{-5} to 10^5, at which literature values only range between 10^1 and 10^3. For μ_{KYNA} parameter values were fitted in the range of 10^{-2} to 10^{-1}, this is in concordance with literature values coinciding with μ_{QUIN}, whose fitted parameters are also in the range of parameters found in the literature. For the parameter $\mu_{TNF-\alpha}$, values range between 10^{-4} and 10^{-1}, parameters from literature are all higher. At which the fitted parameters of μ_{SER} are ten times higher than the parameter reported in the literature. No literature values were found for k and μ_{LPS} as well as $FoodSupplyLPS$ and $FoodSupplyNaCl$. For parameter k, only the parameter fitted on data of LPS experiment I is tiny, values obtained from fits to data of 1-MT/LPS experiment, subset LPS-treated parameters are in the range of 10^{-1}.
In conclusion, calculated parameters vary from the parameters reported in the literature. But those parameters are measured in other organisms than the fitted parameters. Based

on the literature values, one can state that the metabolism of human, rodents, primates and pigs differ. An overview of the fitted parameters and values found in literature are given in the appendix C.

4.7. Parameter Scan

To get an estimate for the variability of optimized parameter values, parameter fitting was performed 100 times. This was based on the approach of Stavrum et al. [15], where each optimization was repeated 20 times to get an estimate for the variability of optimized gene expression values. They set the boundaries of each parameter to the minimal and maximal literature value. This fixing was done since the parameter search space for expression values was huge, and there could be several optimal parameter combinations that would result in similar simulations [15]. In this thesis, optimization was repeated five times more often compared to Stavrum et al. [15], since literature values did not limit the search space. In general, such parameter scans are a standard tool [167, 233], but the number of runs differs between the studies from 20 [15] to 50 [167]. At which not every parameter scan is described in detail, and information on the number of runs is missing (e.g., in Cowan et al. [234]). The process can be very time-consuming since parameter scanning usually involves running the same simulation many times [235]. A rule of thumb to determine the number of runs has yet to be available in the current literature. Thus, further methodical investigations have to be performed. One possible approach is to differ the number of runs for a multiplicity of mathematical models. For each model, a characteristic number (e.g., LL, AIC, BIC) has to be determined. The *in silico* experiment revealing the lowest characteristic number is the best. This experiment is repeated for each model, and those results must be interpreted. The number of fitted parameters, the size of the parameter ranges, and the amount of data the parameters are fitted to must be considered.

4.8. Limitations

In this study, data from pigs measured in different experiments were used to fit the parameters of models of the TRP metabolism using MM kinetics. Unfortunately, those parameters did not reproduce the dynamics of all data sets used in this thesis. Therefore, a complex procedure accompanied with several limitations regarding parameters and their reproducibility, and modeling approaches was used. Those different approaches led to different results. It was already reported that different ODE models could deliver similar results [236], demonstrating the limitations of ODE modeling. The limitations of this thesis are discussed below.

4.8.1. Using LL, AIC, and BIC for Model Selection

The AIC and the BIC are the most often used penalized model selection criteria [237]. In this thesis, LL, AIC, and BIC were compared to select the most likely model. The LL can be used for non-nested models, but in this thesis, nested models were applied. Models are nested because hyp 4 to 7 are combinations of hyp 1, 2, and 3. Thus the LL should not be used as a characteristic number to compare the models.
Penalized criteria such as AIC and BIC allow comparisons of non-nested, and nested models [237]. They can be used to select the best model out of a set of two or more models [238]. Here the best model was determined by using the smallest value. A limitation of this thesis is that the difference to the next likely value was not considered. To account for this, weighted information criteria are generally used to make AIC and BIC values more comparable [239, 240, 241] by reflecting the probability of each model given the data and the candidate models [236]. It was also shown that the model chosen by AIC and BIC differ and that the best ODE model selected by BIC has fewer parameters than the best models selected by AIC [242]. This results from the BIC calculation rule since a number of parameters higher than 7 penalized. If the BIC is used, the assumption was made that the simpler the model is, the more likely it is. In this thesis, it was assumed that instead one then two or three degradation processes lead to the increase of TRP and KYNA after 1-MT administration, leading to Hyp 2.

4.8.2. Different Approaches Reveal Different Results

In this thesis three approaches to process biological problems with the 1-MT and 1-MT/LPS ODE models were used. Each approach fits the parameters of 1-MT's degradation pathway and its inhibitory effects on IDO differently. For each approach, another result was obtained, not expected but already reported by others [243, 244].
Polynikis et al. [243] worked on ODE modeling approaches for gene regulatory networks. Also they recognized that while some qualitative behavior is preserved when making different assumptions, the quantitative predictions of different models can be surprisingly different. This difference was also shown for different modeling methodologies in the face of mRNA translation and protein synthesis. Those studies reveal that different models give broadly similar trends, but also essential differences arise [244].
In this study, a simple ODE model was used. However, there are also other methods to model dynamics, like multiple compartment ODE models [14] or agent-based models. Comparing those methods revealed different results [112, 245].

4.8.3. Reduced Reproducibility of Parameters

Parameters fitted to the data of pigs cannot be transferred to a different data set due to several aspects. The first aspect refers to the method of data collection. In the experiments, data were measured with an MS2 mass spectrometer. In general, the accuracy of an MS2 mass spectrometer is about one to five ppm [246], slightly less compared to

other methods [247]. In addition, the precision and accuracy of this method have been questioned [248, 249]. The accuracy of the measured data cannot be determined since there were no technical replicates. Deviations, e.g., of KYNA and TRP levels between LPS experiment I/II and 1-MT/LPS experiment vary between small and enormous. The slight deviations may originate from a reduced accuracy. At which the deviations of TRP levels are huge. They are more than four times higher than the TRP levels measured in LPS experiments I and II. The source of errors is presumed to be human errors, the greatest source of error [232]. Errors can be diverse [250] and are only sometimes nameable.
Currently, an active research area is minimizing errors called „batch effects“[251]. A batch is a set of samples processed and analyzed by the same experimental procedure uninterruptedly[252]. Batch effects appear if the quantitative results of different batches significantly differ due to irrelevant factors [253]. There is no standard for dealing with batch effects in metabolomics [251], but there are multipe of methods to correct for batch effects. The requirements on the measurements of the samples can group those methods. There are methods with no requirements, methods for isotope-labeled internal standards, quality control samples, quality control metabolites, and chemical isotope labeling [251]. Since the samples are already evaluated, only methods with no experimental requirements could have been considered. However, some are not suitable for dealing with the situation that metabolites vary in different patterns or the data must have a balanced batch-group design [251]. Moreover, batch effect removal may lead to unpredictable outcomes to the results since adjustments extensively modify the original data [254].
Another reason for the variation in the measurements is the season when the experiments were conducted. It was shown that the level of TRP metabolites differs between seasons [231]. These differences are also valid for carbohydrate metabolism [255] or TRP metabolism during allergy [256]. Altered enzyme activities can cause altered metabolite levels. Therefore, MM parameters fitted to data measured in the summer season (LPS experiment I/II) cannot be transferred to data measured in the winter season (1-MT/LPS experiment).

4.8.4. Literature Values and Calculated Parameters

Several parameters of the model were fixed to literature values to reduce the complexity of parameter fitting. Literature values are parameters determined by former experiments, which do not necessarily underlie the same conditions as the present experiment. For this study, no literature values were found that were determined based on experiments conducted in pigs or cells of pigs. For K_m and degradation parameters μ, literature values were mainly obtained from experiments conducted in cells of rodents or humans. It was shown that e.g., proteins of mice differ from humans significantly higher than the proteins of pigs differ from humans [226]. However, also pigs differ from humans in several eintire immune system-related pathways [226].
The second limitation on parameter interpretability is based on different mediums of

measurement. Literature values of K_m-values or degradation rates were mostly calculated upon cell experiments. However, the data used in this study were obtained from samples taken from blood. Cells and blood can differ in e.g., the pH-value, ionic composition, or substrate concentration leading to alterations of the enzyme kinetics between compartments [257]. In addition, different variants of enzymes occur in different organs/compartments. Thus, the concentration in blood is based on different turnover rates. For example, there are four different variants of KAT occurring in different compartments of the body with different enzyme activities [186, 193, 258, 259, 260]. The parameter K_{KAT} was fixed to a literature value of KATI measured in human brain cells [187]. In contrast, the validation experiment was performed with KATIV. A value for KATIV was not found in the literature.

4.8.5. Mathematical Modeling of the Tryptophan Metabolism

A mathematical model has to be as simple as possible [90] but as detailed as needed to answer particular questions [90, 99]. For modeling the TRP metabolism, MM kinetics were used. Nevertheless, to apply MM kinetics, several assumptions were made. For example, the substrate concentration saturates the enzyme. In this study, this was not proved since enzyme concentrations were not measured. Also, the decomposition of enzyme and substrate complex to enzyme and substrate [117] is neglected. To account for this takes a lot of work. The measurements in the blood are mixtures of all enzyme activities from different organs/compartments. To account for the constraints of MM-kinetics, it is necessary to measure the substrate concentration for all enzymes in all compartments. However, this is not feasible for an experimental set-up, where samples were taken from each pig over a while in parallel with enzymes active in essential organs. The here-developed model of the TRP metabolism was simplified in several aspects. The reactions of TRP to SER, from TRP to KYN, and from KYN to QUIN were condensed from two or three reactions to only one due to the lack of measurements of the intermediate metabolites.

4.9. Future Directions

The direct degradation of 1-MT to KYNA was the most likely degradation process of 1-MT in the presented analysis. This hypothesis might be able to explain the increased values of TRP and KYNA, while the intermediate metabolite KYN stayed unchanged. Deciphering the detailed degradation process of 1-MT to KYNA needs experiments, including measurements differentiated by time points for 1-MT, TRP, KYN, and KYNA and all intermediate metabolites, as well as a precise determination of the degree of 1-MT's contamination with TRP.
1-MT administration led to increased survival in mice in which sepsis was induced. Since this 1-MT administration is associated with a substantial increase in KYNA, KYNA could be used as a therapeutic agent [62]. Exclusively KYNA could be administered in sepsis, animals to monitor their survival. KYNA is an immunomodulatory agent with

anti-inflammatory and immunosuppressive functions [62]. It prevents an overshooting immune response by activating T_{reg}-cells via TGF-β and IL-6 in early-phase sepsis. A prolonged synthesis of KYNA leads to immunoparalysis, often resulting in the dead [1]. Nevertheless, elevated KYNA levels in the brain are associated with psychotomimetic effects like schizophrenia [261, 262] and also affect the gut motility [35]. Due to these side effects of KYNA, treated patients need comprehensive monitoring [28, 32, 33] and treatment strategies to counteract schizophrenia [263] or reduced motility of the intestine [35].
Moreover, calibration on dynamics of single pigs would improve the fitting results. Individual-based models account for individual effects, commonly used to model the activation of the immune system [264]. Therefore, the most sensitive parameters are individualized [265].
In this study, the „bottom-up“ approach was used. This approach uses quantitative and dynamic information for calibrating mathematical models with high predictive power. On the contrary, the „top down“ approach combines omics data, including qualitative and static information, to analyze network topologies [115]. To enhance the knowledge gain of the here presented models, the „bottom up“ and the „top down“ approach should be combined to decipher regulatory mechanisms to predict dynamics or the impact of pharmaceutical intervention [115].
In this study, three approaches were used to fit the model parameters to the model. Fitting non-identifiable parameters to data revealed the same results for correlated data sets. Whether this approach consistently returns the best result; has to be determined.

4.10. Conclusion

This thesis gives an explanation of the altered levels of TRP metabolites during 1-MT administration in pigs. Moreover, KYNA and its catalyzing enzymes KATI-IV are proposed to be potential drug targets. First hints to the 1-MT induced process of increasing levels of TRP and KYNA were given, while the intermediate metabolite KYN did not change. The best results of modeling IDO inhibition by 1-MT were yielded by approach 3. This approach applies a parameter scan. Thus, no parameters were fixed. The same results were also obtained for the models of the different hypotheses. Many findings, report positive effects of 1-MT [82, 266] *in vivo*. Even though 1-MT did not reach saturation, experiments led to partial inhibition of IDO by 1-MT [86].

5. Summary

Gram-negative bacteria secrete lipopolysaccharides (LPS), leading to a host immune response of proinflammatory cytokine secretion. Those proinflammatory cytokines are TNF-α and IFN-γ, which induce the production of indoleamine 2,3-dioxygenase (IDO) [2, 53, 54]. IDO production is increased during severe sepsis, and septic shock. High IDO levels are associated with increased mortality [59]. This enzyme catalyzes the degradation of tryptophan (TRP) to kynurenine (KYN) along the kynurenine pathway (KP). KYN is further degraded to kynurenic acid (KYNA). Increased IDO levels accompany with increased levels of KYNA [61, 62], which is associated with immunoparalysis [1]. Due to its central role, the KP is a potential target of therapeutic intervention [62]. The degradation of TRP to KYN by IDO was intervened by 1-Methyltryptophan (1-MT), which is assumed to inhibit IDO [81]. By administering 1-MT, the survival of 1-MT-treated mice suffering from sepsis increased compared to mice not treated with 1-MT [82, 83, 84]. The levels of downstream metabolites such as KYN and KYNA were expected to be decreased. Surprisingly, in healthy mice and pigs, an increase in KYNA after 1-MT administration was reported [85, 86]. Those unexpected metabolite alterations after 1-MT administration, and the mode of action, were not the focus of recent research. Hence, there is no explanation for KYNA increase, while KYN did not change. This thesis aims to postulate a possible degradation pathway of 1-MT along the KP with the help of ordinary differential equation (ODE) systems.
Moreover, the developed ODE models were used to determine the ability of 1-MT to inhibit IDO *in vivo*. Therefore, a multiplicity of ODE models were developed, including a model of the KP, an extension by lipopolysaccharide (LPS) administration, and 1-MT administration.
Moreover, seven ODE models were developed, all considering possible degradation pathways of 1-MT. The most likely degradation pathway was combined with the ODE model of LPS administration, including the inhibitory effects of 1-MT.
Those models consist of several dependent equations describing the dynamics of the KP. For each component of the KP, one equation describes the alterations over time. Equations for TRP, KYN, KYNA, and quinolinic acid (QUIN) were developed.
Moreover, the alterations of serotonin (SER) were also included. All together belong to the TRP metabolism. They include the degradation of TRP to SER and to KYN, which is further degraded to KYNA and QUIN. Every degradation is catalyzed by an enzyme. Therefore, Michaelis-Menten (MM) equations were used employing the substrate constant K_m and the maximal degradation velocity V_{max}. To reduce the complexity of parameter calculation, K_m values of the different enzymes were fixed to literature values. The remaining parameters of the equations were determined so that the trajectories of the calculated metabolite levels correspond to data. The parameters of different mod-

els were determined. To propose a degradation pathway of 1-MT leading to increased KYNA levels, seven models were developed and compared. The most likely model was extended to test whether the inhibitory effects of 1-MT on IDO can be determined.
Three different approaches determined the ODE model parameters of the different hypothesis of 1-MT degradation. In the first approach, ODE model parameters were fixed to values fitted to an independent data set. In the second approach, parameters were fitted to a subset of the data set, which was used for simulations of the different hypotheses. The third approach calculated ODE model parameters 100 times without fixed parameters. The parameter set ending up in trajectories of the TRP metabolites, which have the smallest distance to the data, was assumed to be the most likely. The ODE model parameters were fitted to data measured in pigs [86, 149]. Two different experimental models delivered data used in this thesis. The first experimental model activates IDO by LPS administration in pigs [149]. The second one combines the IDO activation by LPS with the administration of 1-MT in pigs.
The most likely hypothesis, according to approach 1 was the degradation of 1-MT to KYNA and TRP. For the second data set the most likely one was the direct degradation of 1-MT to KYNA. With approach 2 the most likely degradation pathways were the combination of all degradation pathways and the degradation of 1-MT to TRP and TRP to KYNA. With approach 3 the most likely way of KYNA increase was given by the direct degradation of 1-MT to KYNA. In summary, the three approaches revealed hypothesis 2, the direct degradation of 1-MT to KYNA most frequently. A cell-free assay validated this result. This experiment combined 1-MT or TRP with or without the enzyme kynurenine aminotransferase (KAT). KAT was already shown to degrade TRP directly to KYNA [160]. The levels of TRP, KYN and KYNA were measured. The highest KYNA levels were yielded with an assay adding KAT to 1-MT, corresponding to hypothesis 2. The models describing the inhibitory effects of 1-MT revealed that the model without inhibitory effects of 1-MT on IDO was more likely for all three approaches.
The correctness of hypothesis 2 has to be confirmed by further *in vitro* experiments. It also has to be investigated which reactions promote the degradation of 1-MT to KYNA. The missing inhibitory properties of 1-MT on IDO, determined by the *in silico* ODE models, align with previous research. It was shown that the saturation of 1-MT was too low, e.g. in pigs [162], to inhibit IDO efficiently.
In this study, the first possible degradation pathway of 1-MT along the KP is proposed. The reliability of the results depends on the quality of the experimental data, and the season, when data were measured. Moreover, the results vary between the different approaches of parameter fitting. Different approaches of parameter fitting have to be included in the analysis to get more evidence for the correctness of the results.

Bibliography

[1] E. Wirthgen and A. Hoeflich, "Endotoxin-induced tryptophan degradation along the kynurenine pathway: the role of indolamine 2, 3-dioxygenase and aryl hydrocarbon receptor-mediated immunosuppressive effects in endotoxin tolerance and cancer and its implications for immunoparalysis," *Journal of Amino Acids*, vol. 2015, 2015.

[2] O. Takikawa, "Biochemical and medical aspects of the indoleamine 2, 3-dioxygenase-initiated l-tryptophan metabolism," *Biochemical and biophysical research communications*, vol. 338, no. 1, pp. 12–19, 2005.

[3] J. Peters, "Tryptophan nutrition and metabolism: an overview," *Kynurenine and serotonin pathways*, pp. 345–358, 1991.

[4] J. G. Hensler, "Serotonin," in *Basic neurochemistry*, pp. 300–322, Elsevier, 2012.

[5] R. Hardeland, S. Pandi-Perumal, and D. P. Cardinali, "Melatonin," *The international journal of biochemistry & cell biology*, vol. 38, no. 3, pp. 313–316, 2006.

[6] K. Charlton, T. Johnson, A. Hamed, and D. Clarke, "Cardiovascular actions of kynuramine and 5-hydroxykynuramine in pithed rats," *Journal of Neural Transmission*, vol. 57, no. 4, pp. 199–211, 1983.

[7] B. Widner, A. Laich, B. Sperner-Unterweger, M. Ledochowski, and D. Fuchs, "Neopterin production, tryptophan degradation, and mental depression—what is the link?," *Brain, behavior, and immunity*, vol. 16, no. 5, pp. 590–595, 2002.

[8] R. Dantzer and K. W. Kelley, "Twenty years of research on cytokine-induced sickness behavior," *Brain, behavior, and immunity*, vol. 21, no. 2, pp. 153–160, 2007.

[9] R. Dantzer, J. C. O'connor, G. G. Freund, R. W. Johnson, and K. W. Kelley, "From inflammation to sickness and depression: when the immune system subjugates the brain," *Nature reviews neuroscience*, vol. 9, no. 1, pp. 46–56, 2008.

[10] W. Merens, A. W. Van der Does, and P. Spinhoven, "The effects of serotonin manipulations on emotional information processing and mood," *Journal of affective disorders*, vol. 103, no. 1-3, pp. 43–62, 2007.

[11] K. W. Kelley, R.-M. Bluthé, R. Dantzer, J.-H. Zhou, W.-H. Shen, R. W. Johnson, and S. R. Broussard, "Cytokine-induced sickness behavior," *Brain, behavior, and immunity*, vol. 17, no. 1, pp. 112–118, 2003.

[12] M. W. Taylor and G. Feng, "Relationship between interferon-γ, indoleamine 2, 3-dioxygenase, and tryptophan catabolism," *The FASEB Journal*, vol. 5, no. 11, pp. 2516–2522, 1991.

[13] S. R. Thomas and R. Stocker, "Redox reactions related to indoleamine 2, 3-dioxygenase and tryptophan metabolism along the kynurenine pathway," *Redox Report*, vol. 4, no. 5, pp. 199–220, 1999.

[14] L. Rios-Avila, H. F. Nijhout, M. C. Reed, H. S. Sitren, and J. F. Gregory III, "A mathematical model of tryptophan metabolism via the kynurenine pathway provides insights into the effects of vitamin b-6 deficiency, tryptophan loading, and induction of tryptophan 2, 3-dioxygenase on tryptophan metabolites," *The Journal of nutrition*, vol. 143, no. 9, pp. 1509–1519, 2013.

[15] A.-K. Stavrum, I. Heiland, S. Schuster, P. Puntervoll, and M. Ziegler, "Model of tryptophan metabolism, readily scalable using tissue-specific gene expression data," *Journal of Biological Chemistry*, vol. 288, no. 48, pp. 34555–34566, 2013.

[16] L. V. Sinclair, D. Neyens, G. Ramsay, P. M. Taylor, and D. A. Cantrell, "Single cell analysis of kynurenine and system l amino acid transport in t cells," *Nature communications*, vol. 9, no. 1, pp. 1–11, 2018.

[17] N. Venkateswaran and M. Conacci-Sorrell, "Kynurenine: An oncometabolite in colon cancer," *Cell Stress*, vol. 4, no. 1, p. 24, 2020.

[18] R. Schwarcz, "The kynurenine pathway of tryptophan degradation as a drug target," *Current opinion in pharmacology*, vol. 4, no. 1, pp. 12–17, 2004.

[19] H. Schievelbein and K. Löschenkohl, "3-hydroxykynurenine," in *Methods of Enzymatic Analysis*, pp. 1731–1735, Elsevier, 1974.

[20] H. Adegbusi, "Kynurenine and serotonin pathways: A review," *Bayero Journal of Pure and Applied Sciences*, vol. 5, no. 2, pp. 156–159, 2012.

[21] G. J. Guillemin, "Quinolinic acid, the inescapable neurotoxin," *The FEBS journal*, vol. 279, no. 8, pp. 1356–1365, 2012.

[22] H. Mori and M. Mishina, "Structure and function of the nmda receptor channel," *Neuropharmacology*, vol. 34, no. 10, pp. 1219–1237, 1995.

[23] F. Fazio, L. Lionetto, M. Curto, L. Iacovelli, M. Cavallari, C. Zappulla, M. Ulivieri, F. Napoletano, M. Capi, V. Corigliano, *et al.*, "Xanthurenic acid activates mglu2/3 metabotropic glutamate receptors and is a potential trait marker for schizophrenia," *Scientific reports*, vol. 5, no. 1, pp. 1–14, 2015.

[24] R. Grant, S. Coggan, and G. A. Smythe, "The physiological action of picolinic acid in the human brain," *International journal of tryptophan research*, vol. 2, pp. IJTR–S2469, 2009.

[25] R. Kapoor, E. Okuno, R. Kido, and V. Kapoor, "Immuno-localization of kynurenine aminotransferase (kat) in the rat medulla and spinal cord," *Neuroreport*, vol. 8, no. 16, pp. 3619–3623, 1997.

[26] Q. Han, T. Cai, D. A. Tagle, and J. Li, "Structure, expression, and function of kynurenine aminotransferases in human and rodent brains," *Cellular and Molecular Life Sciences*, vol. 67, no. 3, pp. 353–368, 2010.

[27] P. Guidetti, E. Okuno, and R. Schwarcz, "Characterization of rat brain kynurenine aminotransferases i and ii," *Journal of neuroscience research*, vol. 50, no. 3, pp. 457–465, 1997.

[28] R. Schwarcz, J. P. Bruno, P. J. Muchowski, and H.-Q. Wu, "Kynurenines in the mammalian brain: when physiology meets pathology," *Nature Reviews Neuroscience*, vol. 13, no. 7, pp. 465–477, 2012.

[29] C. Chang, K. R. Fonseca, C. Li, W. Horner, L. E. Zawadzke, M. A. Salafia, K. A. Welch, C. A. Strick, B. M. Campbell, S. S. Gernhardt, *et al.*, "Quantitative translational analysis of brain kynurenic acid modulation via irreversible kynurenine aminotransferase ii inhibition," *Molecular Pharmacology*, vol. 94, no. 2, pp. 823–833, 2018.

[30] T. Kita, P. F. Morrison, M. P. Heyes, and S. Markey, "Effects of systemic and central nervous system localized inflammation on the contributions of metabolic precursors to the l-kynurenine and quinolinic acid pools in brain," *Journal of neurochemistry*, vol. 82, no. 2, pp. 258–268, 2002.

[31] S. Fukui, R. Schwarcz, S. I. Rapoport, Y. Takada, and Q. R. Smith, "Blood–brain barrier transport of kynurenines: implications for brain synthesis and metabolism," *Journal of neurochemistry*, vol. 56, no. 6, pp. 2007–2017, 1991.

[32] C. Lavebratt, S. Olsson, L. Backlund, L. Frisen, C. Sellgren, L. Priebe, P. Nikamo, L. Träskman-Bendz, S. Cichon, M. Vawter, *et al.*, "The kmo allele encoding arg452 is associated with psychotic features in bipolar disorder type 1, and with increased csf kyna level and reduced kmo expression," *Molecular psychiatry*, vol. 19, no. 3, pp. 334–341, 2014.

[33] S. K. Olsson, C. Sellgren, G. Engberg, M. Landén, and S. Erhardt, "Cerebrospinal fluid kynurenic acid is associated with manic and psychotic features in patients with bipolar i disorder," *Bipolar disorders*, vol. 14, no. 7, pp. 719–726, 2012.

[34] G. S Jayawickrama, R. R Sadig, G. Sun, A. Nematollahi, N. A Nadvi, J. R Hanrahan, M. D Gorrell, and W. Bret Church, "Kynurenine aminotransferases and the prospects of inhibitors for the treatment of schizophrenia," *Current Medicinal Chemistry*, vol. 22, no. 24, pp. 2902–2918, 2015.

[35] J. Kaszaki, D. Érces, G. Varga, A. Szabó, L. Vécsei, and M. Boros, "Kynurenines and intestinal neurotransmission: the role of n-methyl-d-aspartate receptors," *Journal of Neural Transmission*, vol. 119, no. 2, pp. 211–223, 2012.

[36] H. Bjorkbacka, K. A. Fitzgerald, F. Huet, X. Li, J. A. Gregory, M. A. Lee, C. M. Ordija, N. E. Dowley, D. T. Golenbock, and M. W. Freeman, "The induction of macrophage gene expression by lps predominantly utilizes myd88-independent signaling cascades," *Physiological Genomics*, vol. 19, no. 3, pp. 319–330, 2004.

[37] H. d'Hauteville, S. Khan, D. J. Maskell, A. Kussak, A. Weintraub, J. Mathison, R. J. Ulevitch, N. Wuscher, C. Parsot, and P. J. Sansonetti, "Two msbb genes encoding maximal acylation of lipid a are required for invasive shigella flexneri to mediate inflammatory rupture and destruction of the intestinal epithelium," *The Journal of Immunology*, vol. 168, no. 10, pp. 5240–5251, 2002.

[38] G. Elson, I. Dunn-Siegrist, B. Daubeuf, and J. Pugin, "Contribution of toll-like receptors to the innate immune response to gram-negative and gram-positive bacteria," *Blood*, vol. 109, no. 4, pp. 1574–1583, 2007.

[39] S. A. Khan, P. Everest, S. Servos, N. Foxwell, U. Zähringer, H. Brade, E. T. Rietschel, G. Dougan, I. G. Charles, and D. J. Maskell, "A lethal role for lipid a in salmonella infections," *Molecular microbiology*, vol. 29, no. 2, pp. 571–579, 1998.

[40] K. B. Low, M. Ittensohn, T. Le, J. Platt, S. Sodi, M. Amoss, O. Ash, E. Carmichael, A. Chakraborty, J. Fischer, *et al.*, "Lipid a mutant salmonella with suppressed virulence and tnfα induction retain tumor-targeting in vivo," *Nature biotechnology*, vol. 17, no. 1, pp. 37–41, 1999.

[41] A. Silipo, C. D. Castro, R. Lanzetta, M. Parrilli, and A. Molinaro, "Lipopolysaccharides," in *Prokaryotic cell wall compounds*, pp. 133–153, Springer, 2010.

[42] S. M. Dauphinee and A. Karsan, "Lipopolysaccharide signaling in endothelial cells," *Laboratory investigation*, vol. 86, no. 1, pp. 9–22, 2006.

[43] D. J. Kahler and A. L. Mellor, "T cell regulatory plasmacytoid dendritic cells expressing indoleamine 2, 3 dioxygenase," *Dendritic Cells*, pp. 165–196, 2009.

[44] G. Zhang and S. Ghosh, "Molecular mechanisms of nf-κb activation induced by bacterial lipopolysaccharide through toll-like receptors," *Journal of endotoxin research*, vol. 6, no. 6, pp. 453–457, 2000.

[45] F. Salazar, D. Awuah, O. H. Negm, F. Shakib, and A. M. Ghaemmaghami, "The role of indoleamine 2, 3-dioxygenase-aryl hydrocarbon receptor pathway in the tlr4-induced tolerogenic phenotype in human dcs," *Scientific reports*, vol. 7, no. 1, pp. 1–11, 2017.

[46] H. J. Ball, A. Sanchez-Perez, S. Weiser, C. J. Austin, F. Astelbauer, J. Miu, J. A. McQuillan, R. Stocker, L. S. Jermiin, and N. H. Hunt, "Characterization of an indoleamine 2, 3-dioxygenase-like protein found in humans and mice," *Gene*, vol. 396, no. 1, pp. 203–213, 2007.

[47] R. Metz, J. B. DuHadaway, U. Kamasani, L. Laury-Kleintop, A. J. Muller, and G. C. Prendergast, "Novel tryptophan catabolic enzyme ido2 is the preferred biochemical target of the antitumor indoleamine 2, 3-dioxygenase inhibitory compound d-1-methyl-tryptophan," *Cancer research*, vol. 67, no. 15, pp. 7082–7087, 2007.

[48] A. L. Mellor, P. Chandler, G. K. Lee, T. Johnson, D. B. Keskin, J. Lee, and D. H. Munn, "Indoleamine 2, 3-dioxygenase, immunosuppression and pregnancy," *Journal of reproductive immunology*, vol. 57, no. 1-2, pp. 143–150, 2002.

[49] D. H. Munn, M. D. Sharma, D. Hou, B. Baban, J. R. Lee, S. J. Antonia, J. L. Messina, P. Chandler, P. A. Koni, A. L. Mellor, *et al.*, "Expression of indoleamine 2, 3-dioxygenase by plasmacytoid dendritic cells in tumor-draining lymph nodes," *The Journal of clinical investigation*, vol. 114, no. 2, pp. 280–290, 2004.

[50] A. L. Mellor, B. Baban, P. Chandler, B. Marshall, K. Jhaver, A. Hansen, P. A. Koni, M. Iwashima, and D. H. Munn, "Cutting edge: induced indoleamine 2, 3 dioxygenase expression in dendritic cell subsets suppresses t cell clonal expansion," *The Journal of Immunology*, vol. 171, no. 4, pp. 1652–1655, 2003.

[51] D. M. Alvarado, B. Chen, M. Iticovici, A. I. Thaker, N. Dai, K. L. VanDussen, N. Shaikh, C. K. Lim, G. J. Guillemin, P. I. Tarr, *et al.*, "Epithelial indoleamine 2, 3-dioxygenase 1 modulates aryl hydrocarbon receptor and notch signaling to increase differentiation of secretory cells and alter mucus-associated microbiota," *Gastroenterology*, vol. 157, no. 4, pp. 1093–1108, 2019.

[52] E. Kwidzinski, J. Bunse, O. Aktas, D. Richter, L. Mutlu, F. Zipp, R. Nitsch, and I. Bechmann, "Indolamine 2, 3-dioxygenase is expressed in the cns and down-regulates autoimmune inflammation," *The FASEB Journal*, vol. 19, no. 10, pp. 1347–1349, 2005.

[53] N. J. King and S. R. Thomas, "Molecules in focus: indoleamine 2, 3-dioxygenase," *The international journal of biochemistry & cell biology*, vol. 39, no. 12, pp. 2167–2172, 2007.

[54] R. P. Darveau, T.-T. T. Pham, K. Lemley, R. A. Reife, B. W. Bainbridge, S. R. Coats, W. N. Howald, S. S. Way, and A. M. Hajjar, "Porphyromonas gingivalis lipopolysaccharide contains multiple lipid a species that functionally interact with both toll-like receptors 2 and 4," *Infection and immunity*, vol. 72, no. 9, pp. 5041–5051, 2004.

[55] Y.-W. He, H.-S. Wang, J. Zeng, X. Fang, H.-Y. Chen, J. Du, and X.-y. Yang, "Sodium butyrate inhibits interferon-gamma induced indoleamine 2, 3-dioxygenase expression via stat1 in nasopharyngeal carcinoma cells," *Life sciences*, vol. 93, no. 15, pp. 509–515, 2013.

[56] U. M. Litzenburger, C. A. Opitz, F. Sahm, K. J. Rauschenbach, S. Trump, M. Winter, M. Ott, K. Ochs, C. Lutz, X. Liu, *et al.*, "Constitutive ido expression in human cancer is sustained by an autocrine signaling loop involving il-6, stat3 and the ahr," *Oncotarget*, vol. 5, no. 4, p. 1038, 2014.

[57] O. Hayaishi *et al.*, "Catalytic properties and reaction mechanism of indoleamine 2, 3-dioxygenase.," 1975.

[58] S. Lancellotti, L. Novarese, and R. De Cristofaro, "Biochemical properties of indoleamine 2, 3-dioxygenase: from structure to optimized design of inhibitors," *Current medicinal chemistry*, vol. 18, no. 15, pp. 2205–2214, 2011.

[59] P. Tattevin, D. Monnier, O. Tribut, J. Dulong, N. Bescher, F. Mourcin, F. Uhel, Y. Le Tulzo, and K. Tarte, "Enhanced indoleamine 2, 3-dioxygenase activity in patients with severe sepsis and septic shock," *The Journal of infectious diseases*, vol. 201, no. 6, pp. 956–966, 2010.

[60] W. J. Frazier and M. W. Hall, "Immunoparalysis and adverse outcomes from critical illness," *Pediatric Clinics of North America*, vol. 55, no. 3, pp. 647–668, 2008.

[61] A. De Luca, C. Montagnoli, T. Zelante, P. Bonifazi, S. Bozza, S. Moretti, C. D'Angelo, C. Vacca, L. Boon, F. Bistoni, *et al.*, "Functional yet balanced reactivity to candida albicans requires trif, myd88, and ido-dependent inhibition of rorc," *The Journal of Immunology*, vol. 179, no. 9, pp. 5999–6008, 2007.

[62] E. Wirthgen, A. Hoeflich, A. Rebl, and J. Günther, "Kynurenic acid: the janus-faced role of an immunomodulatory tryptophan metabolite and its link to pathological conditions," *Frontiers in immunology*, vol. 8, p. 1957, 2018.

[63] F. Balkwill, "Tnf-α in promotion and progression of cancer," *Cancer and Metastasis Reviews*, vol. 25, no. 3, pp. 409–416, 2006.

[64] C. M. Forrest, S. R. Gould, L. G. Darlington, and T. W. Stone, "Levels of purine, kynurenine and lipid peroxidation products in patients with inflammatory bowel disease," in *Developments in Tryptophan and Serotonin Metabolism*, pp. 395–400, Springer, 2003.

[65] L.-M. Chen, C.-H. Bao, Y. Wu, S.-H. Liang, D. Wang, L.-Y. Wu, Y. Huang, H.-R. Liu, and H.-G. Wu, "Tryptophan-kynurenine metabolism: a link between the gut and brain for depression in inflammatory bowel disease," *Journal of Neuroinflammation*, vol. 18, no. 1, pp. 1–13, 2021.

[66] X. Zheng, M. Hu, X. Zang, Q. Fan, Y. Liu, Y. Che, X. Guan, Y. Hou, G. Wang, and H. Hao, "Kynurenic acid/gpr35 axis restricts nlrp3 inflammasome activation and exacerbates colitis in mice with social stress," *Brain, Behavior, and Immunity*, vol. 79, pp. 244–255, 2019.

[67] C. Kiank, J.-P. Zeden, S. Drude, G. Domanska, G. Fusch, W. Otten, and C. Schuett, "Psychological stress-induced, ido1-dependent tryptophan catabolism: implications on immunosuppression in mice and humans," *PLoS One*, vol. 5, no. 7, p. e11825, 2010.

[68] J. Wang, N. Simonavicius, X. Wu, G. Swaminath, J. Reagan, H. Tian, and L. Ling, "Kynurenic acid as a ligand for orphan g protein-coupled receptor gpr35," *Journal of biological chemistry*, vol. 281, no. 31, pp. 22021–22028, 2006.

[69] Z. Tiszlavicz, B. Németh, F. Fülöp, L. Vécsei, K. Tápai, I. Ocsovszky, and Y. Mándi, "Different inhibitory effects of kynurenic acid and a novel kynurenic acid analogue on tumour necrosis factor-α (tnf-α) production by mononuclear cells, hmgb1 production by monocytes and hnp1-3 secretion by neutrophils," *Naunyn-Schmiedeberg's archives of pharmacology*, vol. 383, no. 5, pp. 447–455, 2011.

[70] A. Baj, E. Moro, M. Bistoletti, V. Orlandi, F. Crema, and C. Giaroni, "Glutamatergic signaling along the microbiota-gut-brain axis," *International journal of molecular sciences*, vol. 20, no. 6, p. 1482, 2019.

[71] S. L. Gaffen, R. Jain, A. V. Garg, and D. J. Cua, "Il-23-il-17 immune axis: discovery, mechanistic understanding, and clinical testing," *Nature reviews. Immunology*, vol. 14, no. 9, p. 585, 2014.

[72] L. Z. Agudelo, D. M. Ferreira, I. Cervenka, G. Bryzgalova, S. Dadvar, P. R. Jannig, A. T. Pettersson-Klein, T. Lakshmikanth, E. G. Sustarsic, M. Porsmyr-Palmertz, *et al.*, "Kynurenic acid and gpr35 regulate adipose tissue energy homeostasis and inflammation," *Cell metabolism*, vol. 27, no. 2, pp. 378–392, 2018.

[73] B. Akkaya and E. M. Shevach, "Regulatory t cells: Master thieves of the immune system," *Cellular immunology*, vol. 355, p. 104160, 2020.

[74] M. O. Li, Y. Y. Wan, S. Sanjabi, A. Robertson, R. A. Flavell, *et al.*, "Transforming growth factor-beta regulation of immune responses," *Annual review of immunology*, vol. 24, p. 99, 2006.

[75] S. Murch, C. Braegger, J. Walker-Smith, and T. MacDonald, "Location of tumour necrosis factor alpha by immunohistochemistry in chronic inflammatory bowel disease.," *Gut*, vol. 34, no. 12, pp. 1705–1709, 1993.

[76] J. G. Herman, "Hypermethylation of tumor suppressor genes in cancer," in *Seminars in cancer biology*, vol. 9, pp. 359–367, Elsevier, 1999.

[77] O. Shibayama, K. Yoshiuchi, M. Inagaki, Y. Matsuoka, E. Yoshikawa, Y. Sugawara, T. Akechi, N. Wada, S. Imoto, K. Murakami, *et al.*, "Association between adjuvant regional radiotherapy and cognitive function in breast cancer patients treated with conservation therapy," *Cancer medicine*, vol. 3, no. 3, pp. 702–709, 2014.

[78] Y. Guo, F. Xu, T. Lu, Z. Duan, and Z. Zhang, "Interleukin-6 signaling pathway in targeted therapy for cancer," *Cancer treatment reviews*, vol. 38, no. 7, pp. 904–910, 2012.

[79] S. G. Cady and M. Sono, "1-methyl-dl-tryptophan, β-(3-benzofuranyl)-dl-alanine (the oxygen analog of tryptophan), and β-[3-benzo (b) thienyl]-dl-alanine (the sulfur analog of tryptophan) are competitive inhibitors for indoleamine 2, 3-dioxygenase," *Archives of biochemistry and biophysics*, vol. 291, no. 2, pp. 326–333, 1991.

[80] F. Qian, J. Liao, J. Villella, R. Edwards, P. Kalinski, S. Lele, P. Shrikant, and K. Odunsi, "Effects of 1-methyltryptophan stereoisomers on ido2 enzyme activity and ido2-mediated arrest of human t cell proliferation," *Cancer immunology, immunotherapy*, vol. 61, no. 11, pp. 2013–2020, 2012.

[81] S. Chackalamannil, D. Rotella, and S. Ward, *Comprehensive medicinal chemistry III*. Elsevier, 2017.

[82] I. D. Jung, M.-G. Lee, J. H. Chang, J. S. Lee, Y.-I. Jeong, C.-M. Lee, W. S. Park, J. Han, S.-K. Seo, S. Y. Lee, *et al.*, "Blockade of indoleamine 2, 3-dioxygenase protects mice against lipopolysaccharide-induced endotoxin shock," *The Journal of Immunology*, vol. 182, no. 5, pp. 3146–3154, 2009.

[83] M. Hoshi, Y. Osawa, H. Ito, H. Ohtaki, T. Ando, M. Takamatsu, A. Hara, K. Saito, and M. Seishima, "Blockade of indoleamine 2, 3-dioxygenase reduces mortality from peritonitis and sepsis in mice by regulating functions of cd11b+ peritoneal cells," *Infection and Immunity*, vol. 82, no. 11, pp. 4487–4495, 2014.

[84] H. S. Yim, K. M. Choi, B. Kim, I. D. Jung, Y.-M. Park, Y. K. Kang, and M.-G. Lee, "Effect of 1-methyl-d-tryptophan and adoptive transfer of dendritic cells on polymicrobial sepsis induced by cecal content injection," *Microbiology and immunology*, vol. 57, no. 9, pp. 633–639, 2013.

[85] E. Wirthgen, A. K. Leonard, C. Scharf, and G. Domanska, "The immunomodulator 1-methyltryptophan drives tryptophan catabolism toward the kynurenic acid branch," *Frontiers in Immunology*, vol. 11, p. 313, 2020.

[86] E. Wirthgen, W. Otten, M. Tuchscherer, A. Tuchscherer, G. Domanska, J. Brenmoehl, J. Günther, D. Ohde, W. Weitschies, A. Seidlitz, *et al.*, "Effects of 1-methyltryptophan on immune responses and the kynurenine pathway after

lipopolysaccharide challenge in pigs," *International journal of molecular sciences*, vol. 19, no. 10, p. 3009, 2018.

[87] E. Fox, T. Oliver, M. Rowe, S. Thomas, Y. Zakharia, P. B. Gilman, A. J. Muller, and G. C. Prendergast, "Indoximod: an immunometabolic adjuvant that empowers t cell activity in cancer," *Frontiers in oncology*, vol. 8, p. 370, 2018.

[88] G. C. Prendergast, C. Smith, S. Thomas, L. Mandik-Nayak, L. Laury-Kleintop, R. Metz, and A. J. Muller, "Indoleamine 2, 3-dioxygenase pathways of pathogenic inflammation and immune escape in cancer," *Cancer immunology, immunotherapy*, vol. 63, no. 7, pp. 721–735, 2014.

[89] J. Günther, J. Däbritz, and E. Wirthgen, "Limitations and off-target effects of tryptophan-related ido inhibitors in cancer treatment," *Frontiers in immunology*, vol. 10, p. 1801, 2019.

[90] E. Klipp, W. Liebermeister, C. Wierling, and A. Kowald, *Systems biology: a textbook*. John Wiley & Sons, 2016.

[91] J. D. Murray, *Mathematical biology: I. An introduction*. Springer, 2002.

[92] I. Thiele, S. Sahoo, A. Heinken, J. Hertel, L. Heirendt, M. K. Aurich, and R. M. Fleming, "Personalized whole-body models integrate metabolism, physiology, and the gut microbiome," *Molecular systems biology*, vol. 16, no. 5, p. e8982, 2020.

[93] C. Zitzmann and L. Kaderali, "Mathematical analysis of viral replication dynamics and antiviral treatment strategies: from basic models to age-based multi-scale modeling," *Frontiers in microbiology*, vol. 9, p. 1546, 2018.

[94] A. L. Jenner, T. Cassidy, K. Belaid, M.-C. Bourgeois-Daigneault, and M. Craig, "In silico trials predict that combination strategies for enhancing vesicular stomatitis oncolytic virus are determined by tumor aggressivity," *Journal for immunotherapy of cancer*, vol. 9, no. 2, 2021.

[95] M. Ilea, M. Turnea, M. Rotariu, *et al.*, "Ordinary differential equations with applications in molecular biology," *Rev Med Chir Soc Med Nat Iasi*, vol. 116, no. 1, pp. 347–352, 2012.

[96] C. Guldberg and P. Waage, "Über die chemische affinität [on chemical affinity]," *Erdmann's Journal für practische Chemie*, vol. 127, pp. 69–114, 1879.

[97] C. M. Guldberg and P. Waage, *Etudes sur les affinités chimiques*. Imprimerie de Brøgger & Christie, 1867.

[98] A. Kremling, *Kompendium Systembiologie*. Springer, 2012.

[99] I. Dattner, "Differential equations in data analysis," *Wiley Interdisciplinary Reviews: Computational Statistics*, vol. 13, no. 6, p. e1534, 2021.

[100] R. Serban and A. C. Hindmarsh, "Cvodes: the sensitivity-enabled ode solver in sundials," in *International Design Engineering Technical Conferences and Computers and Information in Engineering Conference*, vol. 47438, pp. 257–269, 2005.

[101] "SUNDIALS: SUite of Nonlinear and DIfferential/ALgebraic Equation Solvers." `https://computing.llnl.gov/projects/sundials`. Accessed: 2022-11-22.

[102] A. B. Owen, "A central limit theorem for latin hypercube sampling," *Journal of the Royal Statistical Society: Series B (Methodological)*, vol. 54, no. 2, pp. 541–551, 1992.

[103] T. Toni, D. Welch, N. Strelkowa, A. Ipsen, and M. P. Stumpf, "Approximate bayesian computation scheme for parameter inference and model selection in dynamical systems," *Journal of the Royal Society Interface*, vol. 6, no. 31, pp. 187–202, 2009.

[104] H. Akaike, "A new look at the statistical model identification," *IEEE transactions on automatic control*, vol. 19, no. 6, pp. 716–723, 1974.

[105] A. A. Neath and J. E. Cavanaugh, "The bayesian information criterion: background, derivation, and applications," *Wiley Interdisciplinary Reviews: Computational Statistics*, vol. 4, no. 2, pp. 199–203, 2012.

[106] M. D. Morris, "Factorial sampling plans for preliminary computational experiments," *Technometrics*, vol. 33, no. 2, pp. 161–174, 1991.

[107] C. Zitzmann, B. Schmid, A. Ruggieri, A. S. Perelson, M. Binder, R. Bartenschlager, and L. Kaderali, "A coupled mathematical model of the intracellular replication of dengue virus and the host cell immune response to infection," *Frontiers in microbiology*, vol. 11, p. 725, 2020.

[108] M. Binder, N. Sulaimanov, D. Clausznitzer, M. Schulze, C. M. Hüber, S. M. Lenz, J. P. Schlöder, M. Trippler, R. Bartenschlager, V. Lohmann, *et al.*, "Replication vesicles are load-and choke-points in the hepatitis c virus lifecycle," *PLoS pathogens*, vol. 9, no. 8, p. e1003561, 2013.

[109] A. L. Hill, "Mathematical models of hiv latency," *HIV-1 latency*, pp. 131–156, 2017.

[110] A. M. Smith, "Validated models of immune response to virus infection," *Current Opinion in Systems Biology*, vol. 12, pp. 46–52, 2018.

[111] A. M. Smith, J. A. McCullers, and F. R. Adler, "Mathematical model of a three-stage innate immune response to a pneumococcal lung infection," *Journal of theoretical biology*, vol. 276, no. 1, pp. 106–116, 2011.

[112] D. Gammack, S. Ganguli, S. Marino, J. Segovia-Juarez, and D. E. Kirschner, "Understanding the immune response in tuberculosis using different mathematical models and biological scales," *Multiscale Modeling & Simulation*, vol. 3, no. 2, pp. 312–345, 2005.

[113] A. L. Jenner, R. A. Aogo, S. Alfonso, V. Crowe, X. Deng, A. P. Smith, P. A. Morel, C. L. Davis, A. M. Smith, and M. Craig, "Covid-19 virtual patient cohort suggests immune mechanisms driving disease outcomes," *PLoS pathogens*, vol. 17, no. 7, p. e1009753, 2021.

[114] K. P. Burnham and D. R. Anderson, "Multimodel inference: understanding aic and bic in model selection," *Sociological methods & research*, vol. 33, no. 2, pp. 261–304, 2004.

[115] J. Bachmann, A. Raue, M. Schilling, V. Becker, J. Timmer, and U. Klingmüller, "Predictive mathematical models of cancer signalling pathways," *Journal of internal medicine*, vol. 271, no. 2, pp. 155–165, 2012.

[116] C. H. Taubes, *Modeling differential equations in biology*. Cambridge University Press, 2008.

[117] L. Michaelis, M. L. Menten, *et al.*, "Die kinetik der invertinwirkung," *Biochem. z*, vol. 49, no. 333-369, p. 352, 1913.

[118] G. E. Briggs and J. B. S. Haldane, "A note on the kinetics of enzyme action," *Biochemical journal*, vol. 19, no. 2, p. 338, 1925.

[119] K.-E. Biebler, K. Schreiber, and R. Bode, "Solutions to the michaelis-menten kinetics are not necessarily unique," in *AIP Conference Proceedings*, vol. 1148, pp. 37–40, American Institute of Physics, 2009.

[120] M. D. McKay, R. J. Beckman, and W. J. Conover, "A comparison of three methods for selecting values of input variables in the analysis of output from a computer code," *Technometrics*, vol. 42, no. 1, pp. 55–61, 2000.

[121] M. Stein, "Large sample properties of simulations using latin hypercube sampling," *Technometrics*, vol. 29, no. 2, pp. 143–151, 1987.

[122] G. Claeskens, N. L. Hjort, *et al.*, "Model selection and model averaging," *Cambridge Books*, 2008.

[123] E. Wit, E. v. d. Heuvel, and J.-W. Romeijn, "'all models are wrong...': an introduction to model uncertainty," *Statistica Neerlandica*, vol. 66, no. 3, pp. 217–236, 2012.

[124] A. Karagrigoriou, "Claeskens, g. & hjort, nl (2009). model selection and model averaging.," 2011.

[125] MATLAB, *version 7.10.0 (R2021a)*. Natick, Massachusetts: The MathWorks Inc., 2021.

[126] A. Raue, C. Kreutz, T. Maiwald, J. Bachmann, M. Schilling, U. Klingmüller, and J. Timmer, "Structural and practical identifiability analysis of partially observed dynamical models by exploiting the profile likelihood," *Bioinformatics*, vol. 25, no. 15, pp. 1923–1929, 2009.

[127] A. Saltelli, S. Tarantola, and F. Campolongo, "Sensitivity analysis as an ingredient of modeling," *Statistical Science*, pp. 377–395, 2000.

[128] A. Franczyk, "Using the morris sensitivity analysis method to assess the importance of input variables on time-reversal imaging of seismic sources," *Acta Geophysica*, vol. 67, no. 6, pp. 1525–1533, 2019.

[129] S. Kucherenko and S. Song, "Derivative-based global sensitivity measures and their link with sobol'sensitivity indices," in *Monte Carlo and Quasi-Monte Carlo Methods*, pp. 455–469, Springer, 2016.

[130] S. Kucherenko, M. Rodriguez-Fernandez, C. Pantelides, and N. Shah, "Monte carlo evaluation of derivative-based global sensitivity measures," *Reliability Engineering & System Safety*, vol. 94, no. 7, pp. 1135–1148, 2009.

[131] A. B. Owen and C. Prieur, "On shapley value for measuring importance of dependent inputs," *SIAM/ASA Journal on Uncertainty Quantification*, vol. 5, no. 1, pp. 986–1002, 2017.

[132] M. Lamboni, B. Iooss, A.-L. Popelin, and F. Gamboa, "Derivative-based global sensitivity measures: General links with sobol'indices and numerical tests," *Mathematics and Computers in Simulation*, vol. 87, pp. 45–54, 2013.

[133] J. E. Oakley and A. O'Hagan, "Probabilistic sensitivity analysis of complex models: a bayesian approach," *Journal of the Royal Statistical Society: Series B (Statistical Methodology)*, vol. 66, no. 3, pp. 751–769, 2004.

[134] K. Doksum and A. Samarov, "Nonparametric estimation of global functionals and a measure of the explanatory power of covariates in regression," *The Annals of Statistics*, pp. 1443–1473, 1995.

[135] I. M. Sobol, "Sensitivity analysis for non-linear mathematical models," *Mathematical modelling and computational experiment*, vol. 1, pp. 407–414, 1993.

[136] A. Saltelli and I. M. Sobol, "About the use of rank transformation in sensitivity analysis of model output," *Reliability Engineering & System Safety*, vol. 50, no. 3, pp. 225–239, 1995.

[137] M.-H. Chun, S.-J. Han, and N.-I. Tak, "An uncertainty importance measure using a distance metric for the change in a cumulative distribution function," *Reliability Engineering & System Safety*, vol. 70, no. 3, pp. 313–321, 2000.

[138] E. Borgonovo, "A new uncertainty importance measure," *Reliability Engineering & System Safety*, vol. 92, no. 6, pp. 771–784, 2007.

[139] F. Campolongo, J. Cariboni, and A. Saltelli, "An effective screening design for sensitivity analysis of large models," *Environmental modelling & software*, vol. 22, no. 10, pp. 1509–1518, 2007.

[140] A. Saltelli, F. Campolongo, and J. Cariboni, "Screening important inputs in models with strong interaction properties," *Reliability Engineering & System Safety*, vol. 94, no. 7, pp. 1149–1155, 2009.

[141] Q. Ge and M. Menendez, "An efficient sensitivity analysis approach for computationally expensive microscopic traffic simulation models," *International Journal of Transportation*, vol. 2, no. 2, pp. 49–64, 2014.

[142] X. Wang, M. Yang, Y. Zhang, and M. Kiang, "A screening approach for nonparametric global sensitivity analysis," *Journal of Statistical Computation and Simulation*, vol. 86, no. 4, pp. 656–675, 2016.

[143] M. Alahdal, D. Sun, L. Duan, H. Ouyang, M. Wang, J. Xiong, and D. Wang, "Forecasting sensitive targets of the kynurenine pathway in pancreatic adenocarcinoma using mathematical modeling," *Cancer science*, vol. 112, no. 4, pp. 1481–1494, 2021.

[144] A. Chakwizira, J. Ahlstedt, H. Nittby Redebrandt, and C. Ceberg, "Mathematical modelling of the synergistic combination of radiotherapy and indoleamine-2, 3-dioxygenase (ido) inhibitory immunotherapy against glioblastoma," *The British journal of radiology*, vol. 91, no. 1087, p. 20170857, 2018.

[145] R. G. Ruddell, D. A. Mann, and G. A. Ramm, "The function of serotonin within the liver," *Journal of hepatology*, vol. 48, no. 4, pp. 666–675, 2008.

[146] J. Yao, H. Lu, Z. Wang, T. Wang, F. Fang, J. Wang, J. Yu, and R. Gao, "A sensitive method for the determination of the gender difference of neuroactive metabolites in tryptophan and dopamine pathways in mouse serum and brain by uhplc-ms/ms," *Journal of Chromatography B*, vol. 1093, pp. 91–99, 2018.

[147] E. Wirthgen and A. Hoeflich, "Endotoxin-induced tryptophan degradation along the kynurenine pathway: The role of indolamine 2, 3-dioxygenase and aryl hydrocarbon receptor-mediated immunosuppressive effects in endotoxin tolerance and cancer and its implications for immunoparalysis," *Journal of amino acids*, vol. 2015, 2015.

[148] E. Wirthgen, W. Otten, M. Tuchscherer, A. Tuchscherer, G. Domanska, J. Brenmoehl, J. Günther, D. Ohde, W. Weitschies, A. Seidlitz, *et al.*, "Effects of 1-methyltryptophan on immune responses and the kynurenine pathway after lipopolysaccharide challenge in pigs," *International journal of molecular sciences*, vol. 19, no. 10, p. 3009, 2018.

[149] E. Wirthgen, M. Tuchscherer, W. Otten, G. Domanska, K. Wollenhaupt, A. Tuchscherer, and E. Kanitz, "Activation of indoleamine 2, 3-dioxygenase by lps in a porcine model," *Innate immunity*, vol. 20, no. 1, pp. 30–39, 2014.

[150] W. E. Knox and A. H. Mehler, "The conversion of tryptophan to kynurenine in liver i. the coupled tryptophan peroxidase-oxidase system forming formylkynurenine," *Journal of Biological Chemistry*, vol. 187, no. 1, pp. 419–430, 1950.

[151] O. Takikawa, "Biochemical and medical aspects of the indoleamine 2, 3-dioxygenase-initiated l-tryptophan metabolism," *Biochemical and biophysical research communications*, vol. 338, no. 1, pp. 12–19, 2005.

[152] K. A. Johnson and R. S. Goody, "The original michaelis constant: translation of the 1913 michaelis–menten paper," *Biochemistry*, vol. 50, no. 39, pp. 8264–8269, 2011.

[153] S. Fujigaki, K. Saito, K. Sekikawa, S. Tone, O. Takikawa, H. Fujii, H. Wada, A. Noma, and M. Seishima, "Lipopolysaccharide induction of indoleamine 2, 3-dioxygenase is mediated dominantly by an ifn-γ-independent mechanism," *European journal of immunology*, vol. 31, no. 8, pp. 2313–2318, 2001.

[154] N. J. King and S. R. Thomas, "Molecules in focus: indoleamine 2, 3-dioxygenase," *The international journal of biochemistry & cell biology*, vol. 39, no. 12, pp. 2167–2172, 2007.

[155] R. P. Darveau, T.-T. T. Pham, K. Lemley, R. A. Reife, B. W. Bainbridge, S. R. Coats, W. N. Howald, S. S. Way, and A. M. Hajjar, "Porphyromonas gingivalis lipopolysaccharide contains multiple lipid a species that functionally interact with both toll-like receptors 2 and 4," *Infection and immunity*, vol. 72, no. 9, pp. 5041–5051, 2004.

[156] H. J. Ball, H. J. Yuasa, C. J. Austin, S. Weiser, and N. H. Hunt, "Indoleamine 2, 3-dioxygenase-2; a new enzyme in the kynurenine pathway," *The international journal of biochemistry & cell biology*, vol. 41, no. 3, pp. 467–471, 2009.

[157] S. Dunzendorfer, H.-K. Lee, K. Soldau, and P. S. Tobias, "Tlr4 is the signaling but not the lipopolysaccharide uptake receptor," *The Journal of Immunology*, vol. 173, no. 2, pp. 1166–1170, 2004.

[158] A. Shnyra and A. A. Lindberg, "Scavenger receptor pathway for lipopolysaccharide binding to kupffer and endothelial liver cells in vitro.," *Infection and immunity*, vol. 63, no. 3, pp. 865–873, 1995.

[159] E. Topchiy, M. Cirstea, H. J. Kong, J. H. Boyd, Y. Wang, J. A. Russell, and K. R. Walley, "Lipopolysaccharide is cleared from the circulation by hepatocytes via the low density lipoprotein receptor," *PloS one*, vol. 11, no. 5, p. e0155030, 2016.

[160] Q. Han, T. Cai, D. A. Tagle, H. Robinson, and J. Li, "Substrate specificity and structure of human aminoadipate aminotransferase/kynurenine aminotransferase ii," *Bioscience reports*, vol. 28, no. 4, pp. 205–215, 2008.

[161] L. Guerra-Calderas, R. González-Barrios, L. A. Herrera, D. C. de León, and E. Soto-Reyes, "The role of the histone demethylase kdm4a in cancer," *Cancer genetics*, vol. 208, no. 5, pp. 215–224, 2015.

[162] E. Wirthgen, E. Kanitz, M. Tuchscherer, A. Tuchscherer, G. Domanska, W. Weitschies, A. Seidlitz, E. Scheuch, and W. Otten, "Pharmacokinetics of 1-methyl-l-tryptophan after single and repeated subcutaneous application in a porcine model," *Experimental Animals*, pp. 15–0096, 2015.

[163] A. Raue, B. Steiert, M. Schelker, C. Kreutz, T. Maiwald, H. Hass, J. Vanlier, C. Tönsing, L. Adlung, R. Engesser, *et al.*, "Data2dynamics: a modeling environment tailored to parameter estimation in dynamical systems," *Bioinformatics*, vol. 31, no. 21, pp. 3558–3560, 2015.

[164] R Core Team, *R: A Language and Environment for Statistical Computing*. R Foundation for Statistical Computing, Vienna, Austria, 2013.

[165] H. Wickham, *Ggplot2: Elegant graphics for data analysis*. Use R!, Cham, Switzerland: Springer International Publishing, 2 ed., June 2016.

[166] F. Weber, S. Theers, D. Surmann, U. Ligges, and C. Weihs, "Sensitivity analysis of ordinary differential equation models," 2018.

[167] T. W. Cornforth and H. Lipson, "Inference of hidden variables in systems of differential equations with genetic programming," *Genetic programming and evolvable machines*, vol. 14, no. 2, pp. 155–190, 2013.

[168] A. Raue, B. Steiert, M. Schelker, C. Kreutz, T. Maiwald, H. Hass, J. Vanlier, C. Tönsing, L. Adlung, R. Engesser, *et al.*, "Data2dynamics: a modeling environment tailored to parameter estimation in dynamical systems," *Bioinformatics*, vol. 31, no. 21, pp. 3558–3560, 2015.

[169] D. G. Altman and J. M. Bland, "Standard deviations and standard errors," *Bmj*, vol. 331, no. 7521, p. 903, 2005.

[170] E. R. Werner, G. Werner-Felmayer, D. Fuchs, A. Hausen, G. Reibnegger, and H. Wachter, "Influence of interferon-gamma and extracellular tryptophan on indoleamine 2, 3-dioxygenase activity in t24 cells as determined by a non-radiometric assay," *Biochemical Journal*, vol. 256, no. 2, pp. 537–541, 1988.

[171] Y. Ozaki, J. F. Reinhard Jr, and C. A. Nichol, "Cofactor activity of dihydroflavin mononucleotide and tetrahydrobiopterin for murine epididymal indoleamine 2, 3-dioxygenase," *Biochemical and biophysical research communications*, vol. 137, no. 3, pp. 1106–1111, 1986.

[172] J. Basran, S. A. Rafice, N. Chauhan, I. Efimov, M. R. Cheesman, L. Ghamsari, and E. L. Raven, "A kinetic, spectroscopic, and redox study of human tryptophan 2, 3-dioxygenase," *Biochemistry*, vol. 47, no. 16, pp. 4752–4760, 2008.

[173] E. Pfefferkorn, S. REBHUN, and M. ECKEL, "Characterization of an indoleamine 2, 3-dioxygenase induced by gamma-interferon in cultured human fibroblasts," *Journal of interferon research*, vol. 6, no. 3, pp. 267–279, 1986.

[174] E. Fukumura, H. Sugimoto, Y. Misumi, T. Ogura, and Y. Shiro, "Cooperative binding of l-trp to human tryptophan 2, 3-dioxygenase: resonance raman spectroscopic analysis," *Journal of biochemistry*, vol. 145, no. 4, pp. 505–515, 2009.

[175] F. Hirata and O. Hayaishi, "New degradative routes of 5-hydroxytryptophan and serotonin by intestinal tryptophan 2, 3-dioxygenase," *Biochemical and biophysical research communications*, vol. 47, no. 5, pp. 1112–1119, 1972.

[176] Y. Ohta, H. Kubo, K. Yashiro, K. Ohashi, Y. Tsuzuki, N. Wada, Y. Yamamoto, and K. Saito, "Effect of water-immersion restraint stress on tryptophan catabolism through the kynurenine pathway in rat tissues," *The Journal of Physiological Sciences*, vol. 67, no. 3, pp. 361–372, 2017.

[177] M. K. Stachowiak, E. M. Stricker, J. H. Jacoby, and M. J. Zigmond, "Increased tryptophan hydroxylase activity in serotonergic nerve terminals spared by 5,7-dihydroxytryptamine," *Biochemical Pharmacology*, vol. 35, no. 8, pp. 1241 – 1248, 1986.

[178] L. Neckers, G. Biggio, E. Moja, and J. Meek, "Modulation of brain tryptophan hydroxylase activity by brain tryptophan content.," *Journal of Pharmacology and Experimental Therapeutics*, vol. 201, no. 1, pp. 110–116, 1977.

[179] M. Sawada, T. Nagatsu, I. Nagatsu, K. Ito, R. Iizuka, T. Kondo, and H. Narabayashi, "Tryptophan hydroxylase activity in the brains of controls and parkinsonian patients," *Journal of neural transmission*, vol. 62, no. 1-2, pp. 107–115, 1985.

[180] C. M. D'Sa, R. E. Arthur Jr, J. C. States, and D. M. Kuhn, "Tryptophan hydroxylase: cloning and expression of the rat brain enzyme in mammalian cells," *Journal of neurochemistry*, vol. 67, no. 3, pp. 900–906, 1996.

[181] S. Hosoda, "Further studies on tryptophan hydroxylase from neoplastic murine mast cells," *Biochimica et Biophysica Acta (BBA)-Enzymology*, vol. 397, no. 1, pp. 58–68, 1975.

[182] F. Takeuchi, H. Otsuka, and Y. Shibata, "Purification and properties of kynureninase from rat liver," *The Journal of Biochemistry*, vol. 88, no. 4, pp. 987–994, 1980.

[183] S. Lima, S. Kumar, V. Gawandi, C. Momany, and R. S. Phillips, "Crystal structure of the homo sapiens kynureninase-3-hydroxyhippuric acid inhibitor complex: insights into the molecular basis of kynureninase substrate specificity," *Journal of medicinal chemistry*, vol. 52, no. 2, pp. 389–396, 2008.

[184] H. A. Walsh, K. C. O'Shea, and N. P. Botting, "Comparative inhibition by substrate analogues 3-methoxy-and 3-hydroxydesaminokynurenine and an improved 3 step purification of recombinant human kynureninase.," *BMC biochemistry*, vol. 4, no. 1, p. 13, 2003.

[185] Q. Han, J. Li, and J. Li, "ph dependence, substrate specificity and inhibition of human kynurenine aminotransferase i," *European journal of biochemistry*, vol. 271, no. 23-24, pp. 4804–4814, 2004.

[186] P. Guidetti, E. Okuno, and R. Schwarcz, "Characterization of rat brain kynurenine aminotransferases i and ii," *Journal of neuroscience research*, vol. 50, no. 3, pp. 457–465, 1997.

[187] H. Baran, E. Okuno, R. Kido, and R. Schwarcz, "Purification and characterization of kynurenine aminotransferase i from human brain," *Journal of neurochemistry*, vol. 62, no. 2, pp. 730–738, 1994.

[188] S. Udenfriend and H. Weissbach, "Turnover of 5-hydroxytryptamine (serotonin) in tissues.," *Proceedings of the Society for Experimental Biology and Medicine*, vol. 97, no. 4, pp. 748–751, 1958.

[189] C. Speciale, U. Ungerstedt, and R. Schwarcz, "Effect of kynurenine loading on quinolinic acid production in the rat: studies in vitro and in vivo," *Life sciences*, vol. 43, no. 9, pp. 777–786, 1988.

[190] M. P. Heyes and P. F. Morrison, "Quantification of local de novo synthesis versus blood contributions to quinolinic acid concentrations in brain and systemic tissues," *Journal of neurochemistry*, vol. 68, no. 1, pp. 280–288, 1997.

[191] I. P. Lapin, L. G. Mutovkina, I. V. Ryzov, and S. Mirzaev, "Anxiogenic activity of quinolinic acid and kynurenine in the social interaction test in mice," *Journal of Psychopharmacology*, vol. 10, no. 3, pp. 246–249, 1996.

[192] R. Boni, M. Heyes, J. Bacher, J. Yergey, X.-D. Ji, F. Abramson, and S. Markey, "Stable isotope-labeled tryptophan as a precursor for studying the disposition of quinolinic acid in rabbits," in *Kynurenine and Serotonin Pathways*, pp. 481–484, Springer, 1991.

[193] C. Chang, K. R. Fonseca, C. Li, W. Horner, L. E. Zawadzke, M. A. Salafia, K. A. Welch, C. A. Strick, B. M. Campbell, S. S. Gernhardt, *et al.*, "Quantitative translational analysis of brain kynurenic acid modulation via irreversible kynurenine aminotransferase ii inhibition," *Molecular pharmacology*, vol. 94, no. 2, pp. 823–833, 2018.

[194] A. Moreira, E. P. Sampaio, A. Zmuidzinas, P. Frindt, K. A. Smith, and G. Kaplan, "Thalidomide exerts its inhibitory action on tumor necrosis factor alpha by enhancing mrna degradation.," *Journal of Experimental Medicine*, vol. 177, no. 6, pp. 1675–1680, 1993.

[195] S. Saks and M. Rosenblum, "Recombinant human tnf-alpha: preclinical studies and results from early clinical trials.," *Immunology series*, vol. 56, pp. 567–587, 1992.

[196] K. Van Zee, S. A. Stackpole, W. J. Montegut, M. A. Rogy, S. E. Calvano, K. C. Hsu, M. Chao, C. L. Meschter, H. Loetscher, and D. Stüber, "A human tumor necrosis factor (tnf) alpha mutant that binds exclusively to the p55 tnf receptor produces toxicity in the baboon.," *Journal of Experimental Medicine*, vol. 179, no. 4, pp. 1185–1191, 1994.

[197] H. Akaike, "A new look at the statistical model identification. ieee transactionson automatic control, 19 (6), 716–723," 1974.

[198] K. P. Burnham and D. R. Anderson, "Practical use of the information-theoretic approach," in *Model selection and inference*, pp. 75–117, Springer, 1998.

[199] S. K. Schmidt, S. Siepmann, K. Kuhlmann, H. E. Meyer, S. Metzger, S. Pudelko, M. Leineweber, and W. Däubener, "Influence of tryptophan contained in 1-methyltryptophan on antimicrobial and immunoregulatory functions of indoleamine 2, 3-dioxygenase," 2012.

[200] E. Wirthgen, S. Goumon, M. Kunze, C. Walz, M. Spitschak, A. Tuchscherer, J. Brown, C. Höflich, L. Faucitano, and A. Hoeflich, "Effects of transport duration and environmental conditions in winter or summer on the concentrations of insulin-like growth factors and insulin-like growth factor-binding proteins in the plasma of market-weight pigs," *Frontiers in endocrinology*, vol. 9, p. 36, 2018.

[201] H. Qian, C. Tao, A. T. Danilo, and J. L. Howard ROBINSON, "Substrate specificity and structure of human aminoadipate aminotransferase/kynurenine aminotransferase ii," *Bioscience reports*, vol. 28, no. 4, p. 205, 2008.

[202] I. D. Jung, M.-G. Lee, J. H. Chang, J. S. Lee, Y.-I. Jeong, C.-M. Lee, W. S. Park, J. Han, S.-K. Seo, S. Y. Lee, *et al.*, "Blockade of indoleamine 2, 3-dioxygenase protects mice against lipopolysaccharide-induced endotoxin shock," *The Journal of Immunology*, vol. 182, no. 5, pp. 3146–3154, 2009.

[203] L. Zhou, R. Zhu, Y. Lan, J. Yang, Y. Sun, Y. Hou, X. Ma, and Y. Liu, "Simultaneous determination of 1-methyltryptophan and indoleamine 2, 3-dioxygenase biomakers of tryptophan and kynurenine in mice tumors by hplc–ms/ms," *Chromatographia*, vol. 84, no. 7, pp. 623–634, 2021.

[204] H. C. Lewis, R. Chinnadurai, S. E. Bosinger, and J. Galipeau, "The ido inhibitor 1-methyl tryptophan activates the aryl hydrocarbon receptor response in mesenchymal stromal cells," *Oncotarget*, vol. 8, no. 54, p. 91914, 2017.

[205] A. Karmen, F. Wróblewski, J. S. LaDue, *et al.*, "Transaminase activity in human blood," *The Journal of clinical investigation*, vol. 34, no. 1, pp. 126–133, 1955.

[206] Y.-P. Wang, Z.-G. Sun, C.-Y. Zhang, Q.-Z. Zhang, X.-W. Guo, and D.-G. Xiao, "Comparative transcriptome analysis reveals the key regulatory genes for higher alcohol formation by yeast at different α-amino nitrogen concentrations," *Food Microbiology*, vol. 95, p. 103713, 2021.

[207] P. Khanna and M. S. Jorns, "Characterization of the fad-containing n-methyltryptophan oxidase from escherichia coli," *Biochemistry*, vol. 40, no. 5, pp. 1441–1450, 2001.

[208] W. J. Roth, C. B. Kissinger, R. R. McCain, B. R. Cooper, J. N. Marchant-Forde, R. C. Vreeman, S. Hannou, and G. T. Knipp, "Assessment of juvenile pigs to serve as human pediatric surrogates for preclinical formulation pharmacokinetic testing," *The AAPS journal*, vol. 15, no. 3, pp. 763–774, 2013.

[209] M. Platten, N. von Knebel Doeberitz, I. Oezen, W. Wick, and K. Ochs, "Cancer immunotherapy by targeting ido1/tdo and their downstream effectors," *Frontiers in immunology*, vol. 5, p. 673, 2015.

[210] A. Bessede, M. Gargaro, M. T. Pallotta, D. Matino, G. Servillo, C. Brunacci, S. Bicciato, E. Mazza, A. Macchiarulo, C. Vacca, *et al.*, "Aryl hydrocarbon receptor control of a disease tolerance defence pathway," *Nature*, vol. 511, no. 7508, pp. 184–190, 2014.

[211] E. Wirthgen, A. Hoeflich, A. Rebl, and J. Günther, "Kynurenic acid: the janus-faced role of an immunomodulatory tryptophan metabolite and its link to pathological conditions," *Frontiers in immunology*, vol. 8, p. 1957, 2018.

[212] A. Bianchi-Smiraglia, A. Bagati, E. E. Fink, H. C. Affronti, B. C. Lipchick, S. Moparthy, M. D. Long, S. R. Rosario, S. M. Lightman, K. Moparthy, *et al.*, "Inhibition of the aryl hydrocarbon receptor/polyamine biosynthesis axis suppresses multiple myeloma," *The Journal of clinical investigation*, vol. 128, no. 10, pp. 4682–4696, 2018.

[213] B. Tuvshintulga, E. Vannier, D. S. Tayebwa, S. Gantuya, T. Sivakumar, A. Guswanto, P. J. Krause, N. Yokoyama, and I. Igarashi, "Clofazimine, a promising drug for the treatment of babesia microti infection in severely immunocompromised hosts," *The Journal of infectious diseases*, vol. 222, no. 6, pp. 1027–1036, 2020.

[214] R. Mirnejad, A. Asadi, S. Khoshnood, H. Mirzaei, M. Heidary, L. Fattorini, A. Ghodousi, and D. Darban-Sarokhalil, "Clofazimine: A useful antibiotic for drug-resistant tuberculosis," *Biomedicine & Pharmacotherapy*, vol. 105, pp. 1353–1359, 2018.

[215] A. Nematollahi, G. Sun, G. S. Jayawickrama, and W. B. Church, "Kynurenine aminotransferase isozyme inhibitors: a review," *International journal of molecular sciences*, vol. 17, no. 6, p. 946, 2016.

[216] H.-Q. Wu, M. Okuyama, Y. Kajii, A. Pocivavsek, J. P. Bruno, and R. Schwarcz, "Targeting kynurenine aminotransferase ii in psychiatric diseases: promising effects of an orally active enzyme inhibitor," *Schizophrenia bulletin*, vol. 40, no. Suppl_2, pp. S152–S158, 2014.

[217] A. B. Dounay, M. Anderson, B. M. Bechle, B. M. Campbell, M. M. Claffey, A. Evdokimov, E. Evrard, K. R. Fonseca, X. Gan, S. Ghosh, *et al.*, "Discovery of brain-penetrant, irreversible kynurenine aminotransferase ii inhibitors for schizophrenia," *ACS medicinal chemistry letters*, vol. 3, no. 3, pp. 187–192, 2012.

[218] M. Turska, P. Paluszkiewicz, W. A. Turski, and J. Parada-Turska, "A review of the health benefits of food enriched with kynurenic acid," *Nutrients*, vol. 14, no. 19, p. 4182, 2022.

[219] M. Turska, R. Rutyna, M. Paluszkiewicz, P. Terlecka, A. Dobrowolski, J. Pelak, M. P. Turski, B. Muszyńska, W. Dabrowski, T. Kocki, *et al.*, "Presence of kynurenic acid in alcoholic beverages–is this good news, or bad news?," *Medical Hypotheses*, vol. 122, pp. 200–205, 2019.

[220] D. D. Bell and I. Zucker, "Sex differences in body weight and eating: organization and activation by gonadal hormones in the rat," *Physiology & behavior*, vol. 7, no. 1, pp. 27–34, 1971.

[221] R. W. Johnson and E. Von Borell, "Lipopolysaccharide-induced sickness behavior in pigs is inhibited by pretreatment with indomethacin," *Journal of animal science*, vol. 72, no. 2, pp. 309–314, 1994.

[222] F. W. Sosulski and G. I. Imafidon, "Amino acid composition and nitrogen-to-protein conversion factors for animal and plant foods," *Journal of agricultural and food chemistry*, vol. 38, no. 6, pp. 1351–1356, 1990.

[223] "Fasting in rodents guidelines on fasting." `https://norecopa.no/media/6351/food-deprivation.pdf`. Accessed: 2022-09-27.

[224] N. Verma, A. W. Rettenmeier, and S. Schmitz-Spanke, "Recent advances in the use of sus scrofa (pig) as a model system for proteomic studies," *Proteomics*, vol. 11, no. 4, pp. 776–793, 2011.

[225] H. Rothkötter, E. Sowa, and R. Pabst, "The pig as a model of developmental immunology," *Human & experimental toxicology*, vol. 21, no. 9-10, pp. 533–536, 2002.

[226] H. D. Dawson, A. D. Smith, C. Chen, and J. F. Urban Jr, "An in-depth comparison of the porcine, murine and human inflammasomes; lessons from the porcine genome and transcriptome," *Veterinary microbiology*, vol. 202, pp. 2–15, 2017.

[227] S. P. Golovan, H. A. Hakimov, C. P. Verschoor, S. Walters, M. Gadish, C. Elsik, F. Schenkel, D. K. Chiu, and C. W. Forsberg, "Analysis of sus scrofa liver proteome and identification of proteins differentially expressed between genders, and conventional and genetically enhanced lines," *Comparative Biochemistry and Physiology Part D: Genomics and Proteomics*, vol. 3, no. 3, pp. 234–242, 2008.

[228] G. González-Parra, H. M. Dobrovolny, D. F. Aranda, B. Chen-Charpentier, and R. A. G. Rojas, "Quantifying rotavirus kinetics in the reh tumor cell line using in vitro data," *Virus Research*, vol. 244, pp. 53–63, 2018.

[229] L. Milazzo, J. L. Bown, A. Eberst, G. Phillips, and J. W. Crawford, "Modelling of healthcare associated infections: a study on the dynamics of pathogen transmission by using an individual-based approach," *Computer methods and programs in biomedicine*, vol. 104, no. 2, pp. 260–265, 2011.

[230] J. Ferrer, C. Prats, D. López, and J. Vives-Rego, "Mathematical modelling methodologies in predictive food microbiology: a swot analysis," *International Journal of Food Microbiology*, vol. 134, no. 1-2, pp. 2–8, 2009.

[231] G. Ciprandi, M. De Amici, M. Tosca, and D. Fuchs, "Tryptophan metabolism in allergic rhinitis: the effect of pollen allergen exposure," *Human immunology*, vol. 71, no. 9, pp. 911–915, 2010.

[232] S. J. Lehotay, K. Mastovska, A. Amirav, A. B. Fialkov, P. A. Martos, A. De Kok, and A. R. Fernández-Alba, "Identification and confirmation of chemical residues in food by chromatography-mass spectrometry and other techniques," *TrAC Trends in Analytical Chemistry*, vol. 27, no. 11, pp. 1070–1090, 2008.

[233] A. Ramanathan, C. A. Steed, and L. L. Pullum, "Verification of compartmental epidemiological models using metamorphic testing, model checking and visual analytics," in *2012 ASE/IEEE International Conference on BioMedical Computing (BioMedCom)*, pp. 68–73, IEEE, 2012.

[234] A. E. Cowan, I. I. Moraru, J. C. Schaff, B. M. Slepchenko, and L. M. Loew, "Spatial modeling of cell signaling networks," in *Methods in cell biology*, vol. 110, pp. 195–221, Elsevier, 2012.

[235] X. Liu, J. Jiang, O. Ajayi, X. Gu, D. Gilbert, and R. O. Sinnott, "Bionessie-a grid enabled biochemical networks simulation environment," *Studies in Health Technology and Informatics*, vol. 138, pp. 147–157, 2008.

[236] J. A. Koziol, T. J. Falls, and J. E. Schnitzer, "Different ode models of tumor growth can deliver similar results," *BMC cancer*, vol. 20, no. 1, pp. 1–10, 2020.

[237] J. Kuha, "Aic and bic: Comparisons of assumptions and performance," *Sociological methods & research*, vol. 33, no. 2, pp. 188–229, 2004.

[238] R. Kuiper, "Aic-type theory-based model selection for structural equation models," *Structural Equation Modeling: A Multidisciplinary Journal*, vol. 29, no. 1, pp. 151–158, 2022.

[239] D. Anderson and K. Burnham, "Model selection and multi-model inference," *Second. NY: Springer-Verlag*, vol. 63, no. 2020, p. 10, 2004.

[240] H. Akaike, "On the likelihood of a time series model," *Journal of the Royal Statistical Society: Series D (The Statistician)*, vol. 27, no. 3-4, pp. 217–235, 1978.

[241] E.-J. Wagenmakers and S. Farrell, "Aic model selection using akaike weights," *Psychonomic bulletin & review*, vol. 11, no. 1, pp. 192–196, 2004.

[242] H. Miao, C. Dykes, L. M. Demeter, and H. Wu, "Differential equation modeling of hiv viral fitness experiments: model identification, model selection, and multimodel inference," *Biometrics*, vol. 65, no. 1, pp. 292–300, 2009.

[243] A. Polynikis, S. Hogan, and M. di Bernardo, "Comparing different ode modelling approaches for gene regulatory networks," *Journal of theoretical biology*, vol. 261, no. 4, pp. 511–530, 2009.

[244] Y.-B. Zhao and J. Krishnan, "mrna translation and protein synthesis: an analysis of different modelling methodologies and a new pbn based approach," *BMC systems biology*, vol. 8, no. 1, pp. 1–24, 2014.

[245] G. P. Figueredo, P.-O. Siebers, and U. Aickelin, "Investigating mathematical models of immuno-interactions with early-stage cancer under an agent-based modelling perspective," in *BMC bioinformatics*, vol. 14, pp. 1–20, BioMed Central, 2013.

[246] T. Kind, H. Tsugawa, T. Cajka, Y. Ma, Z. Lai, S. S. Mehta, G. Wohlgemuth, D. K. Barupal, M. R. Showalter, M. Arita, *et al.*, "Identification of small molecules using accurate mass ms/ms search," *Mass spectrometry reviews*, vol. 37, no. 4, pp. 513–532, 2018.

[247] J. F. Krey, P. A. Wilmarth, J.-B. Shin, J. Klimek, N. E. Sherman, E. D. Jeffery, D. Choi, L. L. David, and P. G. Barr-Gillespie, "Accurate label-free protein quantitation with high-and low-resolution mass spectrometers," *Journal of proteome research*, vol. 13, no. 2, pp. 1034–1044, 2014.

[248] W. X. Schulze, B. Usadel, *et al.*, "Quantitation in mass-spectrometry-based proteomics," *Annual review of plant biology*, vol. 61, no. 1, pp. 491–516, 2010.

[249] M. Bantscheff, S. Lemeer, M. M. Savitski, and B. Kuster, "Quantitative mass spectrometry in proteomics: critical review update from 2007 to the present," *Analytical and bioanalytical chemistry*, vol. 404, no. 4, pp. 939–965, 2012.

[250] J. J. Morelli, "Thermal analysis using mass spectrometry: a review," *Journal of analytical and applied pyrolysis*, vol. 18, no. 1, pp. 1–18, 1990.

[251] W. Han and L. Li, "Evaluating and minimizing batch effects in metabolomics," *Mass Spectrometry Reviews*, vol. 41, no. 3, pp. 421–442, 2022.

[252] R. Wehrens, J. Hageman, F. van Eeuwijk, R. Kooke, P. J. Flood, E. Wijnker, J. J. Keurentjes, A. Lommen, H. D. van Eekelen, R. D. Hall, *et al.*, "Improved batch correction in untargeted ms-based metabolomics," *Metabolomics*, vol. 12, no. 5, pp. 1–12, 2016.

[253] J. T. Leek, R. B. Scharpf, H. C. Bravo, D. Simcha, B. Langmead, W. E. Johnson, D. Geman, K. Baggerly, and R. A. Irizarry, "Tackling the widespread and critical impact of batch effects in high-throughput data," *Nature Reviews Genetics*, vol. 11, no. 10, pp. 733–739, 2010.

[254] V. Nygaard, E. A. Rødland, and E. Hovig, "Methods that remove batch effects while retaining group differences may lead to exaggerated confidence in downstream analyses," *Biostatistics*, vol. 17, no. 1, pp. 29–39, 2016.

[255] R. J. Collier, K. G. Gebremedhin, *et al.*, "Thermal biology of domestic animals," *Annu. Rev. Anim. Biosci*, vol. 3, no. 1, pp. 513–532, 2015.

[256] J. M. Gostner, K. Becker, H. Kofler, B. Strasser, and D. Fuchs, "Tryptophan metabolism in allergic disorders," *International archives of allergy and immunology*, vol. 169, no. 4, pp. 203–215, 2016.

[257] K. M. Brindle, "Nmr methods for measuring enzyme kinetics in vivo," *Progress in Nuclear Magnetic Resonance Spectroscopy*, vol. 20, no. 3, pp. 257–293, 1988.

[258] R. Kapoor, E. Okuno, R. Kido, and V. Kapoor, "Immuno-localization of kynurenine aminotransferase (kat) in the rat medulla and spinal cord," *Neuroreport*, vol. 8, no. 16, pp. 3619–3623, 1997.

[259] Q. Han, T. Cai, D. A. Tagle, and J. Li, "Structure, expression, and function of kynurenine aminotransferases in human and rodent brains," *Cellular and Molecular Life Sciences*, vol. 67, no. 3, pp. 353–368, 2010.

[260] R. Schwarcz, J. P. Bruno, P. J. Muchowski, and H.-Q. Wu, "Kynurenines in the mammalian brain: when physiology meets pathology," *Nature Reviews Neuroscience*, vol. 13, no. 7, pp. 465–477, 2012.

[261] S. Erhardt, L. Schwieler, L. Nilsson, K. Linderholm, and G. Engberg, "The kynurenic acid hypothesis of schizophrenia," *Physiology & behavior*, vol. 92, no. 1-2, pp. 203–209, 2007.

[262] E. Plitman, Y. Iwata, F. Caravaggio, S. Nakajima, J. K. Chung, P. Gerretsen, J. Kim, H. Takeuchi, M. M. Chakravarty, G. Remington, *et al.*, "Kynurenic acid in schizophrenia: a systematic review and meta-analysis," *Schizophrenia bulletin*, vol. 43, no. 4, pp. 764–777, 2017.

[263] S. Erhardt, S. K. Olsson, and G. Engberg, "Pharmacological manipulation of kynurenic acid," *CNS drugs*, vol. 23, no. 2, pp. 91–101, 2009.

[264] P. Brodin and M. M. Davis, "Human immune system variation," *Nature reviews immunology*, vol. 17, no. 1, pp. 21–29, 2017.

[265] A. Surendran, J. Le Sauteur-Robitaille, D. Kleimeier, J. L. Gevertz, K. P. Wilkie, A. L. Jenner, and M. Craig, "Approaches to generating virtual patient cohorts with applications in oncology," *bioRxiv*, 2022.

[266] D. Čepcová, I. P. Kema, M. Sandovici, L. E. Deelman, K. Šišková, J. Klimas, P. Vavrinec, and D. Vavrincová-Yaghi, "The protective effect of 1-methyltryptophan isomers in renal ischemia-reperfusion injury is not exclusively dependent on indolamine 2, 3-dioxygenase inhibition," *Biomedicine & Pharmacotherapy*, vol. 135, p. 111180, 2021.

[267] "Protein molecular weight." `https://www.bioinformatics.org/sms/prot_mw.html`. Accessed: 2019-03-25.

[268] "Uniprotkb." `https://www.uniprot.org/uniprot/B3GDZ6.fasta`. Accessed: 2019-03-25.

A. Data Description

To estimate parameters representing the dynamics of the TRP metabolism, published data from experiments conducted in pigs were used [149, 162, 86]. Those experiments include LPS administration, 1-MT administration and a combination of 1-MT, and LPS administration. They have been performed to establish a pig model of IDO activation and to investigate the protective and immunomodulatory effects of 1-MT. Therefore, the TRP metabolites TRP, SER, KYN, KYNA, QUIN, and 1-MT were measured by MS2 mass spectrometry. Due to analytical issues with internal standards, the scale of TRP metabolites was different between different experiments. Moreover, TNF-α was measured after stimulation by LPS with an ELISA kit to measure the immune system-activating properties of LPS. As the basis for further investigations, control animals data were used for parameter fitting of a standard model of the TRP metabolism. This model was extended by IDO activating LPS administration. Parameters of this model were fitted to data from LPS-treated pigs [149]. The estimated parameters of this model were validated on a similar data set. To investigate the 1-MT induced increase of TRP and KYNA, parameters were fitted to data from 1-MT-treated pigs [162, 86]. Moreover, to test whether the developed model can represent the dynamics of TRP metabolism, including 1-MT's inhibitory effects, data from 1-MT and LPS-treated pigs were used. All blood samples were taken from the anterior vena cava. The TRP metabolites (TRP, KYN, KYNA, QUIN, SER) and, depending on the experiment, 1-MT, TNF-α or both were measured. A detailed explanation of the experimental set-up can be found in the corresponding publications [149, 162, 86]. The experimental set-up is summarized below.

A.1. LPS - Treated Pigs

To fix parameters in the models of 1-MT degradation, parameters were fitted to data representing the dynamics of the TRP metabolism in LPS-treated pigs. Those data were published by Wirthgen et al. [147]. The here presented experiment is called the „LPS experiment I“ below. In Figure A.1 a schematic presentation of the experimental set-up is shown.

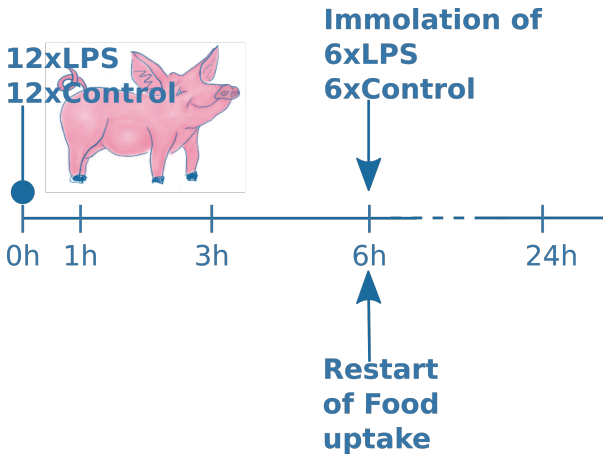

Figure A.1.: **LPS Experiment I and II:** In LPS experiment I, 24 pigs, and in LPS experiment II, 16 pigs were treated at 0 h with either LPS or NaCl as control. At 0 h, 1 h, 3 h, 6 h, and 24 h blood samples were taken and metabolites of the TRP metabolism (TRP, SER, KYN, KYNA, QUIN), and TNF-α were measured (see Figure A.2 and Figure A.3). Before 0 h, food was subducted. 6 h later, food was supplied. At 6 h, twelve pigs of LPS experiment I and eight pigs of LPS experiment II were sacrificed.

Twelve pigs received 100 000 endotoxin units (EU) LPS per kg body weight. The control group consisted of twelve NaCl-treated pigs. 1 h before LPS or NaCl administration, food was removed, but feeding started again 6 h after LPS/NaCl administration. After 6 h, twelve pigs were sacrificed for further studies. Hence, the group size of twelve pigs was reduced to six pigs for LPS and to six pigs for NaCl-treated pigs. TRP, KYN, KYNA, QUIN and SER (TRP metabolites) and TNF-α were measured in blood shortly before LPS administration (0 h), 1 h, 3 h, 6 h and 24 h after LPS/NaCl administration [149]. All metabolites were measured with an MS2 mass spectrometer. The metabolites were indicated in μM, except TNF-α, which was indicated in pg/ml, because it was measured by an ELISA kit. To full fill the requirement of the law of mass action, TNF-α was converted in μM by multiplying with 10^{-9} and by division of the specific molecular weight of TNF-α for pigs (25.26 kD) [267, 268]. Data of LPS experiment I are presented in Figure A.2 and were used to fit parameters representing the dynamics of the TRP metabolism and the activation of IDO by LPS.

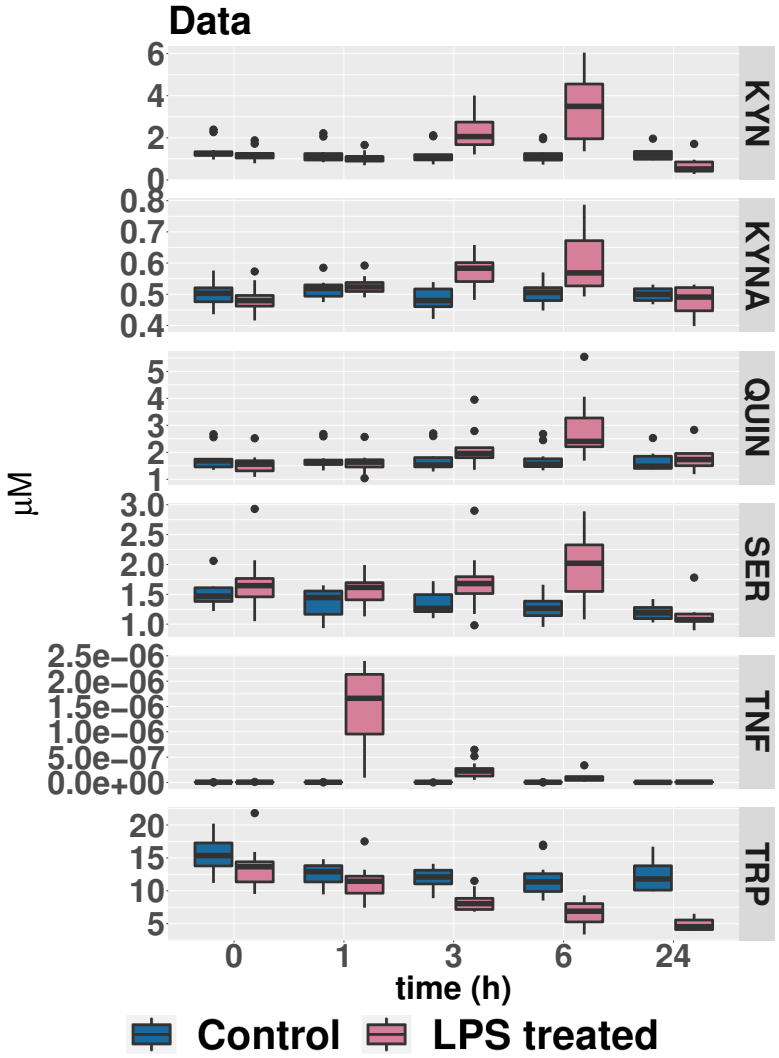

Figure A.2.: **Data measured in LPS experiment I** Measurements of LPS experiment I (compare Figure A.1), twelve LPS and twelve NaCl (as control)-treated pigs have received LPS at 0 h and were starved between 0 h and 6 h. Six LPS and six NaCl-treated pigs were sacrificed at 6 h. This data set is used to fit parameters. Control - NaCl-treated. TRP - tryptophan, KYN - kynurenine, KYNA - kynurenic acid, QUIN - quinolinic acid, SER - serotonin, TNF - tumor necrosis factor α

A second data set, called the „LPS experiment II“, was used to validate those parameters. Measurements are presented in Figure A.3. The data of this data set is also not normally distributed. Again, the medians are decentered and the whiskers are of different length of each box in Figure A.3.

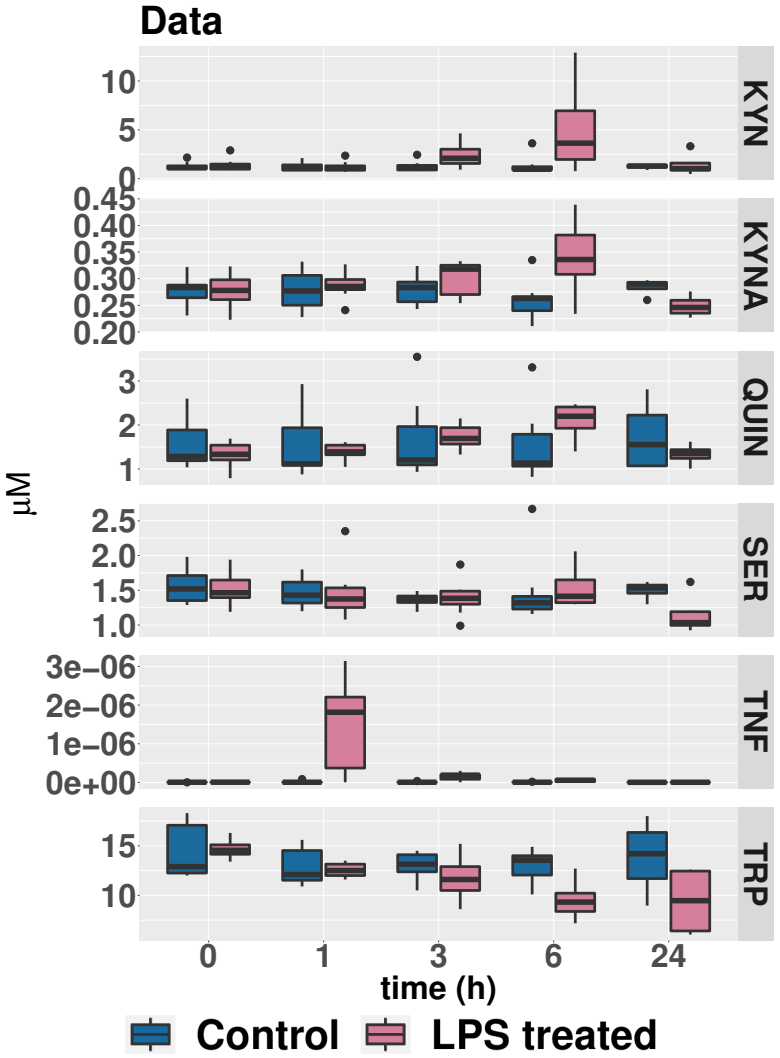

Figure A.3.: **Data measured in LPS experiment II** Measurements of LPS experiment I (compare Figure A.1), eight LPS and eight NaCl (as control)-treated pigs have received LPS at 0 h and were starved between 0 h and 6 h. Four LPS and four NaCl-treated pigs were sacrificed at 6 h. This data set is used to validate parameters fitted to data of LPS experiment I. Control - NaCl-treated. TRP - tryptophan, KYN - kynurenine, KYNA - kynurenic acid, QUIN - quinolinic acid, SER - serotonin, TNF - tumor necrosis factor α

This experiment was conducted the same way as LPS experiment I, except the number of pigs varied. In LPS experiment II, 16 pigs were included, eight LPS-treated and eight NaCl-treated pigs. At 6 h, four pigs of the LPS-treated pigs, and four pigs of the NaCl-treated pigs were sacrificed. Thus, four LPS and four NaCl-treated pigs remained. Due to the differing numbers of pigs, LPS experiment I was used for parameter fitting and LPS experiment II for parameter validation.

A.2. 1-MT and LPS-treated Pigs

Additionally to parameters fitted to data of LPS experiment I (see Figure A.2), parameters were fitted to a subset of the data set presented in this section. Moreover, this data set was used to fit the parameters of models explaining the degradation of 1-MT, and its inhibitory effects on IDO. Those data were already published by Wirthgen et al. [162, 86] and are called the „1-MT/LPS experiment“ below. 16 pigs were included in this experiment. Eight pigs received five times every 24 h 1 g 1-MT (see Figure A.4).

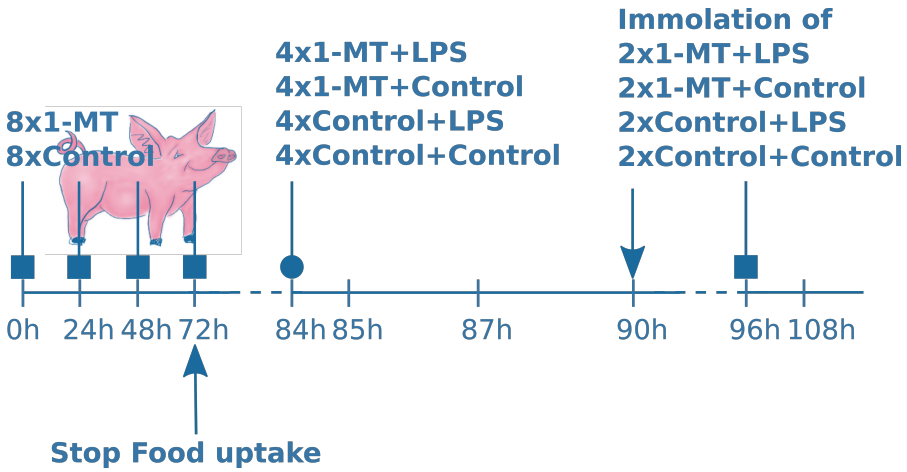

Figure A.4.: **1-MT/LPS experiment:** At 0 h, 24 h, 48 h, 72 h, and 96 h (arrows with square arrowheads) 16 pigs were treated with 1-MT or Myritol as control. At 84 h, pigs received either LPS or NaCl as control. At 90 h, half of the pigs were sacrificed (eight of 16 remained, each treatment group was of equal group size). Pigs were starved from 72 h on till the end of the experiment. At each indicated (0 h, 24 h, 48 h, 72 h, 84 h, 85 h, 86 h, 87 h, 90 h, 96 h, and 108 h) samples from blood were taken, measurements of TRP metabolites and 1-MT are shown in Figure A.5

The control group, consisting of eight pigs, received Myritol (carrier solution for 1-MT). Blood samples were taken at 0 h, 24 h, 48 h, 72 h, and 96 h. Hence, after each 1-MT/Myritol administration. 12 h after the fourth application (at 84 h) of 1-MT, eight pigs received 150 000 EU/kg LPS. Four of them were treated with 1-MT, and four pigs were treated with Myritol. The control group received NaCl consisting of four 1-MT-treated pigs and four Myritol-treated pigs. Thus, this leads to four treatment groups (each with four pigs):

- 1-MT & LPS - pigs that were treated with 1-MT and LPS

- 1-MT, Control - pigs that were treated with 1-MT and NaCl
- Control, LPS - pigs that were treated with Myritol and LPS
- Control & Control- that which were treated with Myritol and NaCl

At 85 h, 87 h, 90 h, 96 h (before the fifth 1-MT application), and at 108 h after LPS/NaCl administration blood samples were taken, too. Half of the treated animals were sacrificed distributed in the four treatment groups after 90 h (see Figure A.1). Thus in each group, two pigs remained. The pigs were starved after the 1-MT administration at 72 h. Feeding was not restarted. All measurements were indicated in μM. TNF-α was indicated in pg/ml. TNF-α measurements were converted to μM as described section A.1 to get uniform units. Measurements of 1-MT, TNF-α, and TRP metabolites are presented in Figure A.5. For parameter fitting, the data set was split up into different subsets according to their purposes.

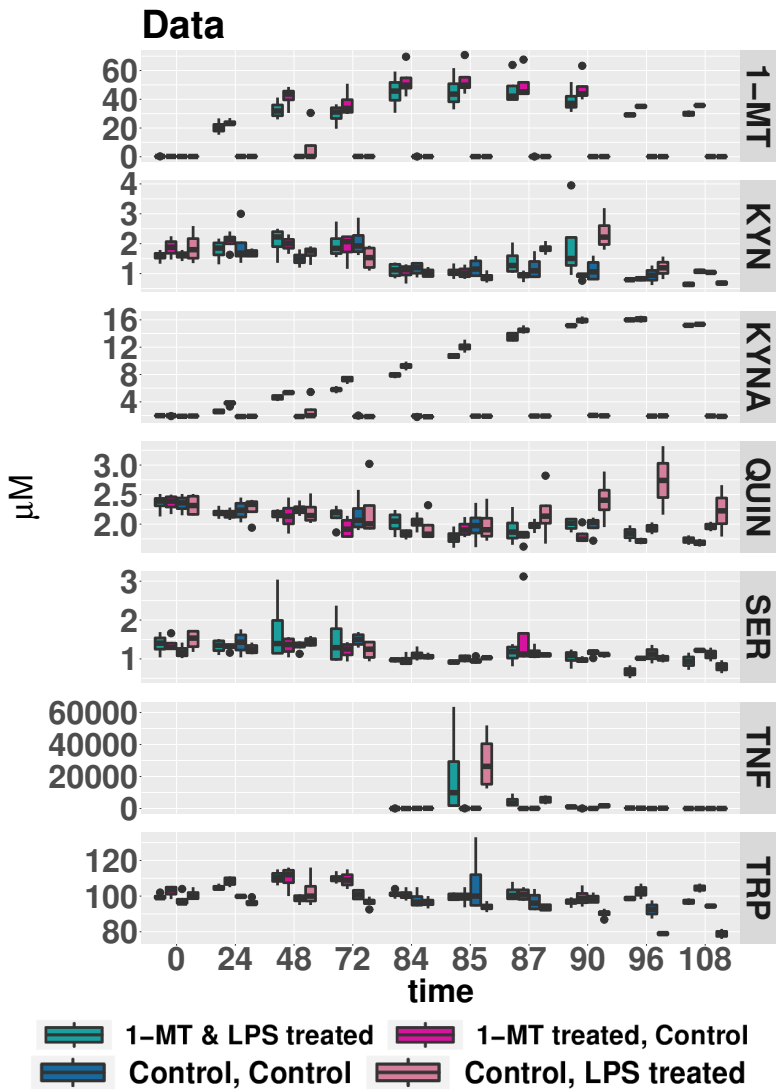

Figure A.5.: **Data measured in 1-MT/LPS experiment:** At 0 h, 24 h, 48 h, 72 h, and 96 h pigs were treated with 1-MT or Myritol (Control) as control, at 84 h pigs received either LPS or NaCl (Control) as control. Four treatment groups resulted (1-MT and LPS - 1-MT & LPS-treated; 1-MT and NaCl - 1-MT-treated, Control; Myritol, and NaCl - Control & Control, Myritol and LPS - Control, LPS-treated). At 90 h, half of the pigs were sacrificed from 16 pigs to eight pigs(equally distributed in the treatment groups). The pigs were starved from 72 h on till the end of the experiment. At each indicated (0 h, 24 h, 48 h, 72 h, 84 h, 85 h, 86 h, 87 h, 90 h, 96 h, and 108 h) samples from blood were taken, TRP metabolites (TRP, SER, KYN, KYNA, QUIN), and 1-MT and TNF-α concentration (only after LPS administration at 84 h) were measured. TRP - tryptophan, KYN - kynurenine, KYNA - kynurenic acid, QUIN - quinolinic acid, SER - serotonin, TNF-α - tumor necrosis factor α

1-MT/LPS experiment, subset LPS-treated pigs To model the dynamics of the LPS induced enzyme IDO concerning the TRP metabolism, the data of the 1-MT/LPS experiment were reduced to pigs only treated with Myritol and afterward with LPS or NaCl. A summary of the experiment with a subset of the pigs is shown in Figure A.6.

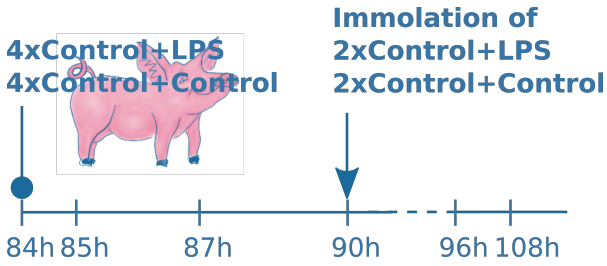

Figure A.6.: **1-MT/LPS experiment, subset LPS-treated** Only a subset of pigs of 1-MT/LPS experiment (see Figure A.4) is considered, Myritol-treated pigs received LPS or NaCl at 84 h, at each indicated (84 h, 85 h, 86 h, 87 h, 90 h, 96 h, and 108 h). At 90 h half of the pigs were sacrificed (four of eight pigs remained). The samples from blood were taken at every indicated . The pigs had no access to food during the whole experiment. The measurements of TRP metabolites and 1-MT are shown in Figure A.7

Only data after 84 h were used for parameter fitting (see Figure A.7). This subset is named „1-MT/LPS experiment, subset LPS-treated pigs“. Pigs were starved for the whole time of this period. Moreover, the number of included pigs is lower than the one in LPS experiment I and II (only eight pigs instead of 24 respective 16 pigs). Moreover, the LPS experiments I and II were conducted during the summer season (August and September) whereas this experiment was conducted in the winter (January). The comparability of results from experiments conducted in different seasons is reduced [255, 256]. In addition, TRP levels are increased by a factor of 5. Experimentalists speculate about human errors. With this subset, results based on the data measured in LPS experiments I and II were validated and parameters only based on 1-MT/LPS experiment, subset LPS-treated pigs, were estimated. Those parameters were also applied to data, to explain the degradation process of 1-MT and its inhibitory effects on IDO.

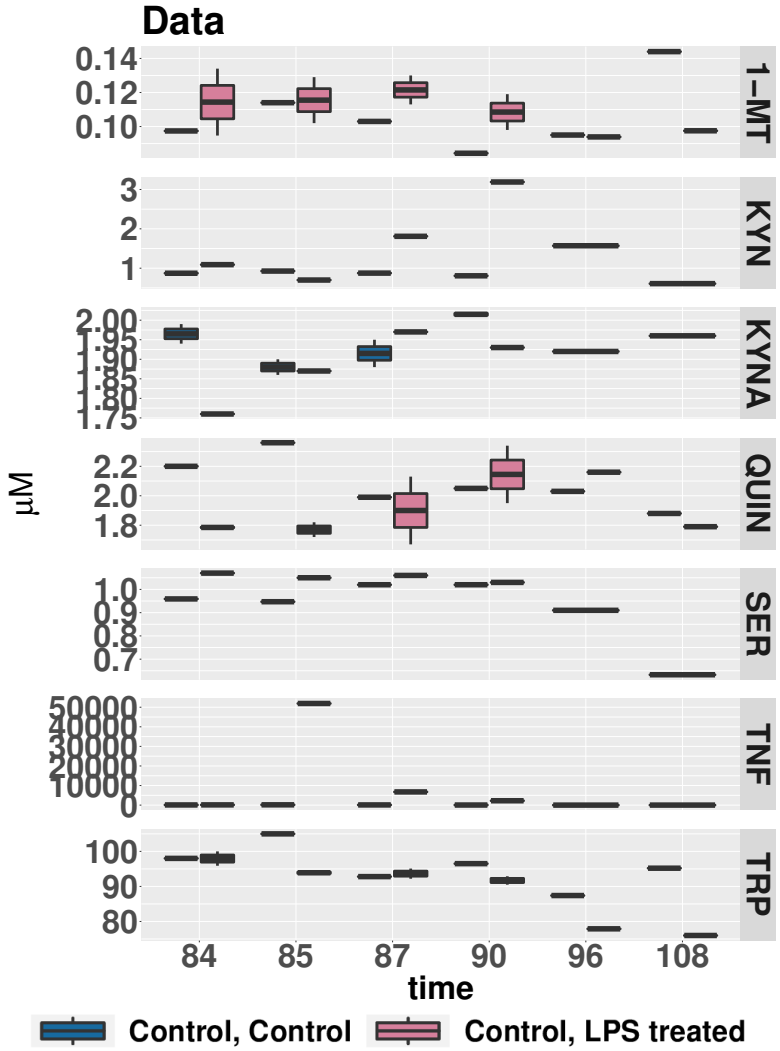

Figure A.7.: **Data measured in 1-MT/LPS experiment, subset LPS-treated:** Only a subset of pigs of the 1-MT/LPS experiment (see Figure A.4) is considered. Myritol-treated pigs received LPS or NaCl at 84 h. At each indicated (84 h, 85 h, 86 h, 87 h, 90 h, 96 h, and 108 h), samples from blood were taken. At 84 h, LPS was administered. The TRP metabolites (TRP, SER, KYN, KYNA, QUIN), and TNF-α concentration were measured. Pigs had no access to food during the whole time. Control & Control - Myritol and NaCl-treated. Control, LPS-treated - Myritol and LPS-treated. TRP - tryptophan, KYN - kynurenine, KYNA - kynurenic acid, QUIN - quinolinic acid, SER - serotonin, TNF-α - tumor necrosis factor α

1-MT/LPS experiment, subset 1-MT-treated pigs The following subset of data measured in the 1-MT/LPS experiment was used to simulate different degradation processes of 1-MT leading to an increase of TRP and KYNA levels at the same time the intermediate metabolite KYN did not change. Thus, only the subset of 1-MT-treated

pigs is needed. Therefore the subset consists of pigs, which were not treated with LPS. Only 1-MT and Myritol-treated pigs were included (see Figure A.8).

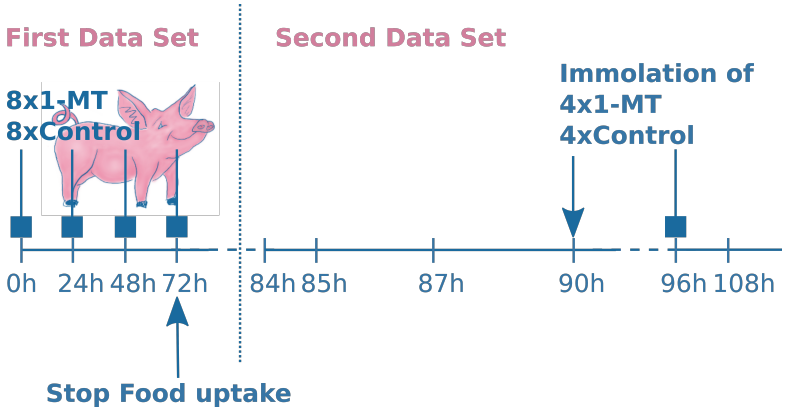

Figure A.8.: **1-MT/LPS experiment, subset 1-MT-treated:** At 0 h, 24 h, 48 h, 72 h, and 96 h (arrows with square arrow heads), pigs were treated with 1-MT or Myritol as control, at 90 h half of the pigs were sacrificed (four of eight pigs remained, equally distributed in the treatment groups), pigs had access to food during s 0 h and 72 h, from 72 h till the end of the experiment pigs straved, at each indicated (0 h, 24 h, 48 h, 72 h, 84 h, 85 h, 86 h, 87 h, 90 h, 96 h, and 108 h) samples from blood were taken, data set was divided in pigs, which received food (first data set) and pigs which did not receive food (second data set), measurements of the TRP metabolites and 1-MT with *FoodSupply* (first data set) are shown in Figure A.9 and without *FoodSupply* (second data set) are shown in Figure A.10

This subset is named 1-MT/LPS experiment, subset 1-MT-treated pigs, and was split up in two periods by the food supply. Since food contains TRP, the increase of TRP due to food intake has to be considered in the models. During the first period, which consists of eight 1-MT and eight Myritol-treated pigs, pigs were fed (see Figure A.8, first data set). Corresponding data are not normally distributed since whiskers are of different lengths and mean values are not centered. The data are presented in Figure A.9.

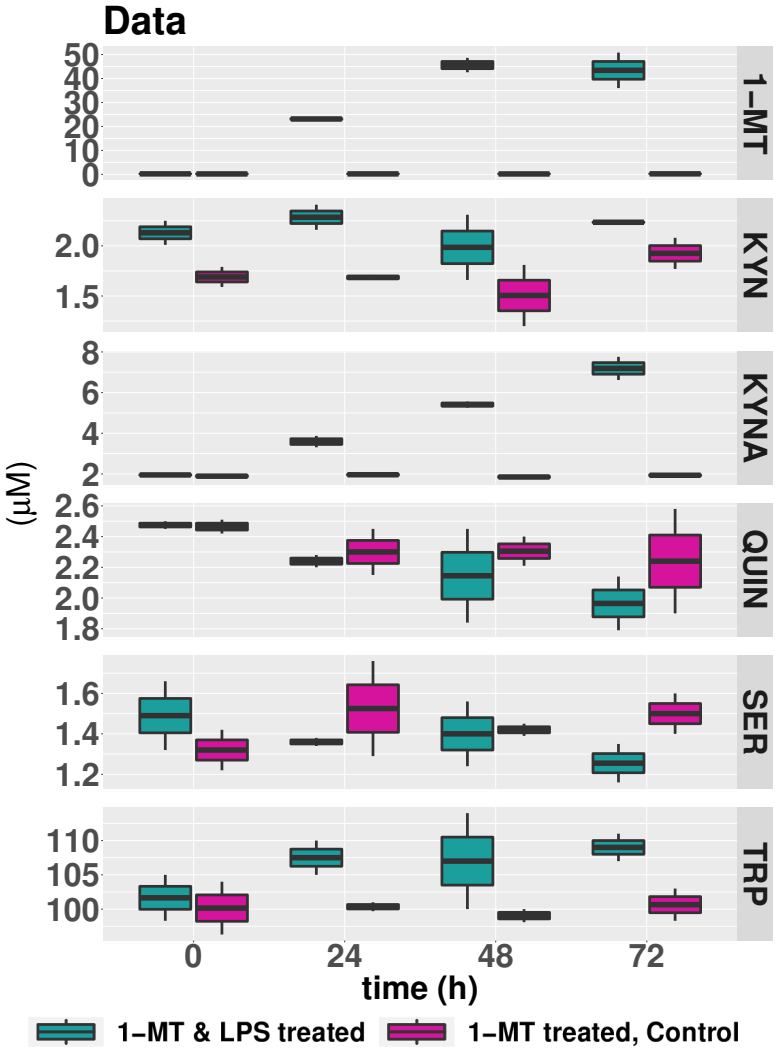

Figure A.9.: **Data measured in 1-MT/LPS experiment, subset 1-MT-treated pigs (first data set):** 16 pigs were treated with 1-MT or Myritol as control, every 24 h (0 h, 24 h, 48 h, 72 h). 1-MT was administered at the indicated time points. Blood samples were taken, and levels of TRP metabolites (TRP, SER, KYN, KYNA, QUIN), and 1-MT concentration were measured. Pigs had access to food for the whole time. 1-MT-treated, Control - 1-MT and NaCl-treated, Control & Control - Myritol and NaCl-treated. TRP - tryptophan, KYN - kynurenine, KYNA - kynurenic acid, QUIN - quinolinic acid, SER - serotonin, 1-MT - 1-methyltryptophan

The second period includes eight pigs, which were starved and were reduced due to immolation at 90 h (see Figure A.8, second data set). Corresponding data are presented in Figure A.10. Again, parameters are not normally distributed, since median values are not centered, and the whiskers are of different lengths. With this subset, parameters estimated on data measured in LPS experiment I and II, and 1-MT/LPS

experiment, subset LPS-treated pigs, were applied on different models, which describe possible degradation processes of 1-MT.

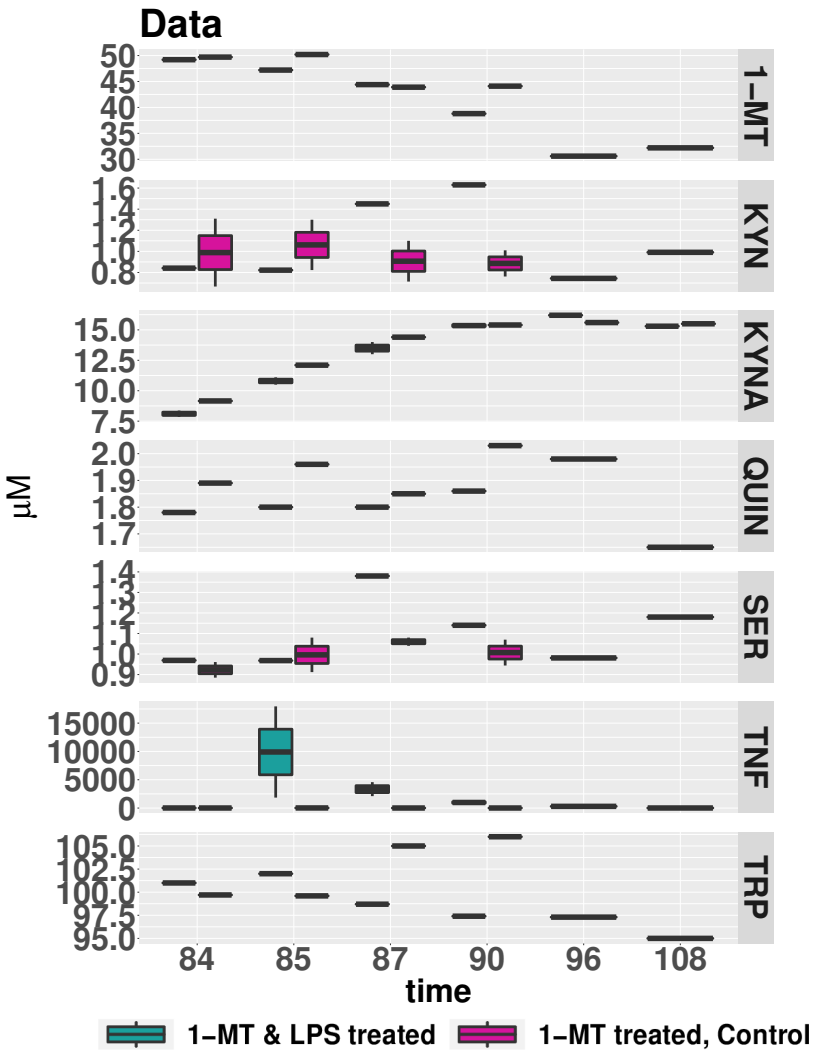

Figure A.10.: **Data measured in 1-MT/LPS experiment, subset 1-MT-treated pigs (second data set):** 16 pigs have been treated with 1-MT or Myritol as control. Every 24 h (0 h, 24 h, 48 h, 72 h, and 96 h), 1-MT was administered. Blood samples were taken at the indicated time points (84 h, 85 h, 87 h, 90 h, 96 h, 108 h). TRP metabolites (TRP, SER, KYN, KYNA, QUIN), and the concentration of 1-MT, were measured. Pigs were starved during the whole time. 1-MT-treated, Control - 1-MT and NaCl-treated, Control & Control - Myritol and NaCl-treated. TRP - tryptophan, KYN - kynurenine, KYNA - kynurenic acid, QUIN - quinolinic acid, SER - serotonin, 1-MT - 1-methyltryptophan

1-MT/LPS experiment, second data set The following subset of data measured in the 1-MT/LPS experiment was used to investigate the ability of the model to reflect 1-MT's inhibitory effects on IDO. Therefore, measurements of pigs treated with 1-MT or Myritol and LPS or NaCl, had to be included. Since LPS was administered at 84 h, only measurements of samples taken at or after 84 h were included. Consequently, this subset consists of pigs treated with LPS or NaCl and 1-MT or Myritol (see Figure A.8, second data set). This subset is called the „1-MT/LPS experiment", second data set. The data are presented in Figure A.11 and are again not normally distributed. This subset was used to fit the parameters of different models. The first one includes the inhibitory effects of 1-MT, and the other does not include inhibitory interactions.

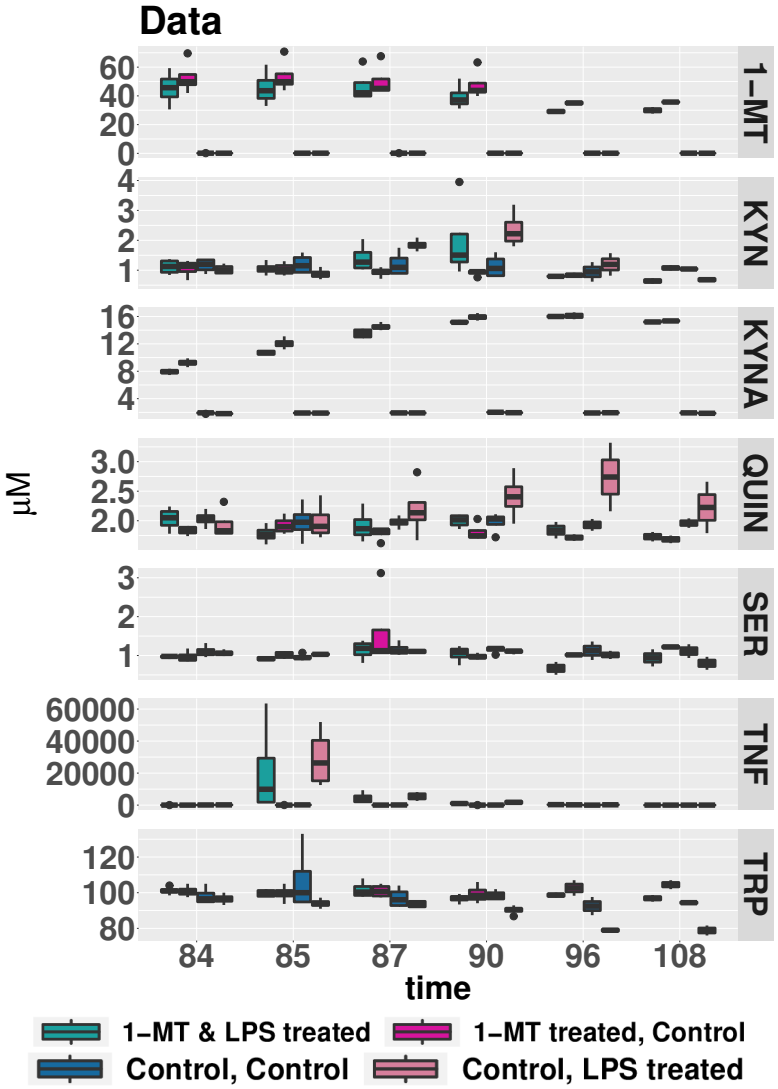

Figure A.11.: **Data measured in 1-MT/LPS experiment (second data set):** 16 pigs were treated with 1-MT or Myritol as control. Four times before the LPS administration at 84 h, 1-MT was administered (0 h, 24 h, 48 h, 72 h, which were omitted), and at 96 h, 1-MT was administered. Blood samples were taken, at the indicated time points (84 h, 85 h, 87 h, 90 h, 96 h, 108 h). TRP metabolites (TRP, SER, KYN, KYNA, QUIN) 1-MT, and $TNF - \alpha$ concentrations, were measured. Pigs were starved during the whole time. 1-MT-treated, Control - 1-MT and NaCl-treated, Control & Control - Myritol and NaCl-treated. TRP - tryptophan, KYN - kynurenine, KYNA - kynurenic acid, QUIN - quinolinic acid, SER - serotonin, TNF-α - tumor necrosis factor α

B. Identifiability Analysis

Table B.1.: **Upper and lower boundary of Identifiability analysis for the LPS model**

parameter	lb	ub	parameter value
V_{KQE}^{max}	1.64	1.7949	1.719
V_{IDO}^{max}	5.3829	5.7898	5.6231
V_{KAT}^{max}	2.5986	2.704	2.6487
V_{TDO}^{max}	0.4452	0.51586	0.48079
V_{TPH}^{max}	-Inf	-0.70297	-1.2354
$FoodSupplyLPS$	1.2594	1.3845	1.3259
$FoodSupplyNaCl$	1.3703	1.4751	1.4249
KYN_0	-0.011572	0.1524	0.077056
$KYNA_0$	-0.31736	-0.27847	-0.29752
$QUIN_0$	0.18013	0.27547	0.22995
SER_0	0.17225	0.22564	0.19997
TRP_0	1.1446	1.1805	1.1627
k	-10.398	-10.132	-10.287
μ_{LPS}	-0.091135	0.25617	0.058797

An identifiability analysis was performed for the parameters fitted to data of LPS experiment I, which are shown in Table C.1 of the LPS model. Parameter identifications are given in the column „parameter“, lower boundary (lb), and upper boundary (ub), and parameter values are given in log_{10}scale in the corresponding column, *species*0 are the fitted initial values of the corresponding species.

C. Comparison of literature and fitted parameters

Table C.1.: **Overview of fitted parameters of the LPS model on different data sets and literature values**

parameter	**I**	**II**	**III**	**IV**	**V**	**VI**
V_{max}^{KAT}	445.35	0.45145	154.73	149.0269	192.9756	$0.271286 - 2820.3$
V_{max}^{TPH}	0.058159	0.10778	0.1531	0.2828675	0.9691421	$78.88 - 81,6 \cdot 10^{12}$
V_{max}^{TDO}	3.0254	0.10778	0.67461	19.0957	129.031	$3934.072 - 94.112 \cdot 10^{6}$
V_{max}^{KQE}	52.36	208.22	107.78	79.06573	25.8605	$1.69218 \cdot 10^{3}$
V_{max}^{IDO}	419880	$119.04 \cdot 10^{-5}$	$5.2925 \cdot 10^{-5}$	21.14442	140.2408	$50 - 14.851 \cdot 10^{3}$
k	5.165110^{-11}	0.16596	0.14364	0.1436183	$5.62472 \cdot 10^{-05}$	-
$FoodSupplyLPS$	21.179	-	-	-	-	-
$FoodSupplyNaCl$	26.6	-	-	-	-	-
μ_{LPS}	1.145	-	-	-	-	-
μ_{KYNA}	-	0.052257	0.028857	0.5520143	4.001432	0.6931472
$\mu_{TNF-\alpha}$	-	0.39988	0.63733	0.6372277	0.0002088248	$0.6931472 - 1.386294$
μ_{QUIN}	-	0.20665	0.52348	0.365035	0.130786	$0.165035 - 1.890401$
μ_{SER}	-	0.076614	0.20665	0.1665	0.030668	0.01444057

The Parameters of the LPS model were fitted multiple times on different data sets. Parameters were fitted to the data of LPS experiment I (**I**) and 1-MT/LPS experiment, subset LPS-treated pigs (**II**). Additionally, parameters were fitted 100 times on the 1-MT/LPS experiment, subset LPS-treated pigs. The parameters of the simulations with the lowest LL are shown in column **III**. The mean values and standard deviation of the parameters of 100 simulations based on data from the 1-MT/LPS experiment, LPS-treated pigs, were calculated. The mean values are shown in column **IV**, and the standard deviation in column **V**. To compare the fitted values to literature values, the minimal and maximal values of literature values according to Table 5 are shown in column (**VI**). For KQE, the value corresponds to the literature value of the enzyme KYNU. For μ_{KYNA}, μ_{SER}, and V_{max}^{KQE} only one literature value was found. All values are indicated in $\mu M/h$.

D. Parameters Fitted to the Data of 1-MT/LPS Experiment, Second Data Set with a Parameter Scan, AIC values

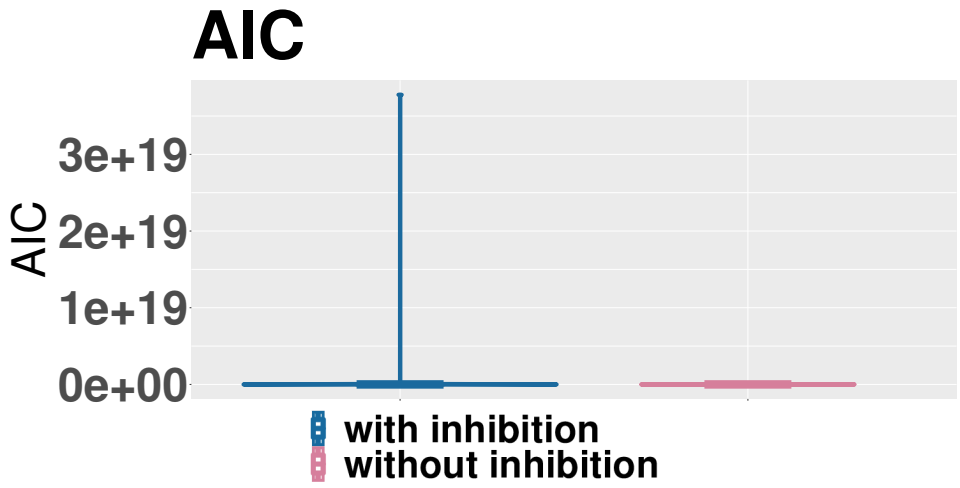

Figure D.1.: **Boxplot of AIC values of hypotheses based on the data of 1-MT/LPS experiment (second data set):** The box plot shows the results of 100 iterations of the model, including inhibition and the model not including inhibition. The curve around the box plot shows the distribution of the data and is mirrored at the whiskers.

Eigenständigkeitserklärung

Hiermit erkläre ich, dass diese Arbeit bisher von mir weder an der Mathematisch-Naturwissenschaftlichen Fakultät der Universität Greifswald noch einer anderen wissenschaftlichen Einrichtung zum Zwecke der Promotion eingereicht wurde. Ferner erkläre ich, dass ich diese Arbeit selbstständig verfasst und keine anderen als die darin angegebenen Hilfsmittel und Hilfen benutzt und keine Textabschnitte eines Dritten ohne Kennzeichnung übernommen habe.

(Unterschrift des Promovenden)